ゴンドワナ・Barapukuria石炭盆地（北西バングラデシュ）の多層・長壁式採炭に伴う地質学的災害危険分析：数値シミュレーションに基づく評価

Geo-environmental hazards associated with multi-slice longwall mining of the Gondwana Barapukuria coal basin, NW Bangladesh: constraints from numerical simulation

A dissertation submitted to the Graduate School of
Engineering and Science, University of the Ryukyus,
as requirement for the degree of Doctor of Philosophy (Science)

June 2009

By

Md. Rafiqul Islam

Marine and Environmental Sciences
Graduate School of Engineering and Science
University of the Ryukyus

Supervisor: Ryuichi Shinjo, Ph.D.

Certificate of the Dissertation Committee

We certify that we have read this thesis and that in our opinion it is fully adequate, in scope and quality, as a dissertation for the degree of Doctor of Philosophy

Professor Dr. Ryuichi Shinjo (Chairman)

Professor Dr. Takeshi Matsumoto

Professor Dr. Masahide Furukawa

Abstract

According to World Coal Institute (WCI), coal is the major fuel used for generating electricity worldwide. Coal provides 26% of global primary energy needs and generates 41% of the world's electricity. Bangladesh is blessed with natural energy resources, especially coals in the northwest region and gas in eastern fold-and-thrust belt region. Natural gas is currently the major indigenous nonrenewable energy resource, which is going to be ended by 2020 if new gas field is not discovered in Bangladesh. The top five Gondwana coal basins of the country where the total in situ reserves over 4500 Mt coals are Jamajgonj, Khalaspir, Phulbari, Barapukuria, and Dighipara. Bangladesh desires to produce coal from the Gondwana coal deposits due to gradually demands of electricity and to safeguard the energy crises in 21th century. Barapukuria is the first and only coal mine in the country.

This dissertation connects the Boundary Element Method (BEM) and Finite Element Method (EFM) with its practical applications to recognize the some mining related geo-environmental hazards associated with the Gondwana Barapukuria Coal Basin of northwest Bangladesh. Several geo-environmental hazards, such as- (i) ground movement and water inrush/inflow, (ii) seam gas outburst (iii) mining-induced fault reactivation, and (iv) rock burst with major roof fall, have been recognized during mining operation which generate adverse impacts on the exploration and underground multi-slice longwall mining in the Barapukuria coal deposits. A summary and problems regarding the present research have been emphasized in the 1st chapter. In the 2nd chapter of this thesis, I discussed general geologic understanding of Bangladesh. In the 3rd chapter, geological, hydrogeological, geotechnical, and tectonic setting of the study area have been focused.

Chapter 4th highlights ground movement and water inrush/inflow hazards into the mine. This chapter deals with current coal mining operations under a mega-aquifer in NW Bangladesh, and presents a case study of underground mining in Barapukuria. The study uses numerical analyses to evaluate stress redistribution, strata failure, and water inflow enhancements that result from these coal extraction operations. A total of three models (A, B, and C) are presented in this study. Two-dimensional numerical modeling was performed to analyze the deformation and failure behavior of rock elements for two different models (A and B). For model A, we used an elastic finite element software package considering a Mohr-Coulomb failure criterion. For

model B, we used boundary element method (BEM). The first two models were applied to determine the stress patterns. Model A provides the tectonic stress pattern of the basin, whereas model B represents the mining-induced stress field. The third model is a schematic model.

The results of model A show that tensional failure of rock elements is concentrated in the Gondwana coal sequences as well as within the Eastern Boundary Fault (EBF) and its surroundings. Failure occurs in the middle to lower part of the model, and the magnitude of tensional stress in the shallow part is much greater than in the deeper part. Contours of τ_{max} magnitudes are attributed to up-bending of the overburden, which would create numerous upward propagating fissures/fractures. The results of model B show that fracture propagation would be about 240 m upward for single-slice (height 3 m) mining extraction. From the contours of mean stress magnitudes, it is observed that the high range of fracture propagation increased upward for multi-slice extraction of coal. It is apparent from the fracture heights that large amounts of caving would occur towards the roof due to the multi-slice extraction of coal, and finally would be linked with the water-bearing Dupi Tila Formation. If this is happened, it would ultimately cause a major water inflow hazard in the mine.

Seam gas outburst related geo-hazards have been focused in the 5th chapter. In this case study, I use two-dimensional Boundary Element Method (BEM) numerical modeling to analyze the deformation and failure behavior of a coal seam and to understand the nature of gas flow into a roadway entering the Barapukuria coal mine in Bangladesh. The Barapukuria basin contains Permian-aged Gondwana coals with high volatile B bituminous rank. Three models (A, B, and C) are presented here. Model A assumes horseshoe-shaped geometry, model B assumes trapezoid-shaped geometry, and model C assumes horseshoe-shaped geometry coupled with a roof fall-induced cave generated by the break-up of rock materials along the vertical dimension of an igneous dyke. The simulation results show that there is little difference in strata deformation between models A and B. In model A, there is no horizontal tensional stress and the overall horizontal stress patterns are compressive, while the distribution and magnitude of vertical stress show higher tensional stresses on the immediate rib sides and floor. In model B, both horizontal and vertical stress distributions indicate low to medium tensional stresses on the immediate roof, floor, and rib sides, but compressive stresses are prominent toward the interior of the coal seam. Deformation vectors indicate that failure extends laterally to about 7.5 m around the excavation geometry.

On the contrary, for model C, the distributions and magnitudes of horizontal and vertical stress show higher tensional stresses in both rib sides of the roof fall zone. The deformation around the dyke-induced perturbation zone affects a large volume of coal. The deformation vectors with high magnitudes are nearly horizontal and propagate laterally up to 30 m; whereas, low–magnitude deformation vectors extend about 25 m toward the roof and 20 m toward the floor. The vertical tensional displacement, which is concentrated in the floor and the left and right hand sides of the roof, propagates about 30 m on both sides and about 22 m in the floor. From these simulation results, it is thought that the extension of the dyke-induced perturbation zone toward the roof, floor, and rib sides of the entry roadway initially creates small tensional cracks that gradually grow into large-scale tensional features. These features could also be responsible for high concentrations of gas, which are emitted into the mine from fractured coals due to insufficient mine ventilation and low atmospheric pressure.

Mining-induced fault reactivation and its impacts on main conveyor belt roadway have been discussed in the 6th chapter. In this chapter, I use same methodology as previously mentioned and the study paper investigates the mining-induced reactivation of faults associated with the main Conveyor Belt Roadway (CBR) and safety of the mine. The stress characteristics and deformation around the faults were investigated by boundary element method (BEM) numerical modeling. The model consists of a simple geometry with two faults (Fb and Fb1) near the CBR and the surrounding rock strata. A Mohr-Coulomb failure criterion with bulk rock properties is applied to analyze the stability and safety around the fault zones, as well as for the entire mining operation. The simulation results illustrate that the mining-induced redistribution of stresses causes significant deformation within and around the two faults. The horizontal and vertical stresses influence the faults, and higher stresses are concentrated near the ends of the two faults. Higher vertical tensional stress is prominent at the upper end of fault Fb. High deviatoric stress values that concentrated at the ends of faults Fb and Fb1 indicate the tendency towards block failure around the fault zones. The deviatoric stress patterns imply that the reinforcement strength to support the roof of the roadway should be greater than 55 MPa along the fault core zone, and should be more than 20 MPa adjacent to the damage zone of the fault. Failure trajectories that extend towards the roof and left side of fault Fb indicate that mining-induced reactivation of faults is not sufficient to generate water inflow into the mine. However, if movement of strata occurs along the fault planes due to regional earthquakes, and if the faults

intersect the overlying Lower Dupi Tila aquiclude, then liquefaction could occur along the fault zones and enhance water inflow into the mine. The study also reveals that the hydraulic gradient and the general direction of groundwater flow are almost at right angles with the trends of faults Fb and Fb1, which could act as barriers to groundwater flow into the mines.

In the 7th chapter, I preferred to rethink about coal bed methane (CBM) resource potential rather than underground mining of Barapukuria coal basin. The coal-bearing sediments are comprised of Gondwana Permian-age sandstones, siltstones, subordinate carbonaceous shales, and six correlated coal seams. Within the structural limits of the basin, approximately 377 Mt coal in-situ has been quantified in the six coal seams that range in depth from 118 to 518 m below surface. About 34 Mt of coal has been estimated as recoverable resources, utilising descensional multi-slice longwall mining. Rest of 343 Mt coal could be used for CBM. The potential of CBM extraction has been investigated as an alternative to underground mining. The study considers the Barapukuria deposit in terms of its geological structure, geothermal gradient, and the rank, porosity and permeability of the coal seams as determined by several phases of exploration of the area. All parameters show supportive of CBM. The methane content of the bituminous coal at Barapukuria varies within the range 6.51-12.68 m^3/t, representing a potential resource of more than 5 Gm^3 of gas.

Acknowledgements

It is a great pleasure to thank my advisor, Professor Dr. Ryuichi Shinjo, for all the guidance and assistance given during my studies at University of the Ryukus. His contagious enthusiasm, accessibility for discussion, and pedagogic skill helped my research greatly. I would like to express my deep hearted gratitude to him for his guidance, motivation, encouragement, constructive criticism, and fruitful discussion on achieving the goal. I would also like to thank the thesis committee members, Professor Dr. Takeshi Matsumoto, and Professor Dr. Masahide Furukawa, for their valuable time on reviewing the thesis and their insightful comments.

I have also appreciated the constructive advice and heartiest support of Professor (Emeritus) Dr. Masaaki Kimura, Professor Dr. Daigoro Hayashi, Professor Dr. Shigeru Ohde, and Professor Dr. MakotoTsuchiya, the Director of the Graduate School of Engineering and Science. I would like to thank the Ministry of Education, Culture, Sports, Science and Technology (Monbukagakusho) of Japan for providing the financial assistance needed to complete this dissertation.

Further, I would like to acknowledge the encouragement of my mother, Shakina Khatun, whose supplication to Allah (SWT) ultimately led to the completion of this dissertation. I would like to thank my wife Mrs. Parul Khatun, my beloved daughter, Israt Jahan (Mim), and my beloved son, Ikbal Hasan Muzahid, for their inspiration and patience throughout my studies. They were always encouraged and gave me full moral support. This dissertation is dedicated to my beloved father, late BAHAS UDDIN MONDOL**,** for his enormous love and supplication for me to Allah (SWT).

Finally, I am forever grateful to my family members, and friends especially Rowich and Tariqul. I am also grateful to Br. M.A. Razzak (Bangladesh), Br. Dr. Sheikh Mohammed Ali (Tanzania), Br. Dr. Islam Salum (Tanzania), Br. Dr. Ibrahim Elsamni (Egypt), Br. Dr. Naser (Egypt), Br. Dr. Basyuni (Indonesia) for their encouragement that has given me the key inspiration to achieve my goal.

Contents

CHAPTER 4: Numerical Simulation of Stress Distributions and Mining Hazards Associated with Ground Movement and Water Inflow of the Barapukuria Coal Mine

CHAPTER 7: Coal Bed Methane (CBM) Resource Potential of the Barapukuria Basin

LIST OF TABLES

CHAPTER 3

CHAPTER 4

CHAPTER 5

CHAPTER 6

CHAPTER 7

LIST OF FIGURES

CHAPTER 1

CHAPTER 2

in Bangladesh and Peninsular India were undisturbed by igneous activity prior to deposition, although some geologic discontinuities like basin boundary faults and intrabasinal faults were generated due to disintegration of super Gondwanaland. After a long period, especially in early cretaceous, the faults in the Gondwana basins area became active and developed tensional ruptures due to movement of Indain plate beneath the Himalaya. These tension ruptures in the upper crust enhanced the magmatic flow to come upward, which finally emplaced as arrested igneous intrusion (dyke) in many coal basins in Bangladesh as well as Peninsular India.

CHAPTER 3

CHAPTER 4

CHAPTER 5

CHAPTER 6

CHAPTER 7

Chapter 1
Introduction

Chapter 1
Introduction

1.1. Background of research

According to World Coal Institute (WCI, coal fact, 2008) (http://www.worldcoal.org), coal is the major fuel used for generating electricity worldwide countries heavily dependent on coal for electricity include: Poland (93%), South Africa (93%), Australia (80%), PR China (78%), Israel (71%), Kazakhstan (70%), India (69%), Morocco (69%), Czech Rep (59%), Greece (58%), USA (50%), and Germany (47%). The top five coal producers countries in the world are China, the USA, India, Australia, and South Africa. Coal production has grown fastest in Asia, while Europe has actually seen a decline in production. Coal provides 26% of global primary energy needs and generates 41% of the world's electricity.

Bangladesh is a miniature rising country of Asia, blessed with scenic wonders and plentiful natural energy resources, especially coals in the northwest region and gas in eastern fold-and-thrust belt region. However, this bounty is accompanied by numerous challenges to solve the problems posed by resource extraction.

Natural gas is currently the major indigenous nonrenewable energy resource. The proven and probable resource, contained within 22 gas fields in the country total is estimated at 804.5 Gm3, of which 580.7 Gm3 is considered recoverable. Approximately 144.5 Gm3 has been consumed to June 2003 leaving a remaining recoverable reserve of 436.2 Gm3. Gas production has increased sharply over the last decade with the result that natural gas resources are likely to be exhausted in 15 to 20 years (National Energy Policy, 2004; Islam and Hayashi, 2008).

The top five coal basins in northwest region of the country where the total in situ reserves over 3258 Mt coals are Jamajgonj (1053 Mt), Khalaspir (828 Mt), Phulbari (over 500 Mt), Barapukuria (377 Mt), and Dighipara (assume to be over 500 Mt) (Islam and Hayashi, 2008). Bangladesh desires to produce coal from the Gondwana coal deposits due to gradually demands of electricity and to safeguard the energy crises in 21th century.

Worldwide coal is mined by two methods: surface or ‘opencast' mining, and underground or ‘deep’ mining. Underground mining method is further divided into two main methods, the longwall mining (Fig.1-1), and room-and-pillar mining (Fig.1-2ab). Another method, longwall top coal caving (LTCC) (Fig.1-3), has successfully been applied in China since the mid 1980s

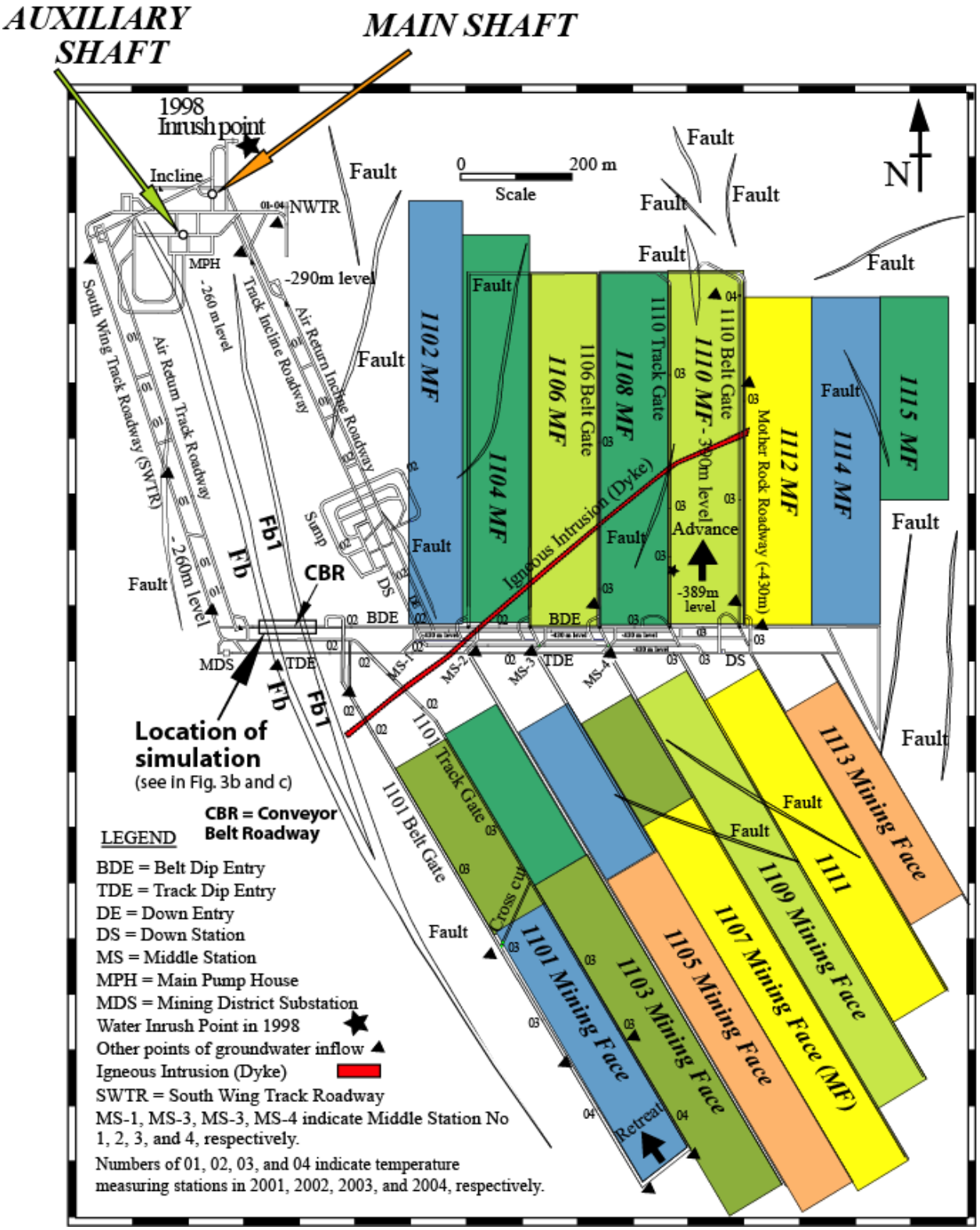

Fig. 1-1. Longwall Mining panels in Barapukuria Coal Mine, Bangladesh (after Barapukuria Coal Mining Co. Ltd, 1998)

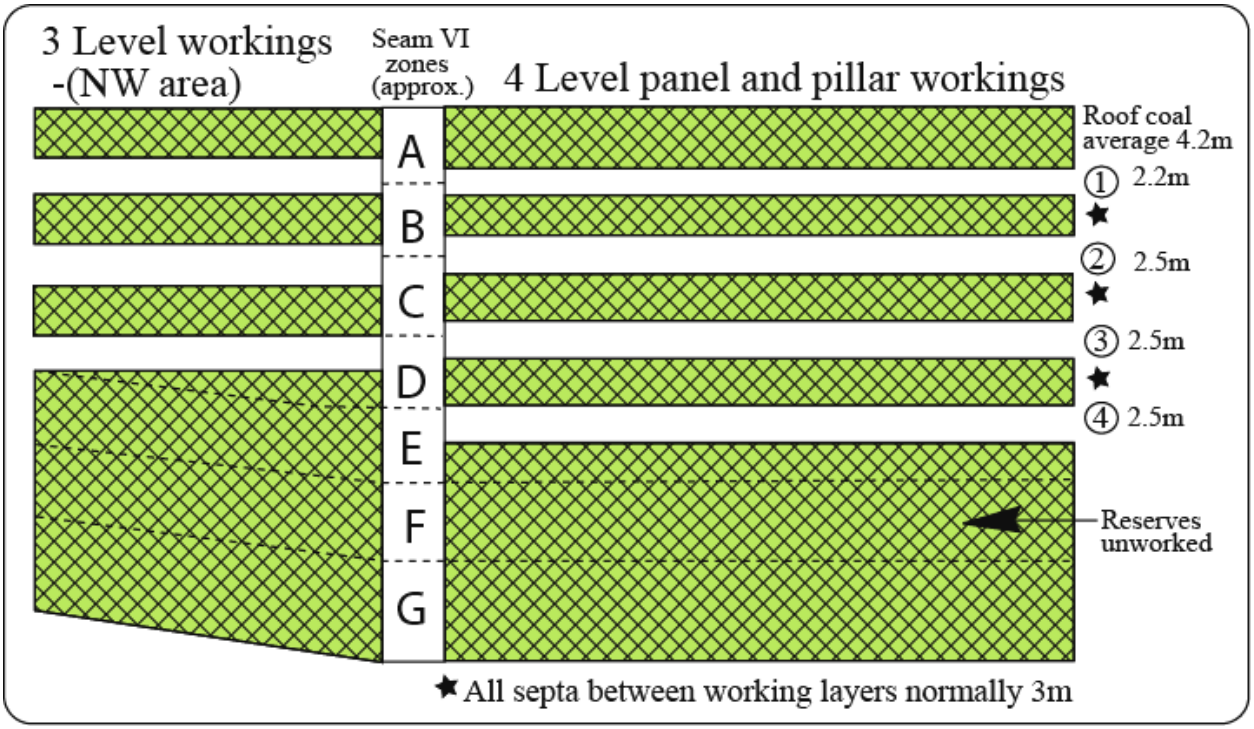

Fig. 1-2a. Panel and Pillar workings

(Xie and Zhou, 2008). This is currently the method preferred in a number of other countries, especially Australia and Turkey. Underground mining currently accounts for about 60% of world coal production; although in several important coal producing countries surface mining is more common. Surface mining accounts for around 80% of production in Australia, while in the USA it is used for about 67% of production (World Coal Institute). About 70–80% of thick coal seams are exploited by means of underground mining methods.

Over the past several decades, mining of thick coal seam, as at Barapukuria deposits, creates hazards in India, Australia, China, Turkey, and other coal producer countries. Hazards have included rib and roof control (due to height and accessibility), pillar stability, spontaneous combustion (due to ventilation difficulties and quantity of slack coal). In Australia, more than six billion tonnes of measured underground mineable coal reserves exist in thick seams (more than 4.5m) in difficult geological conditions. Mining thick seams results in poor resource recovery and high hazards levels. In India, Australia, and China, the current longwall mining methods and designs for thick coal seams in underground mines are inefficient and result in huge losses of valuable coal resources in both countries. The recovery ratio of thick seams in a number of

existing coal mines is below 50% due to the limitations of the traditional mining technologies and complex caving conditions in thick seam environments (Australian Coal Association Research Program, ACARP 2001).

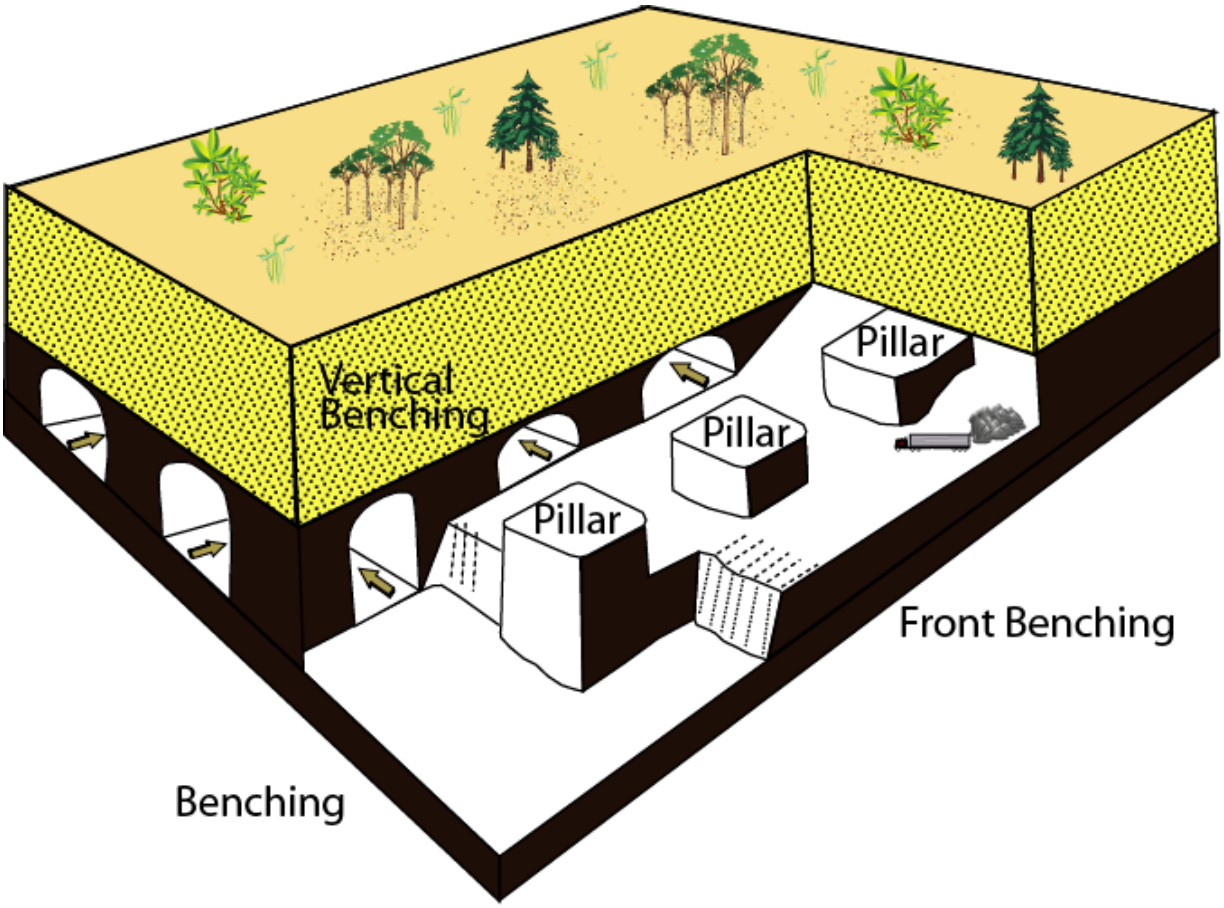

Fig. 1-2b. Schematic view of room-and-pillar mining

Barapukuria is the first and only coal mine to be developed in Bangladesh, with an estimated recoverable reserve of 34 Mt. The remaining measured resource is 343 Mt of in-situ coal. Only Seam VI, out of total seam six, is ever likely to be mined by using multi-slice longwall mining methods. The selection of mining method is largely determined by the geology of the coal deposit. The principal reason for this low recovery ratio (about 10%) are the difficult underground geological structures and conditions for mining.

Water inrush/inflow, major geological discontinuities especially high angle normal faults, seam gas outburst, and rock burst have recognized adverse impacts on the exploration and

mining of underground coal deposits, especially for multi-slice longwall mining in the Barapukuria coal deposits. Normal faults and fractures in the Barapukuria basin are potentially active and created a water flow network between water bearing Dupi Tila aquifer and coal-bearing Gondwana rocks (Wardell Armstrong, 1991; Islam et al., 2009). Geological as well as

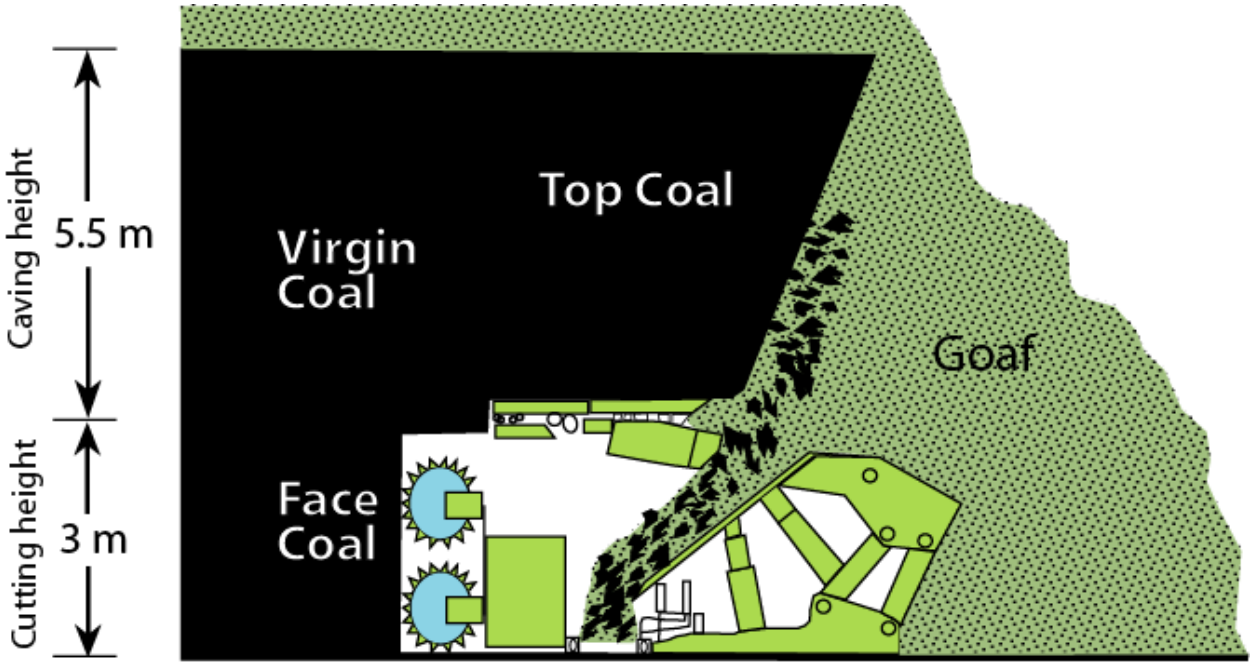

Fig.1-3. Schematic view of Longwall Top Coal Caving (LTCC) (after Simsir and Ozrifat, 2008).

previously mentioned uncertainties may cause significant delays in production schedules, imposed substantial changes to mine plans, reduce expected recoverable coal quantities, adverse affect safety, and heavily influence the financial validity of a mine. As Bangladesh's coal mining industry is becoming increasing reliant upon longwall mining rather than open pit mining, there is a need to implement:

- more effective quantitative and practical approaches to multi-slice longwall mining risk modeling,
- integration of gas outburst as well as rock bursts management,
- Normal faults, at Barapukuria, are related to rift tectonic events. Consequently, it is very essential to understand the regional flow of groundwater and permeability structure of the fault zones in Barapukuria underground mining regions

- uncertainty assessments regarded geological discontinuities,

This will enable mining companies to better plan underground exploration activities and Longwall Top Coal Caving (LTCC) mining operations rather than multi-slice longwall mining methods in Bangladesh.

1.2. Scope of research

There are some particular features about the coal mining operations in the Barapukuria area that may be summarized now as follows:

- The Barapukuria mine is a mine under mega aquifer. With an area of 5.16 km^2, the Barapukuria coal measure is an asymmetrical synclinal deposit of Permian age. It is one of the five largest Gondwana coal basins in Bangladesh,
- Overburden Dupi Tila Formation is highly permeable,
- In 1998, at the preliminary stage of the mining development, a tremendous water inrush happened,
- The coal-bearing Gondwana strata are X-shaped jointed, highly fractured, and faulted,
- The coalfield consists of seams I to VI, of which the lower seam VI is being mined. The thickness of seams varying from 1 m to 42 m. The average thickness of the mineable seam VI is 36 m,
- The multi-slice longwall excavation method is employed with blockade pillars and with trackgate as well as beltgate. This type of mining method could create adverse impacts on socio-environmental systems.
- The depth of mining is currently ranged between 290-420 m. The coal measure rocks in the Barapukuria mining district are weak to moderately strong.
- The in situ stresses (σ_1 and σ_3) at depth are in the order of 2–25 MPa,
- In 2005, the strata relaxation and immense roof fall occurred around an entry roadway with igneous intrusion,
- Gas is released in a higher degree from the neighboring unmined seams and gas bearing strata, which are fractured as mining face advances,
- Gas outburst and rock bursts (violent failure of coal measure rocks caused by high stresses) however occur intermittently during development period and panel extraction.

1.3. Objectives of the research

The objectives of the research are to discriminate a critical assessment of thick (36 m) coal seam mining in Bangladesh with special reference to Barapukuria coal deposits, taking into account:

- constraints on multi-slice mining method due to hazard management imperatives, especially water inflow, igneous intrusion, gas outburst, weak ventilation system, and spontaneous combustion.
- enhanced geotechnical understanding of the driving mechanisms controlling and constraining particular mining systems,
- presentation of both the tectonic and mining-induced stress distribution,
- integration of the calculated results to reveal a concern regarding damage to the overlying aquifer due to multi-slice longwall mining,
- discussion of the adverse environmental impacts, especially damage to the agricultural land as well as the aquifer system.
- reorganization of the strata relaxation zones around the roof, floor, and both rib sides due to mining-induced stress, and
- interpretation of some potential explanations for the enhanced gas emission, including geological structures, coal thickness at the roof and floor, and mine ventilation systems.
- an interpretation of the mining-induced stress distributions to take into account the reactivation of the two major faults associated with the CBR,
- an understanding of the displacements and rock failure trajectories around the two faults,
- a prediction of rock failure loading conditions around the mine roadway, and to then apply that understanding to the development of appropriate reinforcement strategies, and
- an assessment of safety regarding earthquakes induced hazards due to the geotectonic location of the mine, finally
- reflection on Coal Bed Methane (CBM) resource potential rather than multi-slice longwall mining of the Barapukuria coal basin.

1.4. Methodology

Three methods have been used in this study, which are

- Finite Element Method (FEM) modeling for tectonic stress field and gravitational effects,
- Boundary Element Method (BEM) modeling for mining induced stress and displacement,
- Linear Regression Equation Method (LREM) has been used for calculating gas content in coal per tone, and to estimate total gas reserves in place of the Barapukuria coal deposits.

The first two methods describe in brief in the following sections and for details the interested readers are referred to Zienkiewics and Taylor (1989), and Crouch and Starfield (1983). The mathematical bases of the finite element numerical model are available in Islam and Hayashi (2009).

1.4.1. Finite Element Method (FEM)

The FEM (Fig.1-4a) is a valuable tool that can be used to understand the spatial and temporal variations of stress in rock mass. The method is very popular with structural geologists, mining geologists, and mining engineers, although it was developed originally as a concept of structural analysis and until now has mainly been applied to civil engineering problems. The finite element method is a general method of stress analysis in which a continuum or continuous structure is replaced by a finite number of elements interconnected at a finite number of nodal points. The method can be used to determine the displacements of the nodal points and the stresses within the elements developed in two or three-dimensional elastic or viscous structures of arbitrary geometrical and material properties (Stephansson and Berner, 1971).

In the FEM, two important terms *discrete* and *continuous* are applied. In many situations, an adequate model is obtained using a finite number of well-defined components or 'elements' and such problems term as *discrete*. In others case, the subdivision is continued indefinitely and the problem can only be defined using the mathematical fiction of an infinitesimal. This leads to differential equations or equivalent statements, which imply an infinite number of elements and such systems term as *continuous*. With the advent of digital computers, *discrete* problems can generally be solved readily even if the number of element is large. As the capacity of all computers is finite, *continuous* problems can only be solved exactly by mathematical manipulation (Zienkiewics and Taylor, 1989).

1.4.2. Boundary element Method (BEM)

The term 'boundary element' is used to indicate the method whereby the external surface of a domain is divided into a series of elements (Fig.1-4b) over which the functions under consideration can vary in different ways, in much the same manner as in finite elements. In terms of mining engineering, the boundary of the underground excavation is divided into elements and the interior of the rock mass is represented mathematically as an infinite continuum. The BEM has been used as a generic term for a variety of numerical methods that use a boundary or boundary-like discretization. The BEM automatically models the behavior at infinity without the need of deploying a mesh to approximate it. The BEM is indeed an essential part in the inventory of the modern day computational tools. In the contemporary industrial era, mesh preparation is the most labor intensive and the most costly portion in numerical modeling, particularly for the FEM. Without the need of dealing with the interior mesh, the BEM is more cost effective in mesh preparation. For problems involving moving boundaries, the adjustment of the mesh is much easier with the BEM (Watson, J. O., 2003; Cheng and Cheng, 2005).

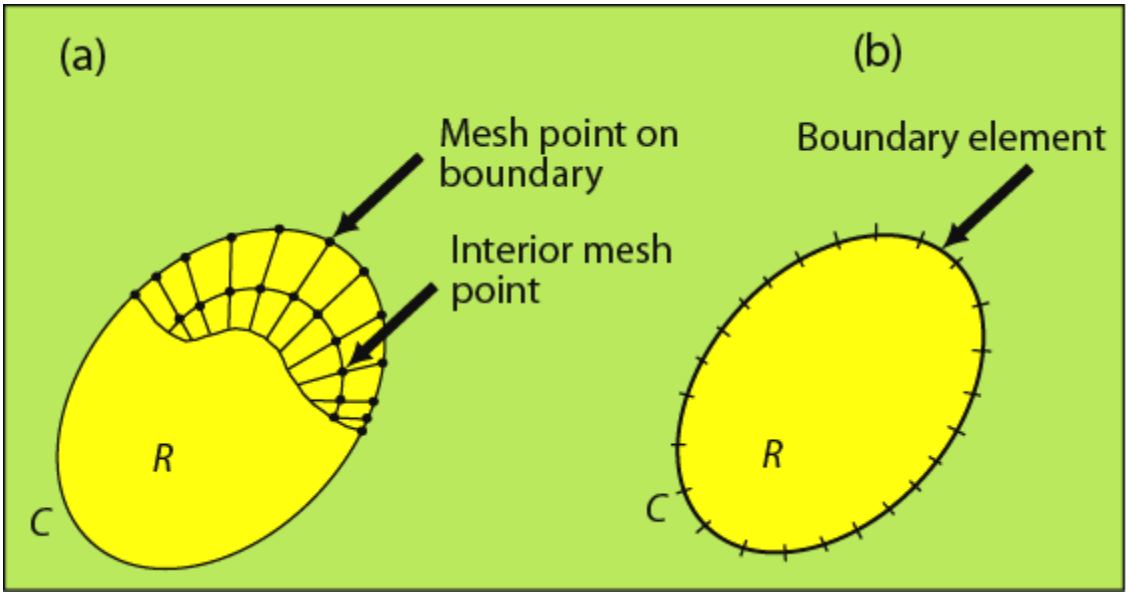

Fig. 1-4. Finite element, Boundary element idealization: (a) finite elements; (c) boundary elements. R represents a two-dimensional plane region bounded by a contour of C (after Crouch and Starfield, 1983)

Comparing to others conventional numerical methods, such as the Finite Element Method (FEM) and the Finite Difference Method (FDM), which can be classified as the domain methods, the BEM distinguish itself as a boundary method. This is why the BEM means that the numerical

discretization is conducted at reduced spatial dimension. For example, for problems in three spatial dimensions, the discretization is performed on the bounding surface only; and in two spatial dimensions, the discretization is on the boundary contour only. This reduced dimension leads to smaller linear systems, less computer memory requirements, and more efficient computation (Cheng and Cheng, 2005).

1.4.3. Linear Regression Equation Method (LREM)

Gas resource = (Gas content)×(density)×(Av. coal thickness)×(Area in Ha)×c

where *Gas content (m^3/t) = [152 + {0.2 × depth (m/0.3048)}] ÷35.3*

and c = tons of coal per hectare metre of coal = 14,593 tonne (av.)

1.5. Dissertation Outline

Chapter 2 presents the basic outline of regional geotectonic setting of Bangladesh/Bengal Basin and its major tectonic divisions with the evolution of Gondwana coal basins in NW Bangladesh as well as peninsular India. Chapter 3 represents detailed geology and regional geotectonic setting of the Barapukuria basin.

Chapter 4 develops an extended example of numerical simulation based on finite element method (FEM) modeling and the Boundary Element Method (BEM). This chapter deals with current coal mining operations in Barapukuria under a mega-aquifer. The study uses numerical analyses to evaluate stress redistribution, strata failure, and water inflow enhancements that result from these coal extraction operations. A total of three models (A, B, and C) are presented in this chapter. Two-dimensional numerical modeling was performed to analyze the deformation and failure behavior of rock elements for two different models (A and B). For model B, I used boundary element method (BEM). The first two models were applied to determine the stress patterns. Model A provides the tectonic stress pattern of the basin, whereas model B represents the mining-induced stress field. The third model is a schematic model.

Chapter 5 presents a number of advanced applications of numerical simulation techniques. The first advanced application is to mining-induced stress state, strata displacements, and problems such as gas outburst in an entry roadway with igneous intrusion (dike). The second application is the use of simulation to characterize better and simulate geological structures. In

this chapter, I used two-dimensional Boundary Element Method (BEM) numerical modeling to analyze the deformation and failure behavior of a coal seam and to understand the nature of gas flow into a roadway entering the Barapukuria coal mine in Bangladesh. Three models (A, B, and C) are presented in this chapter. Model A assumes horseshoe-shaped geometry, model B assumes trapezoid-shaped geometry, and model C assumes horseshoe-shaped geometry coupled with a roof fall-induced cave generated by the break-up of rock materials along the vertical dimension of an igneous dyke. A number of cases are given that show the benefit of accounting for this information.

Chapter 6 corresponds to mining activities approach or breach with two major geologic discontinuities, such as faults. Because thrusts, strike-slip faults, normal faults, igneous intrusions, and recumbent fold hinges, which are referred to as 'tectonic disturbances' are related to highly fractured rock strata and to cause hazardous problems in safe operation of the underground mining. The main objectives of this chapter are to present: an interpretation of the stress distributions to take into account the effect of the tectonic fault including wedge fall, understanding of the deformational behavior of weak roof strata, and prediction of loading conditions around the mine roadway, and to then apply that understanding to the development of appropriate reinforcement strategies.

Chapter 7 focuses on CBM resource potential of the Barapukuria coal basin. The Barapukuria basin contains Permian-aged Gondwana coals with high volatile B bituminous rank. The coal deposit consists of six coal seams. The resultant estimated total gas resource at Barapukuria is 5135.32 Mm^3. Many practical concerns during the employment era (2001-2004) in Barapukuria mine and the numerical model methodology and avenues of research were acknowledged during the preparation of this dissertation.

References

Cheng, A. H.D., Cheng, D. T., 2005. Heritage and early history of the boundary element method. Engineering Analysis with Boundary Elements 29, 268–302.

Crouch, S.L., and Starfield, A.M., 1983. Boundary Element Method in Solid Mechanics. George Allen & Unwin Publishers Ltd, 40 Museum Street, London WC1A 1LU, United Kingdom.

Islam, M.R., and Hayashi, D., 2009. Extensional stresses in the Colombian Eastern Cordillera fold-and-thrust belt, northern Andes: insights from 2D Finite Element Modeling. Geologica Acta 7, 333-350

Islam, M.R., Hayashi, D., and Kamruzzaman, A.B.M., 2009. Finite element modeling of stress distributions and problems for multi-slice longwall mining in Bangladesh, with special reference to the Barapukuria coal mine. International Journal of Coal Geology 78, 91-109.

Islam, M.R., and Hayashi, D., 2008. Geology and coal bed methane resource potential of the Gondwana Barapukuria Coal Basin, Dinajpur, Bangladesh. International Journal of Coal Geology 75, 127-143.

National Energy Policy (NEP), 2004. Government of the People's Republic of Bangladesh, Ministry of Power, Energy and Mineral Resources, Dhaka, Bangladesh.

Simsir, F., and Ozfirat, M. K., 2008. Determination of the most effective longwall equipment combination in longwall top coal caving (LTCC) method by simulation modeling. International Journal of Rock Mechanics & Mining Sciences 45,1015–1023.

Stephansson, O., and Berner, H., 1971. The finite element method in tectonic processes. Phys. Earth Planet. Interiors, 4, 301-321.

Wardell Armstrong, 1991. Techno-Economic Feasibility Study of Barapukuria Coal Project (unpubl.), Dinajpur, Bangladesh.

Watson, J. O., 2003. Boundary Elements from 1960 to the Present Day. Electronic Journal of Boundary Elements 1, 34-46.

Xie, H., and Zhou, H.W., 2008. Application of fractal theory to top-coal caving. Chaos, Solitons and Fractals 36, 797–807.

Zienkiewics, O.C., and Taylor, R.L., 1989. The Finite Element Method. Fourth Edition. Vol. 1. McGraw-Hill Book Company (UK) Limited, London. pp.648.

Chapter 2
Geological outlines of the Bengal Basin/Bangladesh and Origin of the Gondwana Coal Basins in the Dinajpur Craton

Chapter 2

Geological outlines of the Bengal Basin/Bangladesh and Origin of the Gondwana Coal Basins in the Dinajpur Craton

2.1. Introduction

This chapter contains two important outlooks- the first one is the geology and tectonic structures of extensive regions of the Bengal Basin that formed to the northeast part of the peninsular Indian, and the second one is the evolutionary history of the Gondwana coal basins in the northwest Bangladesh. With a view towards understanding the evolutionary history of the Bengal Basin as well Bangladesh, several geophysical, geological, and geotectonic studies have been carried out by the following authors, such as, Khan (1991), Khan and Rahman (1992), Khan and Agarwal (1993), Khan and Chouhan (1996), Alam et al. (2003), Mukherjee et al. (2009), and others. Thus, a here a brief geological review has been considered based on scholarly literatures of the previously mentioned authors.

For understanding the origin of the Gondwana coal basins in northwest Bangladesh, I have studied structures, stratigraphy, and rift basin characteristics of the Gondwana coal deposits in Bangladesh (Islam and Hayashi, 2008; Islam et al., 2009, and Islam and Shinjo, 2009), and India. Then I have discussed on the origin of Gondwana Coal Basins at Dinajpur craton in Bangladesh. The following discussion on geology, tectonic structure and origin of the Gondwana rift basin is thus based on the contributions of different scholars of India.

2.2. Evolutionary history of the Bengal Basin /Bangladesh

2.2.1. Regional geotectonic setting

The Bengal Basin is located in Bangladesh and three eastern states of India including parts of West Bengal, Assam, and Tripura states of India and the Bay of Bengal. Geo-tectonically, the basin is located in the Himalayan foreland at the junction of the Indian, Eurasian, and Burmese plates (Figs. 2-1 and 2-2). The basin is bounded by the Indian shield of craton on the west and the

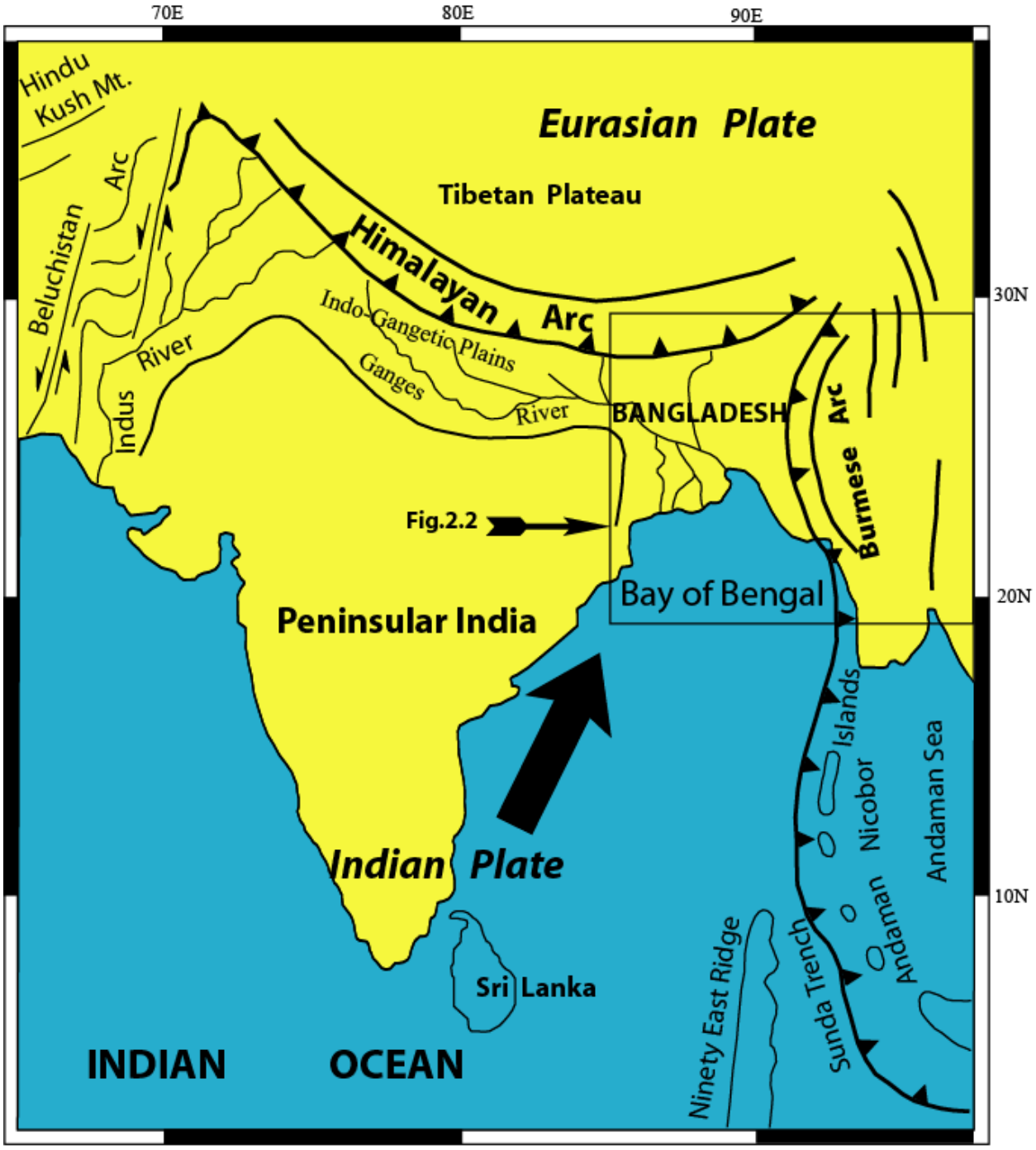

Fig. 2-1. Tectonic map of northeastern Indian plate (after Biswas and Majumder, 1997). Location of Bangladesh is very close to Burmese arc to the east and Himalayan arc to the north, which makes tectonically earthquakes hazard zone. Large arrow represents the direction of Indian plate movement.

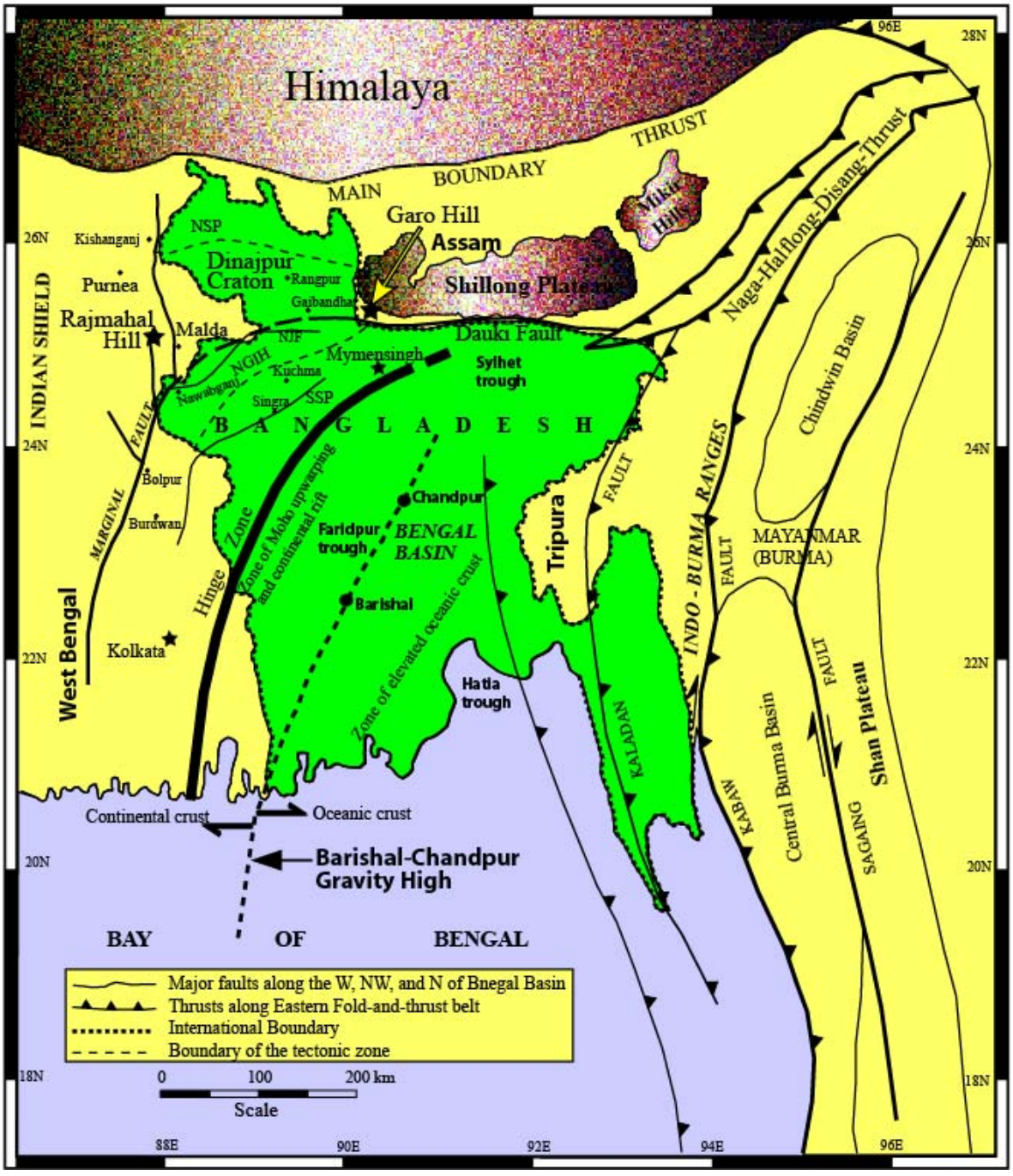

Fig. 2-2. The major geotectonic elements in and around the Bengal Basin. NGIH = Nawabganj-Gaibandha Intracratonic High, NSP = North Slope of the Platform, SSP = Southern Slope of Platform (compiled and modified after Khan, 1991; Khan and Chouhan,1996; Alam et al., 2003). Marginal Fault of the Bengal Basin was taken from Gowd et al. (1992). In the Bangladesh segment, it is named as Nawabganj-Gaibanda Fault. NJF = Nawabganj-Jamalganj Fault (after Khan and Rahman, 1992).

Indo-Burmese fold-and-thrust belts on the east (Alam et al., 2003; Mukherjee et al., 2009). It can be broadly divided into a stable shelf and a foredeep separated by a deep seismic hinge zone (Mukherjee et al.,2009). According to Alam et al. (2003) the Bengal Basin comprises three geo-tectonic provinces: (i) the Stable Shelf zone in the west, (ii) the Central Deep Basin, and (iii) the Chittagong–Tripura Fold Belt in the east.

2.2.2. Dynamics and evolution of the Bengal Basin

The dynamic nature of the basin can be attributed to the interaction of three plates as mentioned above- the Indian plate, Eurasian plate and Burma plate (Alam et al., 2003). These three plates result in the formation of a northeast-southwest trending deep basin zone consisting of numerous sub-basins and surrounded by an almost north-south trending arcuate Tertiary folded belt in the east (the Chittagong–Tripura Fold Belt), an uplifted block of Precambrian shield (Shillong massif) in the north, and a Precambrian basement complex (Stable Shelf zone) of crystalline metamorphics at shallow depths in the west (Fig 2-2). Apart from its tectonic complexities, the Bengal Basin experienced magmatic intrusions and lava extrusions (Rajmahal and Sylhet) in the Cretaceous period (Khan and Chouhan, 1996).

At the beginning of Miocene, the Bengal Basin became a remnant ocean basin (Ingersoll et al., 1995) because of the continuing oblique subduction of Indian plate beneath the Burmese plate. As a remnant ocean basin, Alam et al. (2003) further divided the Bengal Basin into three distinct geo-tectonic provinces such as: (i) Passive to extensional cratonic margin in the west, the Stable Shelf Province; (ii) the Central Deep Basin Province or remnant ocean; and (iii) the subduction-related orogen in the east, the Chittagong–Tripura Fold Belt (CTFB) Province. They stated that the evolution of the Stable Shelf Province and the Central Deep Basin Province commenced with the Early Cretaceous rifting and concomitant volcanic eruptions along the northeastern margin of the Indian Shield.

The basin was initiated at the breakup of Gondwanaland in the late Mesozoic (Mukherjee et al., 2009). It is supposed that Indian plate rifted from the combined Antarctica–Australia part of Gondwanaland and began its spectacular journey, initially northwestward and then northward, sometime in the Early Cretaceous (Curray et al., 1982; Hutchison, 1989; Lee and Lawver, 1995; Acharyya, 1998; Alam et al., 2003; Mukherjee et al., 2009; and others).

2.2.3. Tectonic elements of the Bengal Basin

♦ ***The western limit of the basin:***

The understandings of the tectonic elements in and around the Bengal Basin have been taken from Khan and Chouhan (1996). They noted that the Bengal Basin is bordered by the Indian Peninsular shield in the west. The Peninsular shield with its Archean complex and intracratonic Gondwana basins and late Cretaceous volcanic rocks of Rajmahal hills (McDougall and McElhinny, 1970; Kent et al., 2002) defines the western limit of the basin (Khan and Rahman, 1992; Khan and Agarwal, 1993; Khan and Chouhan, 1996).

♦ ***The northern limit of the basin:***

According to Khan and Chouhan (1996) the Shiilong massif marks the northern limit. The massif is an agglomeration of several blocks such as- (i) the Garo block, (ii) the Khasi-Jaintia block, and (iii) the Mikir block. This massif characterizes the Precambrian rocks with Cretaceous and Tertiary shelf sediments overlying the Sylhet basalt trap flows of Cretaceous age on its southern boundary.

♦ ***Rajmahal-Garo Gap***

The Rajmahal-Garo gap is one of the most important geotectonic units is the northwest part of the Bengal Basin. Most of the Gondwana coal-bearing basins including the Barapukuria Coal Mine and Madhapara Hard Mine is located within this unit (Islam and Hayashi, 2008; Islam et al., 2009). Garo-Rajmahal gap corresponding to a shallow buried basement ridge (Desikachar, 1974) known as the Platform flank zone ((Khan and Rahman, 1992; Khan and Chouhan, 1996). In lies between the exposed Peninsular shield, i.e. Rajmahal Hill to the west and the Garo Hill to the east (Fig. 2-2). In the Bangladesh part, the Rajmahal-Garo gap is known as the 'Rangpur Saddle' (Islam and Hayashi, 2008) or Dinajpur craton (Islam et al., 2009). Khan and Rahman (1992) further divided this platform zone into four sub-zones as follows:

- the Northern Slope of the Platform,
- Stable Platform,
- Nawabganj-Gaibandha lntra-cratonic High, and
- Southern Part of the Platform

Except for the Nawabganj-Gaibanda Intra-cratonic High, the other three platform sub-zones exhibit the occurrence of numerous grabens and half-grabens type basins where coal-bearing Gondwana sediments have been deposited (Khan and Chouhan, 1996; Islam and Hayashi, 2008; Islam et al., 2009). As shown in Fig. 2-2, the north-south trending Maldah-Pumea basin and Ghatal-Burdwan basin forms a segment of the continental rifted basin zone (Khan and Chouhan, 1996).

♦ ***The eastern limit of the basin:***

The Andean types (Islam, 2009) north-south trending Indo-Burman fold-and-thrust belt is the eastern limit of the Bengal Basin. Khan and Chouhan (1996) stated that the folded belt to the east is characterized by a north-south trending arcuate zone of deformed Tertiary sediments. This zone represents westward continuation of Indo-Burman Range. The sediments of Indo-Burman Range and that of the folded belt were deposited in the fore-arc basin and subsequently deformed and uplifted. The "Eastern Thrust" represents an extreme westward margin of the folded belt where most of the structures are thrust faulted (Hossain, 1985).

♦ ***The central deep basin***

The central deep basin zone is characterized by several sub-basins such as- (i) the Sylhet trough, (ii) the Faridpur trough, and (iii) the Hatia trough, which are underlain by oceanic crust. The line separating the deeper basin zone and the zone of Moho unwarping and continental rift is a paleocontinental margin. The NE-SW trending zone marking "elevated oceanic crust" (Fig.2-2) separates the Faridpur trough and the Sylhet trough from that of the Hatia trough (Khan and Chouhan, 1996). The zone of Moho unwarping and continental rift marks a mantle activated continental rift zone along which India has been rifted from Australia (Khan et al., 1994). Alam et al. (2003) proposed that the continent-ocean boundary (COB) beneath the Bengal Basin lies along the Barishal-Chadpur Gravity High (Fig. 2-2). They suggested that the Barishal-Chadpur Gravity High indicate the presence of a rift valley formed during break-up of Gondwanaland and formation of the Indian plate.

♦ ***Hinge Zone***

This is a zone of presumed deep-seated normal faults in the basement complex, and representing the dividing line between the Indian Platform with full thickness of continental crust and the Bengal Foredeep (Fig. 2-2). Although the position of the Hinge Zone within Stable Shelf zone is well established, it is generally shown to truncate against the Dauki Fault in the northeast. The Hinge Zone passes somewhere through the Sylhet Trough of the central deep basin and probably continues towards the Halflong Thrust at the northeastern corner of the Bengal Basin. The Calcutta-Mymensingh Gravity High is not so strong and linear. Hinge Zone represent a probable transition from continental to oceanic crust (Alam et al., 2003).

2.2.4. Stratigraphy

The stratigraphy of the different parts of the basin differs considerably, because of contrast in depositional history within the several sub-basins that were produced by intra-plate tectonic activities associated with ongoing Himalayan orogeny (Mukherjee et al., 2009). The intensity and pattern of plate-to-plate interaction varied with time, affecting the basin architecture and sedimentation style throughout the basin (Alam et al., 2003). Basin sediments overlie Gondwanan basement and vary in thickness from a few hundreds of meters on the stable shelf zone (Islam and Hayashi, 2008; Islam et al., 2009) to more than 18 km sediment thickness in its Central Deep Basin (Khan and Chouhan, 1996). For the details of the stratigraphy of the Bengal Basin, the interested readers are referred to Alam et al. (2003).

2.2.5. Gondwana sediments in the Bengal Basin

The Permian age Gondwana sediments have been recognized only within the Stable Shelf zone or the Platform flank zone in the northwest Bangladesh. The most recognized Gondwana coal basin are: the Barapukuria, Khalaspir, Phulbari, Dighipara, Jamalgonj and others (Islam and Hayashi, 2008; Islam et al., 2009). This tectonic zone is underlain by Indian Shield consisting of an Archean gneissic complex at varying depths over which the Gondwana sediments have been deposited in the intracratonic basins. The Late Cretaceous Rajmahal basaltic trap flows and Cretaceous-Tertiary sediments in turn have been deposited over Gondwana sediments (Khan and Chouhan, 1996).

2.2.6. Intra-plate stress field of the Bengal Basin

Gowd et al. (1992) studied the intra-plate stress field of the Indian subcontinent. They prepared a map of the orientation of maximum horizontal compressive stress (σ_{Hmax}) based on borehole elongation breakouts, in situ hydraulic fracturing measurements, earthquakes focal mechanisms. They recognized four provinces in the Indian subcontinent based on regionally consistent orientations. Their boundaries have been determined taking into consideration regional tectonics and seismicity. These provinces are:

- ***Mid continent province:***

This broad midcontinent included Central and Northern India, Stable Shelf zone of Bangladesh, Shillong Plateau stretching up to great Himalaya, Nepal, and Pakistan. NNE-ENE oriented σ_{Hmax} characterized it. The mean orientation of σ_{Hmax} in this province is about N23^{o}E, which is sub-parallel to the direction of compression expected to arise from the net resistive forces at the Himalayan collision zone. In the shield region of the province, as in Dinajpur craton or Stable Shelf zone of NW Bangladesh, orientations of σ_{Hmax} varying from N31^{o}E to N73^{o}E. This suggests that tectonic stress field in this stress province is largely determined by the tectonic collision processes (Gowd et al.,1992).

- ***The Southern Shield:***

This stress province is characterized by NW oriented $\sigma_{Hmax.}$ These appear close to those of the intra-plate stress field prevailing in the central Indian Ocean (Gowd et al.,1992).

- ***The Bengal Basin:***

This stress province was recognized in the Bengal Basin including parts of West Bengal, Tripura, Monipur, and Mizoram in northeastern India and most of Bangladesh, except Dinajpur craton. This province extends eastward from the marginal fault (Fig.2-2) in the western margin of the Bengal Basin to the Indo-Burma subduction zone. This is bounded on the north by the E-W striking Dauki fault. σ_{Hmax} within the sedimentary pile of the Bengal basin is oriented in E-W direction, while *P* axes of earthquakes within the basement and the crust beneath the basin and within the subducted slab of the Indian plate beneath the Indo-Burman ranges generally trend with N30°E. σ_{Hmax} orientations within the

sedimentary pile of the basin are parallel to the local, approximately E-W, direction of the convergence of Indian and Burmese plates. It is interesting to note that the stress field in the basement and the crust beneath the Bengal basin and in the subducted slab is similar to the one prevailing in the midcontinent stress province (Gowd et al.,1992).

- ***The Assam wedge:***

  This stress region occupies the northeastern corner of the Indian plate, including Upper Assam, Arunachal Pradesh, and much of Nagaland. This region subducts beneath a sharply bent continental collision boundary consisting of the northeastern limb of the Himalayan and northern limb of the Indo-Burman fold belts. As a result, the stress field in this province is depth-differentiated and most likely responsible for the absence of consistent σ_{Hmax} directions (Gowd et al.,1992).

2.3. Evolution of Gondwana Coal Basins in NW Bangladesh and peninsular Indian

The evolution of Gondwana basins is linked with the global tectonic phenomenon, which affected all the components of the Gondwana Supercontinent during the Upper Carboniferous. It is somewhat apparent that the rift zones that evolved to form the Gondwana basins developed almost entirely along the ancient structural grains, such as the contacts of the Precambrian protocontinents (Roy, 2004). He provides some tectonic explanation for the preferential development of the Gondwana basins. He explains that the development of rift zones (grabens) is easier where the extensional stresses act at high angles to the weak structural grains such as palaeo-rifts or the contact zones of proto-continental margins (suture zones). The most significant feature about the Gondwana basins is that these evolved along the contacts of the protocontinents or along the passive rifts (Mahadevan, 1994).The Indian lithosphere underwent significant changes as the result of dismemberment of the Gondwanaland at around 165 Ma ago (Roy, 2004).

The Jurassic break-up of the Gondwanaland, which induced rift type basin opening and sedimentation, has had a pronounced effect on the Indian lithosphere, mainly through the development of sets of new fracture systems. The fracture systems along with the reactivated older tectonic grains, helped to fragment the Indian Shield into a number of rigid crustal blocks. Then it was during the Late Carboniferous when a number of continental rift basins started to

evolve as the receptacle of land-worn sediments. The Gondwana sedimentation took place along several linear intra-continental rift-basins comprising sags and depressions, which at a later stage developed into half or full grabens (Roy, 2004). Manifestations of magmatism in the Gondwana basins are very common in the eastern Indian coal basins like Ranigonj, Rajmahal, and others

The beginning of Bangladesh commenced with separation of the Indian continent from Gondwana during Late Jurassic to Early Cretaceous (Reimann, 1993). Numerous cratonic basins were observed to develop in peninsular India and NW part of Bangladesh starting in latest Permian time following the breakup of Gondwana. At the close of the Archaean era, peninsular India became stabilized as a shield area with the various geosynclines welded into a craton presumably due to compressive forces from the W-SW, SE, and N-NW. Of the various Upper Precambrian intra-cratonic sedimentary basins in India, the more important ones are the Son-Mahanadi Basin, Damodar-Deogarh Basin, Satpura Basin, Pranhita-Godavari Basin and Rajmahal Basin (Fig. 2-3). Intra-cratonic coal-bearing Gondwana basins within the Dinajpur craton of Bangladesh are the Barapukuria, Phulbari, Khalaspir, Dighipara, Nawabgonj, Dangapara, and Jamalgonj (Fig. 2-4) (Uddin and Islam, 1992; Islam and Hayashi, 2008).

The Gondwana basins (Permo-Carboniferous to Jurassic) are relatively smaller units in the Indian (Kailasam, 1976) craton and Dinajpur craton in Bangladesh (Islam and Hayashi, 2008), having been formed in Archaean faulted troughs. The southern and eastern margins are faulted in most of the Gondwana basins in northeast India in which the Lower Gondwana rocks (Permian) are chief coal-bearing formations. These basins are relatively shallow with a total sedimentary thickness varying from 1000 to 2000 m in the Indian segments (Kailasam, 1976), whereas the thickness varying from 118 m in the Barapukuria to about 1200 m in Jamalgonj (Imam et al., 2002; Islam and Hayashi, 2008) of Bangladesh. The Gondwana basins are remains of intra-continental grabens which consist of the Lower Gondwana formation dominated by terrestrial organic matter (coal) of Upper Carboniferous and Permian age, followed by the influx of Triassic to Lower Jurassic clastic sediments (Upper Gondwana) during increasing lateral crustal stretching (Chakrabarti and Mukherjee, 1997).

Fig. 2-3. Coal-bearing Gondwana Basins in Bangladesh and Peninular Indian (after Singh and Singh, 2004). Solid delta close to the Rajmahal Basin indicate approximate location of Rajmahal Hill.

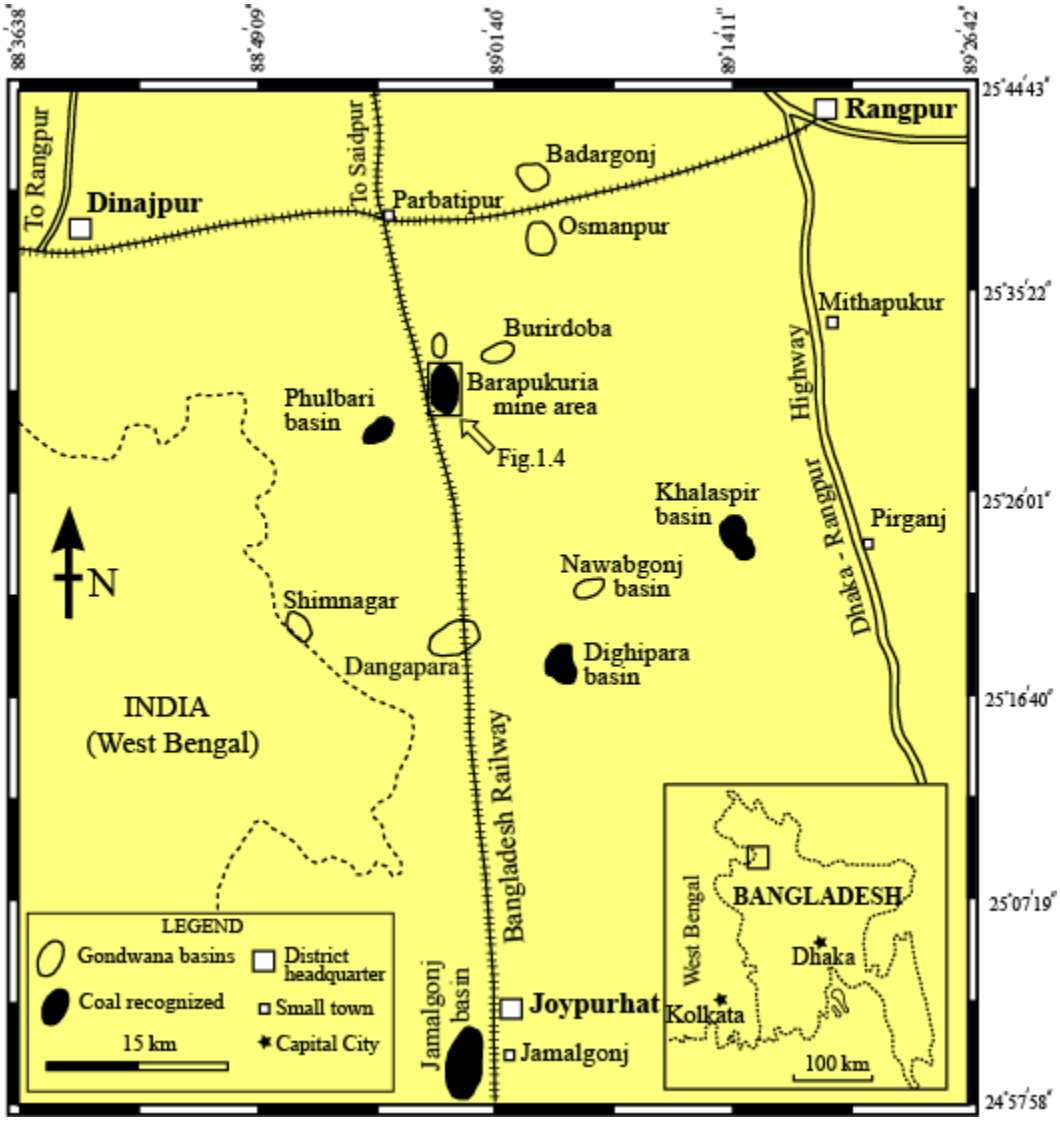

Fig. 2-4. Gondwana coal-bearing basin in NW Bangladesh (after Uddin and Islam, 1992)

2.4. Development of the Barapukuria type craton basin

The origin and development of the Barapukuria type cratonic basins are controversial. According to Klein and Hsui (1987) existing hypotheses to account for cratonic basin formation include:

(1) increase in density of the crust by an eclogite phase transformation (e.g., Williston Basin, Fowler and Nisbet, 1985).

(2) rift associated with intrusion of a thermal plume.

(3) thermal metamorphism of lower crust to boundary conditions of the green-schist and amphibolite facies (Australian craton basins), and

(4) mechanical subsidence caused by isostaticallly uncompensated mass of igneous intrusions (DeRito et al., 1983).

(5) The times of initiation of cratonic basins and Paleozoic passive margins are coeval with the breakup of a late Precambrian supercontinent (Bond et al., 1984).

Klein and Hsui (1987) also stated that several common characteristics of cratonic basins must be considered to explain the origin of the cratonic basins as follows:

- First and foremost are the cause and localization of rifting and common timing of start of thermal subsidence of the cratonic basins themselves.
- Second, major Paleozoic cratonic basins of North America, Africa, and South America all appear to have been initiated during a time of breakup of a major supercontinent between 580 and 500 Ma (Bond et al., 1984),
- Third, sedimentary sequences of cratonic basins in North America, Africa, Asia, Europe, and South America show nearly identical ages for interregional unconformities that separate cratonic sequences as well as identical temporal trends in thickness distribution and volume changes of basin sediment fill.

These observations require a common global explanation, and the near synchroneity of the ages of formation of cratonic basins implies a large-scale process that caused both rifting and thermal subsidence (Klein and Hsui, 1987). The times of initiation of crtonic basins and Paleozoic passive margin are coeval with the breakup of late Precambrian super continent (Bond et al., 1984).

It is apparent from the previously mentioned scholarly reviews that development of the Barapukuria type craton basin is related to rift tectonic activity associated with intrusion of a thermal plume. This prediction is supported by Mahadevan (1994), Khan and Chouhan (1996), Alam et al. (2003), and Roy (2004). The most Gondwana basins in Indian shield evolved along the passive rifts (Mahadevan, 1994) (as shown in Fig. 2-5b). Roy (2004) explains that passive rift zones (grabens) developed in Indian cratons where the tensional stresses act at high angles to the weak structural grains such as ancient rifts. For the case of tensional stresses Bilham et al, (2003) explains that these types of stresses were derived from the far field tectonic activity regarding collision of Indian and Eurasian plates. The ancient rift zones have been invoked as "stress

concentrators" within the Indian plate focusing the approximately NE-directed compressional stress associated with Indo-Asia collision. As mentioned in section 2.2.2, Alam et al., (2003) supports that passive to extensional tectonics occurred in the Stable Shelf zone of NW Bangladesh. Along the northeastern margin of the Indian Shield, the Early Cretaceous rifting and concomitant volcanic eruptions or igneous intrusions are well documented in Rajmahal Hill and Sylhet trough area (Khan and Chouhan 1996; Alam et al., 2003).

2.4.1. Genesis of igneous intrusion with the Barapukuria Cratonic Basin

DeRito et al. (1983) stated that cratonic basins commonly occur over ancient rift zones and reactivation of many cratonic basins occurs simultaneously with large-scale compressional tectonics. Synchronous subsidence of all cratonic basins may occur during periods of active tectonic compression. During the rifting event, the lithosphere is extended or stretched, heat flow in the central region is increased and significant volumes of basalt from the asthenosphere are intruded into the crust and solidifies. In active continental rift, as in Barapukuria, basaltic volcanic activity occurs in the central rift and intrusions of basalts in the central rift are voluminous.

It is assumed that reactivation of Barapukuria cratonic basin occurs simultaneously with large-scale compressional tectonics between Indian and Eurasian plates. Because tensional failure on the weak brittle upper crust of the Dinajpur craton is related to the subduction of Indian plate beneath the Himalayan orogen (Islam and Hayashi, 2008; Islam et al., 2009) (Fig. 2-5c). It is assumed that the Permian coal-bearing Gondwana basins in Bangladesh and Peninsular India were undisturbed by igneous activity prior to deposition. Some geologic discontinuities like basin boundary faults and intra-basinal faults were generated due to disintegration of super Gowandaland in Jurassic period. After a long time, in early Cretaceous, the faults in the Gondwana basins area became reactive and developed tensional ruptures due to movement of Indain plate beneath the Himalaya. These tensional ruptures as well as thin-skinned overburdens in the upper crust enhanced the upward flow of magma (Fig. 2-5d), which finally emplaced as arrested igneous intrusion (dyke) in many coal basins in Bangladesh as well as Peninsular India. These intrusions may be occurred at the same time with Rajmahal volcanics.

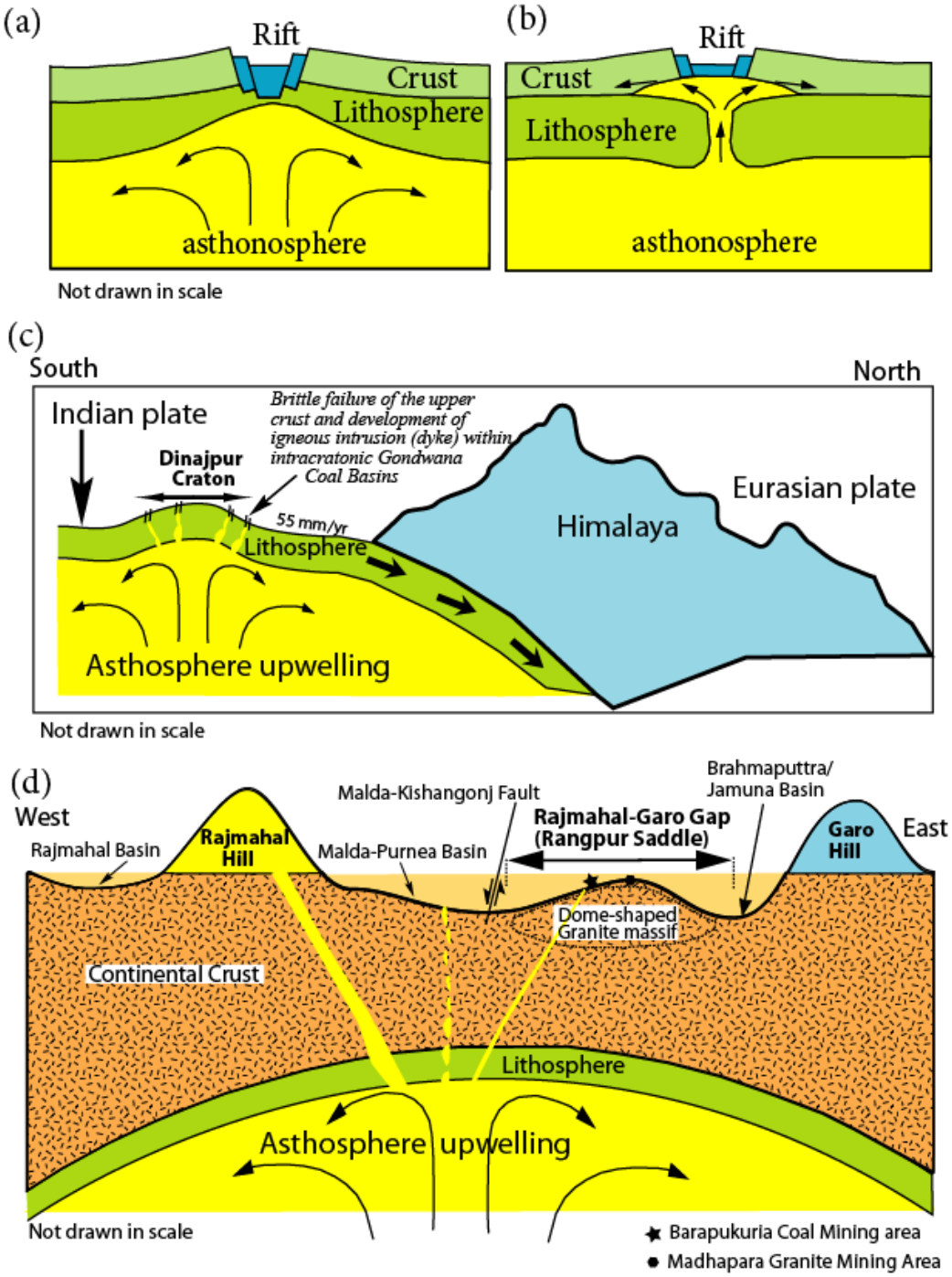

Fig. 2-5. (a) Schematic view of asthenospheric upwelling and evolution of rift basin, (a) active rift basin, (b) passive rift basin (after Turcotte and Emerman, 1983). (c) Showing the subducting Indian plate beneath the Himalayan orogen and generation of tensional failure on the brittle upper crust. (d) It is assumed that the Permian coal-bearing Gondwana Basins in Bangladesh and Peninsular India were undisturbed by igneous activity prior to deposition, although some geologic discontinuities like basin boundary faults and intra-basinal faults were generated due to disintegration of super Gowanda land. After a long time, in early cretaceous, the faults in the

Gondwana basins area became active and developed tensional ruptures due to movement of Indain plate beneath the Himalaya. These tension ruptures in the upper crust enhanced the magmatic flow to come upward, which finally emplaced as arrested igneous intrusion (dyke) in many coal basins in Bangladesh as well as Peninsular India.

References

Acharyya, S.K., 1998. Break-up of the greater Indo-Australian continent and accretion of blocks framing south and east Asia. J. Geodyn. 26, 149– 170.

Alam, M., Alam, M.M., Curray, J., Chowdhury, R.M.L.R., and Gani, M.R., 2003. An overview of the sedimentary geology of the Bengal Basin in relation to the regional tectonic framework and basin-fill history. Sedimentary Geology 155, 179-208.

Bond, G.D., Nicheson, P.A., and Kominz, M.A., 1984. Breakup of supercontinent between 625 Ma and 555 Ma; new evidence and implications for continental histories. Earth and Planetary Science Letters 70, 325-345.

Biswas and Majumder, 1997. Seismicity and tectonics of the Bay of Bengal: Evidence for intraplate deformation of the northern Indian plate. Tectonophysics 269, 323-336.

Chakrabarti, M.K., Mukherjee, B.K., 1997. Sedimentation and hydrocarbon prospects of intracratonic Gondwana rift basins, peninsular India. Indian Journal of Petroleum Geology 6, 60–82.

Curray, J.R., Emmel, F.J., Moore, D.G., Raitt, R.W., 1982. Structure, tectonics and geological history of the northeastern Indian Ocean. In: Nairn, A.E.M., Stehli, F.G. (Eds.), The Ocean Basins and Margins. The Indian Ocean, vol. 6. Plenum, New York, pp. 399– 450.

DeRito, R.F., Cozzarelli, F. A., Hodge, D. S., 1983. Mechanism of subsidence of ancient cratonic rift basins. Tectonophysics 94, 141-168.

Desikacher, S.V., 1974. A review of the tectonic and geological history of eastern India in terms of plate tectonic theory. Journal of Geololical Society of India 15, 134-149.

Fowler, C.M.R., and Nisbet, E.G., 1985. The subsidence of the Williston Basin. Canadian Journal of earth Science 22, 408-415.

Gowd, T. N., Rao, S. V. S., and Gaur, V. K., 1992.Tectonic stress field in the Indian subcontinent. Journal of Geophysical Research 97, 11879–11888.

Hossain K. M., 1985. Plate tectonic theory and the development of the folds of Chittagong and Chittagong Hill Tracts. Bangladesh Journal of Geology 4, 57-67.

Hutchison, C.S., 1989. Geological evolution of South-East Asia.Clarendon Press, London, 368 pp.

Imam, M.B., Rahman, M., Akhter, S.H., 2002. Coalbed Methane prospects of Jamalganj Coalfield, Bangladesh. The Arabian Journal for Science and Engineering 27, 17-27.

Ingersoll, R.N., Graham, S.A., Dickinson, W.R., 1995. Remnant ocean basins. In: Busby, C.J., Ingersoll, R.V. (Eds.), Tectonics of Sedimentary Basins. Blackwell, Oxford, pp. 363–391.

Islam, M.R., and Shinjo, R., 2009. Numerical simulation of stress distributions and displacements around an entry roadway with igneous intrusion and potential sources of seam gas emission of the Barapukuria coal mine, NW Bangladesh. International Journal of Coal Geology (article in press).

Islam, M.R., Hayashi, D., and Kamruzzaman, A. B. M., 2009. Finite Element Modeling of Stress Distributions and Problems for Multi-slice Longwall Mining in Bangladesh, with special reference to the Barapukuria Coal Mine. International Journal of Coal Geology 78, 91-109.

Islam, M.R., 2009. Origin of the regional stress field along the Liquine-Ofqui Fault Zone (LOFZ), Southern Chilean Andes by means of FE Simulation. Journal of Mountain Science 6: 1-13.

Islam, M.R., Hayashi, D., 2008. Geology and Coal Bed Methane Resource Potential of the Gondwana Barapukuria Coal Basin, Dinajpur, Bangladesh. International Journal of Coal Geology 75, 127-143.

Kailasam, N.L., 1976. Geophysical studies of the major sedimentary basins of the indian craton, their deep structural features and evolution. Tectonophysics 36, 225-245.

Kent, R.W., Pringle, M.S., Muller, R.D., Saunders, A.D., and Ghose, N.C., 2002. $^{40}Ar/^{39}Ar$ Geochronology of the Rajmahal Basalts, India, and their relationship to the Kerguelen Plateau. Journal of Petrology 43, 1141-1153.

Khan, F.H., 1991. Geology of Bangladesh, Willey Eastern Limited, 4835/24 Ansari Road, Daryaganj, New Delhi 110002, India, pp. 33-40.

Khan, A.A., and Chouhan, R.K.S., 1996. The crustal dynamics and the tectonic trends in the Bengal basin. Journal of Geodynamics 22, 267-286.

Khan A. A., Sattare G. S., and Rahman, T., 1994. Tectogenesis of the Gondwana rifted basins of Bangladesh in the so-called Garo-Rajmahal gap and their pre-drift regional tectonic correlation. 9th Int. Gond. Symp. Proc., Geological Survey of India, Calcutta, India.

Khan A. A., and Agarwal B. N. P., 1993. Crustal structure of western Bangladesh from gravity data. Tectonophysics 219, 341-353.

Khan A. A., and Rahman T., 1992. An analysis of gravity field and tectonic evaluation of the northwestern part of Bangladesh. Tectonophysics 206, 35 l-364.

Klein, G.., and Hsui, A.T., 1987. Origin of cratonic basins. Geology 15, 1094-1098.

Lee, T.T., Lawver, L.A., 1995. Cenozoic plate reconstruction of Southeast Asia. Tectonophysics 251, 85-38.

Mahadevan, T.M., 1994. Deep continental structures of India: a review. Geol. SOC. India Mem. No. 28, 569p.

McDougall I. and McElhinny M. W. (1970). The Rajmahal traps of India, K-Ar ages and palaeomagnetism. Earth and Planetary Sci. Lett. 9, 372-378.

Mukherjee, A., Fryar, A.E., Thomas, W.A., 2009. Geologic, geomorphic and hydrologic framework and evolution of the Bengal basin, India and Bangladesh. Journal of Asian Earth Sciences 34, 227–244.

Reimann, K.U., 1993. Geology of Bangladesh. Borntraeger, Berlin, p. 160.

Roy, A.B., 2004. The Phanerozoic Reconstitution of Indian Shield as the Aftermath of Break-up of the Gondwanaland. Gondwana Research 7, 387-406.

Singh, B. D. and Singh, A., 2004. Observations on Indian Permian Gondwana Coals Under Fluorescence Microscopy: An Overview. Gondwana Research 7, 143-151.

Turcotte, D.L., and Emerman, S.H., 1983. Mechanisms of active and passive rifting. Tectonophysics 94, 39-50.

Uddin, M.N. and Islam, M.S. 1992. Gondwana basins and their coal resources in Bangladesh. Geology in South Asia-1. Proceedings of the First South Asian Geological Congress, Pakistan. pp. 224-230.

Chapter 3
Geology of the Gondwana Barapukuria Basin

Chapter 3
Geology of the Gondwana Barapukuria Basin

3. 1. Introduction

The Permian age Gondwana Barapukuria coal basin is located at the northwest part of Bangladesh, and is located between longitude 88°56′36″E -88°59′02″E, and latitude 25°34′40″N - 25°31′28″N. This chapter summarizes the results of geological, hydrogeologial and geotechnical field studies conducted during 1989-1990 by Wardell-Armstrong Mining Consultants of the United Kingdom. The overall purpose of that project was to gain a better understanding of the structure of the Barapukuria basin and to assist in the design of the mine and its surface facilities.

3. 2. The Barapukuria coal deposit

Barapukuria has been the subject of the most concentrated exploration and research of all the deposits in Bangladesh, culminating in the development of the country's first producing underground coal mine. This study, is therefore based largely on previously unpublished data resulting from more than 20 years of investigation.

3.2.1. Location, extent and topography

The Barapukuria Coal Basin is located some 50-km east of the district capital Dinajpur, in NW Bangladesh (Figs. 3-1 and 3-2). The basin area covers approximately 5 km^2 within a wide flood plain. Surface topography is flat, with a surface elevation of only +30 to 32 m above mean sea level. Regionally, the surface slopes very gently towards the south and is drained by tributaries of the Jamuna River. Land usage is predominantly agricultural, with the principal crop being rice.

3.2.2. Regional geology

Regionally, Bangladesh is located at the junction of three lithospheric plates: the Indian plate, the Eurasian plate, and the Burmese sub-plate. These three plates form three major tectonic zones in Bangladesh (Fig. 3-1): (i) a platform flank zone in the west named the Dinajpur

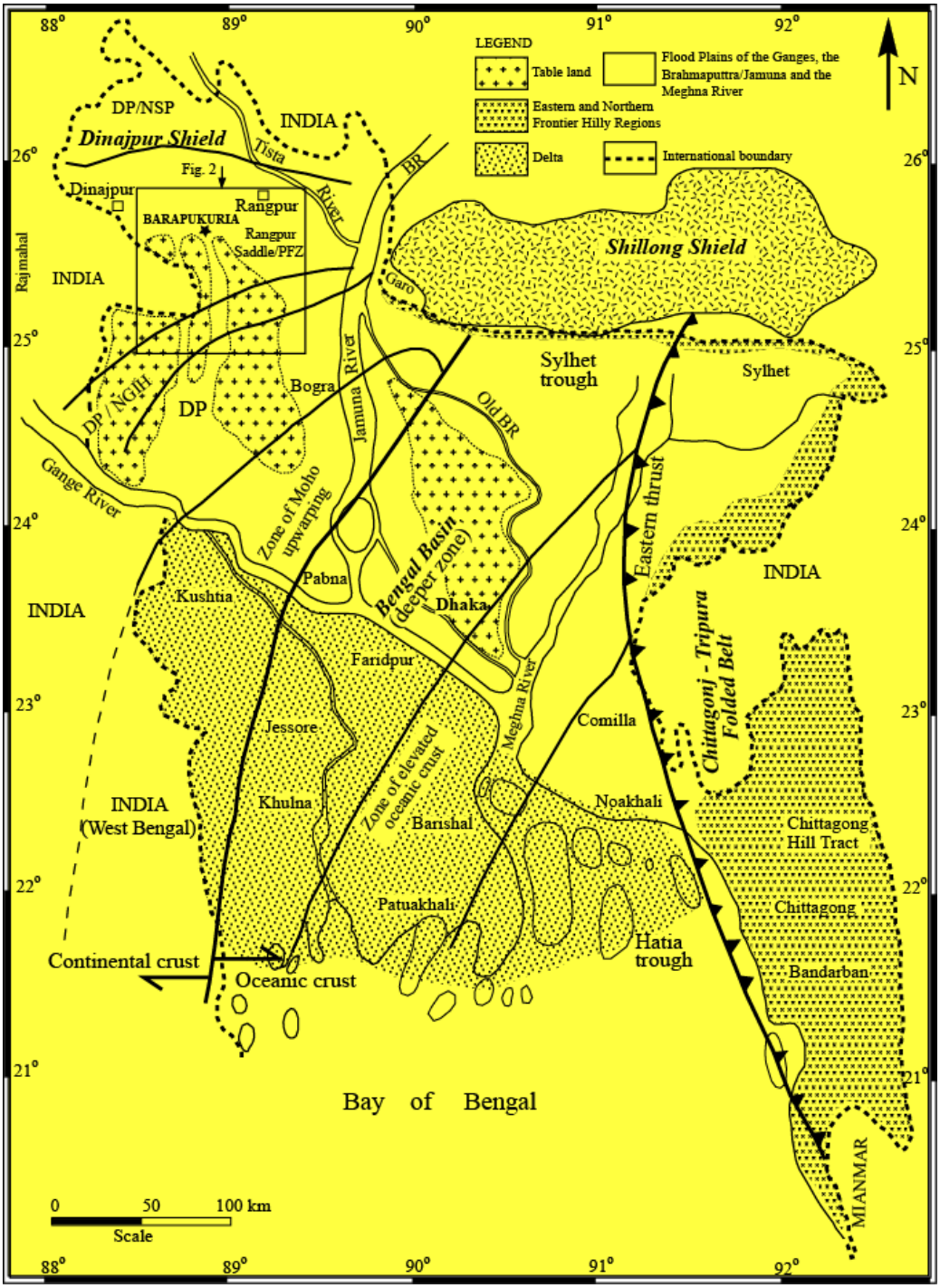

Figure 3-1. Location of the Barapukuria coal basin within the physiographic and geotectonic divisions of Bangladesh. Heavy bold lines indicate boundary of the major tectonic divisions. Medium bold lines in the northwest part indicate tectonic boundary of sub-zones within the Dinajpur Shield. Abbreviations: BR=Brahmaputtra River, DP=Dinajpur Platform, NGIH=Nawabganj-Gaibandha Intracratonic High, NSP=North Slope of the Platform (part of Sud-Himalayan Foredeep), PFZ=Platform Flank Zone (compiled after Khan, 1991; Khan and Chouhan, 1996).

Shield and Platform, (ii) a central deeper basin, the Bengal Basin, and (iii), the folded belt in the east, known as the Chittagong–Tripura Fold Belt (Khan, 1991; Khan and Chouhan, 1996; Alam et al., 2003). Each of these zones is distinguished by a unique tectonic and stratigraphic history (Alam et al., 2003).

The Barapukuria Coal Basin is located in the Dinajpur Shield (Fig. 3-1) of Bangladesh and is surrounded by Himalayan Foredeep to the north, the Shillong Shield/Platform to the east, and the Indian Peninsular Shield to the west. The Garo-Rajmahal gap lies between the exposed Peninsular Shield and the Shillong Shield, which corresponds to a shallow buried basement ridge known as the Platform flank zone (Desikachar, 1974; Khan, 1991). Most of the Gondwana coal basins including Barapukuria, Phulbari, Khalaspir, Dighipara are located within the Bangladesh part of the Garo-Rajmahal gap (known as the 'Rangpur Saddle') (Uddin and Islam, 1992; Bakr et at., 1996; Islam and Islam, 2005).

3.2.3. Exploration history

From 1985-88, surface drilling by the Geological Survey of Bangladesh (GSB) to investigate a negative gravity anomaly identified by geophysical exploration for oil and gas, confirmed the existence of a sequence of Gondwana coal-bearing sediments. Wardell-Armstrong Mining Consultants conducted a Feasibility Study of the mining prospect from 1989-90. This work included the drilling of an additional 12 cored deep exploration boreholes, 11 shallow geotechnical and hydrogeological boreholes, and some two-dimensional seismic surveys. Detailed laboratory analyses were carried out on core samples to determine coal quality, geotechnical and hydrogeological parameters. In 1994, a further 15 boreholes were completed by the China National Machinery Import & Export Corporation (CMC), including one on each of the sites of the two proposed access shafts. Construction and development commenced in 1996. During the development of underground roadways in 1998, a major inflow of water from the overlying Dupi Tila sediments occurred, and resulted in the inundation of the whole mine. Underground development progressed rapidly without further incident, and coal production from 1101 longwall panel, the mine's first mechanised coal face, commenced in September 2005.

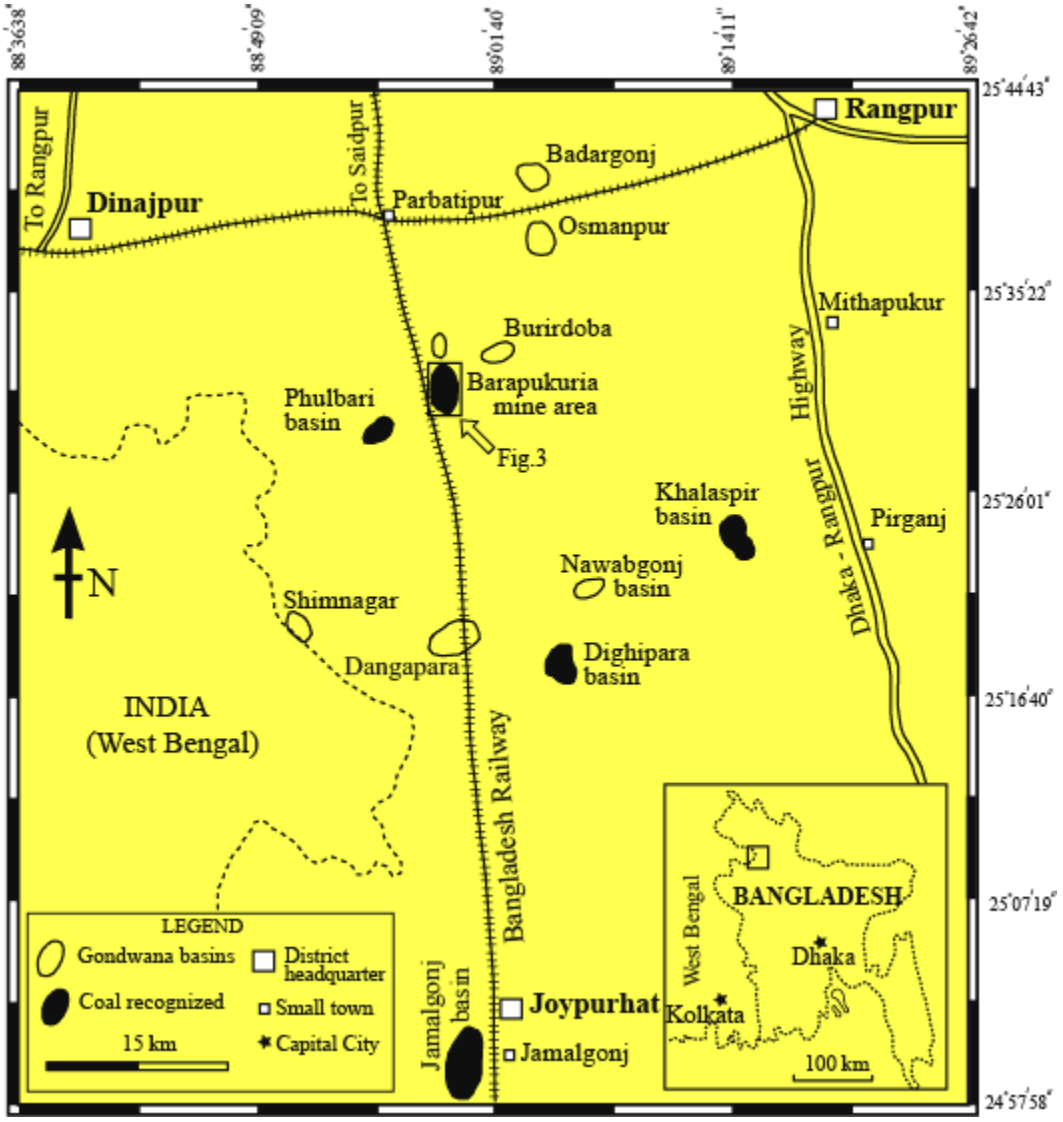

Figure 3-2. Gondwana coal deposits of Bangladesh (modified after Uddin and Islam, 1992)

3.2.4. Geological structure

The general structure (Fig. 3-3) of the basin is of an asymmetrical faulted syncline with an approximately N-S axis. The Permian Gondwana coal-bearing sediments within the syncline rest unconformably on the metamorphic Archaean (Precambrian) basement complex. This sequence is up to 390 m in thickness, and comprises predominantly continental arenaceous sediments, with subordinate siltstones, shales and up to six coal seams (Table 3-1).

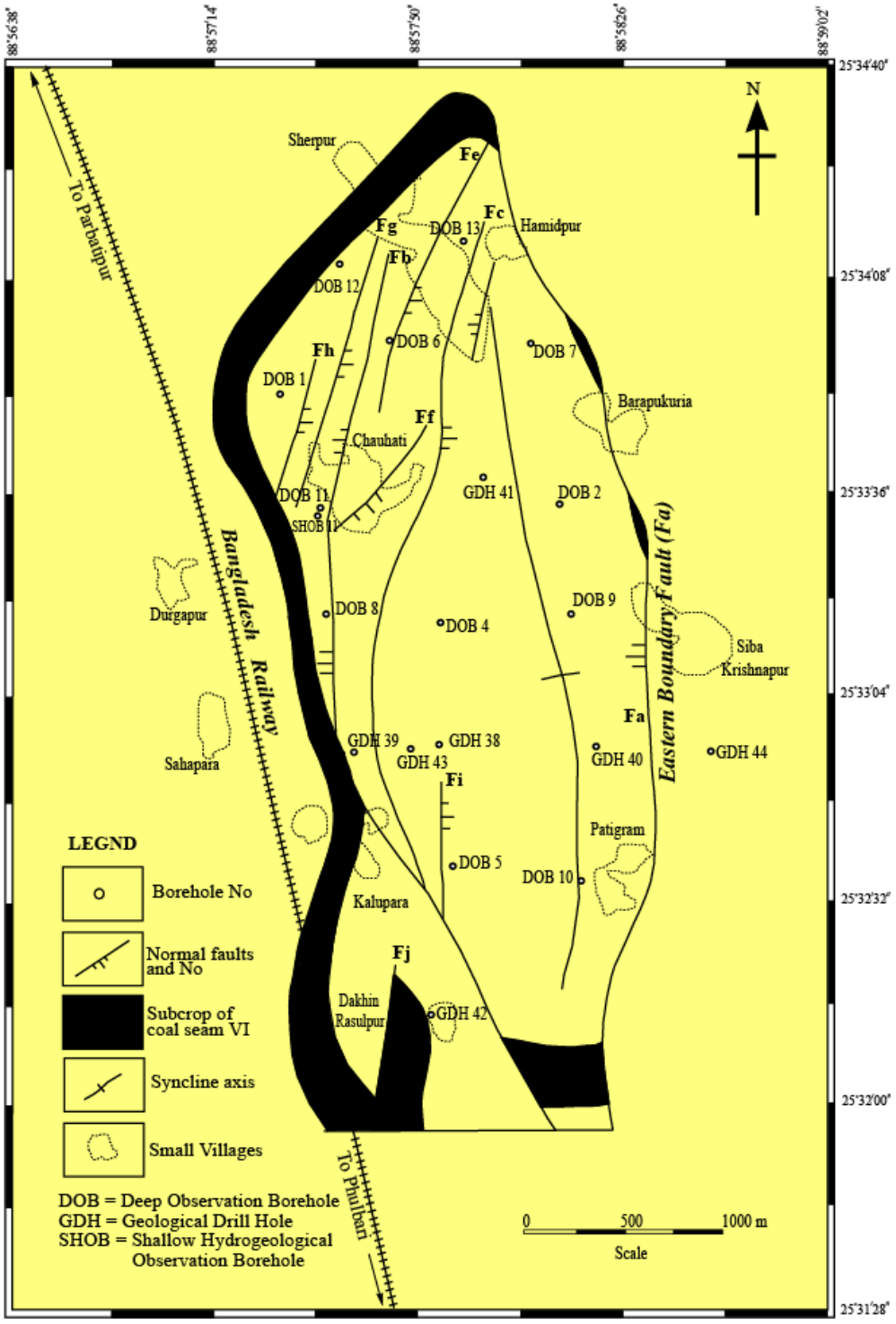

Fig. 3-3. Location of the boreholes, major faults, and structural pattern of the Barapukuria Coal Basin, Dinajpur, Bangladesh (after Wardell Armstrong, 1991; Bakr et al., 1996). See Table 3-2ab for coal seam stratigraphy in the basin.

Accumulation of this relatively thick sequence was probably assisted by contemporaneous subsidence occurring on the down-throw side of a major N-S fault in the Archaean basement, which forms the eastern limit of the coal basin. Faults within the basin are divided into two systems: (1) intra-basinal faults, and (2) boundary faults (Wardell Armstrong 1991; Bakr et al., 1996).

3.2.4.1. Intra-basinal faults

There are numerous faults within the basin which affect the Gondwana sequence; a total of 37 faults are indicated in seismic interpretations (Wardell Armstrong, 1991), which has an estimated vertical resolution of about 10m. In general, these occur in conjugate sets, dipping to the ESE (Fig. 3-3). The largest of these, Fault Fb, strikes NW-SE in the south, deviating to N-S in the north, with a displacement of up to 40 m.

3.2.4.2. Boundary fault

The Eastern Boundary Fault striking NNW-SSE over at least 5 km has controlled sedimentation within the basin. The fault is down thrown to the west and affects formations from the basement to the Tertiary. The fault plane dips at 70-75^{o} towards the west (Fig. 3-4a), with an estimated vertical displacement of more than 200 m with a dominant dip-slip component. This geometry suggests a typical extensional (rift) tectonic structure, resulting in the development of a half-graben type basin with increasing thickness of deposition towards the east and southeast of the basin (Wardell Armstrong, 1991; Bakr et al., 1996).

3.3. Stratigraphy

3.3.1. Madhupur Clay Formation (MCF)

The stratigraphy of the Barapukuria Basin is given in Table 3-1 (Wardell Armstrong, 1991; Bakr el al., 1996). Tables 3-2a and 3-2b show lithologies and thicknesses of the data based on DOB (Deep Observation Borehole) and GDH (Geological Drill Hole) (Figs. 3-5a, 3-5b, and 3-5c). The basin is totally concealed by an unconformable cover of between 100–220 m of the late Miocene/Pliocene Dupi Tila Formation. The sequence is correlated into four formations on the basis of age and lithology (Wardell Armstrong, 1991):

- Madhupur clay

- Dupi Tila (upper and lower)
- Gondwana Group
- Pre-Cambrian Archaean Basement

A summary of the oldest Gondwana Group sedimentary sequence is given below.

3.3.2. Upper Dupi Tila Formation (UDTF)

The upper Dupi Tila Formation, with an average thickness of about 107 m, is divided into two main units:

- An upper unit which is about 65 m in thickness consists of micaceous grey sands and gravel with occasional bands of silt and clay.
- A lower unit which is about 40 m in thickness consists mainly of orange-brown, slightly micaceous sandstones, generally finer than upper unit with more frequent thin beds of silt and clay.

3.3.3. Lower Dupi Tila Formation (LDTF)

The Lower Dupi Tila Formation is absent to the northern parts of the basin, and thickness generally increases to the south. The formation is characterized by firm light grey and white clayey sands and kaoliniteic clays, which were probably derived from the weathering of weak kaolinized Gondana sandstones immediately below. In the south where the formation is at its thickest, the main clay beds are interlaminated with loose silts and sands.

3.3.4. Upper coal sequence

The upper coal sequence (seams I to V) occurs at varying depth from 133-336 m, and is comprised of an interbedded succession of fine to coarse quartzo-feldspathic sandstones with subordinate horizons of siltstone and mudstone. The uppermost Seam I is only present in one borehole (GDH #40) near the centre of the synclinal basin. Progressively lower seams occur over an increasing area: Seams II and IV appear to be the most laterally, varying in thickness between 2.5-15 m. Seams III and V are laterally variable and discontinuous (Wardell Armstrong, 1991; Bakr et al., 1996).

Table 3-1. The generalized stratigraphic succession of the Barapukuria coal basin, Dinajpur, Bangladesh, based on DOB (Wardell Armstrong, 1991) and GDH (Bakr et al., 1996)

Age	Group	Formation		Thickness (m) From	Thickness (m) To	Prime rock types
Holocene - Recent	---	*Soils, Alluvium*		0	1	Clay, very fine silt and sand
Late Pliocene - Pleistocene	---	*Madhupur clay*		3	15	Clay, mostly silty
Late Miocene - Middle Pliocene	Dupi Tila	*Upper Dupi Tila*		94	126	Sand - unconsolidated to partly consolidated, medium to coarse, occasioanly gravelly with bands of silt
		Lower Dupi Tila		0	80	Sandstone, silt and white clay
Permian	Gondwana	*The Upper Coal Sequence*	*Seam I*	0	3	Sandstones - arkose, fine to coarse with occasional conglomerates. Contains coal seams I to V. Occasional siltstones and mudstones.
			Seam II	14	15	
			Seam III	0.30	6	
			Seam IV	3	10	
			Seam V	1	10	
		The Upper sandstone Sequence of Seam VI		15	140	Sandstones - arkose, massive, mostly medium coarse and conglomeratic. Contains no coals and rare siltstones / mudstones.
		Seam VI		22	42	Coals - occasional thin partings of inferior coal, mudstone and sandstone.
		The Lower sandstone Sequence of Seam VI and Seam VII		84	164	Sandstone/Siltstone/Mudstone/Coal- rapid intercalation of mostly fine to medium sandstones with numerous coaly and argillceous bands.
		The Tillites		0	55	Tillites - boulder beds, breccia-conglomerates with occasional ingteranded siltstone, sandstones and rare thin coal bands.
Archaean	---	*Basement Complex*		---		Diorite, meta-diorite, ophlitic gneiss and grranite

Table 3-2a. Summary of lithologies encountered at Deep Observation Borehole (DOB) (after Wardell Armstrong, 1991). See Fig.3 for borehole locations.

Litho-units/Boreholes		**DOB #1**	**DOB #2**	**DOB #4**	**DOB #5**	**DOB #6**	**DOB #7**	**DOB #8**	**DOB #9**	**DOB #10**	**DOB #11**	**DOB #12**	**DOB #13**
Elevation or Wellhead		32.67	31.01	31.28	31.79	31.31	31.22	31.38	30.73	30.18	31.75	30.42	30.79
Madhipur Clay base		3.20	13.30	7.60	12.50	7.40	4.60	12.16	5.20	4.20	12.50	8.80	14.90
Upper Dupi Tila base (m)		103.10	116.50	112.90	109.50	105.50	128.00	117.00	121.60	105.20	114.80	102.70	109.40
Thickness (m)		99.90	103.20	105.30	97.00	98.10	123.40	104.84	116.40	101.00	102.30	93.90	94.50
Lower Dupi Tila base (m)		116.00	NP	132.50	175.20	NP	NP	121.00	132.60	185.80	126.40	NP	NP
Thickness (m)		12.90		19.60	65.70			4.00	11.00	80.60	11.60		
Gondwana Group (main coal seams and sequence)													
Seam I	Roof (m)	NP	NP	NP	NP	NP	NP	NP	NP	NP	NP	NP	NP
Seam II	Roof (m)	NP	NP	NP	NP	NP	NP	NP	155.00	NP	NP	NP	NP
	Floor (m)								168.95				
	Thickness (m)								13.95				
Seam III	Roof (m)		NP	145.30				NP	177.47				
	Floor (m)		NP	147.10				NP	179.80				
	Thickness (m)			1.30					2.33				
Seam IV	Roof (m)	NP	132.90	170.50	NP	NP	NP	NP	208.23	185.34	NP	NP	NP
	Floor (m)		142.50	178.30					218.42	189.14			
	Thickness (m)		9.60	7.80					10.19	3.80			
Seam V	Roof (m)	NP	160.03	206.70	175.20	NP	NP	NP	238.89	208.20	NP	NP	NP
	Floor (m)		162.34	208.10	176.50				241.15	210.38			
	Thickness (m)		2.31	1.40	1.30				2.26	2.18			
Upper sandstone sequence of seam VI	Roof (m)	116.00	162.34	208.10	176.50	105.50	128.00	178.82	241.15	210.38	126.40	102.70	109.60
	Floor (m)	131.80	291.56	331.15	249.10	163.35	199.55	195.80	381.67	312.70	180.64	118.65	162.00
	Thickness (m)	15.80	129.22	123.05	72.60	57.85	71.55	16.98	140.52	102.32	54.24	15.95	52.40
Seam VI	Roof (m)	131.80	291.40	331.15	249.10	163.35	199.55	195.80	381.62	312.70	180.64	118.65	162.00
	Floor (m)	161.20	328.40	373.45	NP	193.72	237.60	217.43	421.37	341.40	213.77	149.49	198.00
	Thickness (m)	29.40	37.00	42.30		30.37	38.05	21.63	39.75	28.70	33.13	30.84	36.00
Lower sandstone sequence of seam VI	Roof (m)	161.20	330.53	373.45	NP	193.90	237.60	217.43	421.37	341.40	213.77	149.49	198.00
	Floor (m)	296.14	NP	NP		NP	NP	NP	NP	NP	361.62	NP	NP
	Thickness (m)	134.94									147.85		
Gondwana Group base (m)		297.00	NP	NP	NP	NP	NP	NP	NP	NP	361.62	NP	NP
Thickness (m)		181.00									235.22		

Table 3-2b. Summary of lithologies encountered at Geological Drill Hole (GDH) (after Bakr et al., 1996). See Figure 3 for borehole locations.

		GDH #38	GDH #39	GDH #40	GDH #41	GDH #42	GDH #43	GDH #44
Elevation or Wellhead		30.50	30.50	29.60	30.50	30.33	31.45	29.67
Madhipur Clay base		12.19	10.06	9.45	9.45	9.14	10.36	9.15
Upper Dupi Tila base (m)		117.38	116.13	135.94	117.96	133.20	114.91	130.45
Thickness (m)		105.19	106.07	126.49	108.51	124.06	104.55	121.30
Lower Dupi Tila base (m)		136.26	170.38	180.44	117.96	190.50	141.12	196.42
Thickness (m)		18.88	54.25	44.50	0.00	57.30	26.21	65.97
Gondwana Group (main coal seams and sequence)								
Seam I	Roof (m)	NP	NP	193.86	NP	NP	NP	NP
	Floor (m)	---	---	196.43	---	---	---	---
	Thickness (m)	---	---	2.57	---	---	---	---
Seam II	Roof (m)	NP	NP	252.68	NP	NP	NP	NP
	Floor (m)	---	---	267.92	---	---	---	---
	Thickness (m)	---	---	15.24	---	---	---	---
Seam III	Roof (m)	NP	NP	276.45	NP	NP	NP	NP
	Floor (m)	---	---	283.05	---	---	---	---
	Thickness (m)	---	---	6.60	---	---	---	---
Seam IV	Roof (m)	162.15	NP	306.17	131.96	NP	NP	NP
	Floor (m)	170.99	---	309.29	140.65	---	---	---
	Thickness (m)	8.84	---	3.12	8.69	---	---	---
Seam V	Roof (m)	197.81	NP	331.01	162.46	NP	161.54	NP
	Floor (m)	208.18	---	336.50	168.86	---	171.75	---
	Thickness (m)	10.37	---	5.49	6.40	---	10.21	---
Upper sandstone sequence of seam VI	Roof (m)	208.18	NP	336.50	168.86	NP	171.75	NP
	Floor (m)	331.62	---	450.19	285.27	---	286.82	---
	Thickness (m)	123.44	---	113.69	116.41	---	115.07	---
Seam VI	Roof (m)	331.62	170.38	450.19	285.27	190.50	286.82	NP
	Floor (m)	371.24	203.00	491.03	321.56	216.10	329.19	---
	Thickness (m)	39.62	32.62	40.84	36.29	25.60	42.37	---
Lower sandstone sequence of seam VI	Roof (m)	371.24	204.27	491.03	321.56	216.10	331.16	NP
	Floor (m)	513.59	288.04	655.62	NP	351.21	473.66	---
	Thickness (m)	142.35	83.77	164.59	---	135.11	142.50	---
Seam VII	Roof (m)	NP	NP	505.97	NP	NP	330.40	NP
	Floor (m)	---	---	506.42	---	---	331.16	---
	Thickness (m)	---	---	0.45	---	---	0.76	---
Gondwana Group base (m)		513.59	288.04	655.62	NP	351.21	473.66	199.03
Thickness (m)		377.33	117.66	475.18	---	160.71	332.54	2.61

3.3.5. Seam VI roof sandstone

Seam VI sediments above are comprised of 15 m to 140 m of relatively homogeneous and massive pale grey to white, medium to coarse-grained sandstones, gritstones, and conglomerates. These arkosic sandstones have been strongly kaolinized, resulting in a white clay matrix which greatly reduces their primary permeability. All of the sandstones in the Gondwana sequence are affected by high angle joints, which are generally tight or mineralized, limiting the sandstone's secondary permeability (Wardell Armstrong, 1991; Bakr et al., 1996).

3.3.6. Seam VI

The thickest and most laterally continuous Seam VI varies across the basin from 22 m to more than 42 m (average 36 m) and is the basal coal seam in the sequence. Seam VI accounts for most of the coal resources at Barapukuria, and is usually overlain and underlain by thick sandstones. A thin mudstone horizon is frequently present as the immediate roof. All of the Barapukuria coal seams have been interpreted as forming in cold to cool temperate environments and were probably deposited in association with lacustrine conditions (Wardell Armstrong, 1991; Bakr et al., 1996).

3.3.7. Seam VI floor sandstone

The succession below seam VI is substantially different from the Gondwana sequence above it, and consists of an interbedded sequence of sandstones, siltstones, and mudstones with occasional thin coal horizons. Above Seam VI sandstones are generally altered and moderately weak, with slight to complete decomposition of the feldspars to kaolinitic clay. Below Seam VI, the sandstones are mostly unweathered, less feldspathic, and moderately strong. There are numerous units of fluviatile sandstones and interbanded sandstone/siltstone sequences with occasional thin and discontinuous coals. (Wardell Armstrong, 1991; Bakr et al., 1996)

3.3.8. Tillites

The basal Gondwana glacial tillites are generally considered to be of Pennsylvanian age. They consists of variable thicknesses of boulder-bed tillites containing clasts of unsorted

sedimentary, igneous, and metamorphic rocks, interbedded with occasional units of mudstone, siltstone, and coal, indicative of periods of interglacial sedimentation and occasional minor peat accumulations (Wardell Armstrong, 1991).

3.4. Fault-related structural controls on stratigraphy

The deposition of the coal seams (I to VI) was controlled to some extent by the N-S Eastern Boundary fault that strikes sub-parallel to the basin axis, and which resulted in a differentially subsiding depositional environment. Strata dips are steepest (up to 45°) in the east, adjacent to the fault. Steep gradients are also present in the west beyond the subcrop of Seam VI (Fig. 3-4a). A number of faults with throws of 10 m or less are present in Seam VI in the area beyond Seam V subcrop. The subcrop of the roof of Seam VI is not well established in the south of the basin, although seismic data indicates that this seam may be present over a large area immediately below the base of the Lower Dupi Tila (Fig. 3-4b). Similarly in the north, Seam VI is though to be present immediately below the base of Tertiary (Fig. 3-4b) (Wardell Armstrong, 1991). Seams I to V appear to be structurally different from the lower Seam VI. The steepest dips (up to 31°) occur on the eastern flanks of the basin.

The Lower Dupi Tila formation varies in thickness rapidly across the basin, unconformably overlying the eroded Gondwana surface and showing a progressive southerly increase in thickness (Figs. 3-4b, and 3-4c). The dip of the base of Tertiary is often steep and the strike is very variable. Thicker lenses of Lower Dupi Tila occur beyond seam subcrops where greater erosion of the Gondwana sandstones has occurred. This formation dips to the east on the downthrow side of the Eastern Boundary Fault, suggesting that this remained active during the Tertiary deposition. No further faulting has been identified in the Tertiary cover. The Upper Dupi Tila formation is a relatively uniform deposit across the basin area. Strata dips up to 11° are present in the lower part of the formation on the downthrow side of the boundary fault.

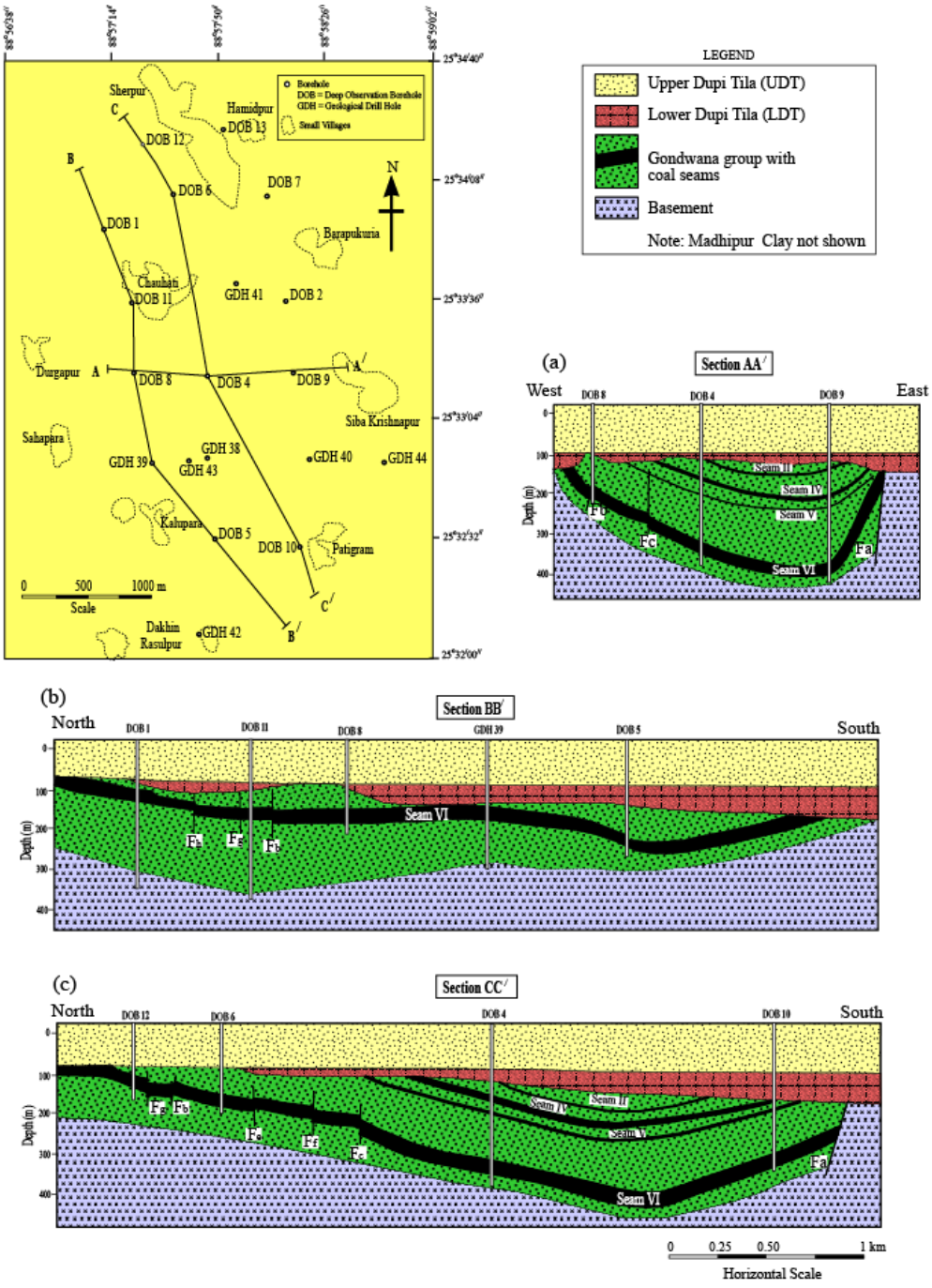

Fig. 3-4. Structure, stratigraphy, and distribution of coal seams of the Barapukuria coal basin (Wardell Armstrong, 1991). Seams II, IV, V, and VI are clearly visible in Figures a, and. c. Seams I and III are not shown in these sections due to small-scale and variable thickness. These two seams are shown in Figure 5b (Seam III in DOB #9) and Figure 5c (Seam I and III in GDH #40).

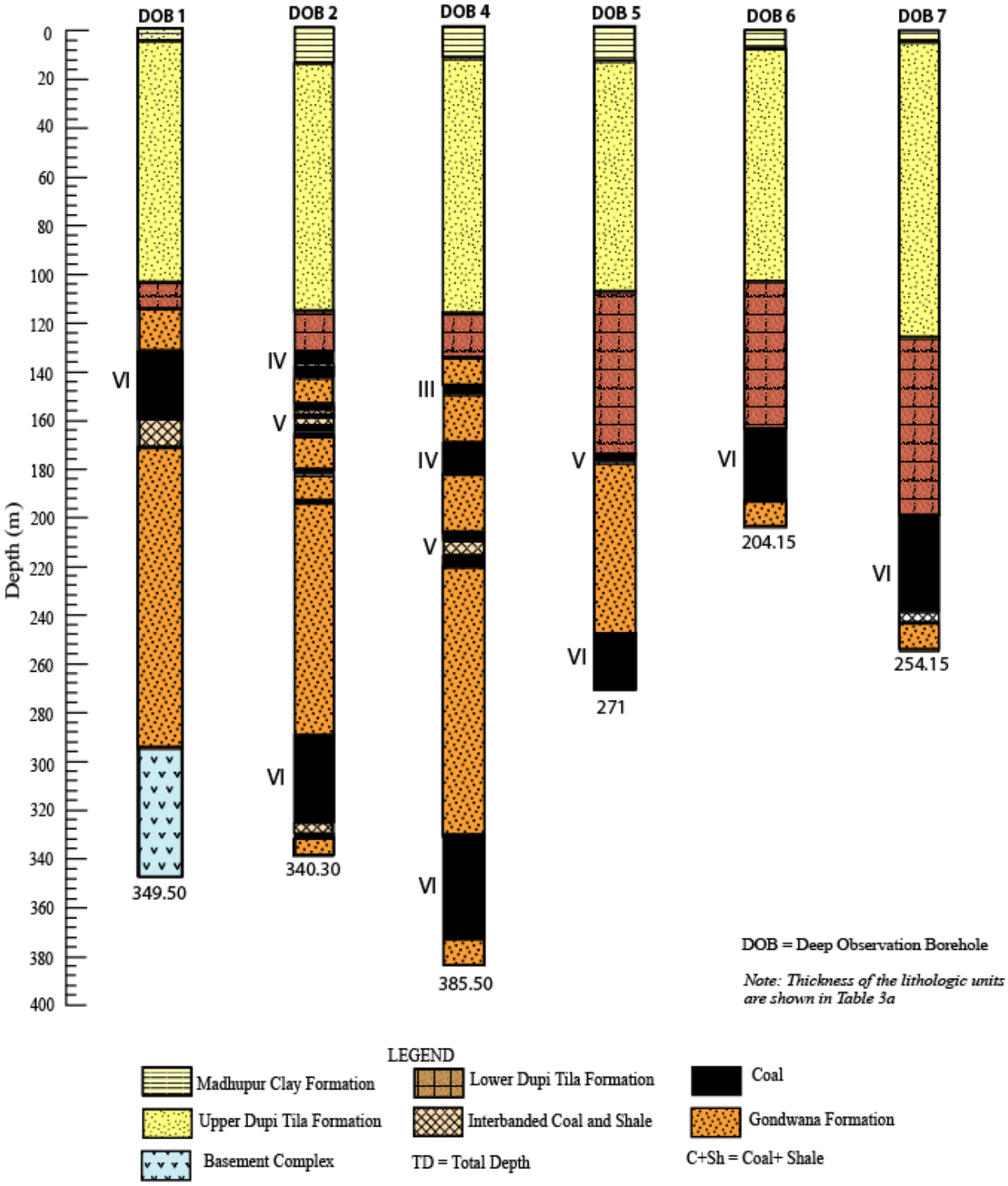

Fig. 3-5a. Stratigraphy and coal seams sequences in DOB #1, #2, #4, #5, #6, and #7 of the Barapukuria Coal Basin, Dinajpur, Bangladesh (see drill hole locations in Figure 3) (Wardell Armstrong, 1991).

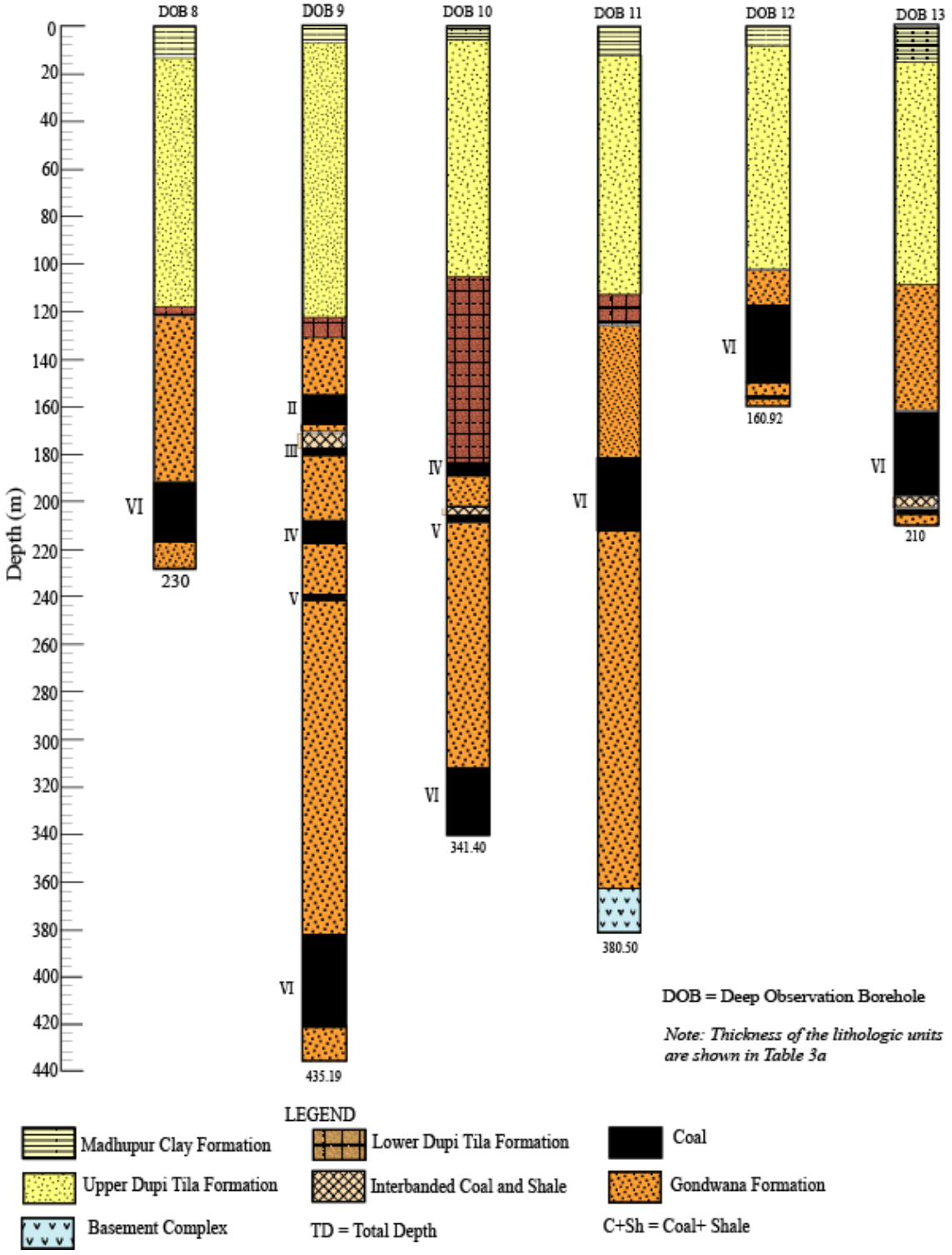

Fig. 3-5b. Stratigraphy and coal seams sequences in DOB #8 to DOB #13 of the Barapukuria Coal Basin, Dinajpur, Bangladesh (see drill hole locations in Figure 3) (Wardell Armstrong, 1991).

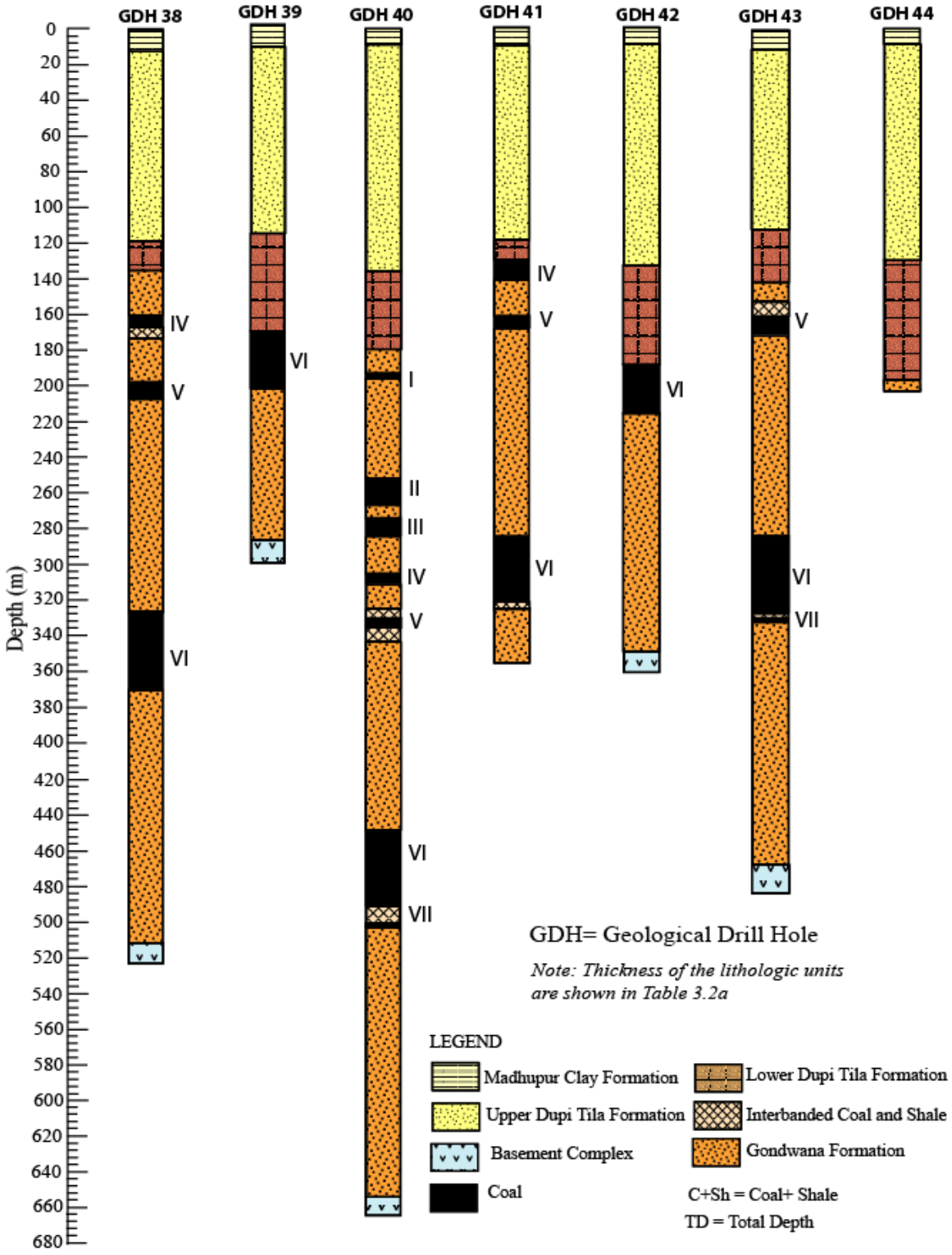

Fig. 3-5c. Stratigraphy and coal seams sequences in GDH #38 to GDH #44 of the Barapukuria Coal Basin, Dinajpur, Bangladesh (see drill hole locations in Figure 3) (Bakr et al, 1996).

3.5. Hydrogeological characteristics of the basin

The hydrodynamic properties of the coal and associated strata are of fundamental importance to the CBM potential of the deposit, and are controlled by the four principal formations as defined in section 2.5. The Upper Dupi Tila aquifer is a prolific groundwater reservoir extending over larger areas of Bangladesh (Khan, 1991). This formation is the source of water for irrigation and domestic supply. The Gondwana Sandstone is a poor aquifer, but is in hydraulic connection with the Upper Dupi Tila aquifer in the northern part of the deposit where the Lower Dupi Tila aquiclude is absent. Despite a finite fractured or "weathered" permeability, the Pre-Cambrian Basement is considered to form a basal aquiclude to the overlying Gondwana and Dupi Tila aquifers (Wardell Armstrong, 1991).

There is a proven potential for groundwater flow from the Upper Dupi Tila into the Gondwana sandstones. In the north of the coal basin where the Lower Dupi Tila aquiclude is absent, the Gondwana sandstones are recharged at the Tertiary/Gondwana unconformity. All Gondwana sandstones are typically jointed, although the joints are frequently mineralised or infilled which reduces the secondary permeability of the aquifer. There appears to be a moderate dynamic balance between the Upper Dupi Tila aquifer and the underlying Gondwana, with an almost flat hydraulic gradient (0.0004-0.0006). Average transmissivity, specific yield, storage coefficient, and velocities were 1200m^2/day, 25% to 30%, 0.0004, and 0.02m/day respectively (Wardell Armstrong, 1991). Porosity, grain density, and permeability data at different depths of the Barapukuria coal deposits are shown in Table 3-3.

Table 3-3. Porosity, grain density, and permeability data at different depths of the Barapukuria coal deposits (Wardell Armstrong, 1991).

Sample No /Borehole	Depth (m)	Lithology	Porosity (%)	Grain density (kg/m^3)	Permeability (forward) (mD)	Permeability (reverse) (mD)
1/DOB 11	118.65	Clayey sand	32.1	2620	0.73	0.58
2/DOB 11	118.70		33.3	2620	0.63	0.51
3/DOB 11	121.55	Banded clay	41.4	2560	0.02	0.04
4/DOB 11	122.27	Interbedded caly,	31.9	2630	0.13	0.03
5/DOB 11	122.35	Interlaminated shale	30.1	2610	0.11	0.11
6/DOB 11	130.35	Clays	35.7	2650	0.12	0.10
7/DOB 11	130.53		32.6	2530	0.11	0.11
8/DOB 9	148.10	Medium-grained sandstone	23.9	2630	12.2	11.2
9/DOB 9	148.95		22.4	2640	75	69
10/DOB 9	173.00	Fine-grained sandstone	17.9	2640	0.86	0.86
11/DOB 9	173.30		18.5	2680	0.67	0.67
12/DOB 9	186.78	Fine-grained sandstone	19.4	2670	0.95	0.93
13/DOB 9	187.10		18.1	2640	0.39	0.40
14/DOB 9	201.12	Very fine-grained sandstone	17.9	2640	0.89	0.89
15/DOB 5	210.40	Thinly bedded mudstone	8.3	2550	0.001	0.001
16/DOB 5	210.87		8.5	2550	0.001	0.001
17/DOB 5	211.10		6.9	2630	<0.001	<0.001
18/DOB 5	219.56	Fine-grained sandstone	15.3	2660	0.55	0.54
19/DOB 5	219.85		14.4	2670	0.21	0.29
20/DOB 9	223.12	Medium-grained sandstone	20.5	2680	0.07	0.07
21/DOB 9	223.39		14.5	2640	0.10	0.10
22/DOB 5	236.72	Medium to coarse-grained sandstone	28.7	2660	59.8	109
23/DOB 5	237.00		30.7	2650	50.9	49.3
24/DOB 9	272.13	Very coarse-rained sandstone	18.2	2630	7.80	7.90
25/DOB 9	272.30		18.30	2640	4.6	4.2
26/DOB 9	283.65	Very coarse-rained sandstone, friable	30.8	2600	522	1340
27/DOB 9	283.80		30.9	2610	213	295
28/DOB 9	289.34	Coarse-rained sandstone	20.6	2640	4.81	4.8
29/DOB 9	289.66		18.0	2630	5.44	5.40
30/DOB 9	308.58	Medium-grained sandstone	14.6	2670	0.23	0.22
31/DOB 9	308.75		16.3	2660	0.43	0.43
32/DOB 9	324.03	Medium to coarse-grained sandstone	19.4	2650	8.97	8.95
33/DOB 9	324.26		19.5	2630	6.09	6.10
34/DOB 9	335.89	Very fine-grained sandstone	5.4	2660	<0.001	<0.001
35/DOB 9	336.10		4.3	2650	<0.001	<0.001
36/DOB 9	373.58	Medium-grained sandstone, friable	19.4	2640	5.52	5.13
37/DOB 9	373.76		19.8	2640	4.08	4.18
38/DOB 9	379.87	Medium-grained sandstone, very friable	21.5	2630	3.67	3.23

3.6. Rock mechanical properties of the Barapukuria coal deposits

Wadell Armstrong Mining Consultant of the UK carried out some specific laboratory tests of the Barapukuria rock sequences to define engineering properties of the various rock formations in order to assist in the design of the mine and its surface facilities. The information upon which this appraisal has been based was obtained from the twelve Deep Observation Boreholes (DOB) and five Shallow Hydrogeological Observation Boreholes (SHOB). These boreholes were selectively cored and subsequently geophysical logged. The Deep Observation Boreholes were constructed to evaluate the lithology, hydrogeology and geotechnical characteristics of the coal-bearing Gondwana Formation. Each borehole was drilled to below the base of the Dupi Tila Formation and into the underlying Gondwana strata using tricon bits and polymer drilling fluids. Within the Gondwana Formation, 63 mm diameter rock cores were obtained in a generally undisturbed condition. When evaluating rocks for the purposes of tunneling, shaft-sinking, and mine design there are several points to be considered as follows:

3.6.1. Ground Control:

Rock properties, which need to be measured to assess the level of support include:

- Unconfined Uniaxial Compressive Strength
- Uniaxial Tensile Strength
- Shear Strength
- Shear Resistance Angle
- Young's Modulus, and
- Poisson's Ratio

The first four parameters relate to the strength of the rock material and indicate its self-supporting characteristics and the level at which stress failure can occur. The last two parameters indicate how the material will react to changes its stress.

3.6.2. Excavation Engineering:

For excavation purposes the rock properties to be measured indlude:

- Unconfined Uniaxial Compressive Strength
- Uniaxial Tensile Strength.

3.6.3. Lithology and rock strength of the Gondwana Formation

Lithologically, the strata comprises a sequence of quartzo-feldspathic, medium and coarse-grained sandstones, interbedded with occasional siltstone and mudstone horizons with four main coal seams. The sandstones, siltstones and mudstones are weak to moderate strong with the weakest strata occurring at or close to the unconformity. In the case of the Barapukuria basin, rock mechanical tests on the Gondwana Formation were examined in four separate subdivisions

- From the base of the Dupi Tila Formation to the base of Seam V,
- Strata from the bellow Seam V to the top of the Seam VI,
- Seam VI, and
- Below Seam VI

3.6.3.1. Overburden: From the base of the Dupi Tila Formation to the base of Seam V

Uniaxial Compressive Strength values for the sandstones ranged from 0.20 to 41.05 MPa indicating weak to moderately strong material. The coals and mudstones exhibited strengths of 18.72 MPa to 19.48 MPa, indicating moderately strong material. Tensile Strength values for the sandstones varied from 1.13 MPa to 1.46 MPa. The mudstone strata gave a low of 0.48 MPa. These are low tensile strength and indicate the materials to be weak to moderately weak under tensile stress. The shear strength values of sandstone range from 6.2 to 6.5 MPa, which is indicative of weak to moderately weak strata (Wardell Armstrong, 1991). Cohesion values of clay, siltstone and sandstone are 10.2, 19.1, and 8.3 MPa, respectively, while the angle of internal friction values are 20, 12, and 34 degrees respectively(Wardell Armstrong, 1991).

3.6.3.2. Overburden: Strata from the bellow Seam V to the top of the Seam VI

Uniaxial Compressive Strength tests on sandstones samples gave values ranging from 0.40 to 55.32 MPa indicating weak to moderately strong material. These values indicate that sandstones are generally weak to moderately strong and occasionally strong. Tensile strength tests carried out on the sandstone gave values ranging from 0.06 to 3.56 MPa. The shear strength values of sandstone range from 6.6 to 12.3 MPa indicating moderately weak rock. The mudstone sample gave a value of 45.3 MPa indicating moderately strong material. Values for Young's Modulus, ranging from 1350 to 20630 MPa are relatively high. They indicate a low degree of

elasticity and tendency to rarest deformation, suggesting that blocky caving would occur in an unsupported excavation (Wardell Armstrong, 1991).

3.6.3.3. Seam VI

Uniaxial Compressive Strengths for the coal ranged from 5.71 to 24.73 MPa (mean 13.67 MPa), indicating moderately weak to moderately strong material. Values for Young's modulus ranged from 3201 to 3239 MPa with a Poisson's ration of 0.1919 to 0.2705 indicating a low degree of elasticity and a tendency for caving to occur (Wardell Armstrong, 1991).

3.6.3.4. Below Seam VI

Uniaxial Compressive Strengths of the basal sandstone ranges from 16.2 to 55.34 MPa. These values indicate moderately strong to occasionally strong rock. Tensile strength values for the sandstones are low ranging from 2.79 to 4.53 MPa. The value for Young's modulus on the sandstone sample was 3164 MPa indicating low elastic properties (Wardell Armstrong, 1991). A summary of rock mechanical parameters as tested by Wardell Armstrong (1991) of Gondwana rock sequences are shown in Table 3.4a-c.

Table 3-4a. Rock mechanical parameters of Gondwana rock sequences (Wardell Armstrong, 1991)

Borehole No	Sample depth (m)		Bulk density (Mg/m^3)	Failure load (MPa)	UCS (MPa)	Young's modulus (MPa)	Poisson's ratio
	From	To					
DOB #2	144.65	144.80	2.33	4.40	14.13	-	-
	158.68	158.83	1.90	1.07	3.48	-	-
	182.82	182.97	2.05	2.73	8.77	-	-
	203.62	203.77	2.14	3.67	11.77	-	-
	212.71	212.87	2.28	10.61	34.04	-	-
	265.17	265.37	2.06	3.95	12.66	7551	0.3861
	280.93	281.10	2.41	8.66	29.33	-	-
DOB #4	163.15	163.39	2.26	13.04	41.05	-	-
	169.25	169.50	2.04	2.29	7.26	-	-
	196.24	196.45	2.24	5.51	17.44	-	-
	205.06	205.70	2.07	1.52	4.81	-	-
	214.29	214.93	2.41	6.95	22.05	-	-
	218.95	219.18	1.98	11.09	35.32	-	-
	312.34	312.58	2.31	6.23	19.83	12650	0.2537
	327.18	327.38	2.22	5.86	18.45	-	-
	330.46	330.76	2.35	5.12	16.31	-	-
	379.57	379.86	2.34	8.37	26.6	-	-
DOB #5	211.78	211.96	2.52	17.29	55.32	14000	0.0908
	245.10	245.27	2.24	7.93	25.13	17990	0.1851
	248.40	248.60	2.14	8.32	26.38	20630	0.1206
DOB #6	136.42	136.65	2.22	4.43	14.42	-	-
	142.14	142.35	2.96	0.54	1.86	-	-
	160.68	160.98	2.05	3.02	9.63	-	-
	195.42	195.58	2.48	11.83	37.86	-	-
	202.90	203.14	2.40	17.40	55.34	-	-
DOB #7	143.35	143.73	2.09	2.10	6.72	-	-
	196.16	196.32	1.93	1.07	3.55	-	-
	238.39	238.55	1.78	0.49	16.0	-	-
	244.85	245.04	2.48	0.15	38.67	-	-
DOB #8	139.25	139.48	2.09	2.43	7.83	-	-
	148.69	148.90	2.12	3.52	11.21	-	-
	169.50	169.70	2.21	4.70	15.17	-	-
	194.70	194.92	2.00	1.32	4.24	-	-
	202.97	203.13	1.33	3.74	12.13	-	-
	219.23	219.45	2.35	7.16	23.44	-	-

(Continued)

Borehole No	Sample depth (m)		Bulk density (Mg/m^3)	Failure load (MPa)	UCS (MPa)	Young's modulus (MPa)	Poisson's ratio
	From	To					
DOB #9	151.58	151.80	1.88	0.92	3.04	-	-
	170.38	170.60	2.10	5.74	18.72	-	-
	195.43	195.67	2.27	8.79	28.11	-	-
	207.45	207.75	2.13	3.52	11.23	-	-
	218.56	218.76	2.29	5.76	18.37	-	-
	233.18	233.46	2.18	2.31	7.37	-	-
	240.57	240.74	1.41	6.10	19.48	-	-
	358.64	358.91	2.91	4.74	15.17	7860	0.3730
	369.20	370.20	1.42	4.07	13.04	-	-
	376.94	377.24	2.52	5.10	16.38	5769	0.2876
	423.52	423.79	2.49	14.73	46.95	-	-
	425.72	425.99	1.50	6.12	19.31	-	-
DOB #10	200.60	200.76	2.31	6.43	21.21	-	-
	217.50	217.64	2.32	5.31	17.32	-	-
	277.67	277.99	3.01	10.28	33.40	9571	0.1144
	311.40	311.51	2.34	9.28	30.14	-	-
	312.06	312.26	2.55	6.56	21.30	11260	0.1144
	318.85	318.99	1.34	6.80	21.93	-	-
	322.17	322.31	1.32	1.75	5.71	-	-
	328.07	328.23	1.39	3.15	10.28	-	-
DOB #11	145.47	145.63	2.08	0.72	2.40	-	-
	149.70	149.88	1.60	1.50	3.86	-	-
	152.84	153.02	2.11	2.95	9.63	-	-
	158.58	158.75	2.19	3.74	12.19	-	-
	163.28	163.46	1.85	0.62	2.26	-	-
	174.42	174.59	2.23	0.27	16.25	-	-
	178.09	178.26	2.35	9.17	29.93	-	-
	179.78	179.96	2.22	2.31	7.41	-	-
	214.66	214.79	1.56	7.65	25.13	-	-
	218.91	219.08	2.51	17.14	54.57	-	-
DOB #12	136.10	136.27	1.38	7.78	24.73	-	-
	144.58	144.74	1.37	2.26	7.21	-	-

Table 3-4b. Tensile strength of Gondwana rock sequences (Wardell Armstrong, 1991)

Borehole No	Sample depth (m)		Failure load (MPa)	Tensile Strength (MPa)
	From	To		
DOB #2	144.52	144.80	0.15	0.48
	184.06	184.16	0.47	1.78
	281.10	281.17	0.65	2.33
	287.99	288.05	0.02	0.06
DOB #4	330.36	330.76	0.71	1.73
DOB #6	132.15	132.20	0.86	2.74
DOB #7		145.69	0.12	0.47
		196.81	0.04	0.16
		251.10	1.03	3.49
DOB #8		151.29	0.42	1.36
		195.00	0.61	1.85
DOB #9		200.73	0.40	1.22
		207.45	0.37	1.13
		233.18	0.46	1.32
		423.52	0.94	2.79
DOB #10	200.48	200.76	0.52	1.46
	217.37	217.64	1.02	3.56
	311.28	311.51	0.82	2.87
DOB #11		149.16	0.12	0.42
		158.75	0.68	2.10
		166.89	0.49	1.50
		174.59	0.67	2.16
		179.96	0.36	0.99
		214.20	1.11	3.58
		215.30	1.41	4.53
DOB #12		117.17	0.29	0.96
		152.08	0.32	1.00

Table 3-4c. Rock mechanical parameters of Gondwana rock sequences as tested from samples of DOB #11 (Wardell Armstrong, 1991)

Borehole No	Sample depth (m)		Bulk density (Mg/m^3)	Failure load (MPa)	UCS (MPa)	Failure load (MPa)	Tensile Strength (MPa)
	From	To					
DOB #11	145.47	145.63	2.08	0.72	2.40	0.12	0.42
	149.70	149.88	1.60	1.50	3.86	0.68	2.10
	152.84	153.02	2.11	2.95	9.63	0.49	1.50
	158.58	158.75	2.19	3.74	12.19	0.67	2.16
	163.28	163.46	1.85	0.62	2.26	0.36	0.99
	174.42	174.59	2.23	0.27	16.25	1.11	3.58
	178.09	178.26	2.35	9.17	29.93	1.41	4.53
	179.78	179.96	2.22	2.31	7.41	0.61	1.85
	214.66	214.79	1.56	7.65	25.13	0.40	1.22
	218.91	219.08	2.51	17.14	54.57	0.37	1.13

References

Alam, M., Alam, M.M., Curray, J., Chowdhury, R.M.L.R., and Gani, M.R., 2003. An overview of the sedimentary geology of the Bengal Basin in relation to the regional tectonic framework and basin-fill history. Sedimentary Geology 155, 179-208.

Bakr, M.A., Rahman., Q.M.A., Islam, M.M., Islam, M.K., Uddin, M.N., Resan, S.A., Haider, M.J., Islam, M.S., Ali, M.W., Choudhury, M.E.A., Mannan, K.M., and Anam, A.N.M.H., 1996. Geology and Coal Deposits of Barapukuria Basin, Dinajpur District, Bangladesh, Records of Geological Survey of Bangladesh. 8, pt 1.

Desikacher, S.V., 1974. A review of the tectonic and geological history of eastern India in terms of plate tectonic theory. J. Geol. Soc. India 15, 134-149.

Islam, M.R., and Islam, M.S., 2005. Water Inrush Hazard in Barapukuria Coal Mine, Dinajpur District, Bangladesh. Bangladesh Journal of Geology 24, 1-17.

Khan, F.H., 1991. Geology of Bangladesh, Willey Eastern Limited, 4835/24 Ansari Road, Daryaganj, New Delhi 110002, India, pp. 33-40.

Khan, A.A., and Chouhan, R.K.S., 1996. The crustal dynamics and the tectonic trends in the Bengal basin. Journal of Geodynamics 22, 267-286.

Uddin, M.N. and Islam, M.S. 1992. Gondwana basins and their coal resources in Bangladesh. Geology in South Asia-1. Proceedings of the First South Asian Geological Congress, Pakistan. pp. 224-230.

Wardell Armstrong, 1991, Techno-Economic Feasibility Study of Barapukuria Coal Project (unpubl.), Dinajpur, Bangladesh.

Chapter 4

Numerical Simulation of Stress Distributions and Mining Hazards Associated with Ground Movement and Water Inflow of the Barapukuria Coal Mine

Chapter 4

Numerical Simulation of Stress Distributions and Mining Hazards Associated with Ground Movement and Water Inflow of the Barapukuria Coal Mine

4.1. Introduction

Over the previous two decades, a variety of studies have documented the environmental impacts of longwall coal mining, including serious effects on aquifers, land subsidence, and the hydraulic properties of the mined strata. These studies also show that the impacts of longwall mining arise not only due to the drainage of groundwater into mined panels but also from changes in the overburden stress regime. Such groundwater hazards present a risk to mining safety that is a common concern of both mine operators and researchers. It is of vital importance to study mining-induced strata failure and the hydraulic parameters of these strata in order to predict and prevent water inflow in coal mines (Hill and Price, 1983; Booth, 1986; Kim et al., 1997; Zhang and Shen, 2004).

The Barapukuria coal mine is the first underground coal mine in Bangladesh. The future of proposed underground mining in the Khalaspir, Phulbari, Dighipara, and Nawabgonj coal basins (see details in Islam and Hayashi, 2008a) depends on the successful operation of the Barapukuria mine because these coal basins have similar geological, tectonic, and structural characteristics. Compared to the other Gondwana coal basins in the Indian subcontinent, the basins in Bangladesh are of exceptional characteristics in their water-bearing formations. The coal-bearing Gondwana Group in the Barapukuria basin, as well as the other basins, is located under a "mega-aquifer" (Islam and Kamruzzaman, 2006), which is named the Dupi Tila Formation. It is a prolific groundwater reservoir extending over larger areas of Bangladesh. Numerous high-angle normal faults, X-shaped joints, and fractures characterize the basins. During a seismic survey carried out by Wardell Armstrong Mining Consultants of the United Kingdom, about 37 faults were detected. At the time of tunnel development (2001-2004), numerous faults with 1-3 m throw were observed. Fracture

intensity within the rock strata of the Gondwana Group ranged from 7-10 per meter, whereas joints ranged from 1-3 per meter. Thus, the coal-bearing Gondwana Group is connected directly or indirectly with the overlying water-bearing Dupi Tila mega-aquifer by diverse joints, faults, and fractures (Islam and Islam, 2005; Islam and Hayashi, 2008a). In addition, there is an open window that is located at the northern extremity of the present mine plan (Islam, 2005).

The hydrogeological conditions in the Barapukuria coal mine are very complex. The most serious issue affecting the safe operation of the coal mine is water inflow from the unconsolidated Upper Dupi Tila (UDT) aquifer. Flooding of the mine from breaches in the Upper

Dupi Tila aquifer occurred frequently during the development of the mine in 1998. When the mining walls had been extended to a total distance of about 1200 m, roof pressure increased dramatically and a small amount of water flowed into the mine from several locations along the roof. Later, mud and sand-laden flows rushed suddenly into the workings (see location in Fig.9), reaching a maximum flow rate of 625 m^3/h (Islam and Islam, 2005).

Despite these geological and hydrogeological complexities, a multi-slice longwall mining plan has been considered for a 34 year mine lifetime, with a target production of 1 million tons per year. If the mine is successfully operated, about 10% of the total coal reserve (about 377 million tons) (Islam and Hayashi, 2008a) will be extracted. At this point, our basic question is whether it is possible to accomplish multi-slice longwall mining in the Barapukuria basin considering its geological and hydrogeological characteristics.

The primary purpose of this study is to focus on hydrogeological complexities that might be encountered in an overlying aquifer during multi-slice mining excavation. Under natural conditions, groundwater is introduced into coal seams by infiltration at the sub-crop with Dupi Tila sands and by vertical movement through the surrounding Gondwana host rocks. Drainage of mining excavation sites located within these seams will cause a redistribution of stress patterns and readjustment of the natural groundwater flow patterns. In general, a lowering of the groundwater potential at the excavation site will lead to the following important changes:

- A higher rate of infiltration from the Dupi Tila into the seam excavation.
- A lower groundwater potential within coal seams relative to surrounding lithologies that will cause increased convergence of groundwater towards the seams.
- Groundwater within the coal seams will converge on the area of excavation and will cause increased movement toward the main cavities including lateral flow along the coal seams.

All of these changes are related to excavation and mining-induced stresses. Although detailed geological studies have been conducted in this half-graben type basin by Wardell Armstrong (1991), Bakr et al. (1996), and Islam and Hayashi (2008a), very little attention has been paid to the tectonic and mining-induced stress pattern of the basin, both of which are important for underground longwall mining. Thus, mining-induced stress patterns and their effects on the aquifer remain uncertain. Using the finite element method, it is possible to determine an approximate pattern of the mining-induced stresses and fracture propagation. The method has been widely used by many researchers, including Obara et al. (2000), McKinnon (2001), Corthesy et al. (2003), Hart (2003), Aksoy et al. (2006), Xu et al. (2006), and Yang et al. (2007).

The main objective of this modeling effort is not to suggest whether mine conditions are good or bad, but rather to address the potential for caving to the height of the aquifer. The basic goals of this study include:

- presentation of both the tectonic and mining-induced stress distribution,
- integration of the calculated results to reveal a concern regarding damage to the overlying aquifer due to multi-slice longwall mining, and
- discussion of the adverse environmental impacts, especially damage to the agricultural land as well as the aquifer system.

To clarify our goal, two types of models are established based on the combined effects of the elastic rock-mechanical parameters. Model A represents the principal stresses from tectonic sources, whereas Model B corresponds to the mining-induced stress field from overburden/gravitational sources. The state of stress in the crust can be caused by two major sources: (1) a gravitational source, and (2) a broad-scale tectonic source. In the case of a

gravitational source, the pressure generated by the weight of the overburden is proportional to the density of the overlying rocks. Broad-scale sources consist of plate boundary forces resulting from geodynamic processes in the crust. Broad-scale tectonic stresses are spatially uniform and control regional faulting and crustal deformation (Zoback and Zoback, 1980; Liu and Zoback, 1992; Zoback, 1992). In the case of the Barapukuria type half-graben basin, it is assumed that both stresses are highly effective. For model A, our database includes an E-W geological cross-section across the Barapukuria basin, and rock physical properties. For model B, we used the Examine2D (www.rocscience.com) software to obtain the mining-induced stress field related to single-slice and multi-slice mining excavation.

4.2. Geological setting

The geology of the Barapukuria coal basin was described in detail by Islam and Hayashi (2008a). A brief outline of the geology is presented here. The Indian plate, the Eurasian plate, and the Burmese sub-plate form three major tectonic zones (Fig. 4-1) in Bangladesh: (i) a platform flank zone in the west named the Dinajpur Shield and Platform, (ii) a deeper basin zone in the middle of the Bengal Basin, and (iii) the Chittagong–Tripura Fold Belt in the eastern extremity (Khan, 1991; Khan and Chouhan, 1996; Alam et al., 2003). The Barapukuria coal basin is located in the Dinajpur Shield (Fig. 4-1) of Bangladesh and is surrounded by the Himalayan Foredeep to the north, the Shillong Shield/Platform to the east, and the Indian Peninsular Shield to the west (Wardell Armstrong, 1991; Khan, 1991; Bakr et al., 1996; Islam and Islam, 2005; Islam and Hayashi, 2008a). The stratigraphic sequence is divided into four formations on the basis of age and lithology (Wardell Armstrong, 1991):

- Madhupur clay
- Dupi Tila (mega-aquifer in Bangladesh)
- Gondwana Group (coal-bearing strata)
- Pre-Cambrian Archaean Basement

The Barapukuria basin (Fig. 4-2) consists of a self-contained, half-graben-controlled sedimentary basin of Gondwana (Permian) age. The basin is asymmetrical and thickened towards a basin-marginal Eastern Boundary Fault (EBF), which is downthrown to the west with a NNW-SSE strike, parallel to the basin. The faults are normal faults, which is a typical feature

of extensional (rift) tectonics. Half-graben development was associated with E-W extension, which is common in Late Cretaceous Indian continental rocks. In the northwestern part of Bangladesh, crustal extension and basin development is widely documented, and may have resulted from several discrete episodes of deformation. Fault Fa appears to have controlled the development of the half-graben, and also appears to have controlled much of the other faulting within the basin. A total of 37 intra-basinal faults were identified in the seismic survey. These intra-basinal faults with throws greater than 10 m are well defined and are mainly distributed above the –250 m level. Overall, the intra-basinal faults Fb, Fc, Fe, Ff, Fg, Fh, Fi, and Fj occur in conjugate sets, most of which dip to the ESE (Wardell Armstrong, 1991; Bakr et al., 1996; Islam and Hayashi, 2008a).

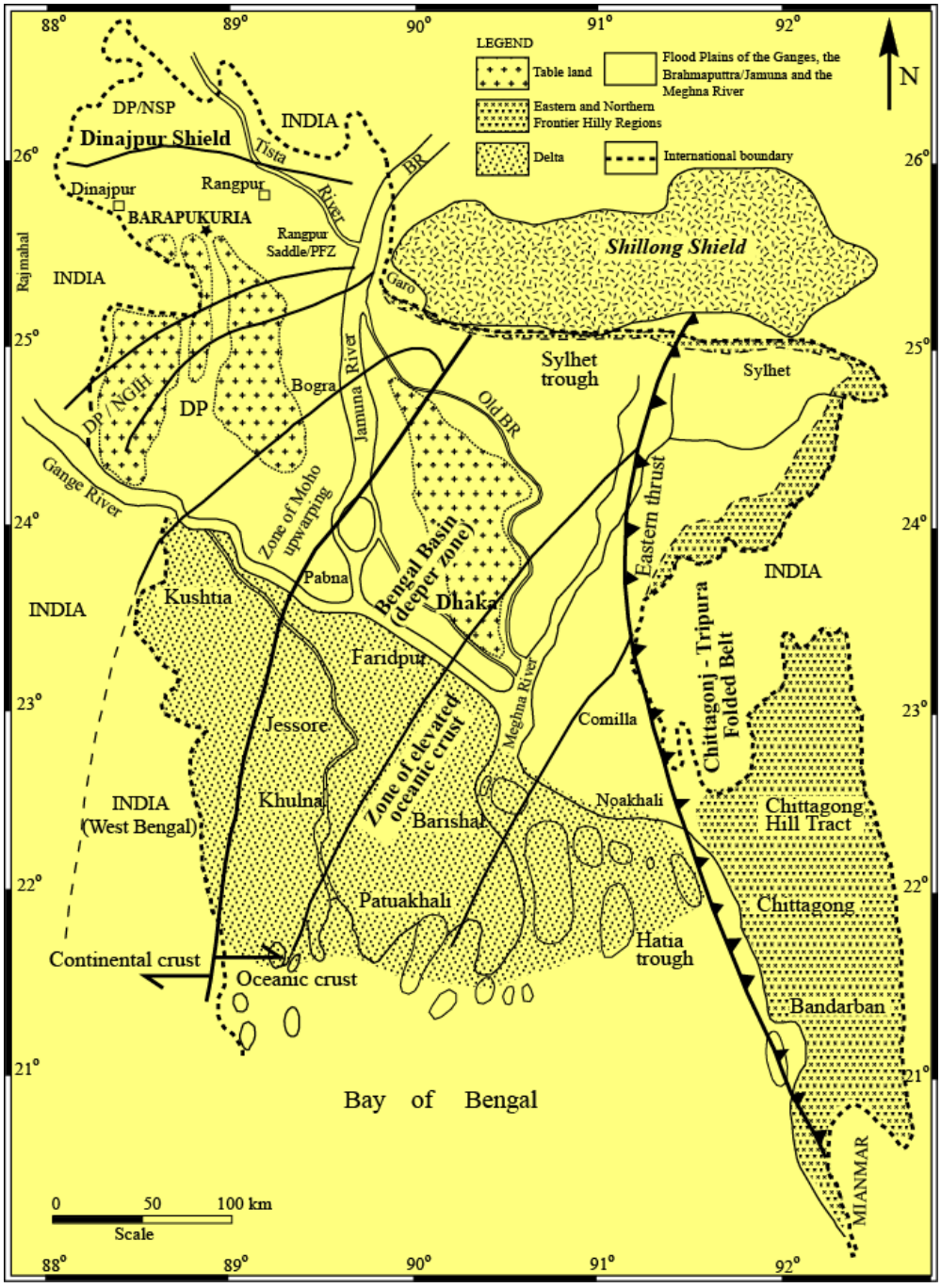

Fig. 4-1. Location of the Barapukuria coal basin within the physiographic and geotectonic divisions of Bangladesh. Heavy bold lines indicate boundary of the major tectonic divisions. Medium bold lines in the northwest part indicate tectonic boundary of sub-zones within the Dinajpur Shield. Abbreviations: BR=Brahmaputtra River, DP=Dinajpur Platform, NGIH=Nawabganj-Gaibandha Intracratonic High, NSP=North Slope of the Platform (part of Sud-Himalayan Foredeep), PFZ=Platform Flank Zone (compiled after Khan, 1991; Khan and Chouhan, 1996).

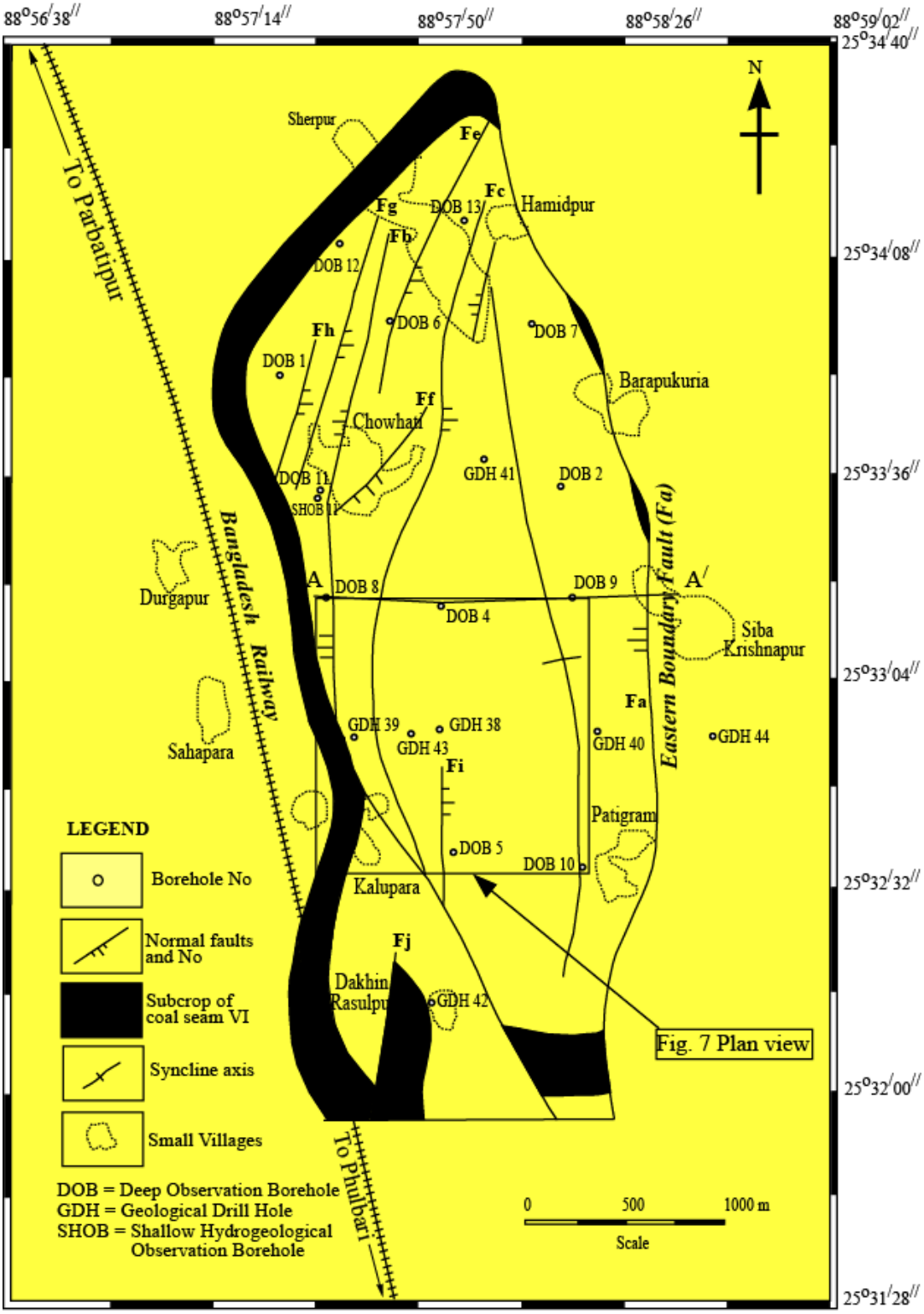

Fig. 4-2. Location of the boreholes, major faults, and structural pattern of the Barapukuria Coal Basin, Northwestern Bangladesh.Abbreviations: DOB=Deep Observation Borehole; GDH=Geological Drill Hole; SHOB=Shallow Hydrogeological Observation Borehole (after Wardell Armstrong, 1991; Bakr et al., 1996; Islam and Hayashi, 2008a).

4.3. Database and methodology

4.3.1. Database

All the necessary data for model A, including the geological cross-section, tectonic structure, geotechnical data, and stratigraphical sequences, were taken from Wardell Armstrong (1991), Bakr et al. (1996), and Islam and Hayashi (2008a). The mining plan for model B was collected from the authority of the Barapukuria Coal Mining Company Limited. The schematic excavation view is drawn based on the first author's practical mining experiences during 2001-2004 in the Barapukuria Coal Mine.

4.3.2. Methodology

We used numerical finite element methods for the analysis of stress-driven problems in rock strata. Model A was constructed based on the finite element (FE) method package program developed by Hayashi (2008). Model B was established on the basis of boundary element methods BEM), where the Examine2D (www.rocscience.com) software package is used. Model A is described in sections 4.4 and 4.5, whereas model B is illustrated in section 4.6 of this chapter.

4.4. Model A and constraints

The state of stress in the crust may be known locally from borehole data down to a few hundred meters depth. In the case of the Barapukuria basin, this type of stress data is not available. Wardell Armstrong Mining Consultants of the United Kingdom collected some core samples during borehole drilling and some laboratory tests were carried out to determine the stress in the rock. The orientations of maximum stress, (σ_{Hmax}) are approximately between N35^{o}E and N45^{o}E, whereas for minimum stress (σ_{Hmin}) the orientations are approximately between N55^{o}W and N45^{o}W (Wardell Armstrong, 1991).

The major normal faults in a half-graben type basin imply a history of deformation under different stress states. Half-grabens are the characteristic of extensional terranes (Melosh and Williams, 1989). The Barapukuria coal basin is one of the largest half-graben type Gondwana coalfields in Bangladesh. The master boundary fault, Fa, together with other faults, controls the structure of the basin. It is assumed that the faults are mainly influenced by a complex interaction of convergence-related tectonic processes of the continental Indian plate with the continental

Eurasian plate. The convergence boundary between the Indian plate and Eurasian plates is located about 200 km N-NE of the basin area. Very strong interaction between the two plates resulted in differential extension and subsidence within the continental crust of the Indian plate and the development of many sedimentary basins, which provide the source rock strata for much of Bangladesh's coal resources. Thus, fault Fa of the Barapukuria basin is related to the rift tectonic activity of the Indian plate (Islam and Hayashi, 2008a). A high density of normal faults associated with numerous fractures demonstrates that the basin was related to the rift tectonic activity (Islam, 2005; Islam and Islam, 2005). In this paper, we present model A considering a simple mechanical parameterization to test the rift tectonic stress pattern across the basin based on the elastic rock properties.

4.4.1. Geometry

A two-dimensional finite element model was constructed primarily based on the geological cross-section (Fig. 4-3c of Wardell Armstrong, 1991). The main tectonic features and the location of the profile $AA^{/}$ are shown in Fig. 4-2. This vertical cross-section through the half-graben basin was represented by a finite element mesh composed of an assembly of 1350 triangular elements and 736 nodes under plane strain conditions. The simplified model (Fig. 4.4a) is extended up to 2000 m and consists of a 650 m thick continental crust. The model consists of four layers, among which the EBF represents the pre-existing boundary fault, which extends to the bottom at a depth of about 550 m. The other three layers correspond to individual crustal units based on density variations and rock mechanical parameters.

4.4.2. Boundary conditions

Half-grabens are characteristically bounded by high-angle planar normal faults, although low-angle extensional faults are common in most of the basins. Large-scale faulting affects the strong and brittle upper crust (Bott, 1997). The basic premise is that an extending elastic layer first fails on a normal fault, which cuts the layer with a dip of approximately 60^{o} in accordance with Anderson's (1951) theory of normal faulting. Slip along this fault flexes the adjacent rock

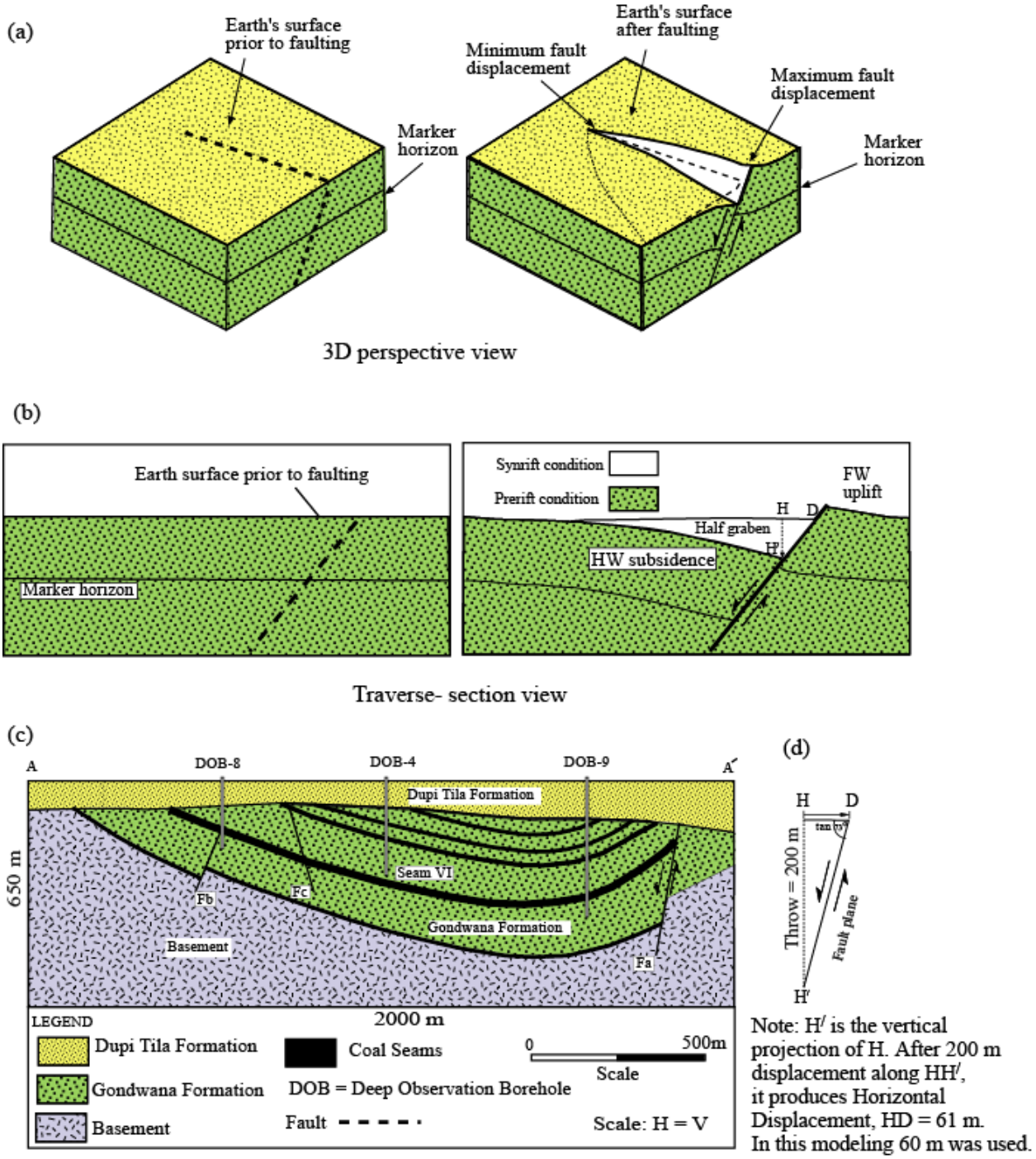

Fig. 4-3. (a) and (b) show schematic views of half-graben basin architecture (modified after Gibson et al., 1989; Morley, 1999). (c) Cross-sectional view (see location in Fig. 4-2 AA/) of the Barapukuria basin. (d) Explanations to show how we assume 60 m horizontal nodal displacement boundary conditions of our modeling. In the case of the eastern boundary fault of the Barapukuria basin, throw is 200 m. Calculated horizontal displacement (HD) is 61 m (approx.), while the dip of the fault plane is 73°.

layers until a new fault forms where the fiber stresses induced by bending are most extensional (Melosh and Williams, 1989). In a gross sense, for the Barapukuria type half-graben basin, displacement is greatest at the center of the fault and decreases to zero at the fault tips, as shown in Fig. 4-3a. The displacement of an initially horizontal surface that intersects the fault is greatest at the fault itself and decreases with distance away from the fault (Fig. 4-3b). This produces footwall uplift and hanging-wall subsidence, the later, which creates the sedimentary basin (e.g., Gibson et al., 1989; Contreras et al., 1997). The structure of the Barapukuria basin is shown in Fig. 4-3c. It is apparent that the basin geometry is affected by fault propagation and that the maximum displacement is accumulated on the boundary fault Fa. Fault Fa cuts all layers (Dupi Tila, Gondwana, and Basement) with a dip of approximately 70-75^{o} and a throw of about 200 m, and accommodated about 61 m of horizontal displacement (Fig. 4-3d).

The source of the extensional stress necessary for half-graben formation is varied. The Barapukuria basin is currently in an active extensional environment (Islam and Hayashi, 2008a), which is the basis of the model presented in this paper. We assumed that the first failure occurred along the extending elastic layer on the EBF, and then it led to the development of a half-graben type basin under the extensional tectonic environment. This assumption is reflected in the boundary conditions used. The half-graben is modeled by fixing the left edge of the grid and applying increasing extension to the right edge. The grid and applied boundary conditions are shown in Fig. 4-4b. The upper part of the model represents the Earth's surface and is free in all directions. The bottom of the grid is prevented from moving in the vertical (y) direction while a uniform body force (gravity) is applied throughout. Arrows at the bottom (along x direction) are not drawn to scale, and the displacement values decrease linearly and gradually from the right side to the left. An equivalent horizontal nodal displacement was applied along the right wall of the model. Free-slip boundary conditions were used along the left wall of the model. The point marked with a triangle is fixed in the horizontal and vertical dimension.

4.4.3. Material properties

We divided the model into four layers, which represent litho-structural sequences from top (Quaternary) to bottom (Pre-Cambrian basement). The rock layers up to 650 m are considered to behave as an elastic material. Five rock mechanical parameters for individual rock layers,

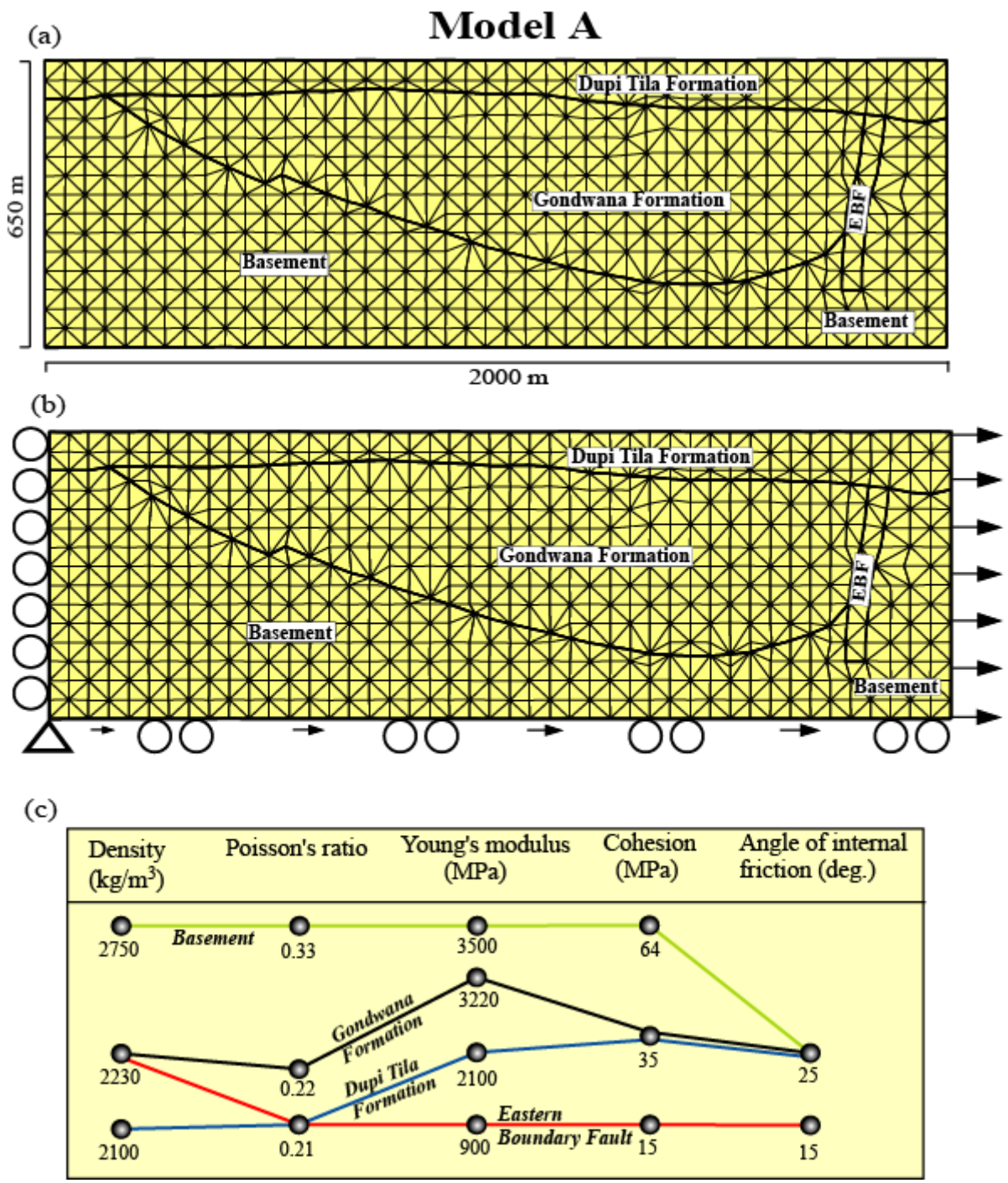

Fig. 4- 4. (a) Layers of model A and finite element grid, which consists of 1350 elements with a network of 736 nodes, (b) applied boundary conditions (see details in text), and (c) graphical presentations of rock physical properties (see in Table 4-1).

Table 4-1. Rock mechanical properties used in the finite element model A. Abbreviations:ρ= density; ν= Poisson's ratio; *E* = Young's modulus; *c* = cohesion;φ= angle of internal friction (in deg.) (see graph in Fig. 4c) (Wardell Armostrong, 1991).

Strata	ρ **(kg/m^3)**	ν	***E*** **(MPa)**	***c*** **(MPa)**	ϕ **(deg.)**
Basement	2750	0.33	3500	64	25
Eastern Boundary Fault	2230	0.21	900	15	15
Gondwana Formation	2230	0.22	3220	35	25
Dupi Tila Formation	2100	0.21	2100	35	25

including density, Poisson's ratio, Young's modulus, angle of internal friction, and cohesion, used in experiments are listed in Table 1, and shown in Fig. 4.4c (Wardell Armstrong, 1991). The average values of density of different rock layers ranged from 2100 kg/m^3 to 2750 kg/m^3. The values of Poisson's ratio used in the model ranged from 0.21 to 0.33, and Young's modulus ranged between 900 to 3500 MPa in accordance with the rock strata.

4.5. Model results

Only a single set of boundary conditions was applied. The modeling scenarios were intended to represent a mechanically weak fault-affected zone, a moderately strong layer, and a strong rock layer due to the influence of extensional displacement. The modeling results were shown as (1) stress distributions orientations, and the magnitudes of the principal stresses, and (2) proximity to failure of elements. Extensional displacements of 40 m, 50 m, and 60 m were applied in the modeling.

4.5.1. Stress distribution

The spatial distributions of the stress orientations and magnitudes are shown in Figs. 4-5a and 4-5b, where σ_1 is the maximum tensional stress, and σ_3 is the minimum compressive stress. The displacement boundary conditions selected in this scenario imply an overall horizontal $\sigma_1$orientation. The stresses in the model are much more uniform in orientation and reflect the overall horizontal extensional setting. In the vicinity of the model, especially the contact line between the Basement and the Gondwana Formation, some stress field reorientations do occur

because of the close contact of the weak rock layer (Gondwana Formation) with the strong layer (Basement complex)

Fig. 4-5c illustrates how the shear stress is partitioned between the various rock layers. The shear stress distribution in the right side of the model is more variable than that on the left-side. The shear stress contour map (Fig. 4-5c) illustrates that the stress increases towards the zone, which is affected by the pre-defined EBF. The shear stress distribution is highly concentrated in and around faulted zone EBF and the maximum deformation of the model is achieved. This prominent high strain zone cutting through the basement up to the base of the Dupi Tila Formation of the model is genetically related to the reactivation of the fault.

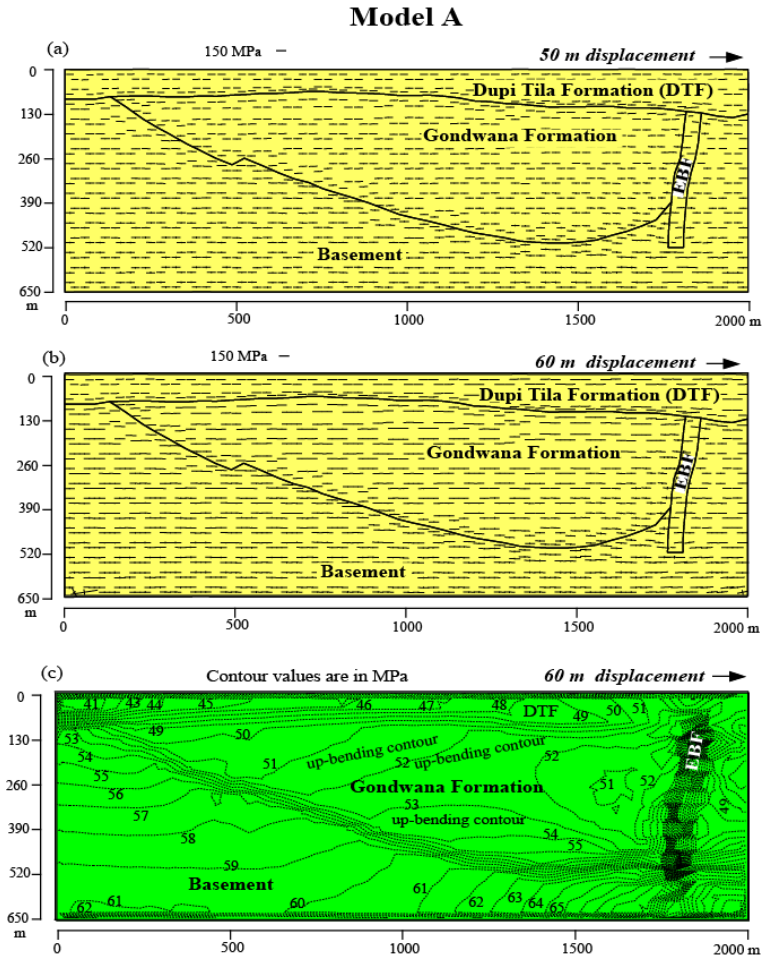

Fig. 4-5. Distributions, orientations, and magnitudes of maximum tensional stress σ_1, and minimum compressive stress σ_3, for: (a) 50 m, and (b) 60 m horizontal displacement. (c) Contours of maximum shear stress (τ_{max}) magnitudes for the model with 60 m horizontal displacement. Shear stress bands are concentrated in and around the EBF. High shear stress extends from the bottom to the top of the Gondwana Formation and nearly reaches the bottom of the water-bearing Dupi Tila Formation.

4.5.2. Proximity to failure of elements

We examined the deformation of the rock strata based on the proximity to failure of elements considering the Mohr-Coulomb failure criterion as applied by Melosh and Williams (1989), Talukder and Hayashi (2006), Islam and Hayashi (2007), Islam and Hayashi (2008b). For 40 m of horizontal nodal displacement, the simulated results (Fig. 4-6a) correspond to failure of the elements occurring mostly within pre-defined EBF zone. There is no evidence for failure of elements within the coal-bearing Gondwana Formation and the basement rock layers. Experimental results also show that the failure of elements changes dramatically with varying nodal displacement. For example, in the case of 50 m displacement, some elements failed at the bottom and right side of coal-bearing Gondwana deposits (Fig. 4-6b). We found reasonable results for 60 m displacement, where most of the failure of elements was concentrated within the coal-bearing Gondwana Formation (Fig. 4-6c). Thus, as the displacement is progressively increased, the failure zone extends from the bottom to the top. The failure of elements propagates from the coal-bearing layer through the middle part of the model, and finally toward the bottom of the water-bearing layer.

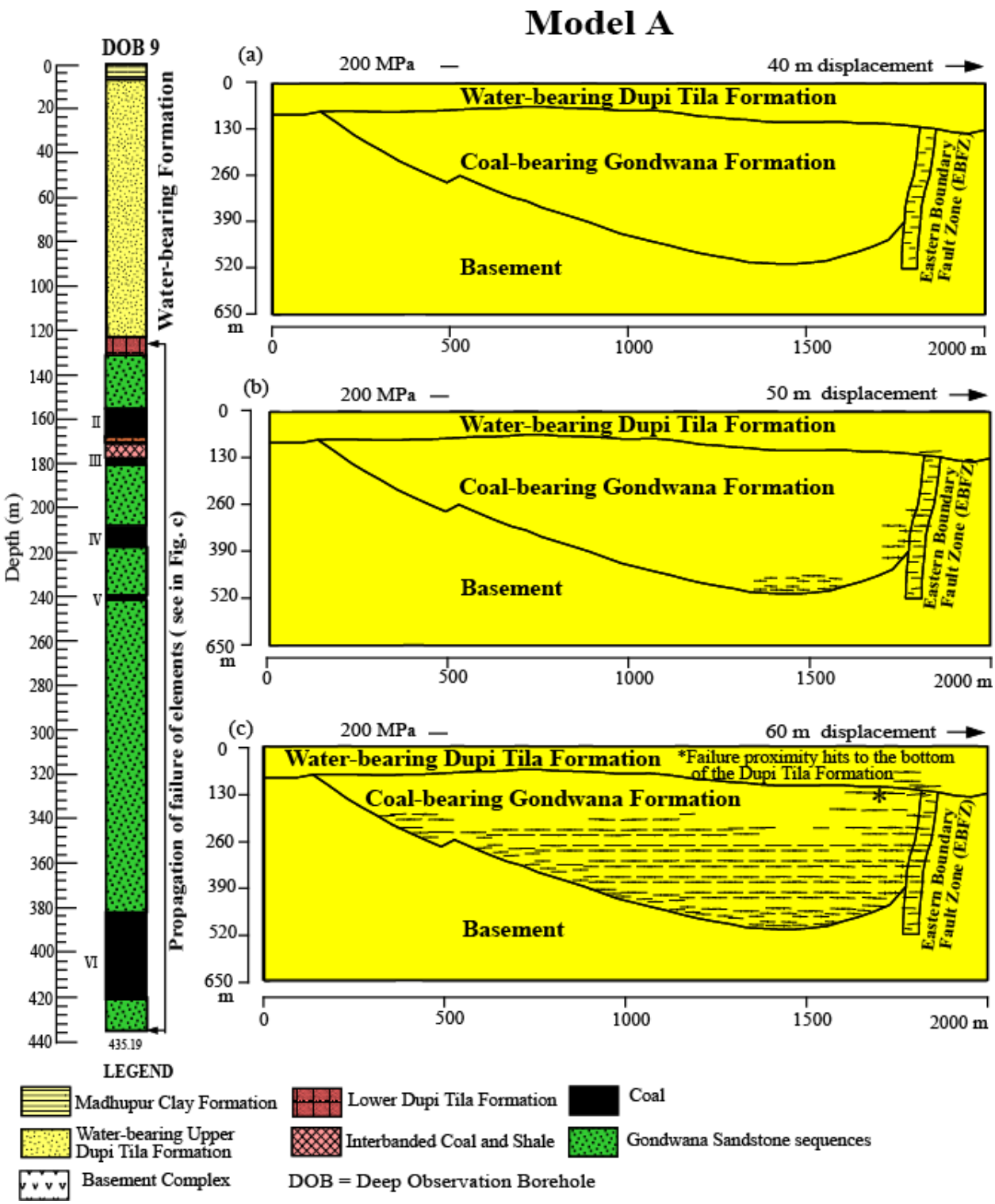

Fig. 4-6. Proximity to failure of elements in the coal-bearing Gondwana Formation, and within the EBF for (a) 40 m, (b) 50 m, and (c) 60 m horizontal nodal displacement. Asterisk in (c) indicates that the zone of proximity to failure of elements cuts the Gondwana Formation and eventually reaches the bottom of the water-bearing Dupi Tila Formation. The approximate effect of failure propagation within the strata is shown in DOB # 9.

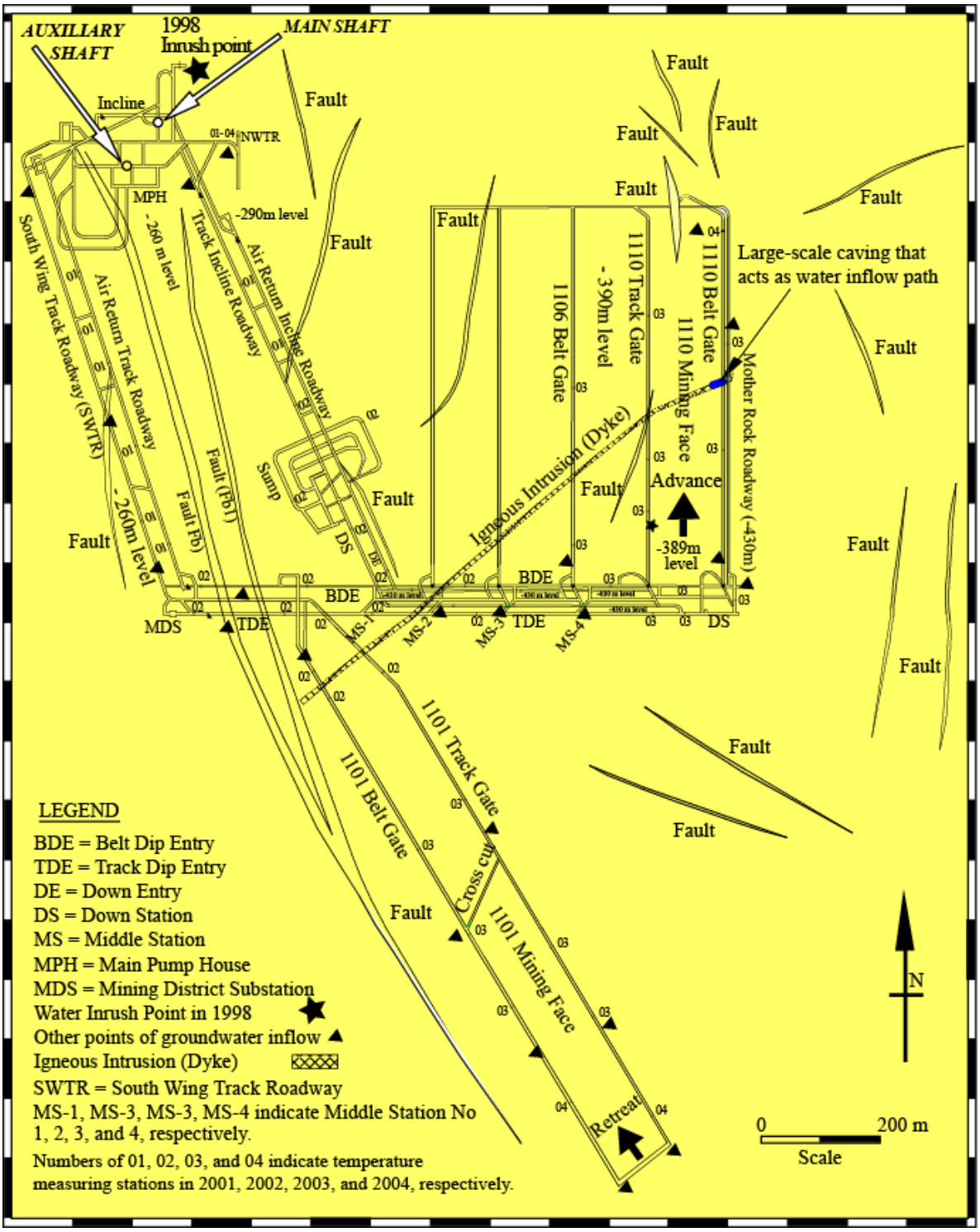

Fig. 4-7. Plan view (from levels -260 m to -420 m) of the Barapukuria Coal Mine (see location in Fig. 4.2). Big asterisk shows the position of water inrush that happened in 1998. Solid delta shows water inflow measuring points. The total inflow comes from different faces and increased simultaneously with mining excavation.

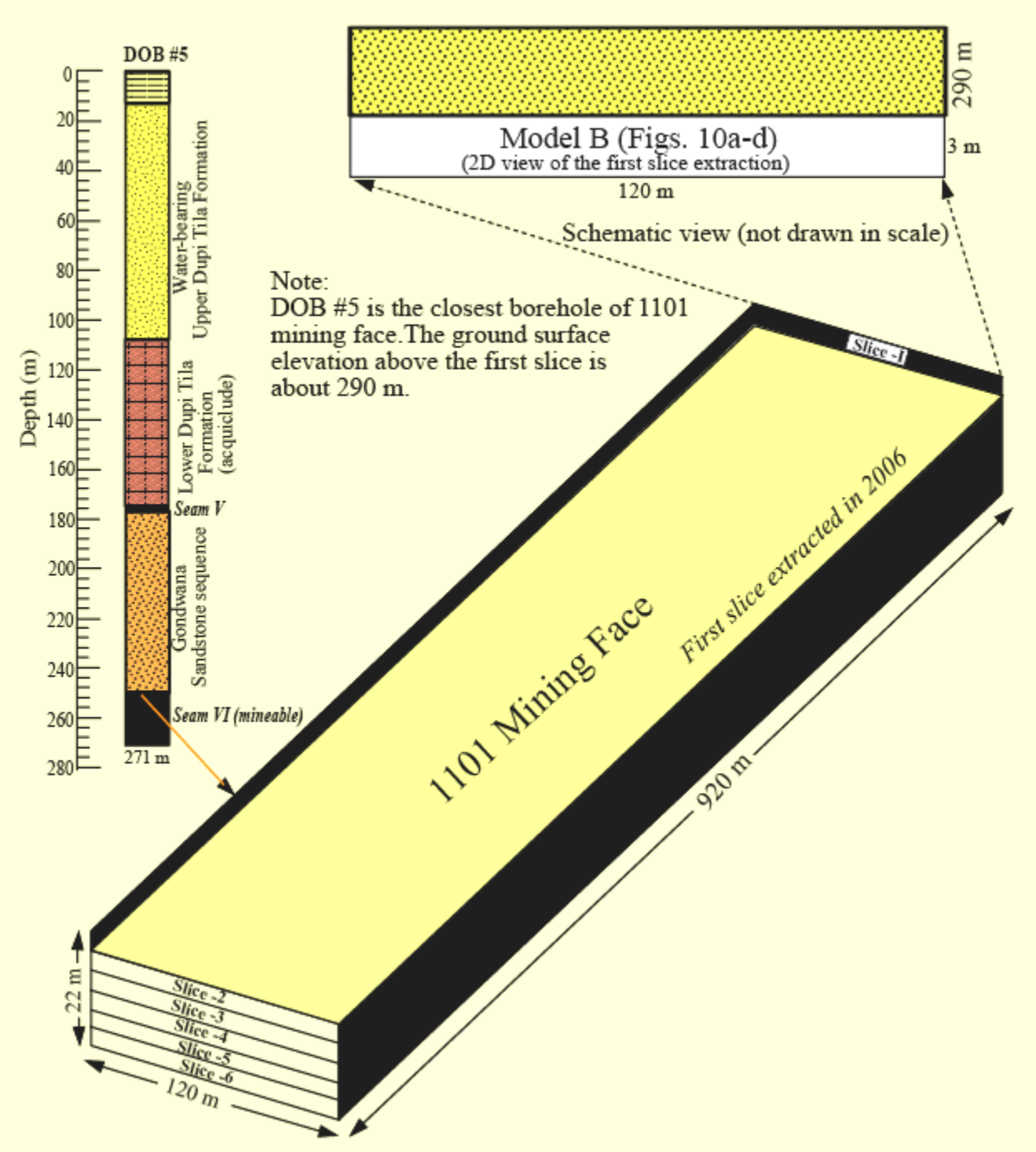

Fig. 4-8. Schematic view of the 1101 mining panel below the Dupi Tila water-bearing aquifer in the Barapukuria coal basin, showing how model B was constructed.

4.6. Model B and constraints

When an underground opening (see plan view in Fig. 4-7) is excavated into a stressed rock mass, the stresses in the vicinity of the new opening are redistributed. It was necessary to make several assumptions, the most significant of which was to use a mining ‘‘slice’’. These mining slices are used for the purposes of the model and represent the mining-induced stress pattern after actual mining excavation. We considered model B, where the stresses induced in the rock surrounding a horizontal rectangular tunnel are illustrated in Fig. 4-8. We present the schematic views of the 1101 mining face, which is presented only as an example of the stress distribution after single-slice and multi-slice extraction of coal. The overburden thickness of the model is about 290 m, and the imposed rock mechanical parameters are shown in Table 4-2.

Table 4-2. Imposed rock mechanical properties (Wardell Armostrong, 1991) in the model B.

Stress field	Type	Gravitational Stress
	Ground Surface Elevation (m)	290
	Overburden Unit Weight (MN/m^3)	0.027
Rock Mass Elastic Properties	Type	Isotropic
	Young’s modulus, *E* (MPa)	3500
	Poison’s ratio, ν	0.22
Rock Mass Strength	Type of failure	Mohr-Coulomb
	Tensile strength (MPa)	6
	cohesion, c (MPa)	15
	angle of internal friction, ϕ (deg.)	30

4.6.1. Model results

The modeling results are represented based on five mechanical parameters, including maximum compressive stress σ_1, minimum compressive stress σ_3, mean stress, deviatoric stress, and deformation vector. Results of these parameters are shown in Figs. 4-9 and 4-10. Contours of the magnitudes of the maximum compressive stress σ_1 and the minimum compressive stress σ_3 are given in Figs. 4.9a-b and 4-10a-b, respectively. These show that the redistribution of stresses is concentrated in the strata close to the excavation, at a distance from the center of the excavation. Mean stress and deviatoric stress contours for the single-slice and multi-slice excavations are shown in Figs. 4-9c-d, and 4-10c-d, respectively.

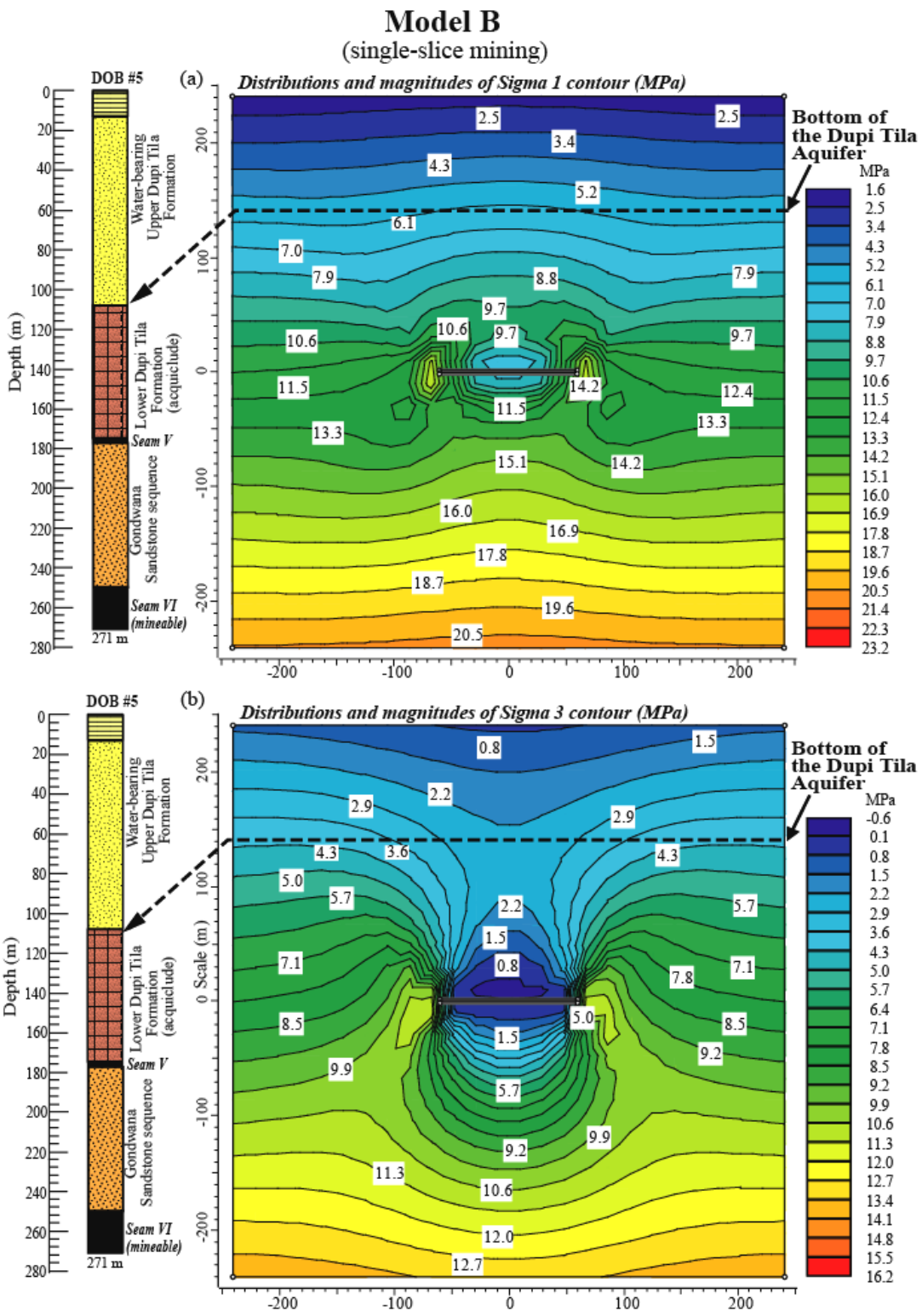

Fig. 4-9. Mining-induced stress field after extraction of 3 m high coal panel from 1101 working face. (a) and (b) show contours of maximum (σ_1) and minimum (σ_3) principal stress magnitudes in the rock strata surrounding a 3 m high and 120 wide coal face, respectively. (c) and (d) represent contours of mean stress and deviatoric stress magnitudes, respectively. Deformation vectors in (d) are represented by red arrows.

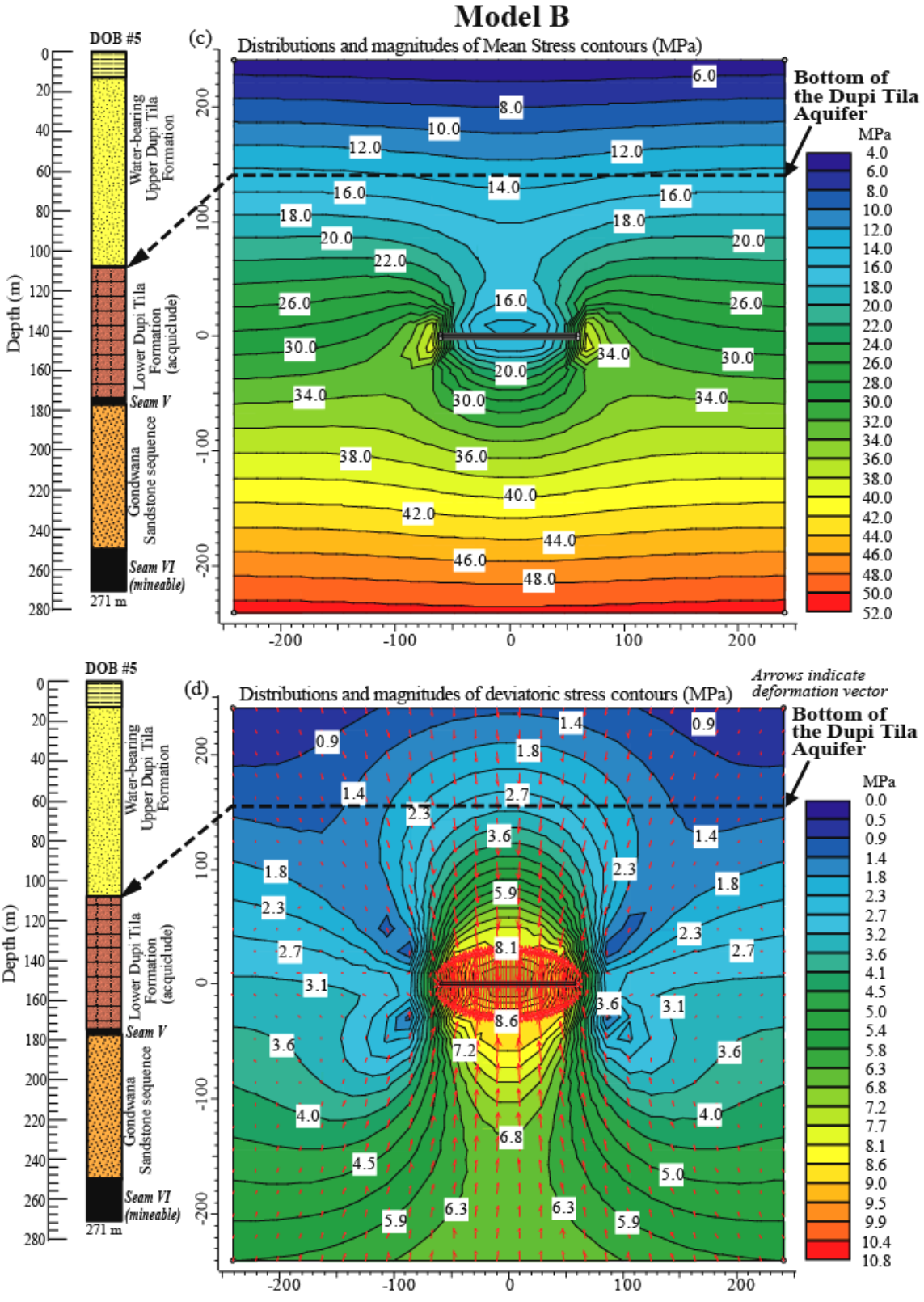

Figure 4.9 (continued)

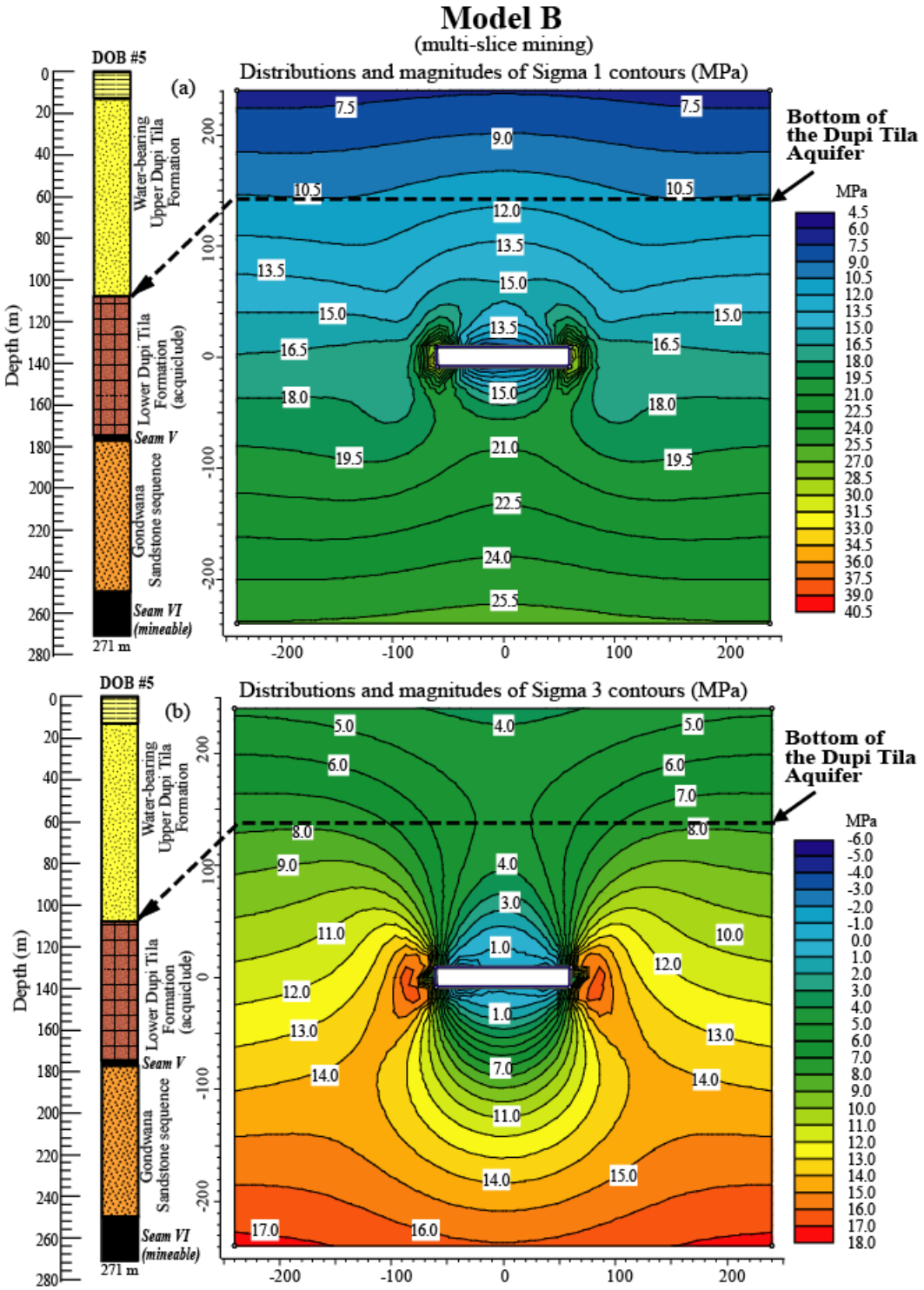

Fig. 4-10. Types of stress patterns that would be generated after extraction of multi-slice (18 m high) coal panel. (a) and (b) show contours of maximum (σ_1) and minimum (σ_3) principal stress magnitudes in the rock strata surrounding an 18 m high and 120 wide coal face, respectively. (c) and (d) represent contours of mean stress and deviatoric stress magnitudes, respectively. Deformation vectors in (d) are represented by red arrows.

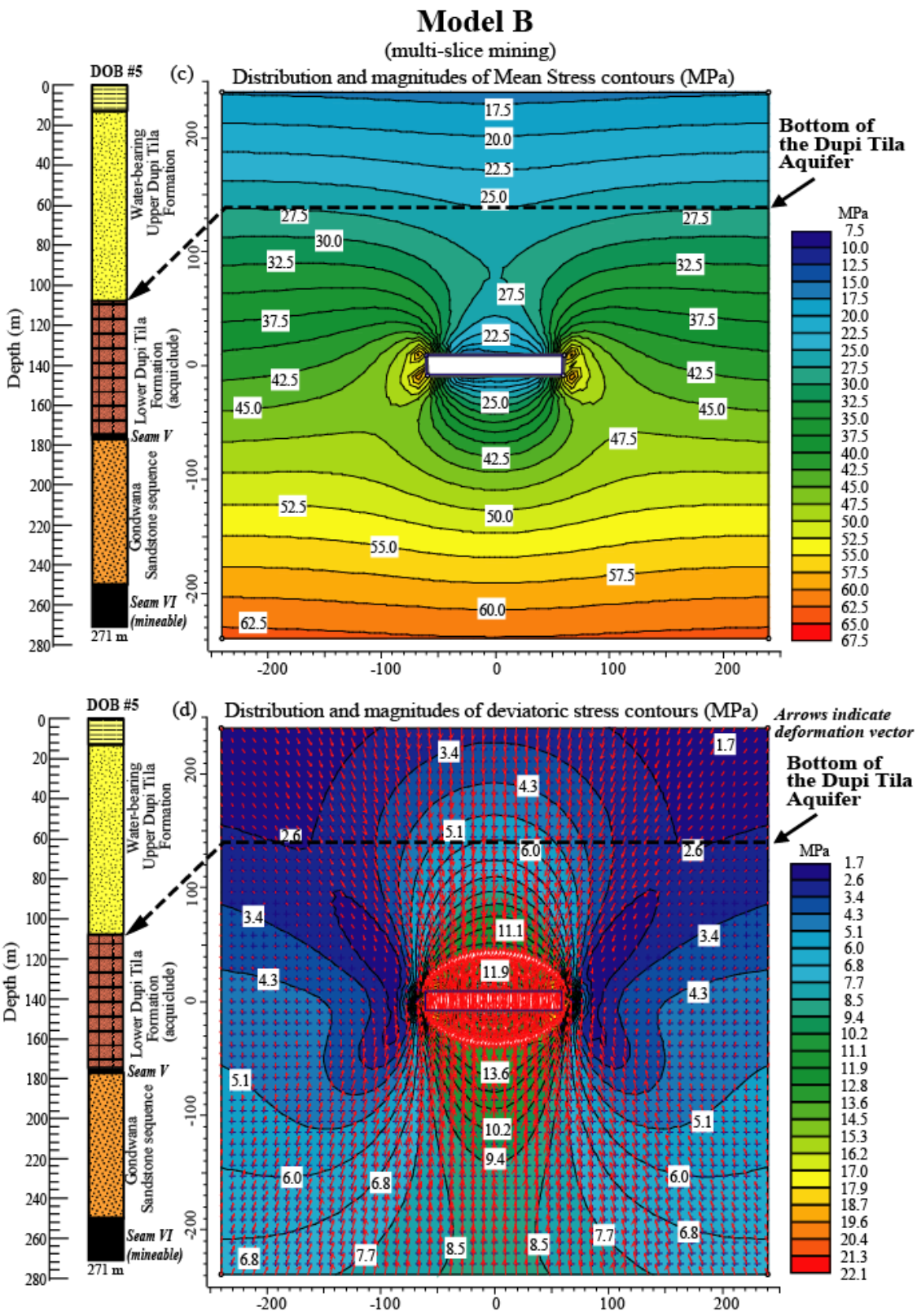

Figure 4.10 (continued)

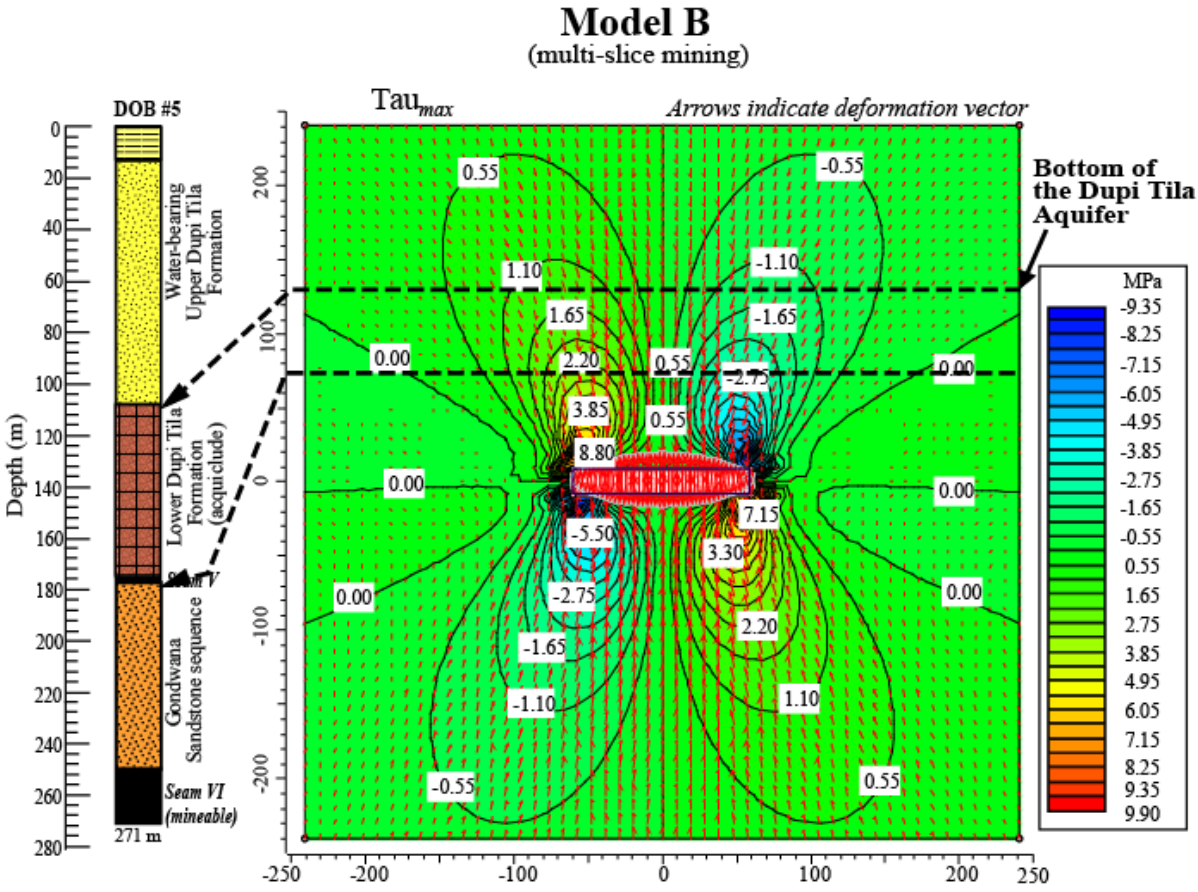

Fig. 4-11. Distribution of maximum shear stress contours (τ_{max}) within the Gondwana Sandstone Sequence (about 2.5-9 MPa), Lower Dupi Tila Aquiclude (about 1.4-2.5 MPa), and Upper Dupi Tila Aquifer about (0.55-1.4 MPa).

4.7. Discussion

4.7.1. Mining Methods

About 70–80% of thick coal seams are exploited by means of underground mining methods. Two mining methods, longwall and room-and-pillar, are generally used for the extraction of coal worldwide. Both of these methods are well suited to extracting the relatively flat coalbeds (or coal seams).

- The basic principle of longwall mining is simple. A seam is selected and blocked out into a panel averaging some meters in width, length, and height, by excavating passageways around its perimeter. Extraction by longwall mining is an almost continuous operation involving the use

of self-advancing hydraulic roof supports, a sophisticated coal-shearing machine, and an armored conveyor paralleling the coal face.

- In contrast, room and pillar mining operations involve cyclical, step-by-step mining sequences. The rooms are the empty areas from which coal has been mined, and the pillars are blocks of coal.
- Another method, Longwall Top Coal Caving (LTCC), has successfully been applied in China since the mid 1980s (Xie and Zhou, 2008). This is currently the method preferred in a number of other countries, especially Australia and Turkey. Production of thick seams using top coal caving is much simpler in comparison to slice mining and requires less development, consequently, the efficiency of production is significantly higher. For thick seams, multi-slice longwall mining is less convenient, less cost-effective, and requires more labor than longwall top coal caving (LTCC) methods (Xie et al., 1999;Yasitli and Unver, 2005; Unver and Yasitli, 2006; Simsir and Ozfirat, 2008).

In the Barapukuria coal basin, six coal seams have been discovered, among which only seam VI (about 36 m thick) has been considered for mining. If the coal thickness was around 3-10 m, single-slice to double-slice mining methods are promising. These types of mining are used in China, USA, Germany, Australia, UK, and India. Single to double-slice mining is not economically beneficial due to high thickness of coal in Barapukuria. Thus, the China National Machinery Import and Export Corporation (CMC) planned to use the multi-slice longwall mining method. For its operation, CMC divided seam VI into 16 panels with 6 slices. Seam VI is blocked out into a panel averaging nearly 120 m in width, 550 m to 900 m in length, and about 3.5 m in height, by excavating passageways around its perimeter. The ultimate height of the fracture zones would be about 22 m for the panel thickness of 3.5 m. The first-slice coal production commenced in 2005 and is continuing with different hazardous environments such as high temperature, humidity, large-caving on the roof, and huge water inflow from the roof.

4.7.2. Geological and hydrogelogical environments

In the Barapukuria basin, although seam VI is fairly flat-lying and extensive, the main problem is that the entire basin is affected by numerous faults and fractures. As described above, the basin is an intracratonic half-graben basin that is crossed by normal faults. The coal bearing

Permian Barapukuria Formation of the Gondwana Group forms a plunging syncline that sub-crops below the Plio-Pleistocene Dupi Tila Formation, which is the water-bearing formation overlying the mineable coal seam as well as the mine plan. Two major extensional faults (Fig. 4-2), Fa and Fb, are major controlling factors for water seepage into the mine (Wardell Armstrong, 1991). The Dupi Tila deposits are comprised of poorly consolidated to unconsolidated sands with high permeability ranging from 4.81 mD to 558 mD. Permeability within the Gondwana is considerably less (3.67 mD to 75 mD) than that of the overlying Dupi Tila aquifer. The upper coal seams have a permeability between 9.8 mD and 137.8 mD because these seams are comparatively soft and, to a varying extent, are in hydraulic continuity with the Upper Dupi Tila aquifer. Seam VI has permeability in the range from 13 mD to 119 mD (Wardell Armstrong, 1991; Islam and Hayashi, 2008a).

Wardell Armstrong Mining Consultants of the United Kingdom carried out pump-tests and sectional-tests to estimate the hydraulic conductivity of the Dupi Tila aquifer and the Gondwana aquifer, respectively. In the Dupi Tila aquifer, the estimated results range from 160-260 m/d for the entire thickness of about 110 m (see Figs. 10ab, borehole DOB#5). Estimated hydraulic conductivity for the Gondwana aquifer is 31 m/d for the entire thickness of about 100 m. The permeability value of the Lower Dupi Tila aquiclude is about 0.15 mD (Wardell Armstrong, 1991).

During the development period (2001-2004) of the mining tunnels in Barapukuria, it was observed that the water inflow rate increased simultaneously with the mining. The water inflow rate in August 1998 was about 620 m^3/hr when the underground mine tunnel length was about 1200 m. In November 2004, it increased up to about 1300 m^3/hr, while the developed tunnel length was about 19,000 m (Islam and Islam, 2005). At present, the total inflow rate is about 1500 m^3/hr (Monthly Progress Report, Barapukuria Coal Mining Co. Ltd, June 2008). This indicates that there is a direct relationship between the opening of the underground mine and the inflow rate of water from the Dupi Tila Formation through coal seams into the excavated mine face.

4.7.3. Model A: influence of proximity to failure of elements and shear stresses

Several major factors, such as overburden pressure or stress, water pressure, geologic structures, and mining parameters control water inrushes (Zhang, 2005). Geologic structures,

particularly faults, play a great role for water inrush. More than 163 longwall mining faces in northern China (Zhang, 2005) have been inundated by major water inrushes that were related to faults. Rock strength in the fault zone is much lower than that of normal rocks. Therefore, rocks in faulted zones fail more easily, and create a larger failure zone.

The tensional failure of elements in our model is concentrated within the Gondwana coal sequences and around the faulted zone EBF, which finally reaches the bottom of the water-bearing Dupi Tila Formation (Fig. 4-6c). The proximity to failure of elements indicates the presence of low strength zones within the coal basin and diverse faults, fractures, and joints that interconnect these zones. Thus, the model shows very good consistency with the observed structural deformation of the coal basin. Our simulation results indicate a potential of water inflow hazard for underground mining because the existence failed elements below the Dupi Tila Formation indicate that some fractured/faulted zones may reduce the distance between the mining face and the aquifer (see Fig. 4-6c, and DOB#9). When faulted/fractured zones are permeable and reach the aquifer, it can cause water inflow once the faults/fractures are exposed by mining. Inflow into the Upper Dupi Tila aquifer may be controlled by the comparatively smaller hydraulic conductivity and permeability of the Gondwana aquifer and the Lower Dupi Tila aquiclude as mentioned in Section 4.7.2.

Shear stress bands are higher along the faulted zone EBF, whereas they are gradually decreased away from the fault. Most of the deformation is observed in a narrow shear zone when τ_{max} ranges from 60 to 65 MPa (Fig. 4-5c). The result shows upward bending effects of the shear stress contours within the Gondwana Formation, where the mining depth ranges from 290 m to 420 m. This indicates that after extraction of large amounts of coal, upward bending would cause numerous large-scale deformations to develop. In addition, zones of fissures/fractures would be developed because of the redistribution of the mining-induced stress field (Islam and Islam, 2005). If multi-slice mining is considered, fracturing of the overburden rock strata would propagate up to the bottom of the Dupi Tila aquifer system (Fig. 4-6c and DOB#9), and would cause a serious water inflow hazard.

4.7.4. Model B: stress distribution of the overburden strata

Model B built can be used to answer the questions of what the relative propagations of fracture towards the roof would be, and if it would generate any problems for mine production.

The model illustrates the impact of the mining-induced stress pattern after the extraction of the single-slice and multi-slice mining. The magnitudes and distribution of minimum compressive stress, σ_3, and the mean stress contours (Figs. 4-9, and 4-10) specify that the intense fracturing of the overburden strata would extend more than 240 m upward. The deformation that occurred at the roof and floor were calculated to be much higher than that on the sidewalls. The deviatoric stress pattern indicates the extent of propagation of the fractured zone as well as the strata subsidence. The deformation vectors indicate that the water-bearing Dupi Tila Formation is vulnerable to being intersected by fractures extending from the roof of the mine.

Fig. 4-11 shows how shear stress changes with the height of an 18 m mining excavation. Notice that shear stress in the roof of the excavation is lower than that in the rib sides. Comparatively higher shear stress concentrations appear near both rib sides of the excavation. In the Gondwana sandstone sequence, which lies immediately above the excavation, the contour value of the shear stress ranges from about 2.5 to 9 MPa. For the Lower Dupi Tila aquiclude and the Upper Dupi Tila aquifer, these values ranged from 1.4 to 2.5 MPa, and 0.55 to 1.4 MPa, respectively.

The safety of the mine is highly dependent on the behavior of overlying rock strata. The 18 m excavation height, as shown in Fig. 4-11, has an influence over the degree and nature of shear stress redistribution around the excavation face. If the Lower Dupi Tila aquiclude, which is very loose, clayey, and unconsolidated, fails due to shear stress (1.4 to 2.5 MPa), it could have adverse effects on the Upper Dupi Tila aquifer.

Determination of stress-depended hydraulic conductivity in the working faces of the Barapukuria coal mine has not yet been carried out. Zhang and Shen (2004) observed that when a coal mine is under an aquifer, the hydraulic conductivity is related to different mining widths. They simulated a model where the depth of the overburden rock strata was 90 m. Their FEM simulation revealed that when the mining width was 220 m, the maximum vertical height of the failure zone in the overlying strata was 42.5 m due to an excavation height of 4 m. Their result suggests that water will flow into the working area when the distance between the coal seam and the aquifer is less than this magnitude. When the mining width was 120 m, then the failure zone in the overlying strata reduced to 30.5 m. They also emphasized that if the aquifer is located directly above the overlying strata, hydraulic conductivity in the vertical direction will dominate

the water flow (Zhang and Shen, 2004). Further study is required in the Barapukuria mine to detect hydraulic conductivity with different mining widths.

For the 120 m width multi-slice mining in Barapukuria, the fracture intensity would be greater than for single-slice mining. If multi-slice longwall mining continues, modeling suggests that damage could occur to the water-bearing Dupi Tila formation. The stress distribution and fracture intensity also indicate serious roof subsidence with deep sinks on the surface. "Hydraulic sand stowing" can be considered as a remedial shield to reduce fracture development, roof subsidence, and the associated potential for water inflow hazards by reducing mining-induced stress from 13.3 MPa to 6.5 MPa. This practice is well-developed in some Indian coal mines such as the Lachhipur, Samla, and Madhusundanpur collieries (Singh et al., 1996).

4.7.5. Model C: strength of rock strata

The results of the numerical analyses were found to be comparable with model C. The model was constructed based on the rock strength factor to understand height of fractures caused by the underground mining. This strength factor was taken from study results of UK coal mines. The rock strength of the Barapukuria Gondwana strata is weak to medium (Wardell Armstrong, 1991). The height of the fracture zones would be about 22 m for weak-strength strata and 37 m for medium-strength strata, respectively, for the panel thickness of 3.5 m (Fig. 4-12a). If multi-slice (six slices) extraction is considered, the panel height would be about 21 m. In this case, the height of the caving/fracture zones would be about of 132 m for weak-strength strata and 222 m for medium-strength strata due to successive roof subsidence of the overburden strata. This result shows good agreement with our simulated model results, where model A indicates tensional failure of elements ranging between 130-520 m depth (Fig. 4-6c), and model B indicates that the effective range of the deviatoric and deformation vector propagation are more than 240 m upward (Figs. 4-9c-d, and 4-10c-d).

4.7.6. Environmental Impacts

Longwall mining is sometimes considered to be destructive or environmentally unsafe because it causes the land above the mined-out panel to sink. At present, large-scale land subsidence has occurred at Kalupara village, south-southeast of the Barapukuria mine, due to

extraction of a 3 m high section of mining panel 1101 (Fig. 4-7). Note that some of the Kalupara village is located just above the 1101 mining panel, from where coal extraction had already been completed by 2006. The 1101 mining panel is about 900 m length. At present, the 1103 mining panel, which is parallel and just east of the 1101 panel, is under consideration for extraction. If in the future multi-slice (about 18 m thick) coal is extracted, at the same time equal heights of land subsidence can be expected to occur. Finally, this adverse effect can damage underground water tables, structures at the surface, and can cause erosion of soil.

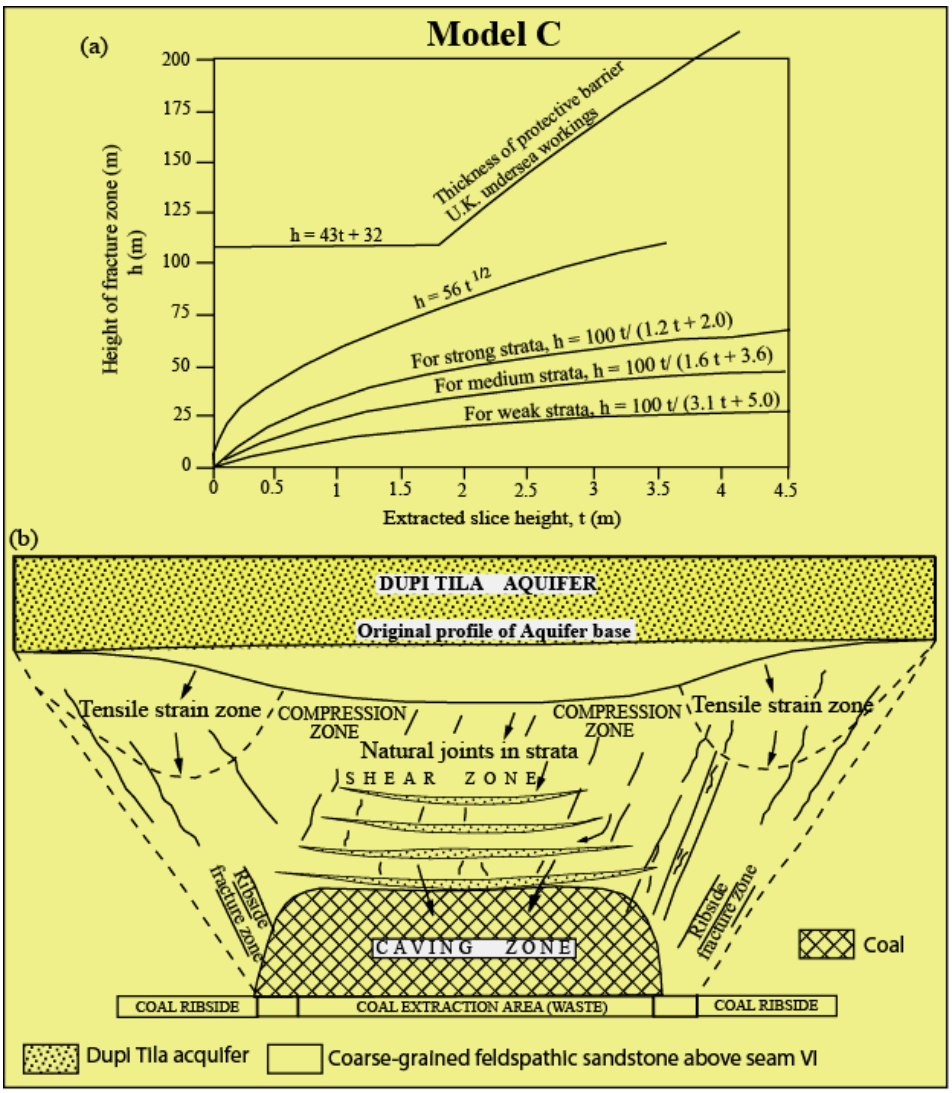

Fig. 4-12. (a) Model C predicts the formula for determining the height of fracture-zones (h) above a longwall mining face for various thicknesses, t (m) of extraction (modified after Whittaker et al., 1992). For the Barapukuria mine, the initial thicknesses of extraction is 3 m. (b) Principal stress zones above longwall mining panel showing potential water inflow paths from a groundwater aquifer (modified after Wardell Armstrong, 1991).

4. 8. Conclusions

(1) This chapter presents a case study of real problems encountered at the Barapukuria underground coal mine. Deformation and failure characteristics were investigated by numerical analysis.

(2) Model A demonstrated that there is a zone of tension resulting from horizontal extension within the coal-bearing Gondwana Formation and around the EBF. This is in agreement with the recorded field observations of Wardell Armstrong (1991).

(3) Model B increased the confidence in our interpretation of the influence of the fracture propagation as a function of the mining sequence. This study supports the hypothesis that the stress redistribution around the coal extraction panel is probably sufficiently altered to induce deformation along the major geological structures like faults and fissures.

(4) The upward bending contours of the deviatoric stress pattern may form a destructive zone and would create preferential flow paths for water into the excavated panel. On a larger-scale, observations of land subsidence near the village of Kalupara also indicate that vertical groundwater flow close to the damage zone is enhanced, which results in discharge of the underlying aquifers.

(5) Therefore, it is reasonable to focus that multi-slice longwall mining in Bangladesh is difficult. The major problems are related to water inflow, damage of aquifers, and the destruction of a large extent of very high productivity agricultural lands.

References

Aksoy, C.O., Onargan, T., Yenice, H., Kucuk, K., Kose, H., 2006. Determining the stress and convergence at Beypazari trona field by three-dimensional elastic-plastic finite element analysis: A case study. International Journal of Rock Mechanics & Mining Sciences 43, 166-178.

Alam, M., Alam, M. M., Curray, J., Chowdhury, R. M. L. R., and Gani, M. R., 2003. An overview of the sedimentary geology of the Bengal Basin in relation to the regional tectonic framework and basin-fill history. Sedimentary Geology 155, 179-208.

Anderson, E.M., 1951. The Dynamics of Faulting and Dyke formation with application to Britain, 2nd edi. Oliver and Boyd, Edinburgh.

Bakr, M.A., Rahman., Q.M.A., Islam, M.M., Islam, M.K., Uddin, M.N., Resan, S.A., Haider, M.J., Islam, M.S., Ali, M.W., Choudhury, M.E.A., Mannan, K.M., and Anam, A.N.M.H., 1996. Geology and Coal Deposits of Barapukuria Basin, Dinajpur District, Bangladesh, Records of Geological Survey of Bangladesh. 8, pt 1.

Booth, C.J., 1986. Strata-movement concepts and the hydrogeological impact of underground coal mining. Ground Water 24, 507-515.

Bott, H.P.R., 1997. Modeling the formation of a half-graben using realistic upper crustal rheology. Journal of Geophysical Research 102, 24605-24617.

Contreras, J., Scholz, C.H., King, G.C.P., 1997. A general model of rift basin evolution: constraints of first order stratigraphic observations. Journal of Geophysical Research 102, 7673-7690.

Corthesy, R., Leite, M.L., Gill, D.E., Gaudin, B., 2003. Stress measurements in soft rocks. Engineering Geology 69, 381-397.

Gibson, J.R., Walsh, J.J, and Watterson, J., 1989. Modeling of bed contours and cross-sections adjacent to planar normal faults. Journal of Structural Geology 11, 317-328.

Hart R., 2003. Enhancing rock stress understanding through numerical analysis. International Journal of Rock Mechanics & Mining Sciences 40, 1089-1097.

Hayashi, D., 2008, Theoretical basis of FE simulation software pakage. Bull. Fac. Sci. Univ. Ryukyus 85, 81-95 (http://ir.lib.u-ryukyu.ac.jp/).

Hill, J. G., and Price, D. R., 1983. The impact of deep mining on an overlying aquifer in western Pennsylvania. Ground Water Monitor Rev. 3, 138-143.

Islam, M.R., 2005. Influence of tectonic structures for the occurrence of gas emission at 1110 working panel in Barapukuria Coal Mine, Bangladesh. Geodynamics and Environment in East Asia (GEEA), International Conference & 5th Taiwan-France Earth Science Symposium, 24-29 November, 2005, Taitung, Taiwan, pp.155-156.

Islam, M.R., and Islam, M.S., 2005. Water Inrush Hazard in Barapukuria Coal Mine, Bangladesh. Bangladesh Journal of Geology 24, 1-17.

Islam, M.R., and Kamruzzaman, A.B.M., 2006. Geochemical and Techno-environmental Behaviour of Gondwana Coals from the Barapukuria coal mine, Bangladesh. Bangladesh Journal of Geology 25, 48-63.

Islam, M.R., and Hayashi, D., 2007. FEM simulation of fold-and-thrust belts in the Southern Central High Andes of Chile and Argentina. Bull. Fac. Sci. Univ. Ryukyus 83, 29-60.

Islam, M.R., and Hayashi, D., 2008a. Geology and coal bed methane resource potential of the Gondwana Barapukuria Coal Basin, Dinajpur, Bangladesh. International Journal of Coal Geology 75, 127-143.

Islam, M.R., and Hayashi, D., 2008b. Extensional stresses in the fold-and-thrust belt of the Southernmost Andes. Bullettino di Geofisica Teorica ed Applicata 49, 223-228.

Kim, J.M., Parizek, R. R., and Elsworth, D., 1997. Evaluation of Fully-Coupled Strata Deformation and Groundwater Flow in Response to Longwall Mining. International Journal of Rock Mechanics & Mining Sciences 34, 1187-1199.

Khan, F.H., 1991. Geology of Bangladesh, 33-40 pp, Willey Eastern Limited, 4835/24 Ansari Road, Daryaganj, New Delhi 110002, India.

Khan, A. A., and Chouhan, R. K. S., 1996. The crustal dynamics and the tectonic trends in the Bengal basin, Journal of Geodynamics 22, 267-286.

Liu, L., and Zoback, M. D., 1992. The effect of topography on the state of stress in the crust: Application to the site of the Cajon Pass Scientific Drilling. Journal of Geophysical Research 97, 5095-5108.

Melosh, H. J., Williams, C.A., 1989, Mechanics of graben formation in crustal rocks: A Finite Element analysis. Journal of Geophysical Research 94,13961-13973.

McKinnon, S.D., 2001. Analysis of stress measurements using a numerical model methodology. International Journal of Rock Mechanics & Mining Sciences 38, 699-709.

Morley, C.H., 1999. Pattern of displacement along large normal faults: Implications for basin evolution and fault propagation, based on examples from east Africa. AAPG Bulletin 83, 613-634.

Obara, Y., Nakamura, N., Kang, S.S., Kaneko, k., 2000. Measurement of local stress and estimation of regional stress associated with stability assessment of an open-pit rock slope. International Journal of Rock Mechanics & Mining Sciences 37, 1211-1221.

Simsir, F., and Ozfirat, M.K., 2008. Determination of the most effective longwall equipment combination in longwall top coal caving (LTCC) method by simulation modeling. International Journal of Rock Mechanics & Mining Sciences 45, 1015–1023.

Singh, R., Singh, T.N., Dhar, B.B., 1996. Coal pillar loading in shallow mining conditions. International Journal of Rock Mechanics & Mining Sciences 33, 757-768.

Stephansson, O., and Berner, H., 1971. The finite element method in tectonic processes. Phys. Earth Planet. Interiors 4, 301-321.

Talukder, M. W., and Hayashi, D., 2006. Numerical simulation of faults in Southern Bolivian and Northern Argentinean Orocline, Central Andes. Bull. Fac. Sci. Univ. Ryukyus 81, 41-70.

Unver, B., and Yasitli, N.E., 2006. Modelling of strata movement with a special reference to caving mechanism in thick seam coal mining. International Journal of Coal Geology 66, 227– 252.

Wardell Armstrong, 1991. Techno-Economic Feasibility Study of Barapukuria Coal Project (unpubl.), Dinajpur, Bangladesh.

Whittaker, B.N., Singh, R.N., Sun, G., 1992, Rock Fracture Mechanics; Principles, Design, and Applications, Elsevier, p.570.

Xu, T., Tang, C.A., Yang, T.H., Zhu, W.C., Liu, J., 2006. Numerical investigation of coal and gas outbursts in underground collieries. International Journal of Rock Mechanics & Mining Sciences 43, 905-919.

Yang, T.H., Liu, J., Zhu, W.C., Elsworth, D., Tham, L.G., Tang, C.A., 2007. A coupled flow-stress-damage model for groundwater outbursts from an underlying aquifer into mining excavations. International Journal of Rock Mechanics & Mining Sciences 44, 87-97.

Yasitli, N.E. and Unver, B., 2005. 3D numerical modeling of longwall mining with top-coal caving. International Journal of Rock Mechanics & Mining Sciences 42, 219–235.

Xie, H., Chen, Z., and Wang, J., 1999. Three-dimensional numerical analysis of deformation and failure during top coal caving. International Journal of Rock Mechanics and Mining Sciences 36, 651-658.

Xie, H., and Zhou, H.W., 2008. Application of fractal theory to top-coal caving. Chaos, Solitons and Fractals 36, 797–807.

Zhang J., and Shen, B., 2004. Coal mining under aquifers in China: a case study. International Journal of Rock Mechanics & Mining Sciences 41, 629-639.

Zhang, J., 2005. Investigations of water inrushes from aquifers under coal seams. International Journal of Rock Mechanics and Mining Sciences 42, 350-360.

Zoback., M. L., 1992. First and second-patterns of stress in the lithosphere: the world stress map project. Journal of Geophysical Research 97, 11703-11728.

Zoback., M. L., and Zoback., M., 1980. State of stress in conterminous United States. Journal of Geophysical Research 85, 6113-6156.

Chapter 5

Simulation of stress distributions and displacements around an entry roadway with igneous intrusion and mining hazards associated with seam gas emission of the Barapukuria Coal Mine

Chapter 5

Simulation of stress distributions and displacements around an entry roadway with igneous intrusion and mining hazards associated with seam gas emission of the Barapukuria Coal Mine

5.1. Introduction

Gas emission from coal seams is a major safety hazard in underground coal mines (Karacan et al., 2008). Up to 90 percent of the methane gas that enters longwall mining may come from adjacent seams. If the coal seam is influenced by mining activities, the seam gas, which is mostly methane, can be emitted into the coal mine. When an underground roadway is excavated into tectonically-stressed coal deposits, the natural stress in the vicinity of the new opening is redistributed. Due to the redistribution of mining-induced stresses, the gas permeability of the coal strata is substantially increased by the development and dilation of joints, bedding planes, fractures, and faults. Various aspects of mine-related stresses, gases and geologic structures have been examined in a worldwide review of the problem of gas emission in coal mines (e.g., Shepherd et al., 1981; Zhang, 1986; Shen and Stephansson, 1994; Lunarzewski et al., 1996; Clayton, 1998; Lunarzewski, 1998; Noack, 1998; Bibler et al., 1998; Zhi et al., 2007; Jia et al., 2007; Karacan et al., 2008; Islam et al., 2009). Based on recent geologic studies of gas emission sites, geologic structures have been identified as a major factor in the occurrence of gas emission (Saghafi et al., 2008). Thrusts, strike-slip faults, normal faults, igneous intrusions, and recumbent fold hinges, which are referred to as 'tectonic disturbances,' are related to highly-fractured coal and thought to cause gas emission hazards (Shepherd et al., 1981; Saghafi et al., 2008). Anomalous stress and gas conditions seem to exist in and around these geologic structures. At such sites, mining-induced fracture systems and abnormally high gas emissions have been recorded (Shepherd et al., 1981).

The process of mining has two main impacts on the production of gas. The first is the internal disruption of coal within the coal seam by extensive fracturing. The second is the opening of pathways through the strata that enable the gas to leave the confines of the seam (Jackson and Kershaw, 1996). The generation and propagation of fracture sets and systems

depend on the fabric configuration and composition of the coals and surrounding rocks involved in the deformation events. The influence of the strata deformation processes on the rock mass is

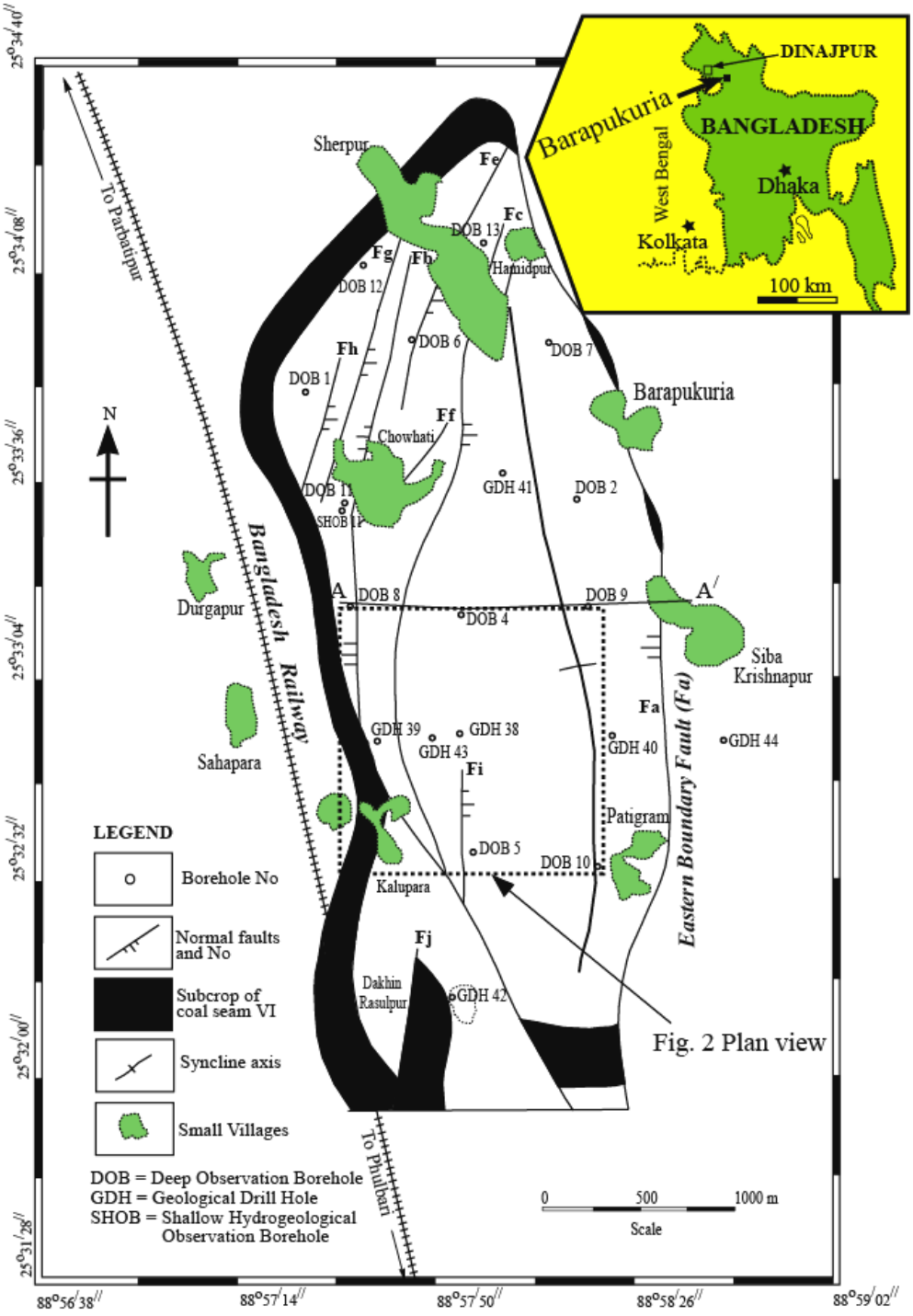

Fig. 5-1. Location of the boreholes, major faults, and structural pattern of the Barapukuria Coal Basin, Northwestern Bangladesh. Abbreviations: DOB=Deep Observation Borehole; GDH=Geological Drill Hole; SHOB=Shallow Hydrogeological Observation Borehole (after Wardell Armstrong, 1991; Bakr et al., 1996; Islam and Hayashi, 2008; Islam et al., 2009).

quite distinct and occurs in the micro- and meso-scopic states. Existing and mining-induced fractures open and develop, maintaining characteristic fracture zones. Mining processes can thus create sudden and unstable gas emission events, which may lead to hazardous underground atmospheric conditions. Seam gas can be released from inactive and active gas resources in either virgin or relaxed strata both prior to and during mining activities (Lunarzewski et al., 1996; Lunarzewski, 1998).

Barapukuira Colliery (Fig. 5-1) is located in the Dinajpur district in the northwest part of Bangladesh. The high volatile B bituminous rank coals of the Barapukuria basin were formed during the Early Permian period (~250 million years ago). Islam and Hayashi (2008) estimated the reservoir gas conditions of the coal seams in the Barapukuria basin. The estimated average gas contents of 8.20 m^3 t^{-1} for seams I to VI and, the resultant estimated total gas resource at Barapukuria is 5135.32 Mm^3. The coal is considered to be part of the coal-bearing Gondwana Formations of northeastern Indian coalfields. The regional geotectonic setting, stratigraphy, depositional systems and geology of the Barapukuria coal deposits are well documented (Islam and Hayashi, 2008). The coalfield consists of seams I to VI, of which the lower seam VI is being mined. The thickness of seams varying from 1 m to 42 m, interbedded with siltstones, sandstones, subordinate carbonaceous shales, and carbonaceous mudstone layers (Islam and Hayashi, 2008; Islam et al., 2009).

In the Barapukuria Group of rocks, the formations from bottom to top are Pre-Cambrian basement, Barapukuria Gondwana Formation (BGF), Dupi Tila Formation (DTF), and Madhupur Clay Formation (MCF). Out of these, only Barapukuria Gondwana Formation is coal-bearing. The Madhupur Clay Formation, varying in thickness between 1-15 m, is the uppermost stratigraphic sequence of the basin. It consists of clay, very fine silt and sand. The basin is entirely covered by an unconformable envelop of between 100–220 m of the Dupi Tila Formation (DTF). This water-bearing formation is comprised mainly of medium to coarse-grained sandstones with some siltstones. The upper coal sequence (seams I to V) occurs at varying depth from 133–336 m, and is comprised of an interbedded sequence of fine to coarse quartzo-feldspathic sandstones with subordinate horizons of siltstone and mudstone. Seams II and IV appear to be the most laterally, varying in thickness between 2.5–15 m. Seams III and V are laterally variable, varying in thickness between 0.30 -10 m. Seam VI roof sandstones are comprised of 15 m to 140 m of relatively homogeneous and, medium to coarse-grained

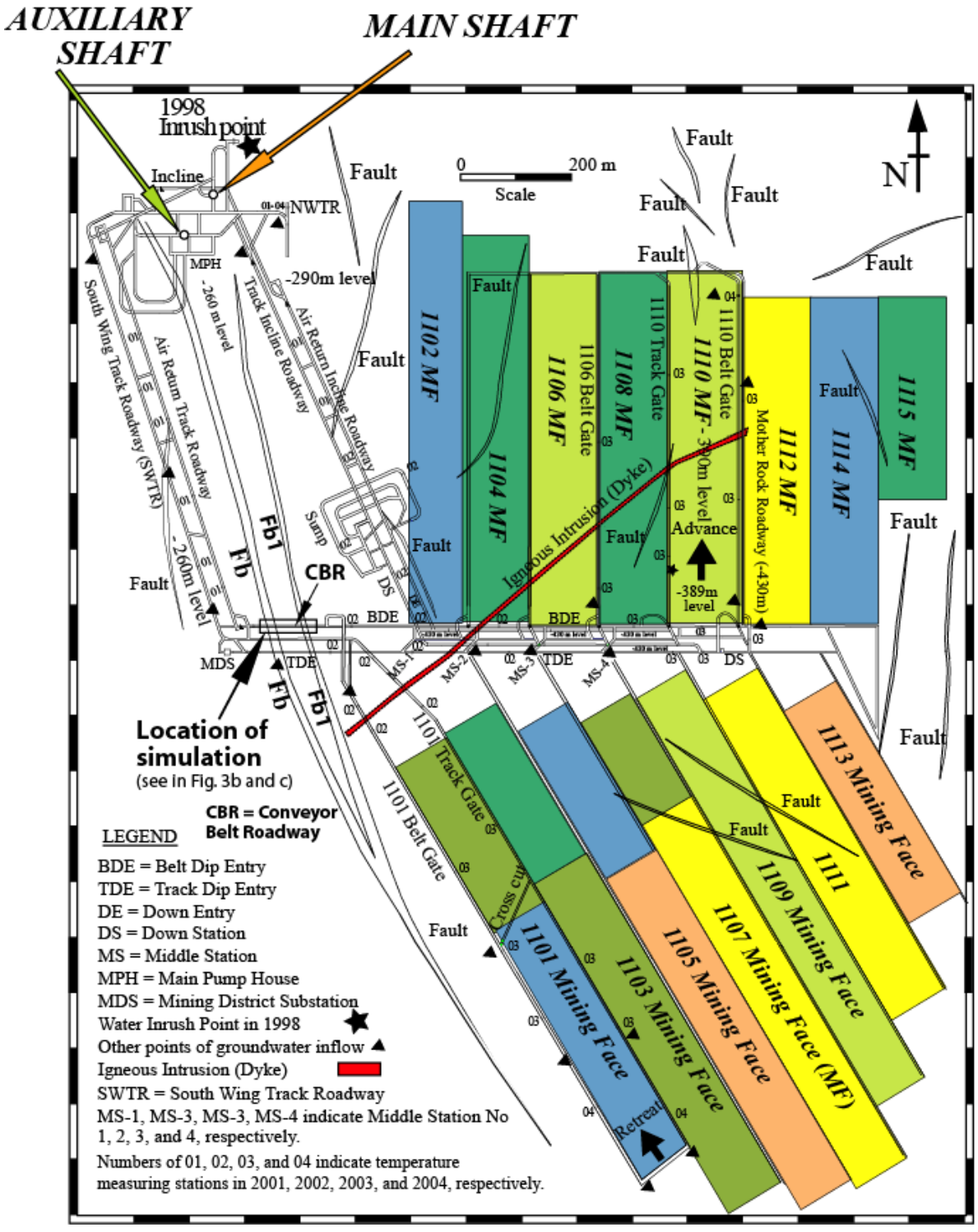

Fig. 5-2. Plan view (from levels -260 m to -420 m) of the Barapukuria Coal Mine (see location in Fig. 5-1). The big asterisk shows the position of water inrush that happened in 1998. The solid delta shows water inflow measuring points. The total inflow comes from different faces and increases simultaneously with mining excavation (after Islam and Hayashi, 2008; Islam et al., 2008). The present study is emphasized in and around the location of Fig. 5-3.

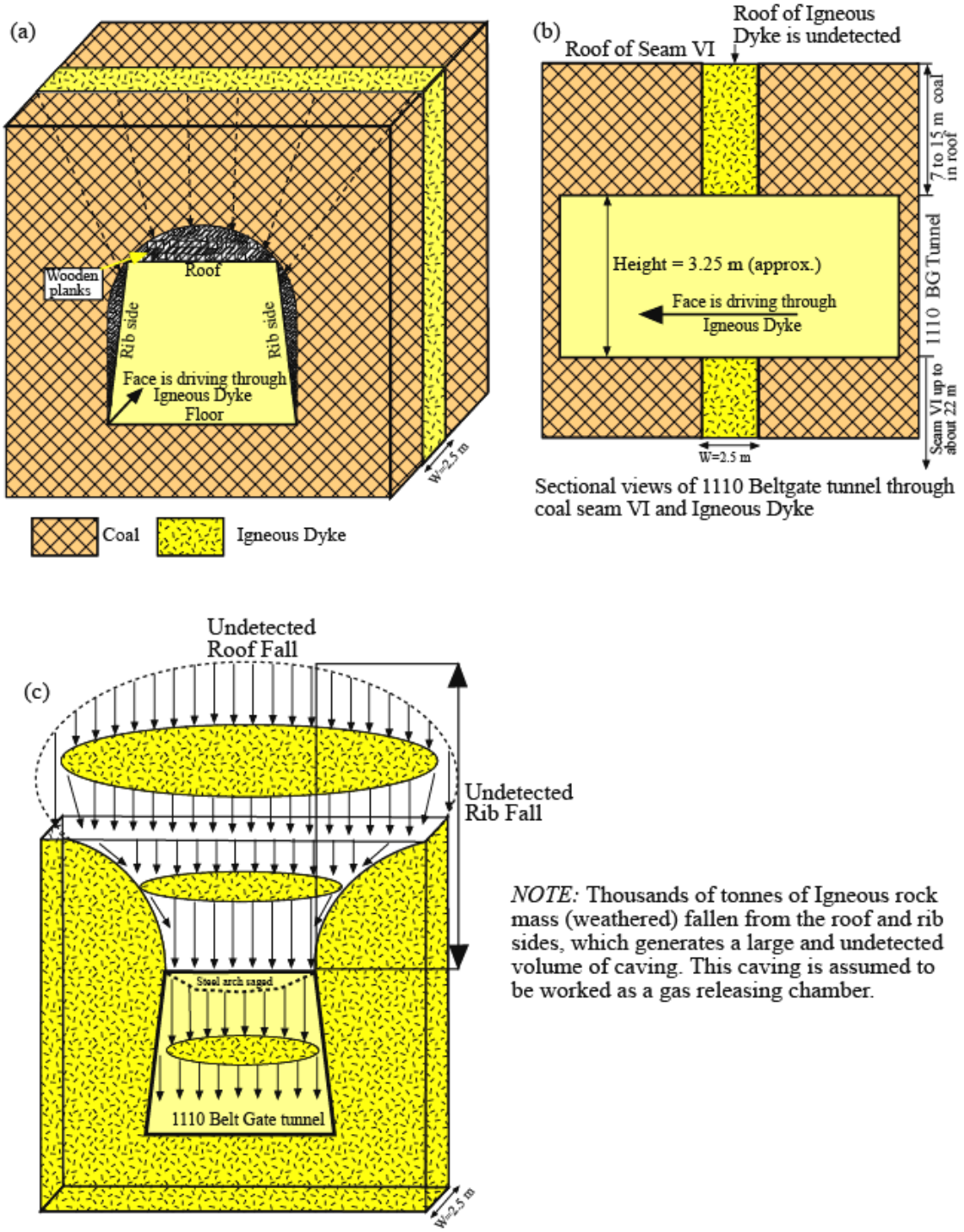

Fig. 5-3. (a) Three-dimensional schematic views of the #1110 belt gate roadway. Initial horseshoe-shaped roadway is reformed to trapezoid-shaped roadway after using steel arches. Some wooden-planks were used to the roof and the both rib sides to fill the caving. Arrows with dash indicate water seepages, which were generated after blasting operations and redistributions of stresses. (b) Sectional views of the #1110 belt gate roadway through coal seam VI and Igneous Dyke. (c) Schematic views to show how roof rock mass of igneous dyke falls and creates large volume of caving at the roof.

sandstones, conglomerates, and gritstones. The thickest Seam VI varies across the basin from 22 m to more than 42 m (average 36 m), and is usually overlain and underlain by thick sandstones. The sequence underneath seam VI is significantly dissimilar from the Gondwana sequence above it, and consists of an interbedded sequence of sandstones, siltstones, and mudstones (Islam and Hayashi, 2008).

In Barapukuria coal mine, emission of methane was observed in an access roadway (see in Fig. 5-2, face #1110) in 2005 (Islam, 2005; Islam and Hayashi, 2008). Numerous extensive fractures and tectonic faults, ranging in size from less than 1 m to 3 m, affect the thickest coal seam (seam VI) of the Barapukuria coal basin. In addition, a long igneous intrusion (dyke) (Fig. 5-2) has been detected throughout roadways under development. When the #1110 gate roadway crossed over an igneous intrusion, a tremendous roof fall occurred and distorted the original shape (Figs. 5-3a-b) of the mining roadway. Thousands of tons of overburden rocks and coal partings containing minor amounts of water were released from the roof and created an undetectable volume of caving (Fig. 5-3c).

The presence of the caving means that the weight of rock above can no longer be supported and thus the stresses in the surrounding rocks are thrown outwards into the strata at the edges of the excavation. The concentration of very large stresses at the edges of the excavation geometry can lead to failure, displacing the peak stress some meters toward the roof, floor and both rib sides. It is assumed that the relaxation of coal strata at the roof, floor, and rib sides allows gas to flow from all gas sources to the underground mine. However, the mining-induced stress patterns and deformation of coal strata related to the tectonic disturbances from the excavation geometry of the gate roadway remain uncertain. The gate roadway will remain closed until December 2008. The intensity of the gas and water inflow depends on the type and strength of the rocks and the degree of strata relaxation.

In this study, the strata relaxation around an entry roadway and the seam gas emission of the Barapukuria coal mine have been modeled using the boundary element method. This computer-based numerical simulation provides an approach to estimate the pattern of strata relaxation in the floor, roof, and rib sides strata and to predict gas emissions associated with longwall mining activities. The two major objectives are:

- to recognize the strata relaxation zones around the roof, floor, and both rib sides due to mining-induced stress, and

- to interpret some potential explanations for the enhanced gas emission, including geological structures, coal thickness at the roof and floor, and mine ventilation systems.

5.2. Geologic conditions of the working face

The geologic conditions of the Barapukuria coal deposit were illustrated in detail by Wardell Armstrong (1991), Bakr et al. (1995), Islam and Hayashi (2008), and Islam et al. (2009). The stratigraphic sequence of the coal deposit is divided into four formations on the basis of age and lithology:

- Madhupur clay from the recent Holocene era,
- a water-bearing Dupi Tila aquifer of Late Miocene-Middle Pliocene age,
- Permian coal-bearing Gondwana rock sequences,
- Igneous intrusion (dyke) of Lower Cretaceous period (Singh et al., 2008), and
- Pre-Cambrian Archean basement.

In this study, only the geologic conditions of the #1110 belt entry roadway are illustrated. The #1110 working panels consist of two roadways: the 1110 belt entry to the east and the 1110 track entry to the west (Fig. 5-2). A detailed geologic map (Fig. 5-4) was prepared during the roadway excavation based on roadway face observations by the author. Although only 37 faults were detected by the seismic survey done by Wardell Armstrong Mining Consultant of the United Kingdom, abundant micro-faults (throw 1-3 m) were detected inside the coal seam during development of the juncture of the working roadway. The intensities of joints (2-3 m^{-1}), fractures (7-10 m^{-1}) and cavities (0.5-1.5 m) were high.

Physically, the coal had low specific gravity, was brittle, was easily friable, had a vitreous to sub-vitreous luster, and was associated with accessory minerals like chalcopyrite and pyrite. No ductile coal laminations were found at the roadway, but highly brittle and granular coal laminations were observed at the roof and the floor. A thick layer of coal (>15 m) was found over the roof of the #1110 belt gate roadway, extending 520 m from its starting point. About 22 m thick coal exists to the floor (Figs. 5-3b and 5-4). During drilling operations intended to detect the roof of coal seam VI, the roof was found to be structurally deformed and associated with intense sub-folds (Islam, 2005). The China National Machinery Import and Export Corporation

(CMC) detected some sub-folds and numerous small-scale faults within the coal seam and the overlying rock sequences during probe drilling operations and roadway advancement.

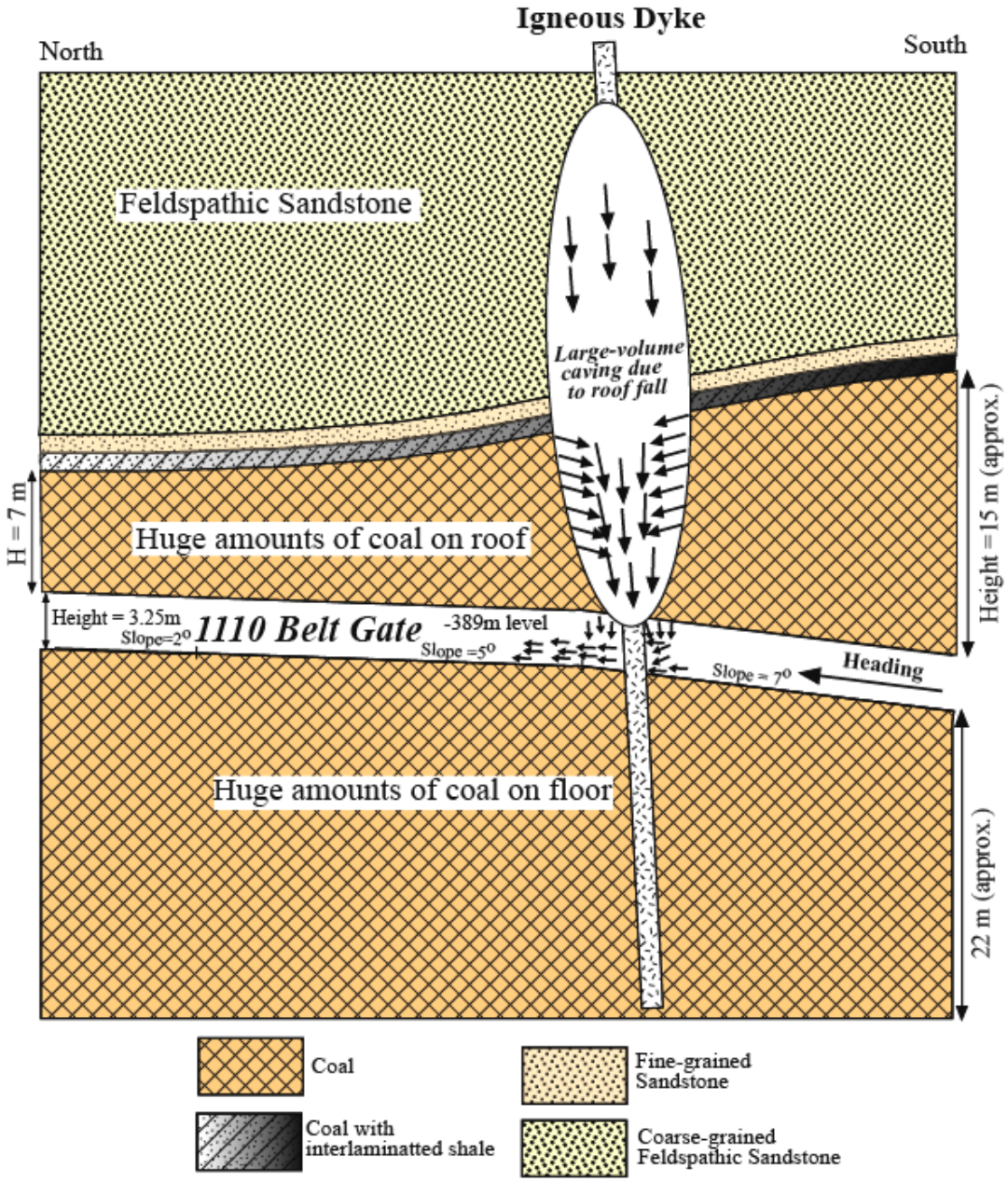

Fig. 5-4. Geologic conditions of the #1110 belt gate roadway (length about 520 m). About 15 m height coal remains at the initial point of the entry and this finally ends about 7 m coal to the roof. This high thickness of coal seams towards the roof and floor create highly fractured and porous media after redistribution of mining-induced stress field along the roadway. Arrows in oval-shaped cave show how gas accumulates from surrounding fractures and porous coals and finally flow into the roadway.

The #1110 belt entry was the first location where gas emission occurred. Methane emissions happened at the end of 2005, and the entry remains fully closed. The buried depth of the working face is 420 m, the coal seam thickness is 36 m, and the coal seam is gently inclined with a dip angle of 15-18^{o}. The roadway height within the coal seam is 3.25 m, and the rocks of the roof are mudstones and clay, coal with interlaminated shales, fine-grained sandstones, and coarse-grained feldspathic sandstones. The immediate roof is clay rock about 0.2-0.3 m thick.

The key and problematic structure in this entry is an igneous dyke. This dyke was not recognized by the Wardell Armstrong Mining Consultant of the United Kingdom at the time of the seismic survey; it was first detected during roadway advancement mining at the #1101 track entry. It was subsequently found at the #1106 track and belt entries and the #1110 track and belt entries (Fig. 5-2). The width of the dyke, nearly 2.5 m, was similar in each entry. At the #1110 entry section, a large and undetectable volume of cave was generated at the roof (Figs. 5-3c and 5-4) due to continuous roof fall (Islam, 2005; Islam and Islam, 2005).

There remains some uncertainty as to whether the origin of the Barapukuria dyke is sedimentary or igneous. A separate study using isotope analysis is needed to address this question. I assume the dyke is linked to igneous intrusion (Islam, 2005) because similar igneous dykes are frequently found in the Gondwana coalfields of India (Singh et al., 2008), Australia (Gurba and Weber, 2001; Golab and Carr, 2004; Golab et al., 2007; Wold et al., 2008), China, Vietnam, Botswana, Uganda, and South Africa. These intrusions are a result of post-depositional volcanism into the rift basins (e.g., Gudmundsson and Loetveit, 2005) and coal seams (e.g., Saghafi et al., 2008). The physical behavior of the dyke material is extremely variable. It is usually moderately hard when dry but very loose when in contact with water (Islam, 2005; Islam and Hayashi, 2008).

5.3. Numerical modeling

In this study, the boundary element method (BEM) was used to predict mining-induced strata deformation and stress dependent parameters. Models were constructed according to the state of plane strain and results were illustrated using the Examine2D software package (www.rocscience.com). All models (Fig. 5-5) considered the vertical cross-section of the mining excavation with proposed geometry, support system, and roof fall occurrence corresponding to

an overburden thickness of about 420 m. The imposed mechanical rock parameters are shown in Table 5-1.

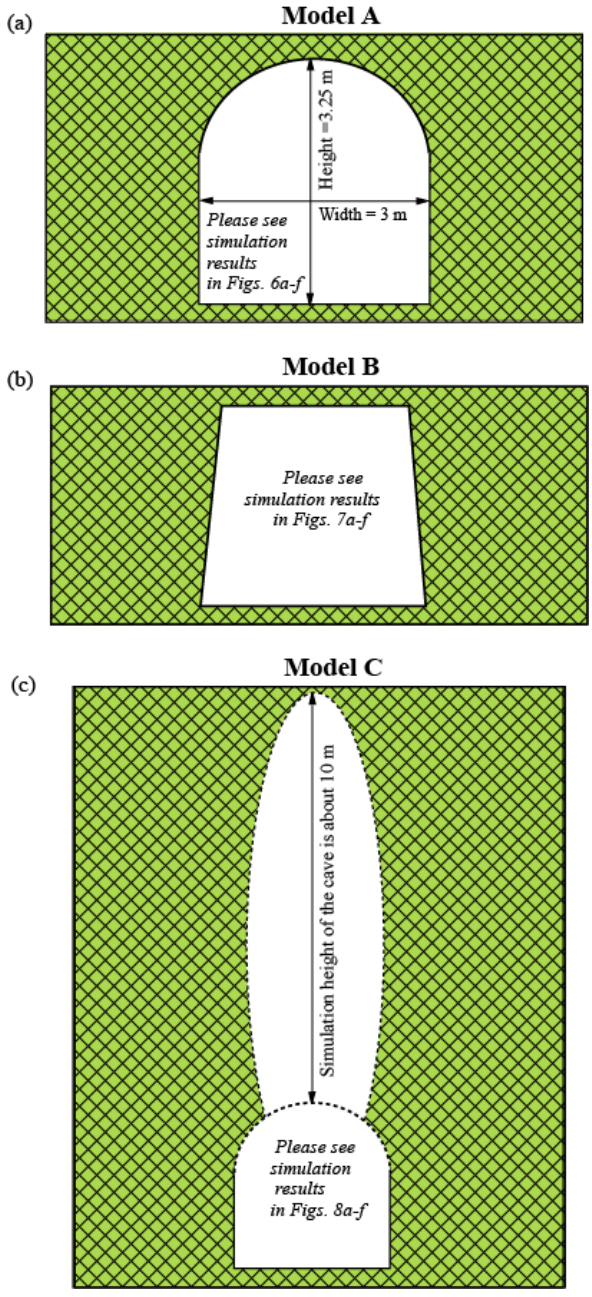

Fig. 5-5. Sectional views of the three models. (a) model A considers the horseshoe-shaped geometry. (b) model B involves the trapezoid-shaped geometry of the #1110 entry roadway, and (c) model C assumes the horseshoe-shaped geometry coupled with a large roof fall due to the weak rocks associated with the igneous dyke.

Table 5-1. Imposed rock mechanical properties (Wardell Armstrong, 1991) in models (A, B, and C)

Stress field	Type	Gravitational Stress
	Ground surface elevation (m)	420
	Overburden unit weight (MN/m^3)	0.026
Rock mass elastic properties	Type	Isotropic
	Young's modulus, *E* (MPa)	3000
	Poison's ratio, ν	0.22
Rock mass strength	Type of failure	Mohr-Coulomb
	Tensile strength (MPa)	3
	cohesion, *c* (MPa)	10
	angle of internal friction, φ (deg.)	20

Detail laboratory tests were carried out by Wardell Armstrong Mining Consultant to determine the rock mechanical parameters on some selected samples. The present numerical model accounts for both coal seam and the overburden sandstones. It is noted that all parameters used in table 1 are mean values of both for the overburden sandstones and coal seam that were taken from Wardell Armstrong (1991).

Three applied geometries were studied successively as follows:

- Model A considers the horseshoe-shaped (Fig. 5-5a) geometry of the #1110 entry roadway.
- Model B involves the trapezoid-shaped geometry of the #1110 entry roadway only (Fig. 5-5b). Arches were used to protect the roof and rib falls. Some wooden planks as shown in Fig. 5-3a were used to fill the gap between the arches and the immediate roof and two rib sides in order to provide support during collapse of the coal strata.
- Model C assumes the horseshoe-shaped geometry coupled with a large roof fall due to the weak rocks associated with the igneous dyke (Fig. 5-5c).

5.4. Modeling results

Modeling results are presented in terms of six mechanical parameters:

- distributions of horizontal compressive stress (σ_1),
- distributions of vertical stress (σ_3),
- horizontal displacement,
- vertical displacement,
- deviatoric stress, and

- shear stress (τ_{max}).

In addition, deformation vectors are shown as red arrows in color figures.

5.4.1. Model A

The distributions of σ_1 and σ_3 stresses from the simulation using model A are shown as colored contours in Fig. 5-6a-b. The horizontal stress was about 8 MPa in both rib sides, about 36 MPa in the roof, and about 24 MPa in the floor (Fig. 5-6a). Horizontal stress values decreased gradually toward the roof and the floor, but showed less gradual changes in both rib sides. The vertical stress (σ_3) was 1.9 MPa at the roof and 0.8 MPa at the sidewalls and floor. Vertical stress values increased gradually, reaching 12.3 MPa around the roadway (Fig. 5-6b).

The simulation resulted in a horizontal displacement of 0.016 mm (Fig. 5-6c, color legend) for the left side of the roadway and -0.012 mm for the right side, leading to an overall horizontal displacement of 0.028 mm. Displacement values decreased gradually from the rib sides to the interior of the coal strata.

Deformation vectors, which are represented by red arrows in Fig. 5-6b, indicate that the coal strata around 7.5 m were affected by mining-induced stress. Near the roadway, major deformation occurred within 5 m of the coal strata. A vertical displacement of -0.003 mm was simulated for the roof, while a displacement of 0.008 mm was simulated for the floor, leading to a total of 0.011 mm vertical displacement (convergence). Displacement values decreased gradually toward the roof and the floor.

High deviatoric stress values were concentrated in two places: the immediate roof and the floor. In the rib sides, these values decreased toward the coal seam. In the immediate roof, the highest calculated stress value was 27 MPa and was eventually reduced to 6 MPa (Fig. 5-6e). In the floor, the highest stress value was 18 MPa and was ultimately reduced to 7.5 MPa. The stress values ranged from 0 to 6 MPa at a distance of 3 m from the rib sides.

The shear stress (τ_{max}) distribution of the representative excavation is illustrated in Fig. 5-6f. Both types of shear stress (compressive and tensional) were concentrated around the roadway. There appeared to be a stress shadow area located in similar regions of the roof and the floor. The compressive shear stress ranged from 0.7 to 10 MPa and was concentrated in an area

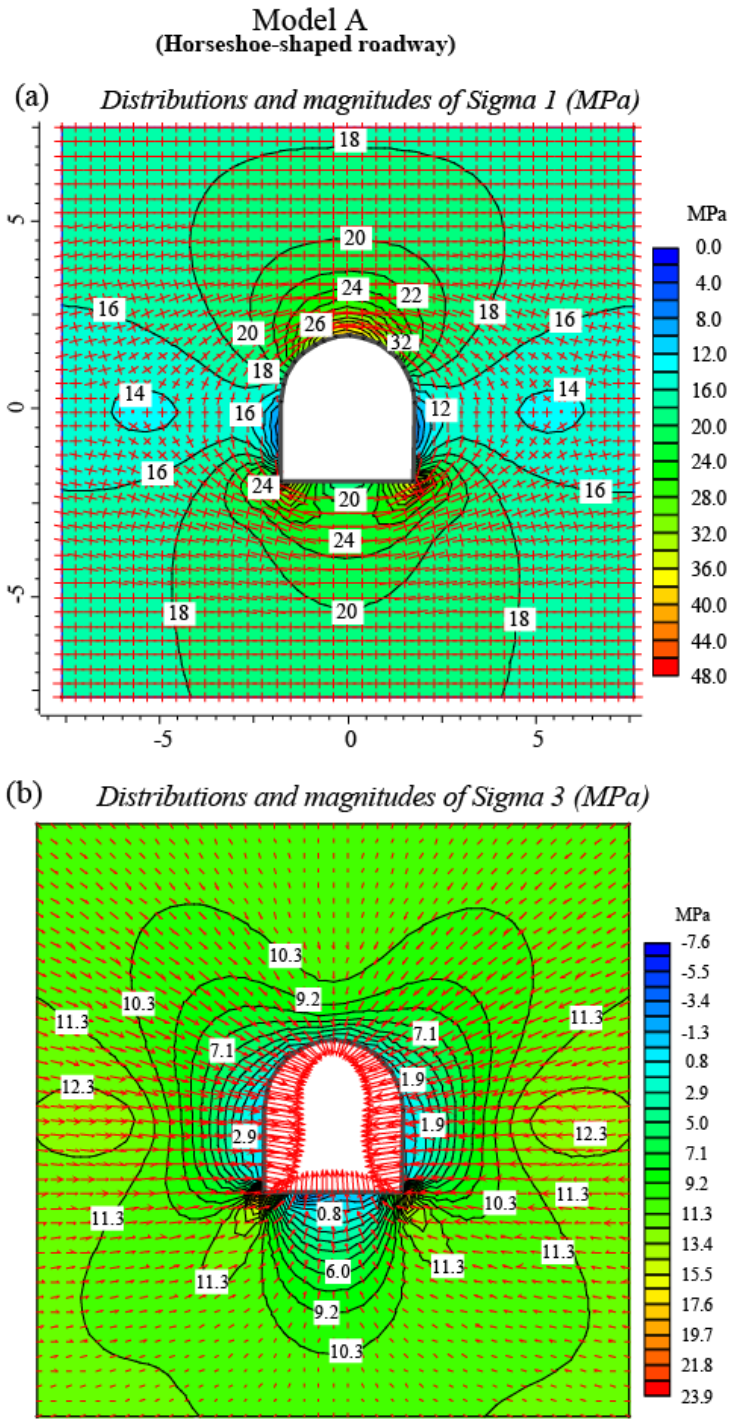

Fig. 5-6. Mining-induced stress redistributions caused by the horseshoe-shaped geometry of the #1110 entry roadway. (a) and (b) show contours of maximum (σ_1) and minimum (σ_3) principal stress magnitudes in the rock strata surrounding a 3.25 m high roadway section, respectively. (c) and (d) represent contours of horizontal displacement and vertical displacement magnitudes, respectively. (e) and (f) represent contours of deviatoric stress magnitudes and shear stress magnitudes, respectively. Deformation vectors in (b, and f) are represented by red arrows.

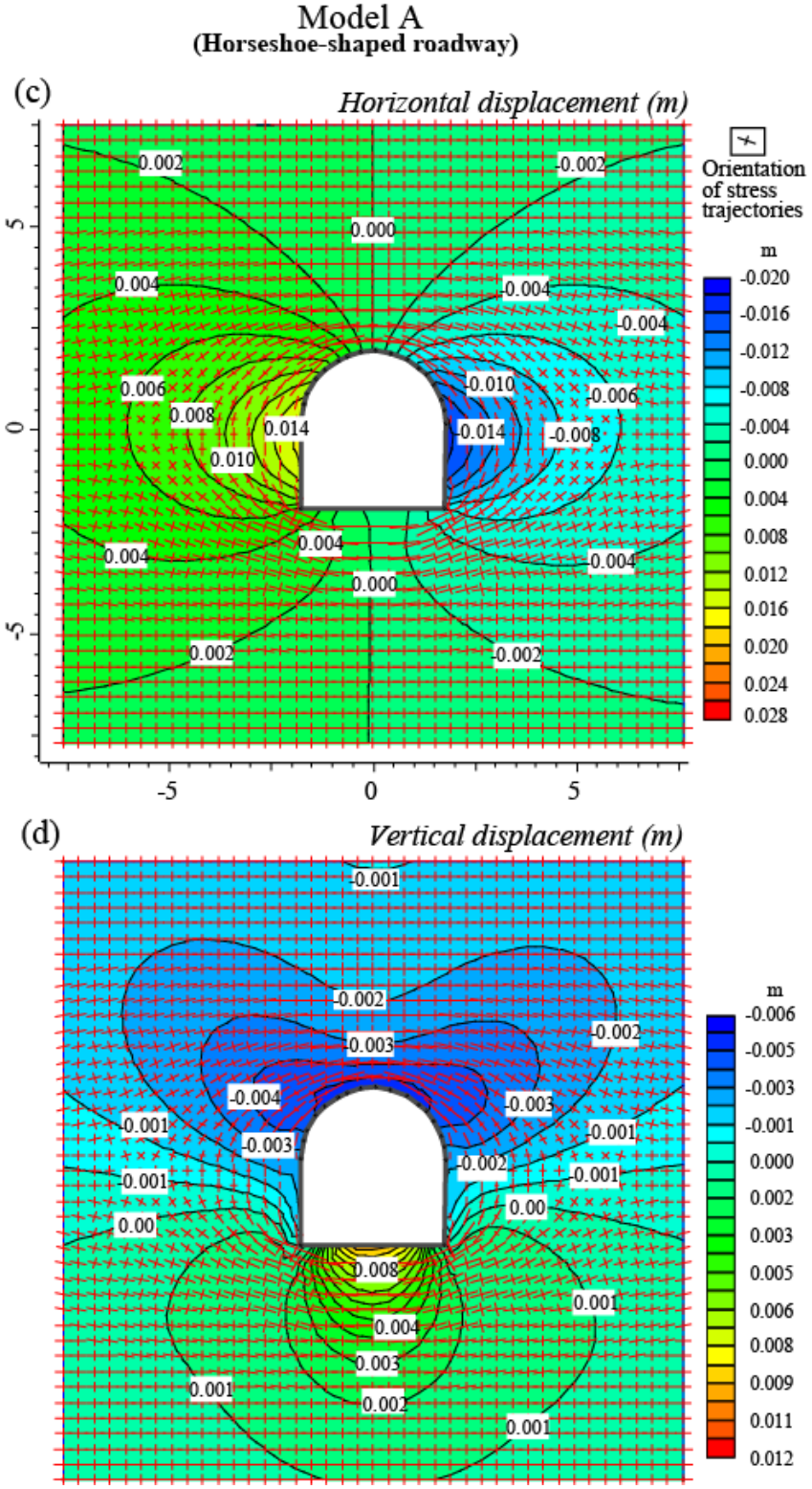

Fig. 5-6 (continued)

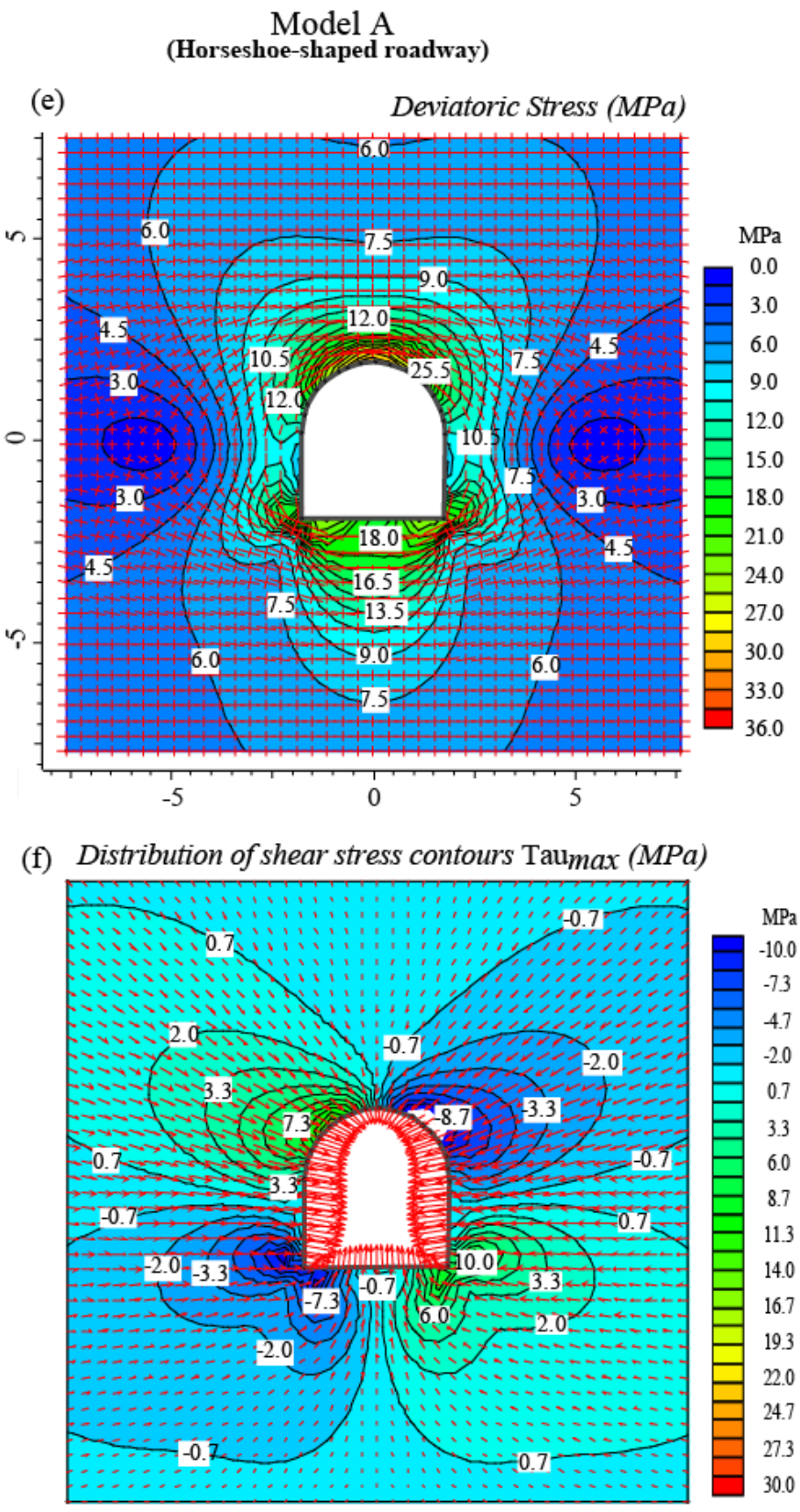

Fig. 5-6 (continued)

that extended to the left hand side of the roof and the right hand side of floor. The tensional shear stress ranged from -10 to -0.2 MPa and was concentrated in an area that extended to the left hand side of the floor and the right hand side of the roof. This configuration was caused by the release of stress by damaged coal strata during mine excavation. The active region of the high stress area extended toward the excavation, corresponding to the damage from the strata movement.

5.4.2. Model B

The results of the numerical analysis for model B are shown in Fig. 5-7a-f. The distribution of σ_1 extends up to 6 m toward the roof and up to 7.5 m toward the floor. The stress contours spread laterally up to 7.5 m in both rib sides. σ_1 was about 22 MPa in the immediate roof and floor of the model and ultimately decreased to 18 MPa in both the roof and the floor. Tensional stress, with values up to -2 MPa, was concentrated in the immediate rib sides. Horizontal compressive stress increased gradually from the rib sides to the interior of the coal strata, ranging from 2 to 18 MPa in both rib sides (Fig. 5-7a).

The distribution of vertical stress (σ_3) was strongly influenced by the trapezoid-shaped geometry. The tensional stress ranged from about -0.9 to -2.7 MPa. The vertical stress of the strata jumped from 9.9 to 0.9 MPa in the roof and floor, but in the rib sides this value decreased gradually from 11.7 to 1.8 MPa (Fig. 5-7b).

The horizontal compressive displacement at the left side of the model was relatively small. The maximum value was 18 mm, but this decreased gradually to 2 mm in the interior of the coal strata. The horizontal tensional displacement was concentrated in the right side of the model. The maximum value was -22 mm and was gradually reduced to -2 mm (Fig. 5-7c). The vertical compressive displacement was concentrated in the floor with values ranging from 2 to 9 mm. On the contrary, vertical tensional displacement was most prominent in the roof. The maximum value was -12 mm and was gradually reduced to -2 mm (Fig. 5-7d).

The distributions of deviatoric stress (Fig. 5-7e) in the roof, floor, and rib sides were obviously dissimilar. High stress values were concentrated in the roof and floor. The maximum value was 16.5 MPa in the immediate roof and floor and gradually decreased to 6 MPa. The maximum deviatoric stress in the rib sides was almost 10 MPa and was eventually reduced to 1.5 MPa.

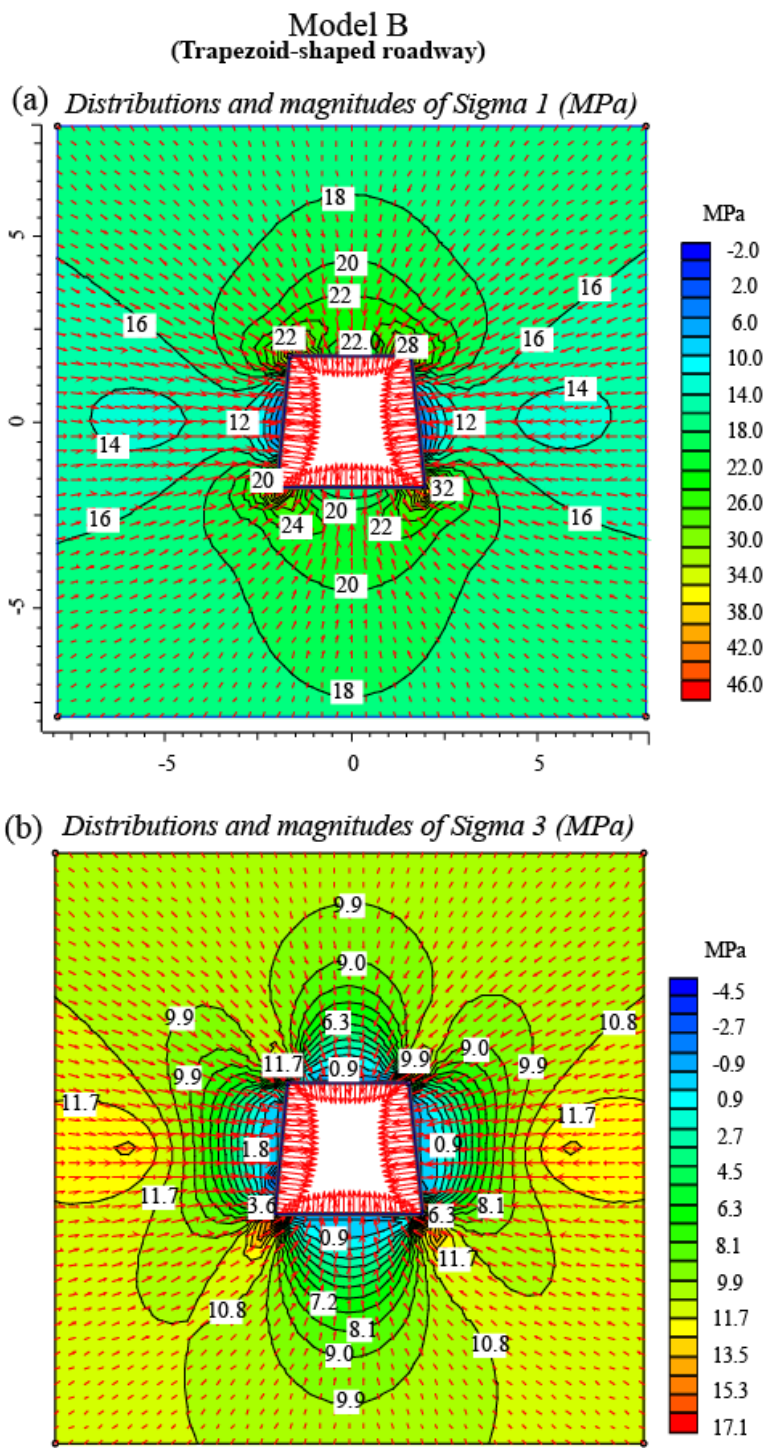

Fig. 5-7. Mining-induced stress redistributions caused by the trapezoid-shaped geometry of the #1110 entry roadway. (a) and (b) show contours of maximum (σ_1) and minimum (σ_3) principal stress magnitudes in the rock strata surrounding a 3 m high roadway section, respectively. (c) and (d) represent contours of horizontal displacement and vertical displacement magnitudes, respectively. (e) and (f) represent contours of deviatoric stress magnitudes and shear stress magnitudes, respectively. Deformation vectors in (a, b, and f) are represented by red arrows.

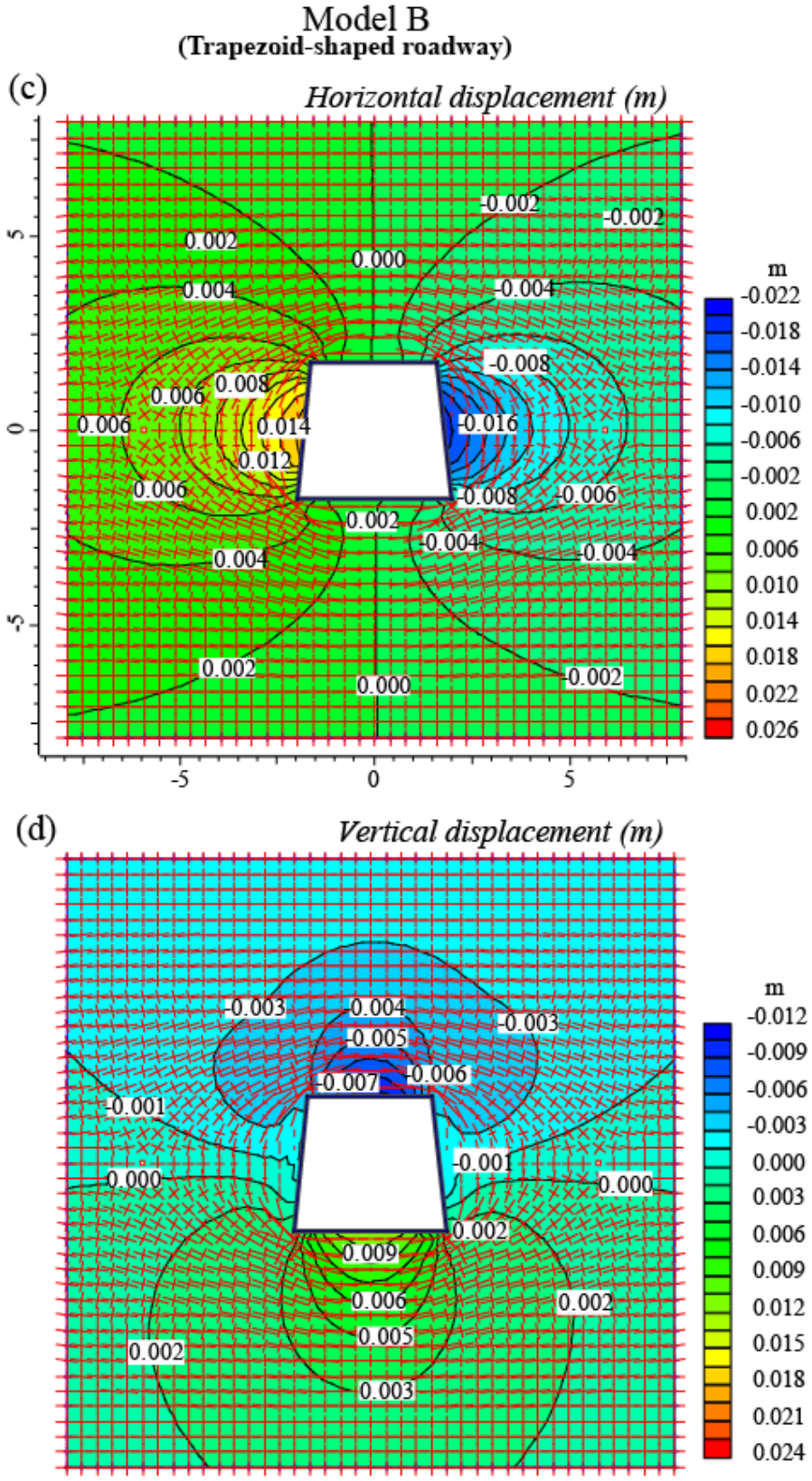

Fig. 5-7 (continued)

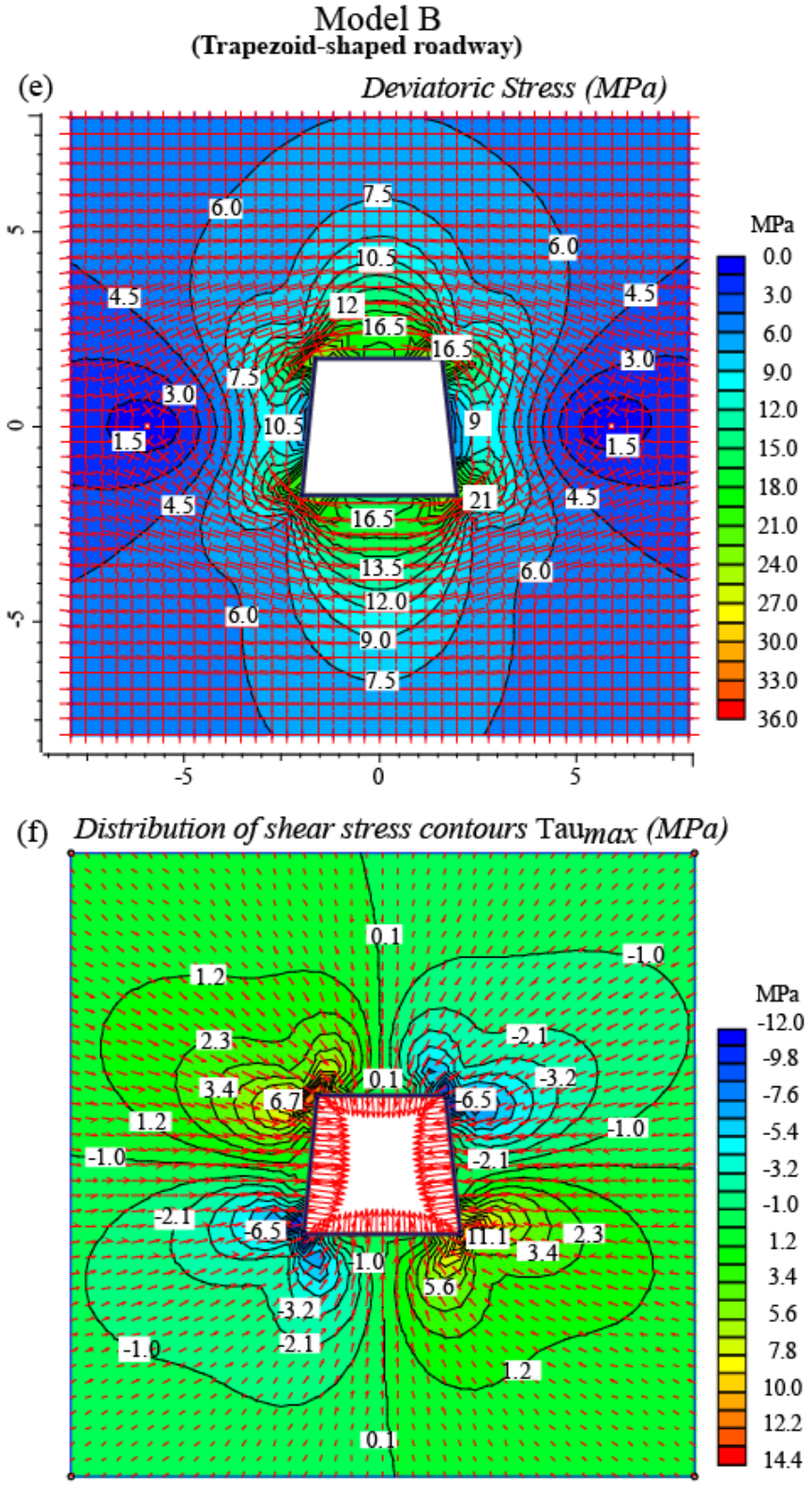

Fig. 5-7 (continued)

The distribution characteristics of shear stress (τ_{max}) are illustrated in Fig. 5-7f. The tensional shear stress was concentrated in the left hand side of the floor and the right hand side of the roof. The maximum value was about -6.5 MPa and was reduced to -1.0 MPa in a stepwise fashion. In contrast, the compressive shear stress was concentrated in the left hand side of the roof and the right hand side of the floor. In the left hand side of the roof, the maximum value was 6.7 MPa and the minimum was 1.2 MPa. In the right hand side of the floor, these values were between 1.2 and 11.1 MPa.

5.4.3. Model C

Model C emphasized the stresses and deformation due to the presence of a roof fall-induced cave embedded within the regular shape of the excavation. This model could be used as a standard way to predict coal seam deformations. Distributions of σ_1 in this simulation extended up to 28 m toward the roof and up to about 18 m toward the floor.

The maximum tensional stress was -5 MPa and was concentrated in the immediate rib sides. It gradually decreased to -1.3 MPa. The overall stress patterns were compressive and extended laterally up to 30 m on both sides. The stress magnitudes ranged from 2.3 to 15.2 MPa. There were no tensional stresses in the immediate roof and floor of the model. The maximum compressive stress in the roof was about 28 MPa and decreased gradually to 17 MPa. In the floor, the maximum value was 35.3 MPa and was eventually reduced to 18.8 MPa (Fig. 5-8a). Distributions of σ_3 extended up to 32 m in the roof and floor. Comparatively high tensional stresses, ranging from -0.3 to -6.7 MPa, were concentrated in both sides of the model and eventually became compressive stresses, ranging between 1.8 and -12.3 MPa. The maximum compressive stresses were concentrated in the immediate roof of the model and varied from 10.2 to 13.3 MPa. These values ranged between 7 and 12.3 MPa in the floor (Fig. 5-8b).

The horizontal compressive displacement of about 54 mm was concentrated in the left side. This value fell gradually to 18 mm in the internal part of the coal strata. The horizontal tensional displacement was concentrated in the right side of the model and the maximum value of -66 mm was gradually reduced to -6 mm (Fig. 5-8c). The vertical tensional displacement was concentrated in the floor and the left and right hand sides of the roof, where the maximum value

was -6 mm and the minimum was -3 mm. The tensional stress propagated up to 30 m in both sides and about 22 m in the floor. On the contrary, vertical compressive displacement was

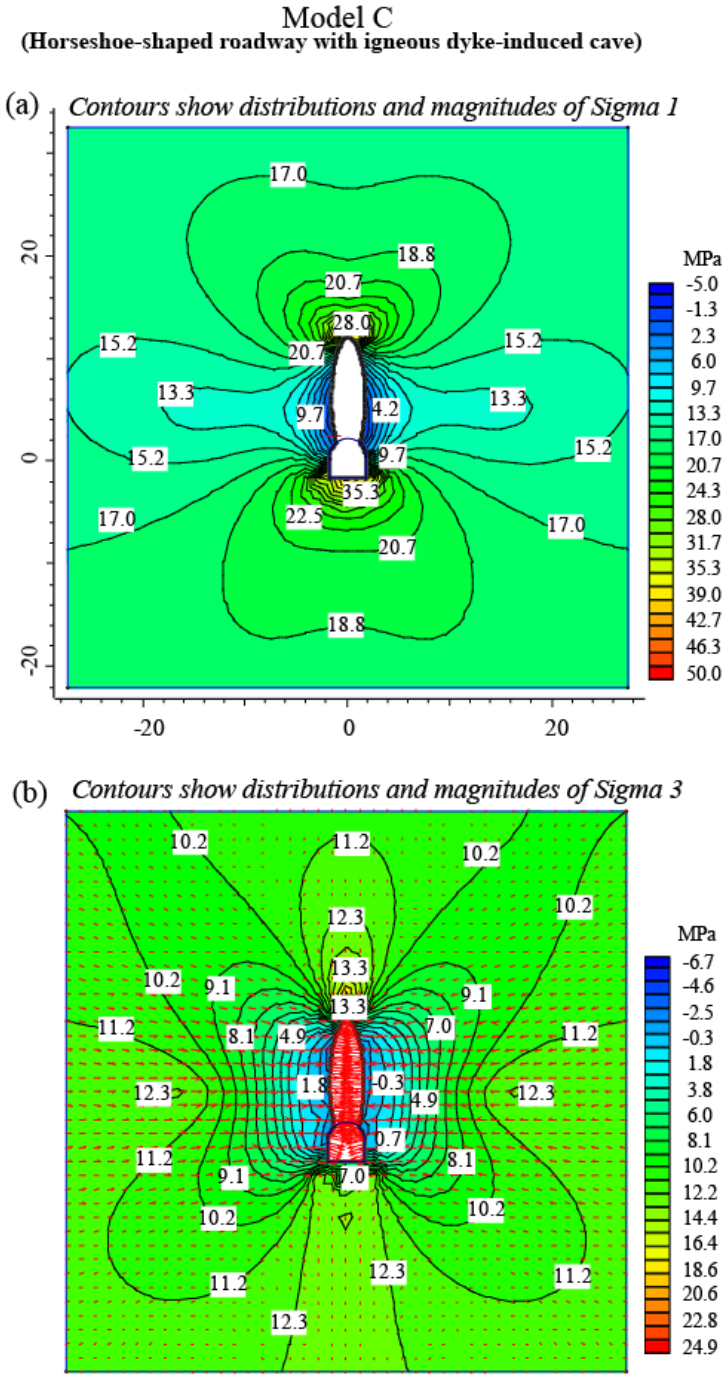

Fig. 5-8. Mining-induced stress redistributions caused by the horseshoe-shaped geometry coupled with a large roof fall due to igneous dyke. (a) and (b) show contours of maximum (σ_1) and minimum (σ_3) principal stress magnitudes in the rock strata surrounding a 3.25 m high roadway section with 10 m high cave to the roof, respectively. (c) and (d) represent contours of horizontal displacement and vertical displacement magnitudes, respectively. (e) and (f) represent contours of deviatoric stress magnitudes and shear stress magnitudes, respectively. Deformation vectors in (b, and f) are represented by red arrows.

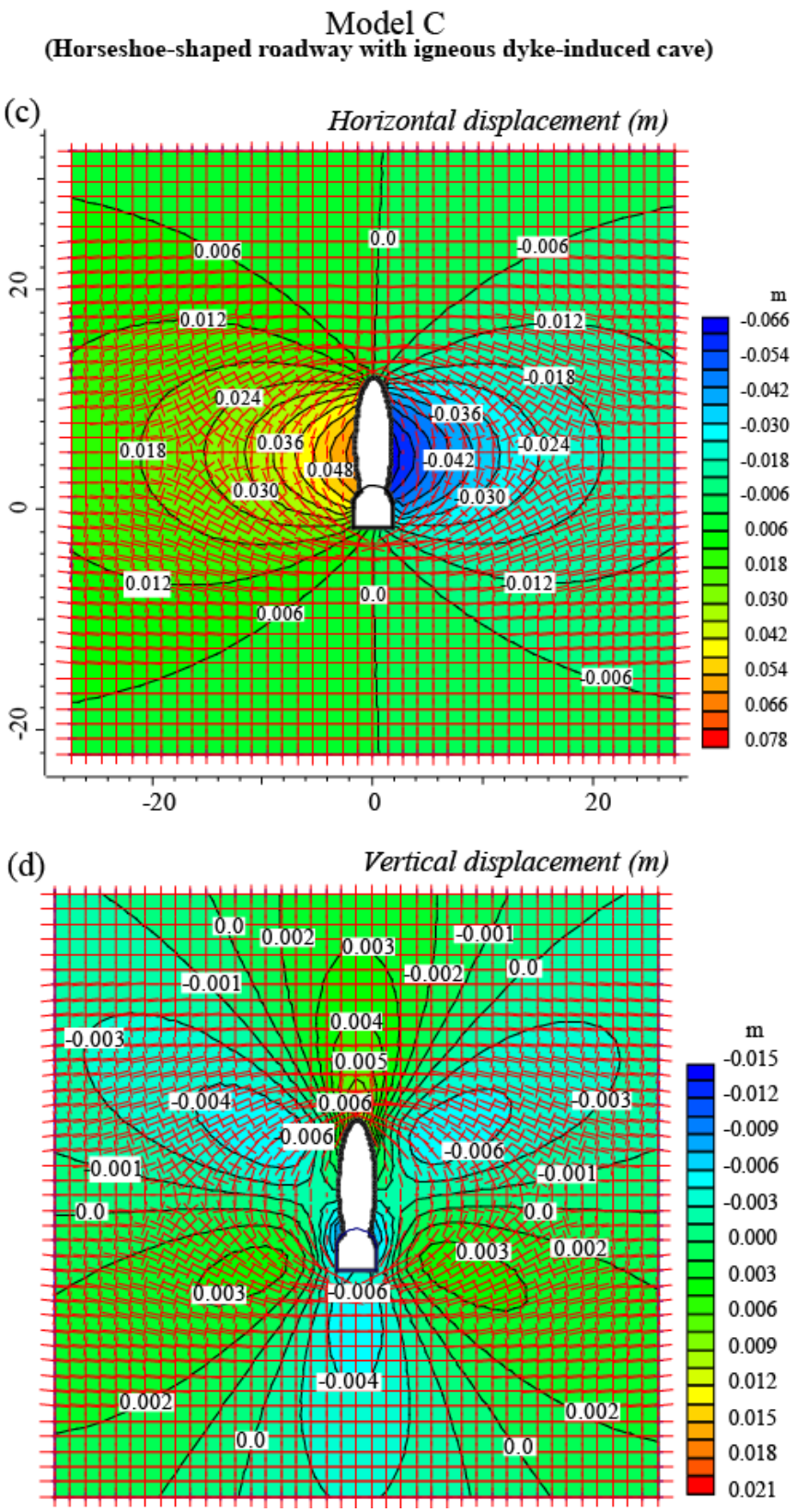

Fig. 5.8 (continued)

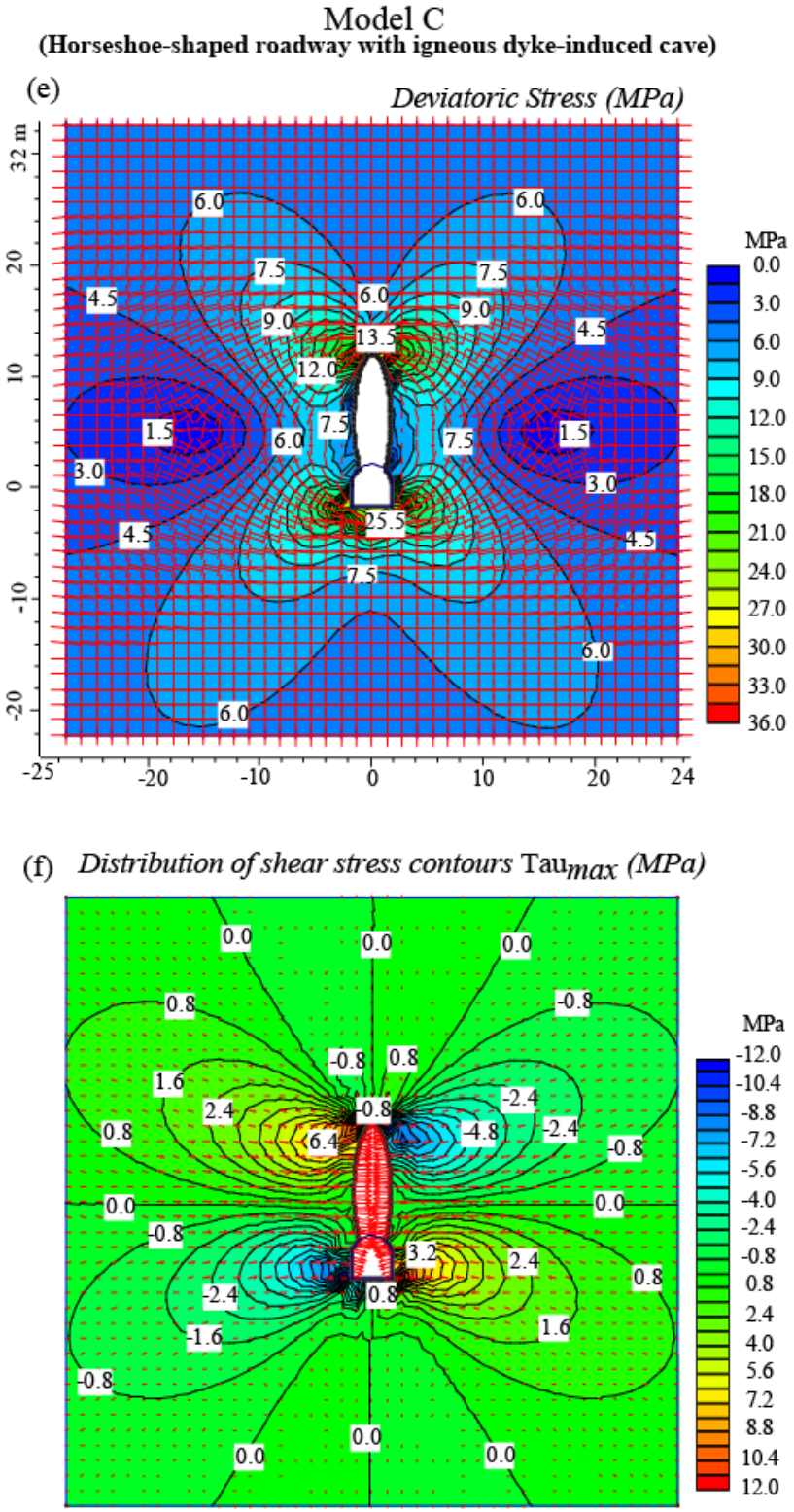

Fig. 5-8 (continued)

prominent in the left and right hand sides of the rib and the immediate roof of the model. The maximum value was 6 mm and was gradually reduced to 2 mm (Fig. 5-8d).

The distribution of deviatoric stress is shown in Fig. 5-8e. High stress values were concentrated in the roof and floor. The magnitude of the stress ranged from 6 to 25. 5 MPa. The maximum deviatoric stress in the rib side was almost 7.4 MPa and was eventually reduced to 1.5 MPa. The distribution of shear stress (τ_{max}) is illustrated in Fig. 5-8f. The compressive shear stresses were concentrated in the left hand side of the roof and the right hand side of the floor. The magnitude of the stress was between 0.8 and 7.2 MPa. In contrast, the tensional shear stresses were concentrated in the left hand side of the floor and the right hand side of the roof. The maximum value was about -12 MPa and was gradually reduced to -0.8 MPa.

5.5. Discussion

Gas emissions from working coal seams have affected underground mining operations for over a century. The emissions observed in the #1110 entry roadway of the Barapukuria coal mine were comparable to those from other underground coal mines worldwide, including mines in China, Australia, Canada, India, Germany, United Kingdom, and France. The emissions stem from gas influx from neighboring coal seams (in the case of a multi-seam deposit) and from associated rock layers. When a coal seam is influenced by mining activities, gas can be emitted into the coal mine workings in one of three ways: (i) it may flow evenly from the pores and fractures of the coal, (ii) it may escape from the coal seam due to major tectonic disruptions, or (iii) it may suddenly burst into the mine in great quantities (Alexeev et al., 2004; Su, et al., 2005; Whittles et al, 2006). In this study, several potential factors have been recognized as possible causes of the gas emission in the Barapukuria coal mine. The most important factors include:

- gas contents in Barapukuria coal,
- geologic features and their relationship to the gas emission,
- igneous intrusions,
- thickness of coal seam at the roof and floor, and
- insufficient mine ventilation.

A brief description of the role of each of these factors is provided in the following sections.

5.5.1. Gas contents in Barapukuria coal and outburst status based on gas emission levels

The Barapukuria coal deposit consists of six coal seams. Of these, only seam VI is being mined. It has an average thickness of about 36 m and a gas content of 6.51–12.68 m^3 t^{-1}, with an average of ~9.6 m^3 t^{-1}. Seam V has a thickness between 1 and 10 m with a gas content of 8.10 m^3 t^{-1}. Seam IV has a thickness of 3-10 m with a gas content of 7.75 m^3 t^{-1}. Seam III has a thickness between 0.30 and 6 m and has a gas content of 8.02 m^3 t^{-1}. Seam II has a thickness between 14 and 15 m and an average gas content of 8.09 m^3 t^{-1}. Seam I was detected only in borehole GDH #40, so its thickness and gas content are unknown. The estimated range of gas concentration in the Barapukuria deposits indicates medium to highly enriched coal, which could easily enhance gas flow in the mine roadway (Islam and Hayashi, 2008).

Continuous gas monitoring system has been performed by Beamish (1990) to assess seam gassiness at the mining face as an indication of outburst-proneness at Collinsville Mine, Queensland, Australia. He concluded that CO_2 emissions less than 2.6 m^3 t^{-1}, no outbursting occurs, and normal mining proceeds. Up to 3.8 m^3 t^{-1}, low-medium outburst-prone conditions exist and mining takes place under controlled procedures. When values exceed 3.8 m^3 t^{-1}, high outburst-prone conditions exist and mining is halted. In Barapukuria, gas emission levels were not calculated and gas drainage thresholds especially horizontal vertical boreholes were not set for shielding the longwall entry against methane inflow.

5.5.2. Geologic features and their relationship to gas emissions

The main sources of coal seam gas are coal seams, porous sandstones above and below the seams, fracture systems, joints and faults (Lunarzewskii, 1998). Some studies (e.g., McCulloch et al., 1975; Thielemann et al., 2001; Li et al., 2003; Wu et al., 2004; Ulery, 2006; Karacan et al., 2008; and others) have also emphasized that anomalous geologic features can play a significant role in gas emission in mines. Gas emission from coalfields has occurred within deformed coal layers, particularly in deformed zones associated with normal faults, reverse faults and intense sub-folds (Cao and Peng, 1995). Li et al. (2003) showed that a shear zone in a coal seam, associated with normal faults, contains a large number of fractures and thus a large quantity gas. The fractures may act as gas conduits from coal formations into the mine.

In Australian underground coal mines, the majority of gas outbursts events have been associated with geological structures within 2.5 m of workings- primarily faults, shear zones and

igneous intrusions, with characteristics dimensions greater at least than the prevailing seam thickness (Wold et al., 2008). Faults and the associated weak zones, especially very weak X-shaped joints and fractures within the coal seam, may also be responsible for the high gas concentrations encountered during mining. Mining activities disturb existing stress equilibrium in the coal seam and change the structural attributes of the affected strata. Mining-induced stress can greatly reduce the strength of fault zones. Redistribution of mining-induced stress could lead to the formation of extensive geologic structures around large-scale faults along with the development of characteristic fracture zones (McCulloch et al., 1975; Lunarzewski, 1998; Karacan et al., 2008).

Numerous normal faults in the coals of the Barapukuria basin (Islam and Hayashi, 2008; Islam et al., 2009) have been recognized as either conduits for gas flow from strata adjacent to the mined coal seam or as barriers for accumulation of large quantities of methane, which could enter the mine when the faults are interrupted (Karacan et al., 2008). Barapukuria coal seams are tectonically highly disturbed. Many small-scale normal faults are distributed within seam VI with throws of 1-3 m. Moreover, there is a high intensity of butt cleat with average spacing of 20-25 m^{-1} and face cleat with average spacing of 8-10 m^{-1}, which could reduce the strength of the coal (Islam and Hayashi, 2008).

It is clear from the simulation results that mining-induced strata deformation enhanced fracture propagations up to 7.5 m from the excavation of the horseshoe- and trapezoid-shaped roadways (Figs. 5-6 and 5-7). The deformation extends up to 25 m around the excavation when roof fall through the vertical direction of the igneous dyke is taken into account (Fig. 5-8). At the time of the gas emission (2005), the working roadway was about 520 m in length with a long exposed wall. From the strata deformation pattern, it is clear that redistribution of mining-induced stresses σ_1 and σ_3 (Figs. 5-6a-b, 5-7a-b, and 5-8a-b) opened numerous faults and fracture networks and connected frequently with coal cleats and X-shaped joints (Islam and Hayashi, 2008; Islam et al., 2009). Ultimately, the concentrated gas in mineable seam VI (6.51–12.68 m^3/ton) (Islam and Hayashi, 2008) was able to flow through the network of faults, fractures, and joints into the mine.

5.5.3. Igneous intrusion (dyke)

A dyke is a magma-driven extensional fracture (Gudmundsson and Loetveit, 2005) that is commonly found in the rift tectonic coal basins of the Indian subcontinent, including those of Bangladesh. Gudmundsson and Loetveit (2005) stated that during rifting episodes, the columnar joints within the coal/rock strata combine to form small tensional cracks that gradually grow into large-scale tensional features and ultimately turn into normal faults. Some dykes follow the normal fault plane for several tens of meters vertically before leaving the fault plane to form additional extensional features. The dyke-induced zone is usually characterized by numerous normal faults and tensional fractures that are zero to several meters in width. Most dykes are injected dykes and do not reach the surface but rather are arrested at some depth in the rift zone. Arrested dykes may cause brittle deformation and encourage dyke-induced tensile stresses to the regions above and at the lateral end of the contacts (Gudmundsson and Loetveit, 2005). The Barapukuria-type rift basin contains normal faults that are composed of rock layers with different mechanical properties (Islam and Hayashi, 2008; Islam et al., 2009). The recognized dyke in the Barapukuria basin is an injected dyke that does not reach the surface. Its measured length is over 1000 m, but its vertical extent has not been determined.

The presence of an igneous dyke in a coal basin is one of the most important factors that can cause gas emission in underground mining. Dykes are common igneous structures in many Australian coal basins, like the Hunter Valley coal basin in the Dartbrook area (Golab and Carr, 2004; Golab et al., 2007), the Southern coalfields of New South Wales, and Bowen basin of Queensland (Wold, et al., 2008). Igneous intrusions are difficult to mine throughout, and their emplacement is accompanied by formation of joints and fractures that cause roof and wall instability of the mining excavations and increase coal permeability allowing more seam gas and ground water to emerge from the coal as mining approaches (Golab et al., 2007). Intrusions also thermally and geochemically alter coal to form coke and produce methane (CH_4) and carbon dioxide (CO_2), increasing the threat of spontaneous combustion and outburst (Golab and Carr, 2004). According to Saghafi et al. (2008), the presence of an igneous dyke indicates a high intensity of gas emission. High gas emissions occur mainly in the vicinity of igneous intrusions due to an unexpected drop in stress. It has been shown that the methane storage capacity and lower diffusivity of dyke material can explain the occurrence of gas pockets observed in the vicinity of intrusions. In this study, it is observed that the magnitudes of σ_1 and σ_3 stresses decrease gradually near the dyke-affected zone due to the weak materials of the dyke (Figs. 5-8a-

b). In contrast, shear stress (τ_{max}) and deviatoric stress (Figs. 5-8e-f) increase around 20 m from the igneous intrusions. However, mining through the igneous dyke created low-pressure zones at horizontal distances of up to 20 m on either side of the dyke (as seen in Figs. 5-8a-b), which allowed the coal to release gas (Saghafi et al., 2008). Mining-induced tensional deformation and fractures (Figs. 5-8b and 5-8f) around the dyke zone served as gas conduits into the mine roadway.

5.5.4. Thickness of coal seam at the roof and floor

The amount of gas emission varies significantly over a wide range of geologic and mining conditions. The stratigraphic section above and below the worked coal seam is of great importance when using longwall mining systems. A significant amount of the methane that enters the underground mine originates from surrounding coal seams and acts as a gas-bearing source. During longwall extraction, the highest levels of gas can be expected when the strata are fully relaxed. The degree to which degassing takes place depends on the particular relaxation behavior of the strata and is especially dependent on the physical properties and geometry of the strata, the thickness and distance between gas sources, and the shape and extent of the relaxed zone (Lunarzewski, 1998; Alexeev et al., 2004). According to Noack (1998), above the worked coal seam up to the 20 m thickness, and below the worked coal seam up to the -11 m thickness, the degree of gas emission is assumed to be 100%. Jackson and Kershaw (1996) concluded that the zone around the coal working is a function of the size of the excavation and the depth of extraction. Both factors serve to increase the stresses obtaining around the working, which both increases the degree of fracture and the size of the fracture zone. Consequently, mining headings tend to release gas from the mined seam alone, while longwall districts release gas from regions up to about 200 m distant.

The #1110 belt gate roadway passes through seam VI, where about 7-15 m of coal remains at the roof of the roadway. The seam thickness is about 22 m at the bottom of the face. This very thick coal seam experiences frequent tectonic disturbances, especially intermittent joints, fractures, and small-scale faults. However, simulation results reveal that deformation vectors (Figs. 5-6b, 5-7a-b) relaxed the coal seam by more than 7 m along the horizontal and vertical directions of the excavation. In the case of the dyke-induced roof fall zone, where a 10 m height cave on the roof is simulated in model C, deformation vectors (Fig. 5-8b) extended up to

30 m toward the roof and up to 22 m toward the floor. The actual height of the cave was more than 10 m. This means that the entire coal seam, and in particular the roof and the floor around the roadway, was fully affected and relaxed by the dyke-induced caving. It is evident that the horseshoe- and trapezoid-arch-shaped geometries of the roadway generated less significant deformation vectors (Figs. 5-6b, 5-7a-b) than the dyke-induced deformation vectors (Fig. 5-8b). As a consequence, the dyke-induced gap above the roadway, which relaxed coal strata on the both rib sides and extended about 20 m horizontally, served as a gas flow channel from the floor, roof and rib sides of the thickened coals.

5.5.5. Insufficient mine ventilation systems

A sufficient supply of ventilated air to the mine can play a significant role in negating the effects of gas emission into a working face. Methane released from coal seams and the surrounding gas-bearing strata mixes with the cleaner ventilation air. Mine gases can accumulate in mine if the ventilation system is insufficient (Donnelly and David, 2000). Inadequate amounts of air in the ventilation system may cause dangerous gas accumulation in mines and can lead to gas explosions under certain conditions (Lunarzewski, 1998). Therefore, the amount of ventilation in the mining roadway is very important. In China, a reasonable amount of ventilation at the working face is at least 650 m^3/min, i.e., 10.83 m^3/sec (He et al., 2008). In the Barapukuria mine, the planned ventilation air flow was 10 m^3/sec; however, the air flow at the #1110 belt entry has not been properly maintained in the region beyond the dyke-induced disturbed zone. It fluctuates inconsistently between 5 and 8 m^3/sec before connecting with the cross-cut flow. At the point furthest from the entry, it can be less than 4 m^3/sec (Monthly Progress Report, Barapukuria Coal Mining Co. Ltd, July 2003). It could therefore be concluded that due to a lack of sufficient ventilation, the strata temperature of the coal rose, the rate of coal oxidation increased, and huge quantities of methane formed and were emitted into the #1110 belt entry. The caved zone of the roof and the ribs of the trapezoid-shaped arch supports formed a region of relatively low stress (σ_3 in Fig. 5-7b). This lighter loading allowed penetration of the ventilation air from the roadway into the caved zone. This ventilation air flow leakage kept the remainder of any strata gases from flowing back into the belt gate.

5.6. Conclusions

In this chapter, BEM was used to simulate a case study of coal strata deformation and gas emission in the Barapukuria coal mine, focusing on an entry roadway that was characterized by a tectonic disturbance. The model simulates the large-scale deformation around the dyke-induced perturbation zone, which defines the potential flow paths of strata gases. Modeling within the coal seam provides information on the propagation of coal fractures that act as gas pathways. The horizons within the roof, floor, and ribs, which are potential gas sources, and the changing stress conditions around the gate roadway, which affect strata deformation and enhanced gas permeability, were also simulated.

The #1110 working panel will remain closed until December 2008. In the near future, if the mine continues to have inadequate air in the ventilation system, there is a high likelihood that coal will be oxidized given the low atmospheric pressure and temperature. This could cause excessive heat in the mine as well as the accumulation of hazardous gas and would lead to gas explosions under certain conditions. The following important points should be considered before further development of the #1110 working face at the Barapukuria coal mine and are also relevant for the proposed underground mines in the Khalaspir, Phulbari, Dighipara, and Nawabgonj coal basins:

(1) Sophisticated two-dimensional or three-dimensional numerical modeling techniques should be applied to recognize the dilation of joints and the mining-induced fractures, where the gas permeability increases substantially.

(2) Gas flow monitoring systems in the mining roadway should be strictly controlled and barometric pressure observations should be examined before work begins.

(3) The ventilation air flow rate at the working face should be controlled following the mine implementation plan. In every entry, the ventilation system should be improved to prevent gas emission.

(4) Air composition should be monitored every hour to find the variation of gas composition and concentration with rising temperature.

(5) The optimum gas level should be determined and should be used to establish a quantitative relationship between coal temperature and the composition and concentration of index gases.

(6) Horizontal boreholes should be preferred parallel to the mining direction for degasification of the mining panel area (Karacan et al., 2008) in advance of mining and also for shielding the longwall entries against methane inflow during development mining and afterwards.

References

Alexeev, A.D., Vasylenko, T.A., Ul'yanova, E.V., 2004. Phase states of methane in fossil coals, Solid State Communications 130, 669–673.

Bakr, M.A., Rahman., Q.M.A., Islam, M.M., Islam, M.K., Uddin, M.N., Resan, S.A., Haider, M.J., Islam, M.S., Ali, M.W., Choudhury, M.E.A., Mannan, K.M., and Anam, A.N.M.H., 1996. Geology and Coal Deposits of Barapukuria Basin, Dinajpur District, Bangladesh, Records of Geological Survey of Bangladesh. 8, pt 1.

Beamish, B.B., 1990. Continuous gas monitoring for the assessment of outburst proneness at a mining face. International Journal of Mining and Geological Engineering 8, 131-147.

Bibler, C.J., Marshall, J.S., and Pilcher, R.C.,1998. Status of worldwide coal mine methane emissions and use. International Journal of Coal Geology 35, 283-310.

Cao, Y.X., and Peng, L.S., 1995. Basic types of coal bedding faults and their effect on controlling gas outburst zones. Journal of China Coal Society 20, 317–413.

Clayton, J.L., 1998. Geochemistry of coalbed gas: A review. International Journal of Coal Geology 35, 159-173.

Donnelly, L.J., and David M.M., 2000. The location of abandoned mine workings using thermal techniques. Engineering Geology 57, 39-52.

Golab, A.N., Hutton, A.C., and French D., 2007. Petrography, carbonate mineralogy and geochemistry of thermally altered coal in Permian coal measures, Hunter Valley, Australia. International Journal of Coal Geology 70, 150–165.

Golab, A.N., and Carr, P.F., 2004. Changes in geochemistry and mineralogy of thermally altered coal, Upper Hunter Valley, Australia. International Journal of Coal Geology 57, 197– 210.

Gudmundsson, A., and Loetveit, I.F., 2005. Dyke emplacement in a layered and faulted zone. Journal of Volcanology and Geothermal Research 144, 311-327.

Gurba, L.W., and Weber, C.R., 2001. Effects of igneous intrusions on coalbed methane potential, Gunnedah Basin, Australia. International Journal of Coal Geology 46, 113–131.

He, X., Zhang, R., Pei, X., Sun, Y., Tong, B., and Huang, H., 2008.Numerical simulation for determining three zones in the goaf at a fully-mechanized coal face. Journal China University of Mining & Technology 18, 199- 203.

Islam, M.R., and Islam, M.S., 2005. Water Inrush Hazard in Barapukuria Coal Mine, Dinajpur District, Bangladesh. Bangladesh Journal of Geology 24, 1-17.

Islam, M.R., 2005. Influence of tectonic structures for the occurrence of gas emission at 1110 working panel in Barapukuria Coal Mine, Bangladesh. In: abstract volume, Geodynamics and Environment in East Asia (GEEA), International Conference & 5th Taiwan-France Earth Science Symposium, 24- 29 November, 2005, Taitung, Taiwan, pp.155-156.

Islam, M.R., and Hayashi, D., 2008. Geology and coal bed methane resource potential of the Gondwana Barapukuria Coal Basin, Dinajpur, Bangladesh. International Journal of Coal Geology 75, 127-143.

Islam, M.R., Hayashi, D., and Kamruzzaman, A.B.M., 2009. Finite element modeling of stress distributions and problems for multi-slice longwall mining in Bangladesh, with special reference to the Barapukuria coal mine. International Journal of Coal Geology, (article in press).

Jackson, P., and Kershaw, S., 1996. Reducing long term methane emission resulting from coal mine. Energy Conversion and Management 37, 801-806.

Jia, X., Bei, Y., Jin, L., Dong, W., 2007. Characteristics of Gas Emission at Super-Length Fully-Mechanized Top Coal Caving Face. Journal China University of Mining & Technology 17, 447- 452.

Karacan, C.O., Ulery, J.P., and Goodman, G.V.R., 2008. A numerical evaluation on the effects of impermeable faults on degasification efficiency and methane emissions during underground coal mining. International Journal of Coal Geology 75, 195-203.

Li, H., Ogawa, Y., Shimida, S., 2003. Mechanism of methane flow through sheared coals and its role on methane recovery. Fuel 82, 1271–1279.

McCulloch, C.M., Diamond, W.P., Bench, B.M., Deul, M., 1975. Selected geologic factors affecting mining of the Pittsburgh Coalbed. Report of Investigations No. 8093. US Dept. of Interior, US Bureau of Mines, Pittsburgh, PA.

Lunarzewski, L., Moelle, K.H.R., Li, G., Dean-Jones, G.L., 1996. The Impact of Seam Gas Emission and Outbursts on Coal Production-Origins, Prediction and Control. The 6th Japan-Australia Joint Tech.Meet. on Coal, Sapporo, Japan.

Lunarzewski, L.W., 1998. Gas emission prediction and recovery in underground coal mines. International Journal of Coal Geology 35, 117-145.

Noack, K., 1998. Control of gas emissions in underground coal mines. International Journal of Coal Geology 35, 57-82

Saghafi, A., Pinetown, K.L., Grobler, P.G., Heerden, J.H.P., 2008. CO_2 storage potential of South African coals and gas entrapment enhancement due to igneous intrusions. International Journal of Coal Geology 73, 74-87.

Shen, B., Stephansson, O., 1994. Modification of the G-criterion for fracture propagation subjected to compression. Engineering Fracture Mechanics 47, 177-189.

Shepherd, J., Rixon, L.K., Griffiths, L., 1981. Outbursts and geological structures in coal mines: a review. Int. J. Rock Mech. Min. Sci. Geomech. Abstr. pp. 267-283.

Singh, A.K., Sharma, M., Singh, M.P., 2008. Genesis of natural cokes: Some Indian examples. International Journal of Coal Geology 75, 40–48.

Su, S., Beath, A., Guo, H., Mallett, C., 2005. An assessment of mine methane mitigation and utilization technologies. Progress in Energy and Combustion Science 31, 123–170.

Thielemann, T., Kroos, B.M., Littke, R., Welte, D.H., 2001. Does coal mining induce methane emissions through the lithosphere/atmosphere boundary in the Ruhr Basin, Germany. Journal of Geochemical Exploration 74, 219–231.

Ulery, J.P., 2006. Managing excess gas emissions associated with coal mine geologic features. In: Kissell, Fred (Ed.), Handbook for Methane Control in Mining. NIOSH Information Circular 9486. US Department of Health and Human Services, Centers for Disease Control and Prevention, National Institute for Occupational Safety and Health, Pittsburgh, Pa.

Wardell Armstrong, 1991, Techno-Economic Feasibility Study of Barapukuria Coal Project, Dinajpur, Bangladesh.

Whittles, D.N., Lowndes, I.S., Kingman, S.W., Yates, C., and Jobling, S., 2006. Influence of geotechnical factors on gas flow experienced in a U.K. longwall coal mine panel. International Journal of Rock Mechanics and Mining Sciences 43, 369-387.

Wold, M.B., Connell, L.D., and Choi, S.K., 2008. The role of spatial variability in coal seam parameters on gas outburst behaviour during coal mining. International Journal of Coal Geology 75, 1–14.

Wu, Q., Wang, M., Wu, X., 2004. Investigations of groundwater bursting into coal mine seam floors from fault zones. International Journal of Rock Mechanics and Mining Sciences 41, 557–571.

Zhi, W., Ling, C., Cong, C., Zhen, L., 2007. Forecast of Geological Gas Hazards for "Three-Soft" Coal Seams in Gliding Structural Areas. Journal of China University of Mining & Technology 17, 484-488.

Zhang, S., 1986. FEM analysis on mixed-mode fracture of CSM-GRP. Engineering Fracture Mechanics 23, 523-535.

Chapter 6

Mining-induced fault reactivation associated with the main Conveyor Belt Roadway and safety of the Barapukuria Coal Mine in Bangladesh: constraints from BEM simulations

Chapter 6

Mining-induced fault reactivation associated with the main Conveyor Belt Roadway and safety of the Barapukuria Coal Mine in Bangladesh: constraints from BEM simulations

6.1. Introduction

The reactivation of a fault in an area undergoing mining subsidence may result in the generation of a fault scarp along the ground surface, accompanied by compression and fissuring (Donnelly, 2006). These types of problems can often be expected when mining activities approach or breach a major geologic discontinuity, such as a fault (Crouch and Starfield, 1983). Thrusts, strike-slip faults, normal faults, and igneous intrusions (dikes and sills), which are referred to as 'geologic discontinuities', are associated with highly fractured rock strata and can cause problems in the safe operation of underground mines (Shepherd et al., 1981; Saghafi et al., 2008; Islam et al., 2009; Islam and Shinjo, 2009). The mining conditions in thick coal deposits in tectonically stressed masses are characterized by a number of features that are manifestations of mine pressure. The distribution of stress around a major fault zone that intersects the mine entry roadway is of considerable importance in determining the stability and safety of mining operations. The redistribution of longwall mining-induced stresses can cause important deformation inside and around the mine openings. Therefore, during mining excavation, special attention should be paid to the presence of major faults and the influence of other geologic discontinuities, especially joints, fractures/fissures, weak and flat laminated bedding planes, and small faults (Homand et al., 1997; Ozbek et al., 2003; Mark and Molinda, 2005; Sunwoo et al., 2006; Donnelly et al., 2008; Islam et al., 2009; Islam and Shinjo, 2009). Major roof collapses and instabilities in the main gate roadways can cause fatalities, injuries, and significant economic losses because these roads provide critical access to the longwall mining operations (Shen et al., 2008).

Barapukuria colliery (Fig. 6-1) is a highly tectonically deformed basin, and is influenced by a complex interaction of convergence-related tectonic processes between the continental Indian

plate with the continental Eurasian plate (Islam and Hayashi, 2008; Islam et al., 2009). Numerous north-south-trending normal faults have been identified in this coal basin. Vertical displacements range from less than 1 m to about 3 m on small faults that lie within the mining levels between –250 m to –430 m. These small-scale faults are detected at the time of mining face inspections. Besides these faults, a total of 37 intra-basinal faults have been interpreted in seismic data, which have an estimated vertical resolution of about 10 m. The largest Eastern Boundary Fault (Fig. 2), which strikes NNW-SSE for at least 5 km, has controlled sedimentation within the basin. The fault plane dips 70-75^{o} towards the east, and has an estimated vertical displacement of more than 200 m with a dominant dip-slip component. These faults correspond to the contemporary tectonic stress field of regional E-W extension along the basin axis that trends almost north-south. This extension is thought to account for the preferred orientation of roof failures in underground coal mines and jointing in roof sandstones. The second largest of these, fault Fb, strikes NW-SE in the south to N-S in the north, and has a displacement of up to 60 m (Wardell Armstrong, 1991; Bakr et al., 1996; Islam, 2005; Islam and Islam, 2005; Islam and Kamruzzaman, 2006; Islam and Hayashi, 2008; Islam et al., 2009). Fault Fb, which is further divided into Fb and Fb1, intersect the main conveyor roadway (CBR) of the Barapukuria mine (Fig. 6-2).

In the case of the Barapukuria rift basin, mining-induced deformation of strata occurred inside and around the gate roads (Islam et al., 2009). Throughout the development stage (2001-2003), it was observed that where the CBR passed through faults Fb and Fb1, the roadway was affected by a large wedge fall along a slickensided fault surface. The CBR has been driven through sandstone, siltstone, and interbedded shales and clays. Continuous collapse of clay bands and slickensided material through the fault planes created major hazards and instability in the roofs of the roadways (Islam, 2005; Islam and Islam, 2005; Islam and Kamruzzaman, 2006).

Knowledge of the mining-induced reactivation of faults, stress propagations, displacements, and deformation characteristics, as well as the failure behavior of rock strata in and around the two major faults that overlie the main CBR, remains limited. No interpretation of the mining-induced stress distribution with respect to the reactivation of the two major faults was realized, although this interpretation is essential in forecasting of mine operations. The main objectives of this paper are to present:

• an interpretation of the mining-induced stress distributions to take into account the reactivation of the two major faults associated with the CBR,

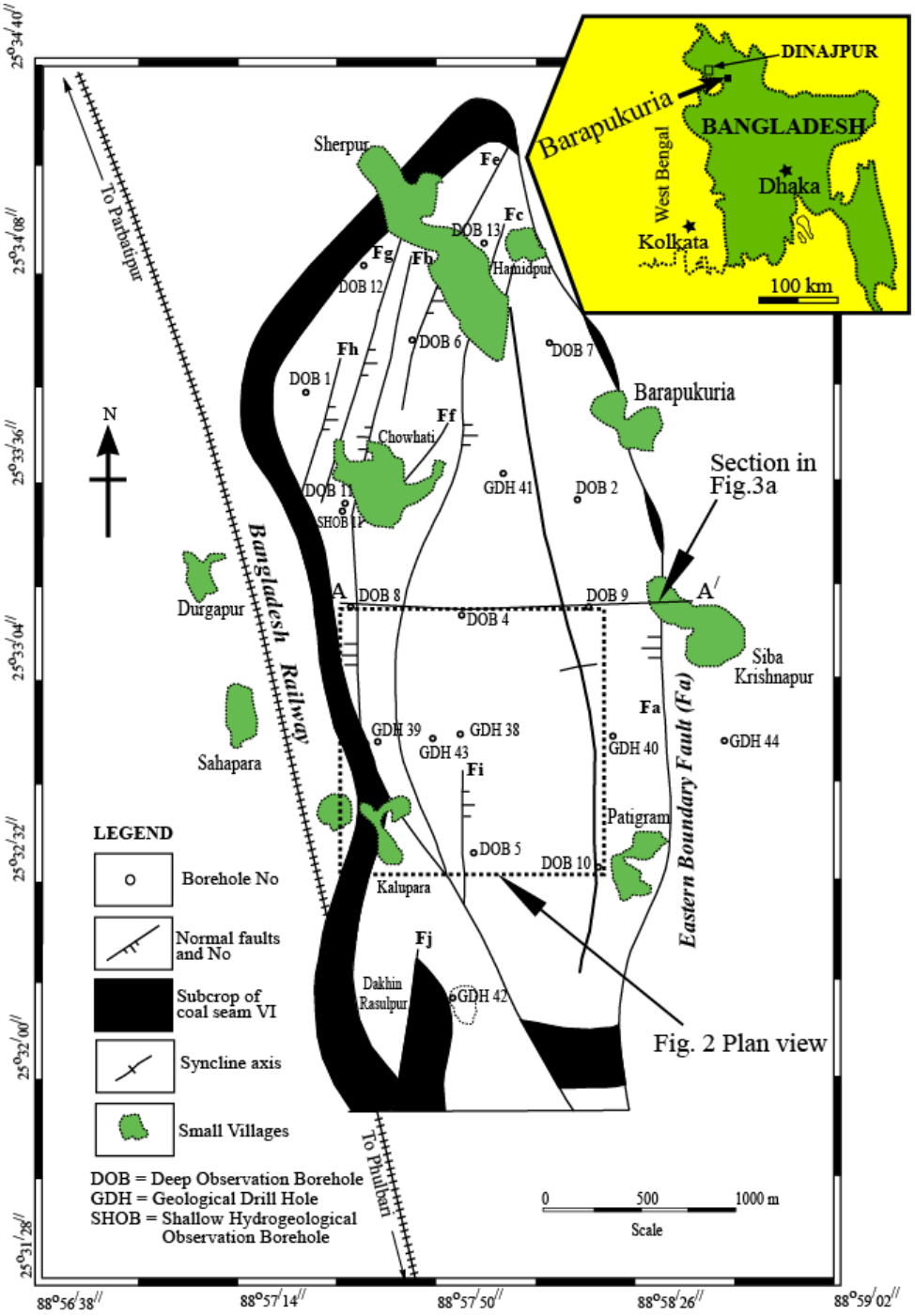

Fig. 6-1. Location of the boreholes, major faults, and structural pattern of the Barapukuria Coal Basin, NW Bangladesh. Abbreviations: DOB=Deep Observation Borehole; GDH=Geological Drill Hole; SHOB=Shallow Hydrogeological Observation Borehole (after Wardell Armstrong, 1991; Bakr et al., 1996; Islam and Hayashi, 2008; Islam et al., 2009).

- an understanding of the displacements and rock failure trajectories around the two faults,
- a prediction of rock failure loading conditions around the mine roadway, and to then apply that understanding to the development of appropriate reinforcement strategies, and
- an assessment of safety regarding earthquakes induced hazards due to the geotectonic location of the mine.

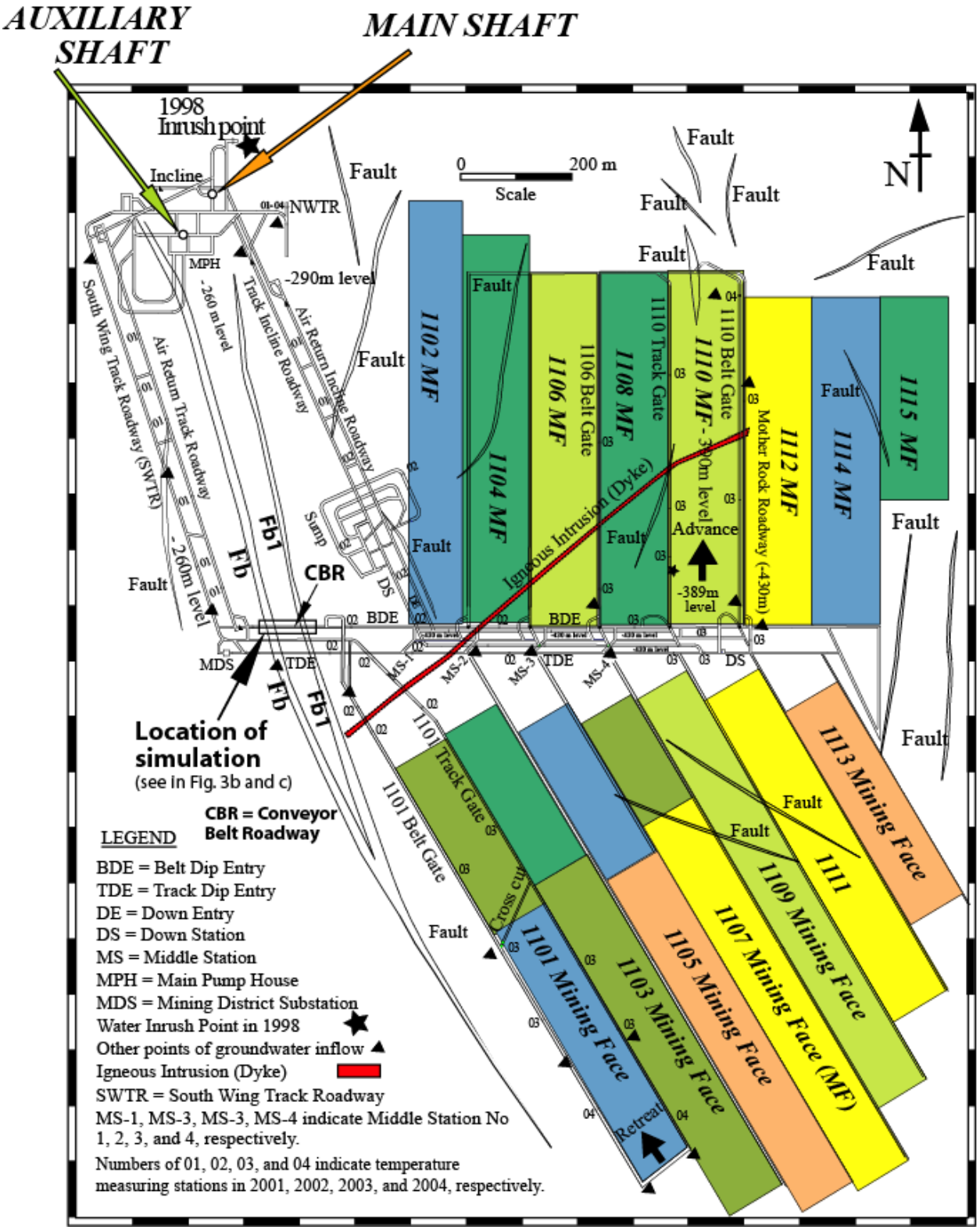

Fig. 6-2. Longwall mining panels in Barapukuria Coal Mine, Bangladesh (after Barapukuira Coal Mining Co. Ltd, 1998; Islam and Shinjo, 2009).

6.2. Geology of the main Conveyor Belt Roadway

The principal constraints on the design of the Barapukuria mine relate to the presence of the 'massive' overlying Gondwana sandstones and the unconsolidated and water-bearing Dupi Tila Formation. The Dupi Tila Formation, and the Gondwana sandstone that is in hydraulic continuity with it, represents a major potential hazard to the mine from water inflow (Wardell Armstrong, 1991; Islam et al., 2009). The entry of water into mine workings is governed by a combination of complex factors related to the formation of either bed separation cavities and/or relaxed zones above the mine excavation. As experienced by the first author (2001-2004) in the Barapukuria mine, water inflow to the mine workings mainly depends upon geological structures and discontinuities. The vertical flow of water from the Dupi Tila aquifer to bed separation cavities took place through the rock mass by intergranular seepage and flow through major faults, joints, and intensely fractured zones within the strata. Bed separation zones above caved panels provide major reservoirs for storing and transmitting water. Local variations in permeability and rates of inflow arise (Islam and Islam, 2005) because of geological features like faults, areas of strata flexure, the presence of lenticular sandstones, and jointing and faulting.

The geology and stratigraphy of the Gondwana Barapukuria coal deposit was illustrated in detail by Islam and Hayashi (2008), Islam et al., (2009), and Islam and Shinjo (2009). Based on the age and lithology, the stratigraphic sequence (Fig. 6-3a) of the Barapukuria coal deposit is divided into four formations and an igneous dike as follows:

- Holocene-recent aged Madhupur Clay Formation, about 1-15 m thick,
- Late Miocene-Middle Pliocene aged water-bearing aquifer Dupi Tila Formation (DTF), about 100-220 m thick,
- Permian-aged coal-bearing Gondwana Formation, about 133- 390 m thick,
- Lower Cretaceous aged igneous intrusion (dike), and
- Pre-Cambrian Achaean basement.

In the present study, the geological conditions of the main CBR are illustrated. A detailed geologic map (Fig. 6-3b) was prepared during the roadway excavation based on roadway face observations by the first author. Permian age Gondwana sandstones, siltstones, and subordinate carbonaceous shales were observed during the roadway excavation. Shales and siltstones around the fault zones were of poor to medium rock quality. Sandstone-siltstone-shale alterations were

observed in the roof and ribs of the roadway. The bedding strike was generally about N30 ^{o}E with dips varying from 10-18^{o}. Fault gauge extended up to about 60 m from the area immediately adjacent to the roof of the roadway. Numerous groundwater seepages caused weathering and decomposition of the shales and sandstone-siltstone alterations along low-angle bedding planes, which caused a decrease in rock strength. A wedge-shaped roof collapse, about 5 m in height (Fig. 6-3c), occurred around the faults where vertical shallow fractures were visible. These fractures provide a clear sign of the effects of high horizontal tensile stresses in and around the faults.

6.3. Numerical modeling

We used Boundary Element Method (BEM) numerical modeling, which emphasizes the role of stresses that lead to the failure of the rock surrounding the two major faults. We attempt to appraise the reactivation and deformation around the core zone and damage zone of the two faults. We applied the software package Examine2D (www.rocscience.com) to analyze the stress reactivation of faults and the deformation of the surrounding rock mass. The conventional BEM is based on the hypothesis of homogeneity of rock materials (e.g., Zhang et al., 2008).

6.3.1. Models and constraints

A model was constructed that incorporates the locations of faults Fb and Fb1 and the CBR, according to plane strain conditions. The model considers a vertical cross-section along the roadway corresponding to an overburden thickness of about 290 m. The geometry of the model is simple and consists mainly of two faults (Fb and Fb1) that sub-vertically overlie the main CBR (Fig. 6-3b). Wardell Armstrong Mining Consultants of the United Kingdom recognized fault Fb during the seismic surveys; however, Fb1 was detected during mine face advancement. The displacement of Fb was not determined exactly, but was assumed to be about 50 m with a positive standard deviation of about 20 m (Wardell Armstrong, 1991). In this modeling, we used 75 m of vertical displacement with a dominant dip-slip component of about 58^{o} for both faults. This geometry represents a typical extensional (rift) tectonic structure (Islam and Hayashi, 2008).

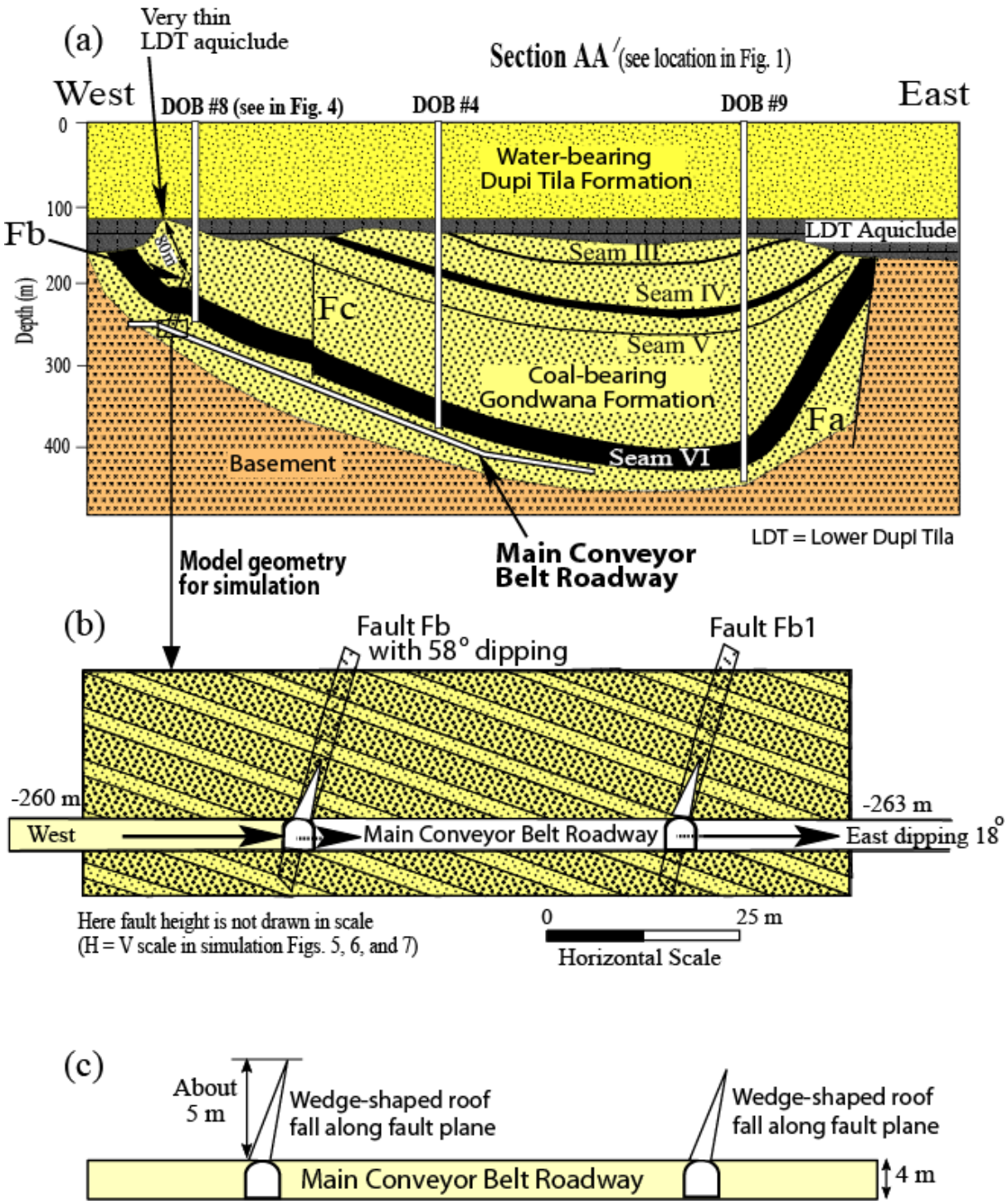

Fig. 6-3. (a) Location of the main conveyor belt roadway (CBR) under mineable seam VI that intersects two tectonic faults, Fb and Fb1. (b) Sectional views of the main conveyor belt roadway (see location in Figs. 2 and 3a) and model geometry for simulation. (c) Wedge-shaped roof fall along fault plane due to collapse of a huge amounts of slickenside materials. Height of roof cavern is about 5 m, whereas height of the roadway is 4 m.

The imposed rock mechanical parameters, which are shown in Table 6-1, are taken from Wardell Armstrong (1991). A Mohr-Coulomb failure criterion was adopted with rock mechanics parameters including overburden unit weight, Young's modulus, Poisson's ratio, tensile strength, cohesion, and angle of internal friction (Table 6-1). The depth-dependent bulk density of the stratified rock, failure loads, unconfined compressive strength (UCS), and tensile strength of some selected samples, which were taken from DOB #8 (Fig. 6-4), were determined by Wardell Armstrong Mining Consultants of the United Kingdom.

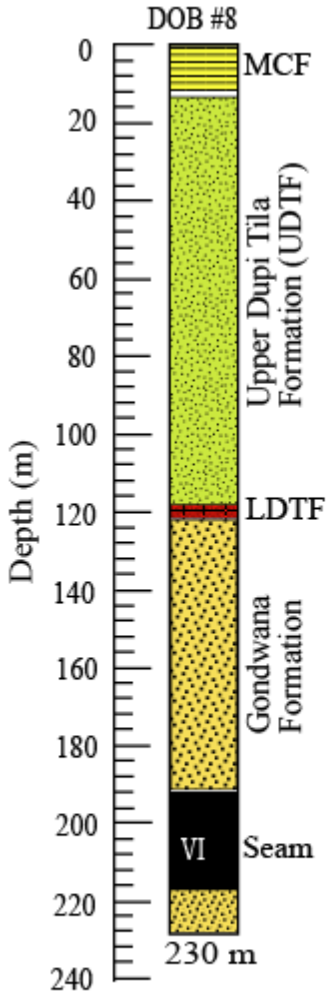

Unconfined Compressive Strength (MPa)

Depth (m)		Bulk density (kg/m^3)	Failure load (MPa)	UCS (MPa)
From	To			
139.25	139.48	2090	2.43	7.83
148.69	148.90	2120	3.52	11.21
169.50	169.70	2210	4.70	15.17
194.70	194.92	2000	1.32	4.24
202.97	203.13	1330	3.74	12.13
219.23	219.4 5	2350	7.16	23.44

UCS = Unconfined Compressive Strength (MPa):
Maximum 23.44 (MPa), and minimum 4.23 (MPa)
Failure load:
Maximum 7.16 (MPa), and minimum 1.32 (MPa)

Tensile Strength (MPa)

Depth (m)		Failure load (MPa)	Tensile Strength (MPa)
From	To		
151.12	151.29	0.42	1.36
194.84	195.00	0.61	1.85

DOB = Deep Observation Borehole
MCF = Madhupur Clay Formation
LDTF = Lower Dupi Tila Formation

Fig. 6-4. Laboratory test results of rock samples from DOB #8 (after Wardell Armstrong, 1991). For the location of DOB#8, please see cross-section AA′ in Fig. 3a.

Table 6-1. Imposed rock mechanical properties (Wardell Armstrong, 1991) in model.

Stress field	Type	Gravitational Stress
	Ground surface elevation (m)	290
	Overburden unit weight (MN/m^3)	0.022
Rock mass elastic properties	Type	Isotropic
	Young's modulus, *E* (MPa)	7550
	Poison's ratio, ν	0.25
Rock mass strength	Type of failure	Mohr-Coulomb
	Tensile strength (MPa)	1.85
	cohesion, *c* (MPa)	15
	angle of internal friction, φ (deg.)	25

6.4. Model results

Results of the simulation are illustrated in Figs. 6-5, 6-6, and 6-7. The modeling results are presented in terms of seven rock mechanical parameters as follows:

6.4.1. Distribution of σ_1 stresses

Fig. 6-5a shows the distribution of the σ_1 stress. The results show good agreement with the study of Wang and Miao (2006). They observed that the areas of decreasing and increasing horizontal stresses are in the hanging wall and the footwall of the fault, respectively. The distribution of horizontal stresses is influenced by the fault, and the stress is concentrated in the rock strata around the two ends of the fault. The maximum value of horizontal stress in our model is about 50 MPa at the bottom of the hanging wall of Fb, which is located to the left of the roof of the roadway. Although the values decreased gradually towards the roof, the contours are highly concentrated around this portion of the roadway. The minimum values of stress at the upper ends of the faults are about 20 MPa. In the region between Fb and Fb1, the stress is about 33 MPa. The horizontal stress decreased gradually toward both rib sides, the roof, and the floor. The tensional horizontal stress is negligible.

6.4.2. Distribution of σ_3 stresses

The distribution of the σ_3 stress is shown in Fig. 6-5b. The distribution of vertical stresses is influenced by the two faults. Wang and Miao (2006) found that for the case of fault reactivation, the high stress within the rock strata is concentrated at the two ends of the faults, which is

supported in our simulation. High tensional stress, about -24 MPa, is located near the roof of the roadway, which is adjacent to the bottom of the hanging wall of Fb. The stress is higher near the upper end of Fb, at about -18.8 MPa. The values decreased gradually up to about 5 m radial distance from the core of the faults, reaching -2.5 MPa within the damage zones of the faults (Fig. 6-5b). For the case of Fb1, the vertical compressional stress is lower compared with that of the tensional stress. This value ranges from 0.2 MPa to 8.3 MPa. The higher value of the vertical tensional stress indicates that the overlying strata are likely to move and deform vertically.

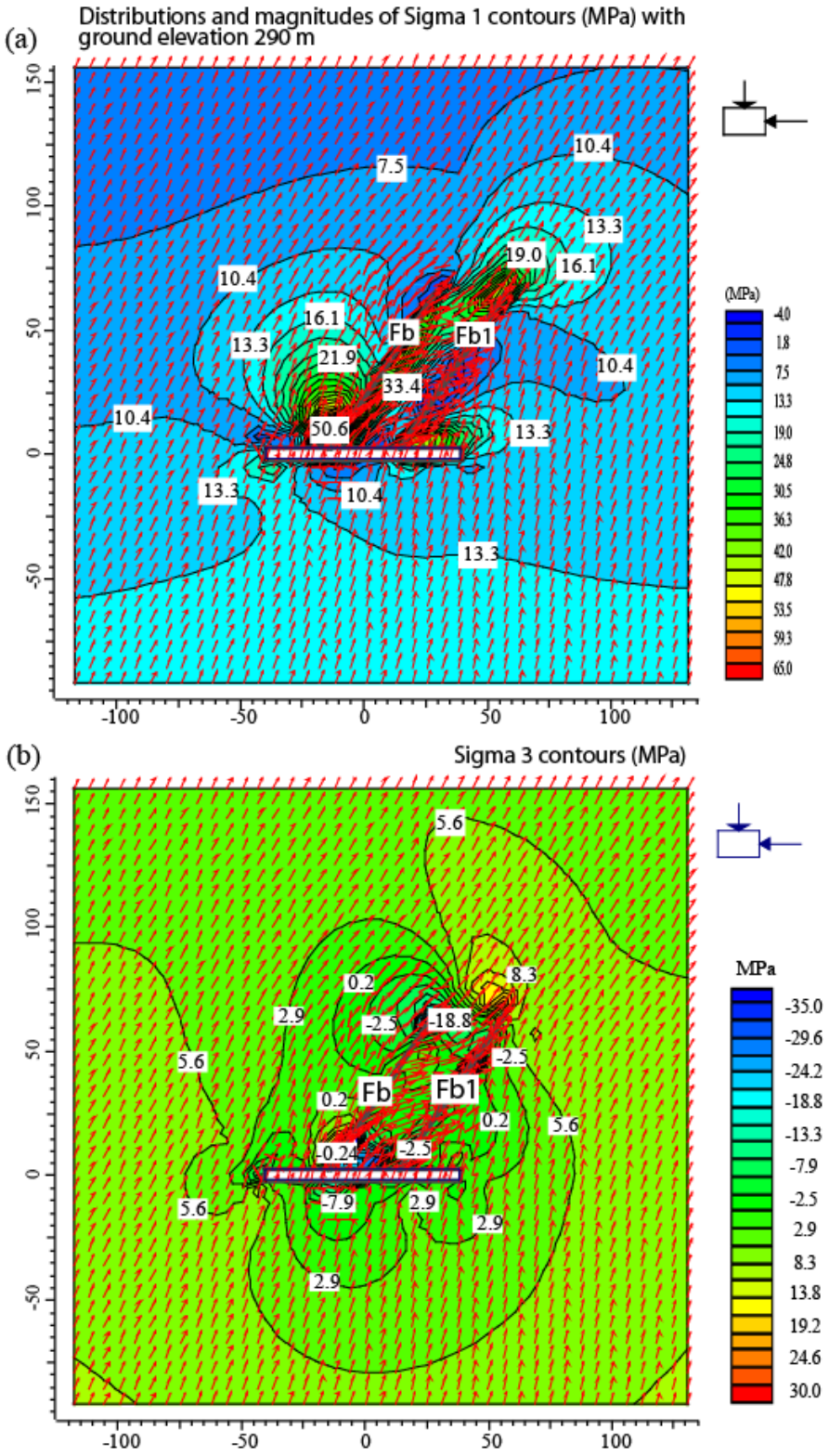

Fig. 6-5. (a) Show contours of horizontal (σ_1), and (b) shows vertical (σ_3) principal stress magnitudes around faults zones.

6.4.3. Distribution of deviatoric stresses

High deviatoric stress values were concentrated in two locations in the model, and especially near the ends of Fb and Fb1. At the bottom of the hanging wall of Fb, the values range from 21 MPa to 56 MPa, whereas at the top of the hanging wall the values range from 25.7 MPa to 34.3 MPa. Likewise, for Fb1, the deviatoric stress at the upper end of the footwall is about 17 MPa, while at the lower end it is about 38.7 MPa. In the rib sides, these values decreased toward the rock strata. In the area between the two faults, the highest calculated stress value was 51.7 MPa at the bottom, and decreased to 25.7 MPa at the upper end (Fig. 6-6a). These results indicate the tendency for either block caving or isolated rock slab failure around the highly stressed fault zone.

6.4.4. Distribution of τ_{max} stresses

The shear stress (τ_{max}) distribution around the representative faults is illustrated in Fig. 6-6b. Both types of shear stress (positive or negative and tensional) were concentrated around the faults. An area of high shear stress concentration was located at the bottom of the hanging wall and just above the main CBR. The positive shear stress ranged from 16 MPa to 32 MPa and was concentrated in an area that extended from the left side to the right side of the roof. The negative shear stress ranged from -20 to –4.0 MPa and was concentrated near the lower end of the hanging wall of Fb, which is close to the roof of the CBR. It is assumed that this configuration was caused by the release of stress during roadway development. The active region of the high stress area extended toward the excavation, corresponding to the damage from strata movement. Regarding these modeling results, we emphasis that the tensional failure due to shear stress indicates a low degree of elasticity and the tendency to resist deformation in the roof of the roadway, suggesting that block caving could occur in an unsupported excavation along the core zone of Fb. Wardell Armstrong (1991) supports this interpretation.

6.4.5. Distribution of failure trajectories within rock strata

The failure trajectories of rock strata due to reactivation of the two faults are illustrated in Figs. 6-6a-b. The failure trajectories indicate damage zones both inside the core and outside the faults. The failure zone extends up to 85 m towards the roof. This forms a narrow tapering zone

at the lower end of the hanging wall of Fb, while it forms an oval-shaped extended failure zone at the upper part of hanging wall. It is important to emphasize that this failure zone is about 80 m

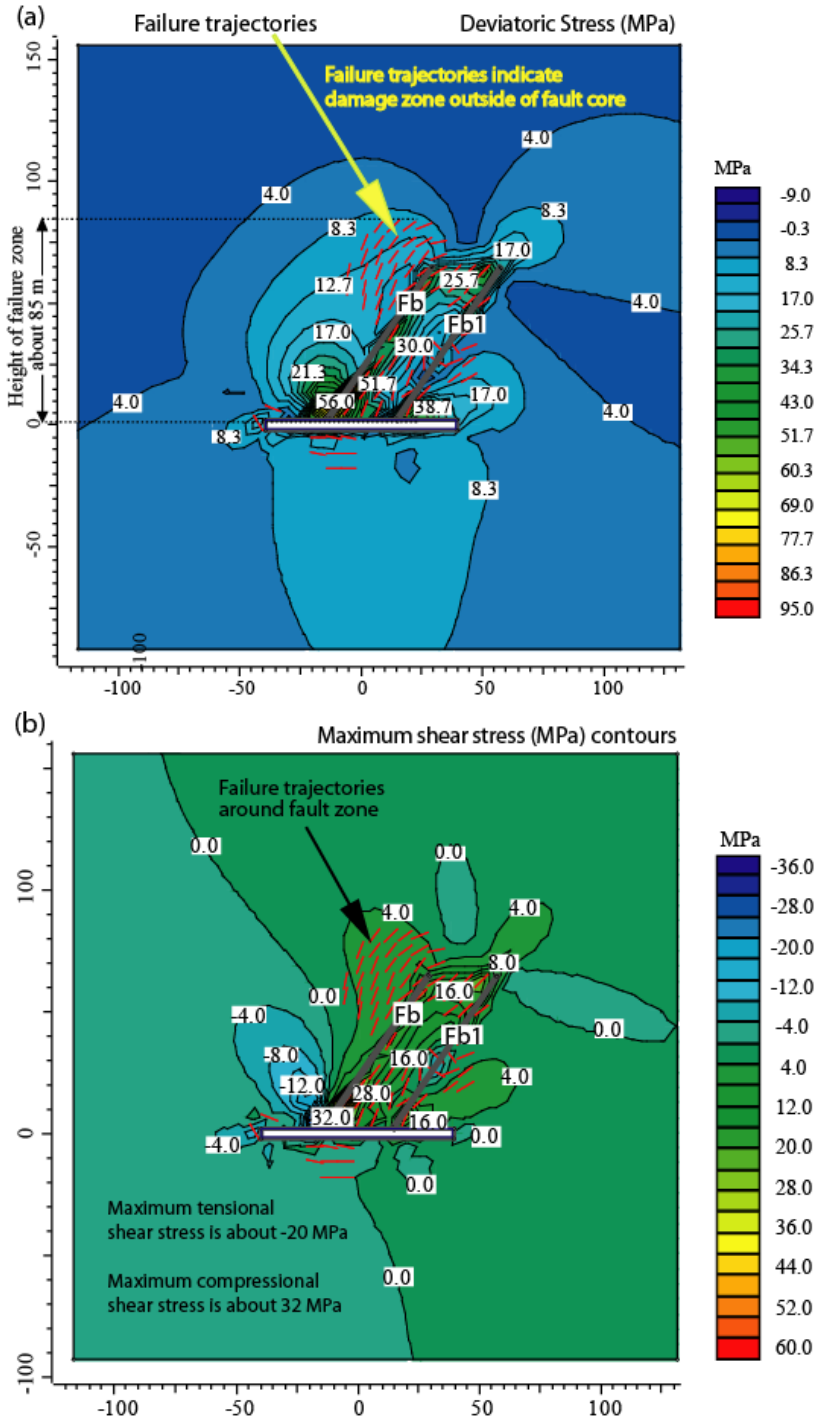

Fig. 6-6. (a) Distributions of deviatoric stress contours and strata failure trajectories around fault zones of both faults Fb and Fb1. (b) Distributions of maximum shear stress (τ_{max}) contours (MPa) and strata failure trajectories around fault zones of both faults. (c) and (d) show safety assessment between failure trajectories zones and LDT aquiclude of geologic section.

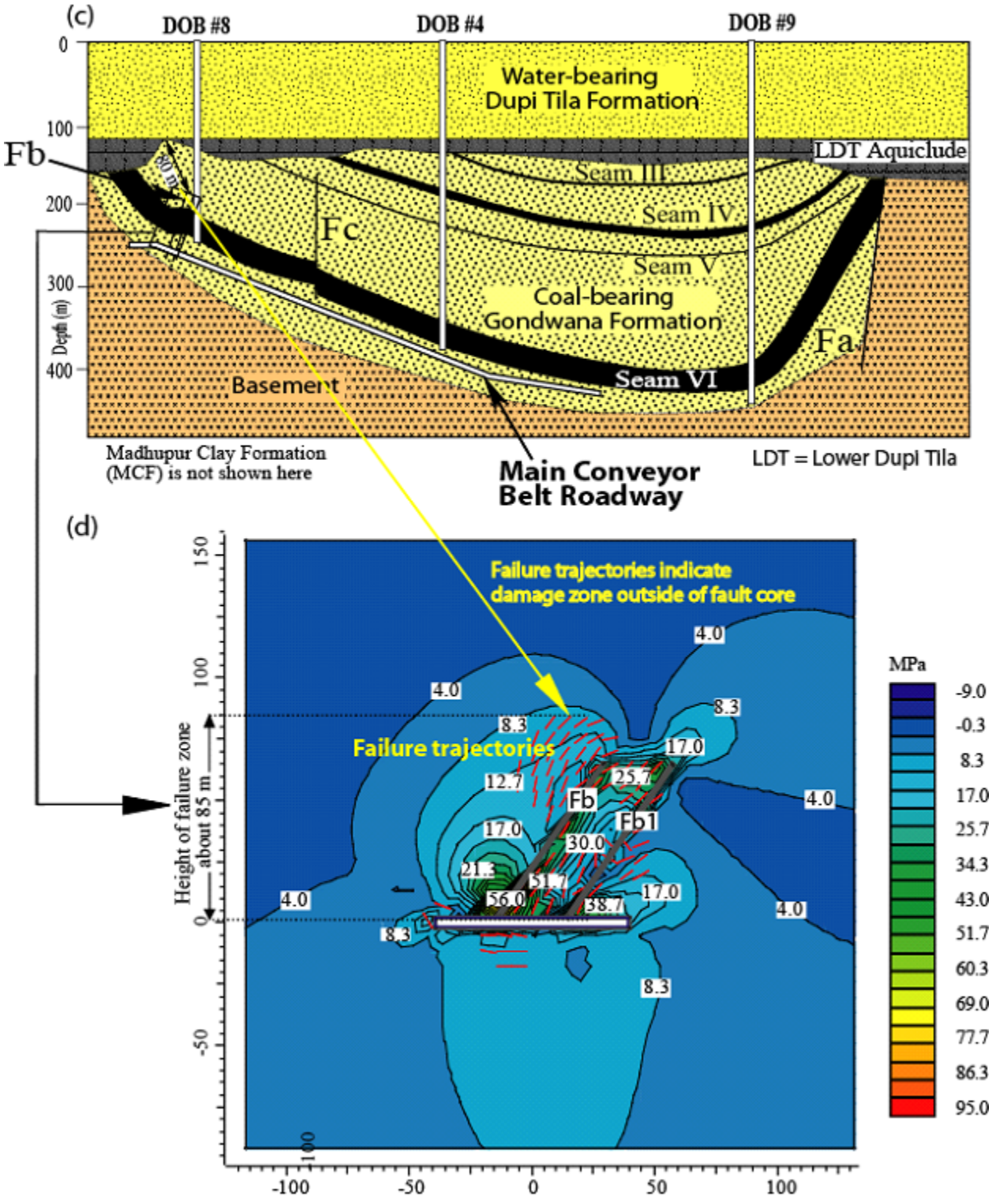

Fig.6-6 (continue)

below the very thin LDT aquiclude (Fig. 6-6c-d). This indicates that the LDT aquiclude will not be compromised because of the present state of strata failure.

6.4.6. Horizontal displacement

Fig. 6-7a shows the distribution of horizontal displacements. The simulation resulted in a horizontal displacement of 66 cm towards the roof, which gradually reduced to 12 cm towards the rib and top sides. Displacement values decreased gradually from the rib sides to the interior of the rock strata.

6.4.7. Vertical displacement

The vertical displacement around the faults is illustrated in Fig. 6-7b. At the lower end of the hanging wall of Fb, a vertical displacement of about 56 cm was simulated at the roof of the CBR, which decreased to 28 cm at a height of 40 m above the roof. The displacement decreased to 22 cm at the lower end of the hanging wall of Fb1, located at the roof above the CBR. It is reasonable to note that the displacement rapidly increased up to 36 cm at the middle of the foot wall of Fb1. These values gradually decreased to 22 cm. The 36 cm displacement contour extends up to about 60 m above the roof strata around the footwall of Fb1. The simulation results indicate that the vertical failure tendency will be limited from 40 m to 60 m toward the immediate roof of CBR.

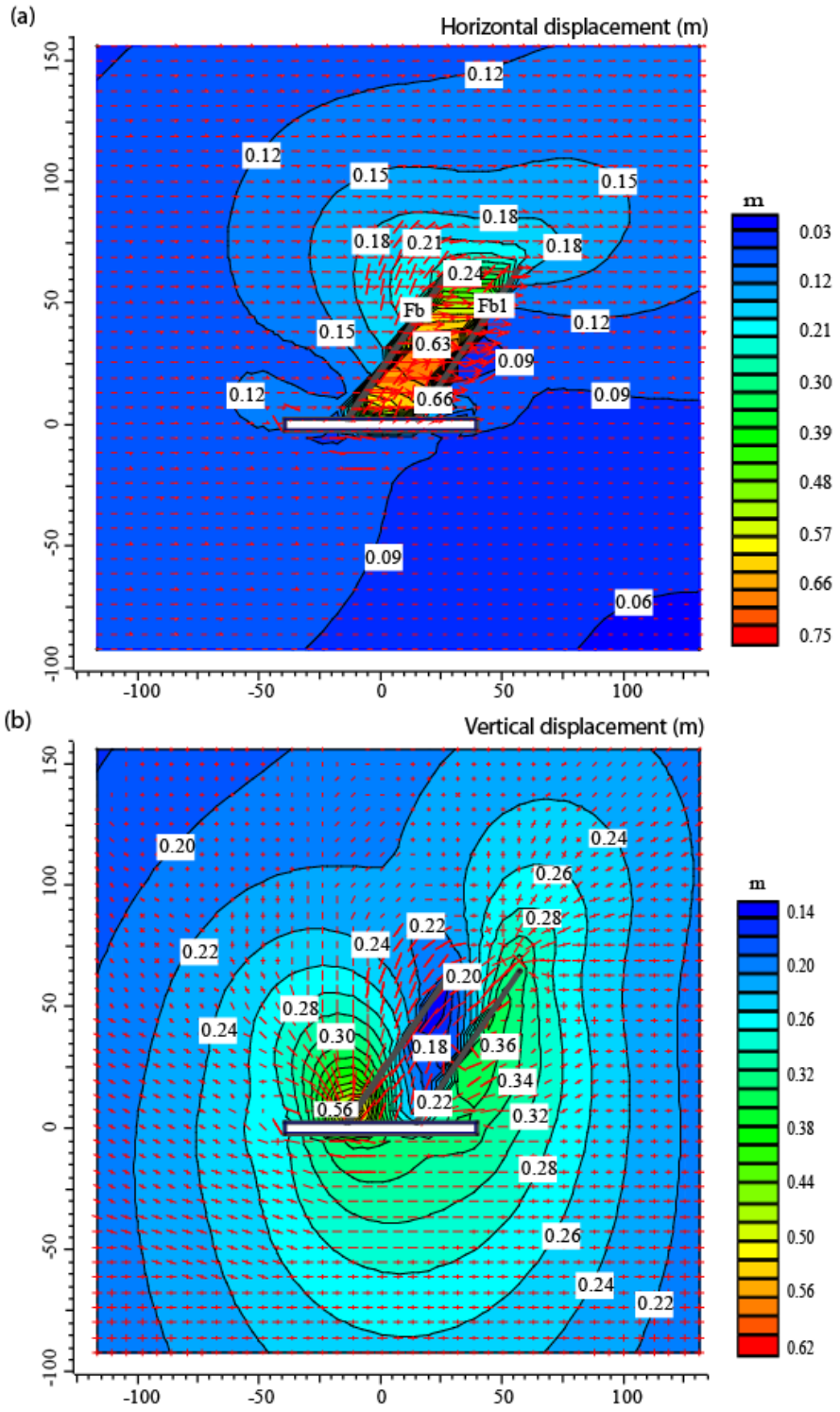

Fig. 6-7. (a) Contours of horizontal displacement (m). Maximum displacement occurs between two faults, which is about 66 cm at the lower end of the footwall of Fb and hanging wall of fault Fb1. (b) Contours of vertical displacement (m). Maximum vertical displacement is about 56 cm at the bottom of the hanging wall of Fb and at the immediate roof of conveyor belt roadway.

6.5. Discussion

The measurements of the various parameters of the stress system in the present study may be the key to successful prediction of fault reactivation and safety in the Barapukuria coal mine. As the first underground coal mine in Bangladesh, Barapukuria is also an experimental mine where the evaluation of different geo-environmental hazards is essential. In our previous two research papers, we focused on water inflow hazards due to multi-slice longwall mining (Islam et al., 2009) and gas outburst problems (Islam and Shinjo, 2009) in the Barapukuria basin. Regardless of these two problems, another difficulty, which is beyond the scope of this study, could arise due to fault reactivation around the mining roadways and equipped faces.

Many studies have shown that faults, fractures, and related zones of weakness, such as at Barapukuria, can be associated with many problems that threaten the safety of miners. Tectonic fault reactivation associated with underground mining is usually related to two major factors, including mining-induced stress redistribution around faults (Donnelly, 2006) and earthquake induced fault movement (McKinnon and Barra, 2003). Both of these can cause water inflow into the mine if the faults intersect an overlying aquifer, as in the Barapukuria basin (Islam and Islam, 2005). The presence of water above the mine strongly influences deformation and ruptures of rocks by controlling the water pressure and the geotechnical properties within fractures and faults. Moreover, groundwater entering mine workings from fault zones can lead to a disaster for mine operations. Fault zones are important because displacement can greatly reduce the strength of the surrounding bedrock due to the creation of zones of weakness and the presence of gauge materials that may be dissolved and become permeable to water (e.g., Long et al., 1991; Wu et al., 2004). Fracture-enhanced permeability depends on the density, orientation, and, importantly, the hydraulic conductivity of the individual fractures and faults. Large geological features like large-scale faults contribute to water flow (Finkdeiner et al., 1997).

In the present simulation, we showed in-situ stress patterns, displacements, and failure tendency of rock strata around two faults associated with the CBR, and emphasized the following factors:

- evaluation of failure conditions around the fault zones connected with the roof of the CBR
- prediction of loading conditions on the mine roadway, and to application of that understanding to the development of appropriate reinforcement strategies,

- hydrogeological effects of faults on underground mining,
- hydrogeological effects of dikes on underground mining, and
- prediction of earthquake-induced hazards and their impact on the safety of the mine

6.5.1. Evaluation of failure conditions around the fault zones and immediate roof of the CBR

Wardell Armstrong (1991) reported that the minimum thickness of the overlying strata, which ranged from 50-130 m, was sufficient to ensure that water inflow to longwall workings is not excessive, except where tensional zones have induced breaks. There are exceptions to this where fault planes and dikes might connect the workings and the aquifer. In places where clay-rich and non-brittle beds are present, a strata thickness of 10 times the extraction height may provide an adequate protective layer. In the 'massive sandstone' at Barapukuria, the natural joints can extend further due to mining extraction, and a protective barrier of up to 20 times the extracted height may be required to prevent excessive water inflow. This means that if the excavation height is 4 m, as in the present mine design and modeling, then 80 m of overburden rock should prevent water inflow.

The model results indicate that an extensive failure zone extends from the upper end of Fb to the left side. If we would not get any failure criterion in the model as shown in Figs. 6-6a-b, mechanical behavior of rock strata would remain smooth. Nevertheless, failure of rock strata creates subject of rethinking. The failure zone remains about 80 m below the very thin LDT aquiclude (Fig. 6-6c-d). Based on the simulation results, it is reasonable to state that the probability of water inflow through the two fault zones into the mine is negligible, unless these two faults are reactivated due to the large regional earthquakes. Fault movements due to earthquakes could damage the LDT aquiclude and connect with the Upper Dupi Tila (UDT) aquifer.

6.5.2. Loading conditions on the mine roadway and appropriate reinforcement strategies

The China National Machinery Import and Export Corporation (CMC) used drilling and blasting as the excavation method. A general support system for the roadway used a combination of rock bolts (1.8 m), wire-mesh (750×1000 mm), steel-arches, and shotcrete (10 cm thick) to prevent roof falls, rib falls, and water inflow. Our modeling results imply that bed separation

cavities would arise if a sufficient support system, with a strength greater than 55 MPa, is not available. The deviatoric stress state implies that the reinforcement strength of the support system at the roof of the roadway should be greater than 55 MPa along the fault core zone, and more than 20 MPa along the damage zone of the fault (Fig. 6-6a). The strength of the roof supporting materials, as revealed in our simulation, should be appropriately maintained for the safety of the roadway. If the strength along the cores of the faults is less than 55 MPa, then bed separation cavities could arise and major aquifers will transmit water to these cavities through the intervening beds by fracture permeability, intergranular permeability, and structural discontinuities.

6.5.3. Hydrogeological effects of faults on underground mining

Faults and fractures in the Barapukuria basin have created a groundwater flow network between the water bearing Dupi Tila aquifer and coal-bearing Gondwana rocks (Wardell Armstrong, 1991; Islam et al., 2009). Studies have revealed that major fault zones consist of two main hydrogeological structures, namely a core and a damage zone (Caine et al., 1995; Evans et al., 1997; Gudmundsson et al., 2001). The core, consisting mainly of breccia and other cataclastic rocks, has a low permeability during interseismic periods. In contrast, the fault damage zone, consisting mainly of fractures of various sizes, has a higher permeability than the core (Babiker and Gudmundsson, 2004). The effect of a fault zone on groundwater flow can be complex. For instance, part of a fault zone may act as a low-permeability barrier to flow, while others act as high-permeability conductors for flow (Gudmundsson, 2000; Babiker and Gudmundsson, 2004). These studies indicated that a fault zone can act as an important conduit, rather than as a barrier for groundwater flow, if the following two conditions are met:

- ***First,*** the permeability of the fault zone must be higher than that of the host rock. This condition implies that the fault zone must be active in the sense of concentrating tensile and shear stresses. These stresses will sustain high permeability by creating new fractures and opening old ones inside the fault zone and in the surrounding area that could largely control groundwater flow (Barton et al., 1995; Mayer and Sharp, 1998; Gudmundsson, 2000; Gudmundsson et al., 2001).
- ***Second,*** the trend of the fault zone must be generally parallel to the hydraulic gradient. For example, if a fault trends at a right angle to the hydraulic gradient, its effect on groundwater

flow is normally small. In contrast, if a high-permeability fault runs subparallel or parallel to the general groundwater flow (the hydraulic gradient), groundwater tends to flow into the fault in its upstream part and out of the fault in its downstream part (Gudmundsson, 2000).

Therefore, from the above-mentioned statements, it is essential to understand the following two factors for the case of the Barapukuria coal mine:

- the concentration of tensile and shear stresses around the faults, and
- the hydraulic gradient and general direction of groundwater inflow in the underground mining regions.

For the first factor, our model results reveal that the horizontal tensile stress is negligible (Fig. 6-5a). However, the vertical tensile stress is higher, about -18.8 MPa, around the upper end of Fb (Fig. 6-5b). Moreover, tensional shear stresses are concentrated from the middle to the lower end of the hanging wall of Fb, ranging from -20 to –4.0 MPa (Fig. 6-6b). Results of these two parameters indicate a tendency to cause high permeability zones, which could cause water inflow into the mine if Fb intersects the overlying aquifer. Nonetheless, failure trajectories (Fig. 6-6b) indicate a low probability of intersecting the overlying aquifer. However, the faults could be triggered due to earthquakes.

For the second factor, Wardell Armstrong Mining Consultants of the United Kingdom investigated the hydraulic gradient and the general direction of groundwater inflow in the Barapukuria area (Figs. 8 and 9). A moderate hydrodynamic balance appears to exist between the Upper Dupi Tila aquifer and the underlying Gondwana units, with an almost flat hydraulic gradient (0.0004–0.0006). Average transmissivity, specific yield, storage coefficient, and velocities were 1200 m^2/day, 25% to 30%, 0.0004, and 0.02 m/day, respectively (Wardell Armstrong, 1991; Islam and Hayashi, 2008). The main lineaments (faults and shear zones) and dikes (see Fig. 6-9) overlie the Achaean basement in the study area. Fb is absent within the Dupi Tila Formation, and the general direction of groundwater is NE-SW. If Fb was within the Dupi Tila Formation (Fig. 6-8), it could act as an important conduit, rather than as a barrier to groundwater flow. Conveniently, Fb is located within the Gondwana Formation (Fig. 6-9), where the general direction of groundwater is NW-SE, W-E, and SW-W-E. The hydraulic gradient and the general direction of groundwater flow are almost at right angles with the trend of Fb in the mining regions. Therefore, Fb could act as a barrier to groundwater flow, i.e., the effect on the

groundwater flow would be small. This conclusion is in good agreement with the Eastern Boundary Fault (EBF) (Figs. 6-8, and 6-9) Fa that acts as a barrier to groundwater in the east part of the Barapukuria basin.

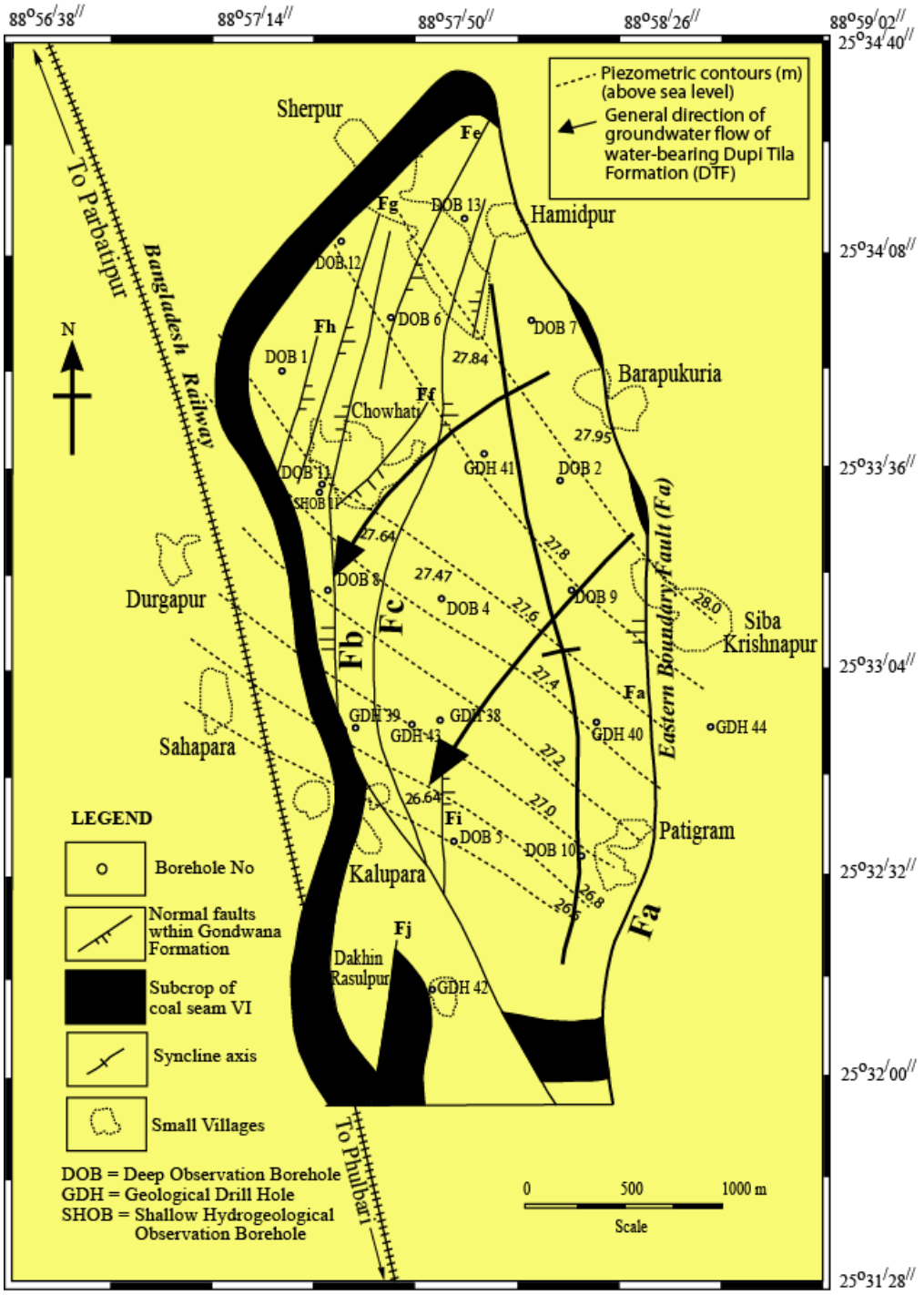

Fig. 6-8. General direction of groundwater flow within water-bearing Dupi Tila Formation (DTF) of Barapukuria coal deposits (after Wardell Armstrong, 1991).

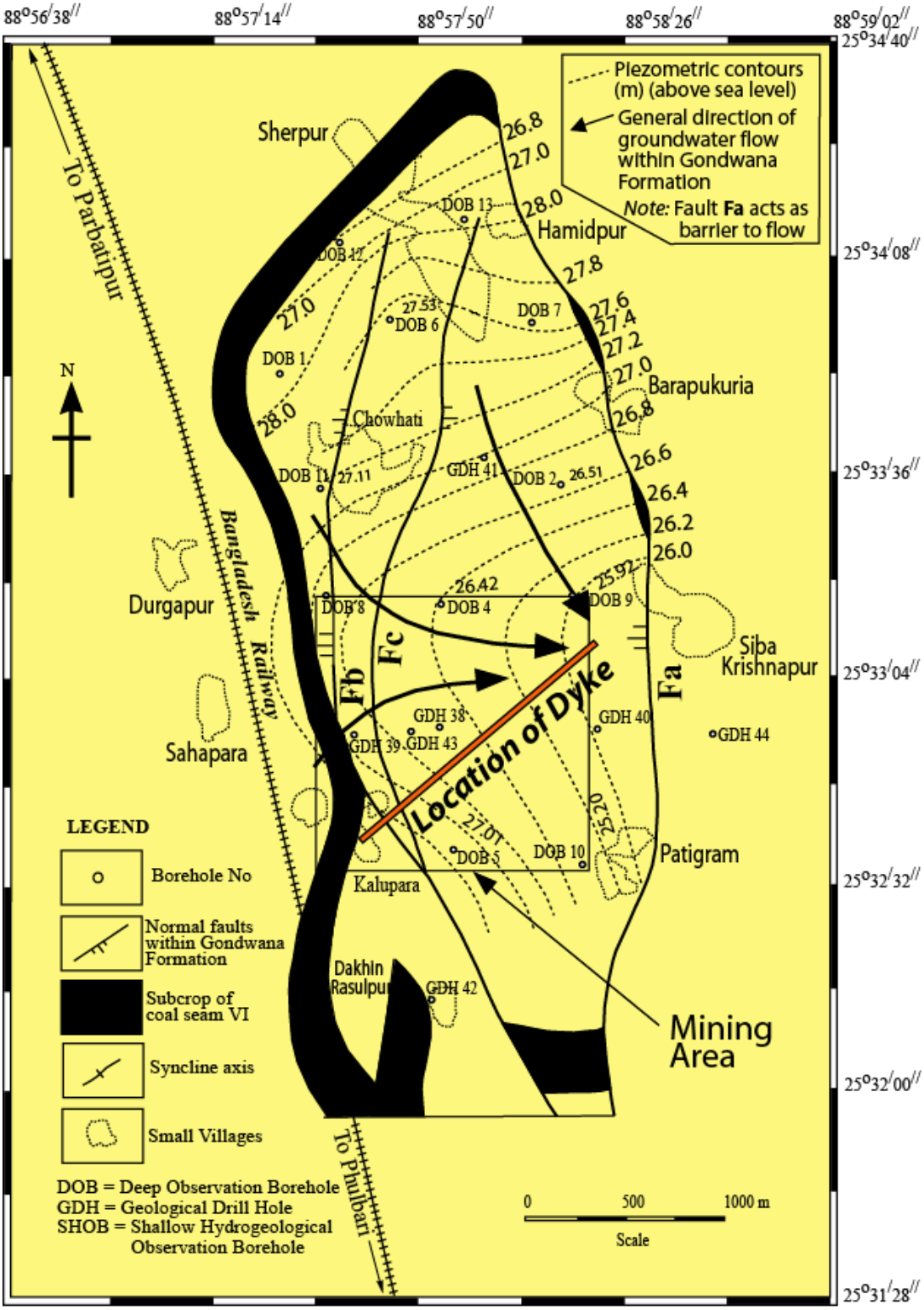

Fig. 6-9. General direction of groundwater flow within Gondwana Formation of the Barapukuria coal deposit (after Wardell Armstrong, 1991).

6.5.4. Hydrogeological effects of dikes on underground mining

Another important geological feature in the Barapukuria coal deposits is an igneous intrusion (dike) that trends NE-SW (Fig. 6-9). Studies (e.g., Babiker and Gudmundsson, 2004) have shown that not only faults, but also dikes, can play important roles in groundwater flow. Dikes can be either barriers or conductors for groundwater flow if they consist of fine-grained rock. The effect of dikes depends on their trends in relation to the hydraulic gradient and the density of the fracture systems in the dikes. Transverse dikes act both as groundwater barriers and as conductors (Babiker and Gudmundsson, 2004). In the case of the igneous dike in the Barapukuria basin, it was observed during the mining development that the dike acts as a barrier rather than a conductor for groundwater flow. A very small amount of water flows through some fracture systems of the dike; however, it was insignificant (Islam et al., 2009).

6.5.5. Prediction of earthquake induced hazard and safety of the mine

Here we discuss studies regarding earthquake induced hazards and the safety of the mine. Past earthquakes around the Barapukuria basin, with moderate to high magnitudes, were controlled by the Shillong Plateau and the Dhubri-Brahmaputra/Jamuna fault to the east and the Himalayan orogen (Fig. 6-10) to the north. Two other subsurface structures associated with earthquakes in 1965 (M 5.9) and in 1980 (M 6.0) are the NW-SE tending Tista and Gangtok lineaments, respectively (Islam and Islam, 2005; Reena and Kayal, 2003; Thakur, 2004). The greater part of the eastern Himalaya, including the Shillong Plateau and Burmese arc, and its foredeep, especially the northwest part of Bangladesh, are seismically active. The seismicity of this region is a result of collision tectonics in the Himalaya (Taponnier and Monlar, 1976; Mukhopadhyay, 1984), and subduction tectonics below the Burmese arc (Verma et al., 1976; Saikia et al., 1987; Nielsen et al., 2004). Most of the seismic activity appears to be associated with a dominant geologic unit, like a lineament. The seismicity in the southern Himalayan foredeep is inferred to mostly correspond to the Tista or other parallel lineaments, like the Padma lineament, and Dhubri-Brahmaputra/Jamuna lineament (Mukhopadhyay, 1984). The earthquakes also occur at considerable distances from the convergent plate margins between the Indian and Eurasian plates (Mukhopadhyay, 1984). Intracratonic normal faulting earthquakes occur at shallow depths (less than 40 km) in the Ganges Plain. The largest intracratonic events in the past 200 years, such as the Assam event in 1897, are apparently inconsistent with the predictions of

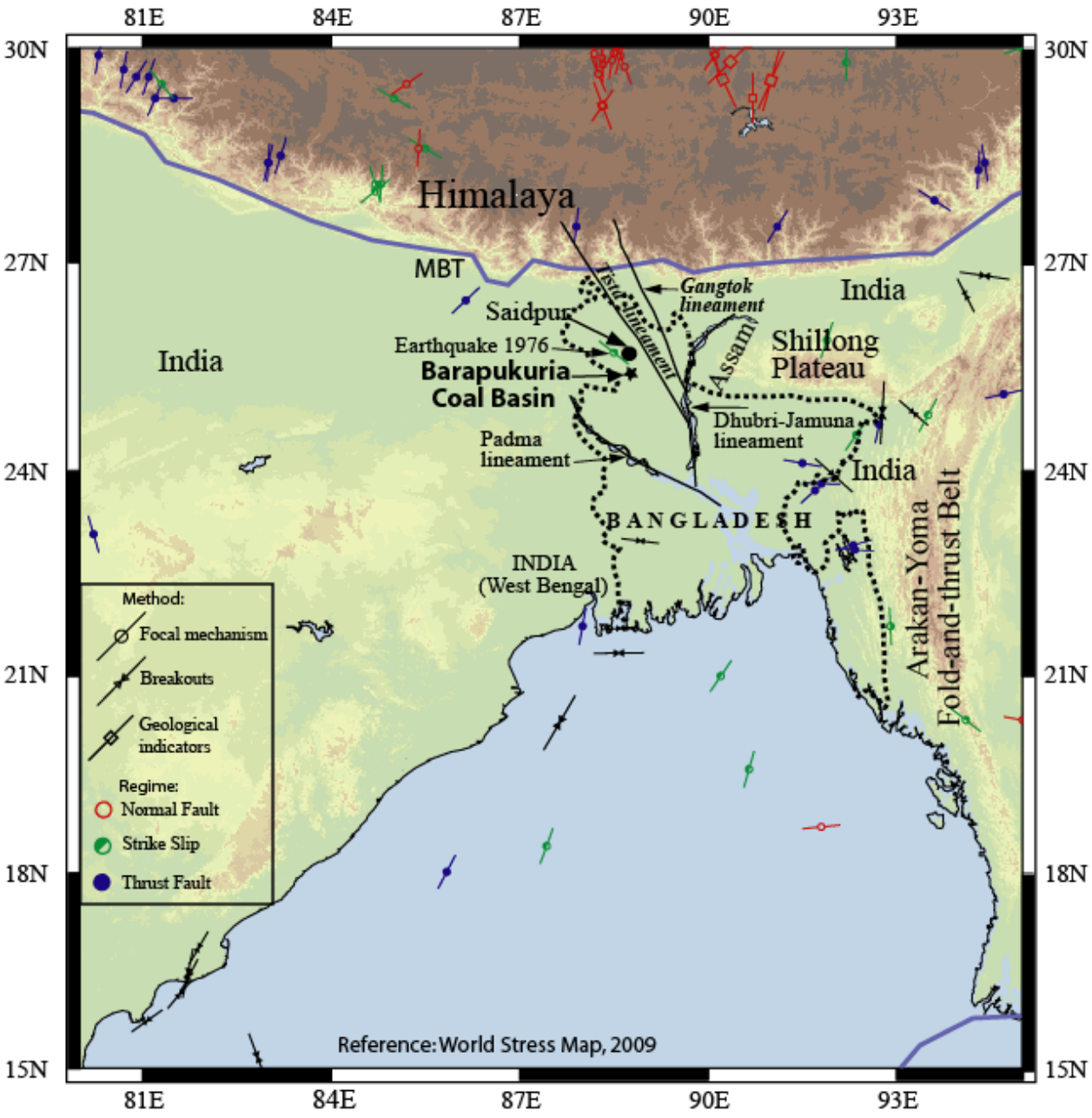

Fig. 6-10. Geotectonic location of the Barapukuria coal basin. The Shillong Plateau and Dhubri-Brahmaputra/Jamuna fault to the east and the Himalayan orogen to the north. Other two subsurface structures associated with earthquakes events in 1965 (M 5.9) and in 1980 (M 6.0) are NW-SE tending Tista, and Gangtok lineaments, respectively (Reena and Kayal, 2003). In 1976, an earthquake (focal depth 33 km, M 5.2) occurred at Saidpur (Khan and Agarwal, 1993), which is about 30 km north to the Barapukuria coal basin. High intensity of faults and fissures within the Gondwana rock sequences and their connection to the water-bearing Upper Dupi Tila Formation plus mining-induced strata failure could cause water inflow through the major fault planes if tectonic movement of the faults occurred due to seismic activity.

the 40 km thick plate (Bilham et al., 2003). The 1897 great Assam earthquake ruptured in a reverse sense, implying compression from 40 km to 9 km depth (Bilham and England, 2001). This suggests that the surface of the Indian plate in this region is in tension and is unable to sustain shallow reverse faulting (Bilham et al., 2003). Wu (2003) stated that for shallow-focus earthquakes (less than 50 km), the accumulated fluid pressure over the fault may have a control on fault movement and earthquakes. In 1976, the Saidpur earthquake (focal depth 33 km, M 5.2) occurred about 30 km north of the Barapukuria coal basin (Fig. 6-10) (Khan and Agarwal, 1993). This event implies that the Barapukuria intracratonic basin is located within a region of active seismicity. The NW-SE trending active Tista lineament is very close, about 35 km, to the Barapukuria basin. This very weak lineament is believed to have the potential for earthquake activity. Studies have shown that earthquakes with moderate magnitudes could reactivate the shallow normal faults in the Barapukuria basin, which could cause problems with multi-slice longwall mining.

Wu (2003) investigated how earthquakes along active faults relate to mining hazards, and concluded that in an active fault zone, physical and chemical interactions between water and rock lead to a softening in the filling materials that lubricates fault planes and changes structures. These processes decrease the cohesion and angle of internal friction in the fault zone and reduce the strength of the active fault planes and filling materials. The decrease in the cohesion and angle of internal friction within tectonically formed slickensides along a slickensided fault-surface has always been a threat to the safety and efficiency of underground coal mines (Singh et al., 1996; Phillipson, 2003; Mark and Molinda, 2005). Roof failures occur due to the presence of slickensided materials and massive and laminated strata overlying the mining excavation (Singh et al., 1996; Hebblewhite and Lu., 2004).

From our model, we obtained the in situ vertical tensional stress (Fig. 6-5b) and higher shear stress (Fig. 6-6b) in the hanging wall of fault Fb. The vertical tensional stress in the upper part of Fb and the failure trajectories in the unfractured rock imply a decrease in the cohesion and angle of internal friction in the fault zone (Wu, 2003). Normal faults, as at Barapukuria, are related to rift tectonic events and are potentially active. This indicates that if faults Fb and Fb1 become active and movement occurs associated with the regionally active Tista lineament or other intracratonic events as at Saidpur (1976), it could have an adverse effect on the safety of the mine. The results of the failure trajectories indicate that that mining-induced reactivation of

the faults is less likely to generate heavy water inflow into the mine. However, if the regional earthquake intensity is higher and movement occurs along the fault planes, and the faults intersect the LDT aquiclude, liquefaction could be generated along the fault zones and enhance water inflow into the mine.

6.6. Conclusions

In this paper, BEM numerical modeling was used to simulate mining-induced fault reactivation associated with a key roadway of the Barapukuria Coal Mine. Previous studies have indicated that reactivation of faults could lead to widespread damage to an underground mine. Disputed causes of fault reactivation (Donnelly, 2006) in underground coal mining have resulted in large-scale roof collapse and damage to mining equipment, fatal accidents, hindering of production, and economic losses. Multi-slice longwall mining operations, such as at Barapukuria, could experience several phases of fault reactivation during the lifetime of the mine. The following important points should be considered for the safety of the mine:

(1) We found an 85 m high zone of failure trajectories that extends above the roof. Conveniently, the zone is about 80 m vertically below the LDT aquiclude. Therefore, the extent of the failure trajectories around reactivated faults implies a low probability of causing water inflow through faults into the mine.

(2) The reinforcement strength should be more than 55 MPa along the fault core zone, and more than 20 MPa adjacent to the damage zone of the fault, in order to support the roof of the CBR.

(3) The general direction of groundwater flow is almost at right angles with the trend of faults Fb and Fb1. This indicates that groundwater flow though the fault is not efficient.

(4) If movement occurs along the faults planes due to a large earthquake, and if the faults intersect the overlying thin Lower Dupi Tila aquiclude, then liquefaction could be generated along the fault zones, which could cause water inflow into the mine.

References

Babiker, M., and Gudmundsson, A., 2004. The effects of dykes and faults on groundwater flow in an arid land: the Red Sea Hills, Sudan. Journal of Hydrology 297, 256–273.

Bakr, M.A., Rahman., Q.M.A., Islam, M.M., Islam, M.K., Uddin, M.N., Resan, S.A., Haider, M.J., Islam, M.S., Ali, M.W., Choudhury, M.E.A., Mannan, K.M., and Anam, A.N.M.H., 1996. Geology and Coal Deposits of Barapukuria Basin, Dinajpur District, Bangladesh, Records of Geological Survey of Bangladesh. 8, pt 1.

Barton, C.A., Zoback, M.D., Moos, D., 1995. Fluid flow along potentially active faults in crystalline rock. Geology 23, 683–686.

Bilham, R., Bendick, R., and Wallace, K., 2003. Flexure of the Indian Plate and Intraplate Earthquakes. Proc. Indian Acad. Sci. (Earth Planet Sci.)112, 1-14.

Bilham, R., and England. P., 2001. Plateau pop-up during the great 1897 Assam earthquake. Nature 410, 806 – 809.

Caine, J.S., Evans, J.P., Foster, C.B., 1995. Fault zone architecture and permeability structure. Geology 24, 1025–1028.

Crouch,S.L., and Starfield, A.M., 1983. Boundary Element Method in Solid Mechanics. George Allen & Unwin Publishers Limited, 40 Museum Street, London WC1A 1LU, UK, pp.321.

Donnelly, L.J., Culshaw, M.G., Bell, F.G., 2008. Longwall mining-induced fault reactivation and delayed subsidence ground movement in British coalfields. Quarterly Journal of Engineering Geology and Hydrogeology 41, 301-314.

Donnelly, L.J., 2006. A review of coal mining induced fault reactivation in Great Britain. Quarterly Journal of Engineering Geology and Hydrogeology 39, 5-50.

Evans, J.P., Foster, C.B., Goddard, J.V., 1997. Permeability of faultrelated rocks and implication for hydraulic structure of fault zones. Journal of Structural Geology 19, 1393–1404.

Finkbeiner, T., Barton, C.A., and Zoback, M.D., 1997. Relationship among in-situ stress, fractures and faults, and fluid flow: Monterey Formation, Santa Maria Basin, California. AAPG Bulletin 81, 1975-1999.

Gudmundsson, A., Berg, S.S., Lyslo, K.B., Skurtveit, E., 2001. Fracture networks and fluid transport in active fault zones. Journal of Structural Geology 23, 343–353.

Gudmundsson, A., 2000. Active fault zones and groundwater flow. Geophys. Res. Lett. 27, 2993–2996.

Hebblewhite, B.K., and Lu, T., 2004. Geomechanical behavior of laminated, weak coal mine roof strata and the implications for a ground reinforcement strategy. International Journal of Rock Mechanics & Mining Sciences 41, 147-157.

Homand, F., Souley, M., Gaviglio, P., and Mamane, I., 1997. Modelling natural stresses in the arc syncline and comparison with in situ measurements. International Journal of Rock Mechanics & Mining Sciences 34, 1091-1107.

Islam, M.R., and Shinjo, R., 2009. Numerical simulation of stress distributions and displacements around an entry roadway with igneous intrusion and potential sources of seam gas emission of the Barapukuria coal mine, NW Bangladesh. International Journal of Coal Geology (article in press).

Islam, M.R., Hayashi, D., and Kamruzzaman, A.B.M., 2009. Finite element modeling of stress distributions and problems for multi-slice longwall mining in Bangladesh, with special reference to the Barapukuria coal mine. International Journal of Coal Geology 78, 91-109.

Islam, M.R., and Hayashi, D., 2008. Geology and coal bed methane resource potential of the Gondwana Barapukuria Coal Basin, Dinajpur, Bangladesh. International Journal of Coal Geology 75, 127-143.

Islam, M.R., and Kamruzzaman, A.B.M., 2006. Geochemical and Techno-environmental Behaviour of Gondwana Coals from the Barapukuria coal mine, Bangladesh. Bangladesh Journal of Geology 25, 48-63.

Islam, M.R., 2005. Influence of tectonic structures for the occurrence of gas emission at 1110 working panel in Barapukuria Coal Mine, Bangladesh. Geodynamics and Environment in East Asia (GEEA), International Conference & 5th Taiwan-France Earth Science Symposium, 24-29 November, 2005, Taitung, Taiwan, pp.155-156.

Islam, M.R., and Islam, M.S., 2005. Water Inrush Hazard in Barapukuria Coal Mine, Dinajpur District, Bangladesh. Bangladesh Journal of Geology 24, 1-17.

Khan, A.A., and Agarwal, B.N.P., 1993. The crustal structure of western Bangladesh from gravity data. Tectonophysics 219, 341-353.

Long, J.C.S., Karasaki, K., Davey, A., Peterson, J., Landsfeld, M., Kemeny, J., and Martel, S., 1991. An inverse approach to the construction of fracture hydrology models conditioned by

geophysical data. International Journal of Rock Mechanics and Mining Sciences & Geomechanics Abstracts 28, 121-142.

Mark, C., Molinda, G.M., 2005. The Coal Mine Roof Rating (CMRR)- a decade of experience. International Journal of Coal Geology 64, 85-103.

Mayer, J.R., Sharp, J.M., 1998. Fracture control of regional groundwater flow in a carbonate aquifer in a semi-arid region. Geol. Soc. Am. Bull. 110, 269–283.

McKinnon, S.D., and Barra, I.G., 2003. Stress field analysis at the El Teniente Mine: evidence for N-S compression in the modern Andes. Journal of Structural Geology 25, 2125-2139.

Mukhopadhyay, M., 1984. Seismotectonics of traverse lineaments in the eastern Himalaya and its foredeep. Tectonophysics 109, 227-240.

Nielsen, C., Rooke, N.C., Rangin, C., Bourdon, E., Han, U,M., Aung, U.T.T., Htin, U.K., Swe, U.M., Farcy, F., and Sun, D.T.H., 2004. From partial to full strain partitioning along the Indo-Burmese hyper-oblique subduction. Marine Geology 209, 303-327.

Ozbek, A., Turkmen, S., and Gul, M., 2003. The deformation evaluation of Kizlac T3A Tunnel (Osmaniye, Turkey). Engineering Geology 67, 309-320.

Phillipson, S.E., 2003. The control of coal bed decollement-related slickensides on roof falls in North American Late Paleozoic coal basins. International Journal of Coal Geology 53, 181-195.

Reena De and Kayal, J.R. 2003. Seismotectonic Model of the Sikkim Himalaya: Constrain from Microearthquake Surveys. Bulletin of Seismological Society of America 93, 1395-1400.

Saghafi, A., Pinetown, K.L., Grobler, P.G., Heerden, J.H.P., 2008. CO_2 storage potential of South African coals and gas entrapment enhancement due to igneous intrusions. International Journal of Coal Geology 73, 74-87.

Saikia, M.M., Kotoky, P., and Duarah, R., 1987. A zone of plate convergence with associated seismic activity- the Indo-Burman arc. Tectonophysics 134, 145-152.

Shen, B., King, A., and Guo, H., 2008. Displacement, stress and seismicity in roadways roofs during mining-induced failure. International Journal of Rock Mechanics & Mining Sciences 44, 672-688.

Shepherd, J., Rixon, L.K., Griffiths, L., 1981. Outbursts and geological structures in coal mines: a review. Int. J. Rock Mech. Min. Sci. Geomech. Abstr. pp. 267-283.

Singh, R., Singh, T.N., Dhar, B.B., 1996. Coal pillar loading in shallow mining conditions. International Journal of Rock Mechanics & Mining Sciences 33, 757-768.

Sunwoo, C., Jung, Y.B., Karanam, U.M.R., 2006. Stability assessment in wide underground mine openings by Mahtews' stability graph method. Tunneling and Underground Space Technology 21, 246.

Tapponier, P., and Monlar, P., 1976. Slip-line theory and large-scale continental tectonics. Nature 264, 319-324.

Thakur, V.C., 2004. Active tectonics of the Himalayan Frontal Thrust and seismic hazards to Ganges Plain. Current Science 86, 1554-1560.

Verma, R.K., Mukhopadhyay, M., and Ahluwalia, M.S.,1976. Earthquakes mechanism and tectonics features of northern Burma. Tectonophysics 32, 387-399.

Wang, L., and Miao, X., 2006. Numerical Simulation of Coal Floor Fault Activation Influenced by Mining. Journal of China Univrsity of Mining & Technology 16, 385-388.

Wardell Armstrong, 1991. Techno-Economic Feasibility Study of Barapukuria Coal Project (unpubl.), Dinajpur, Bangladesh.

Wu, Q., Wang, M., Wu, X., 2004. Investigations of groundwater bursting into coal mine seam floors from fault zones. International Journal of Rock Mechanics & Mining Sciences 41, 557–571.

Wu, Y., 2003. Mechanism analysis of hazards caused by the interaction between groundwater and geo-environment. Environmental Geology 44, 811-819.

Zhang, H.Q., He, Y.N., Tang, C.A., Ahmad, B., and Han, L.J., 2008. Application of an improved flow-stress-damage model to the critically assessment of water inrush in a mine: a case study. Rock Mechanics Rock Engineering, DOI 10.1007/s00603-008-0004-2.

Chapter 7

Coal Bed Methane (CBM) Resource Potential of the Barapukuria Basin

Chapter 7

Coal Bed Methane (CBM) Resource Potential of the Barapukuria Basin

7.1. Introduction

Barapukuria Coal Mine (Fig. 3-1) is sited on a subcropped asymmetrical synclinal deposit of Permian age Gondwana coal measures, a structure first indicated by a negative gravity anomaly in oil and gas exploration. Exploration for the deposit was initiated by the Geological Survey of Bangladesh (GSB), with seven surface boreholes. These boreholes confirmed the existence of a substantial coal deposit, comprising a sequence of up to six coal seams, some of which had the potential for economic exploitation.

From 1988 to 1991, a Feasibility Study of the prospect was undertaken by Wardell Armstrong Mining Consultants Company of the United Kingdom, and the company drilled a further twelve deep surface boreholes, 11 shallow hydrogeological investigation boreholes, and 18 surface seismic survey lines to determine the large scale tectonic structure of the deposit. The broad extent and structure of the Barapukuria deposit was thereby established by Wardell Armstrong Mining Consultants based on drilled boreholes and seismic data. In 1994, the China National Machinery Import and Export Corporation (CMC) completed a further 13 boreholes within the known limits of the deposit.

The thickest and most laterally extensive seam of the deposit is designated Seam VI, with an average thickness of about 36m. The initial design of Barapukuria Coal Mine was undertaken by CMC, and focused on this primary target seam for multi-slicing by longwall mining. Construction and shaft sinking commenced in 1996. The development of the underground pit-bottom and main service roadways was interrupted in April 1998 by a major inflow of water from the overlying Dupi Tila sediments. Subsequent to this serious incident, the original mine design was revised. An additional two surface boreholes were also completed for hydrogeological investigation, and both three- and two-dimensional seismic surveying was carried out. Coal production commenced in 2005 and is continuing at the present time.

The stratigraphy and structure of the basin is now known in some detail, both from the above surface exploration, and direct geological monitoring of the underground developments. To date, however, no analytical investigation has been undertaken on the potential of exploiting coal bed methane (CBM) from the basin. CBM is virtually identical in quality to the conventional natural gas for which exploration continues worldwide. The economic success of CBM exploitation in the USA, Canada, and Australia has prompted other countries to examine their own CBM potential. However, investment and research is usually dependent upon individual government energy policies and priorities and therefore levels of commitment between countries vary greatly.

In Bangladesh, natural gas is currently the major indigenous non-renewable energy resource. The proven and probable resource, contained within 22 gas fields in the country total is estimated at 804.5 Gm^3, of which 580.7 Gm^3 is considered recoverable. Approximately 144.5 Gm^3 has been consumed to June 2003 leaving a remaining recoverable reserve of 436.2 Gm^3. Gas production has increased sharply over the last decade with the result that natural gas resources are likely to be exhausted in 15 to 20 years (National Energy Policy, 2004). Investment in the research and development of alternative energy sources must therefore be prioritised as part of the government's long term energy policy. In this respect, CBM exploitation from coal deposits discovered in the Jamalgonj, Barapukuria, Phulbari, Khalaspir, Dighipara, Nawabgonj, and Dangapara basins (Fig. 3-2) can contribute to the increasing energy demands of the country.

Barapukuria is the first and only coal mine to be developed in Bangladesh, with an estimated recoverable reserve of 34 Mt, and a life of 30 years at the planned production rate. The remaining measured resource is 343 Mt of in-situ coal. The principal reason for this low recovery ratio (9%) are the difficult underground geological conditions for mining. Only Seam VI is ever likely to be mined by underground methods, and following the major water inflow in 1998, planned extraction was limited to the southern area of the deposit. A methane emission occurred on a producing coal face in 2005, indicating that CBM exploitation from the remaining resources in Seam VI and the overlying seams has significant potential as an economic source of energy.

Imam et al. (2002) investigated the CBM potential of the Jamalgonj coal deposit near Joypurhat district of NW Bangladesh, and to date remains the only work completed in this field. This study examines the potential of CBM exploitation from the total in-situ coal resource of the Barapukuria deposit, including a review of previous exploration and the evaluation of the geological structure, coal rank, porosity and permeability, geothermal gradient and other parameters. This has been presented by Wardell Armstrong (1991) and Bakr et al. (1996). The no new data was collected and this paper represents a synthesis of data from the references. We have used the equations of Kim (1977), Mullen (1988), and Nolde and Spears (1998) for the assessment of gas content and gas-in-place.

The study considers:

- Thickness and depth of the coal seams
- Coal rank, composition and maceral content
- Characteristics of coal cleats
- Hydrodynamics
- Porosity and permeability of coal
- Geothermal gradient

CBM technology has the potential to make a significant contribution to the future energy demands of Bangladesh, and could provide an economically attractive alternative to relatively environmentally unfriendly surface and underground coal mining. A summary of the five primary coal deposits identified in Bangladesh to date is given in Table 7-1 and Coal Bed Methane (CBM) resource potential of the Barapukuria deposit is described in detail in the following sections.

Table 7-1. Summary of Coal Deposits, Bangladesh (Ref. Petrobangla, 1994)

Name/ Location	Area (km^2)	No of Coal seams	Depth Range (m below surface)	In-situ Coal Resources (Mt)
Jamalgonj	unproven	7	650-1158	1054*
Khalaspir	12.26	8	257-483	828
Phulbari	unproven	2	150-250	over 500
Dighipara	unproven	1	328-422	unproven
Barapukuria	5.16	6	118-518	377

* Imam et al. (2002)

7.2. Coal Quality

7.2.1. Analytical Basis

Detailed analyses of approximately 450 coal core samples were carried out in UK laboratories as part of the Feasibility Study of Wardell Armstrong Mining Consultants. The coal cores were split longitudinally and samples taken on a continuous 'ply-by-ply' basis throughout each coal seam. Half was retained in permanent storage at the Barapukuria site. The suite of tests included measurement of:

- Moisture
- Ash content
- Volatile Matter
- Fixed Carbon
- Total Sulphur Content
- Gross Calorific
- Ultimate Analysis (Carbon, Hydrogen, Nitrogen, Sulphur, Oxygen)
- Chlorine

Prior to analysis, the coal was ground to a specific size and 'air-dried' to a moisture content in equilibrium with the laboratory environment. Results are quoted on an 'as analysed' or 'air' dried (ad) basis, and usually often also adjusted mathematically to a 'dry' basis (db). The 'air dried' or 'dry' coal qualities are not, however, equivalent to the quality of the coal in-situ, or run-of-mine product which is analysed on an 'as received' (ar) basis. Coal quality characteristics of the Barapukuria coal seams are given in Tables 7-2 and 7-3 (Wardell Armstrong, 1991). The 'in-situ' and 'as mined' moisture content of the coal was measured on 93 composite samples in compliance with the ASTM Standards Test D1412-07(1979) to determine the 'Equilibrium moisture' content. The results of these tests show 'equilibrium moisture' varies within the range of 3% to 9%.

Table 7-2. Proximate analysis of Barapukuria coal (seam II to VI) with a special reference to DOB #9 (see location in Fig. 3) (Wardell Armstrong, 1991).

Sample No	Depth ranges (m)		Results of proximate analyses											
			As Received						Dry Basis					Relative Density
	From	To	Moist (%)	Ash (%)	VL (%)	FC (%)	TS (%)	CV (KCal)	Ash (%)	VL (%)	FC (%)	TS (%)	CV (kcal)	
DOB9/S2/2	155.00	156.99	5.80	45.80	19.90	28.50	1.19	3586	48.60	21.10	30.30	1.26	3807	1.88
S2/3	156.99	158.98	3.80	17.80	28.70	49.70	0.46	6207	18.70	29.80	51.70	0.48	6452	1.45
S2/4	158.98	160.97	8.10	61.90	12.60	17.40	0.29	1674	67.40	13.70	18.90	0.32	1822	2.24
S2/5	160.97	162.96	6.70	30.20	22.30	40.80	1.66	4762	32.40	23.90	43.70	1.78	5104	1.68
S2/6	162.96	164.95	2.60	63.50	12.40	21.50	0.29	2011	65.20	12.70	22.10	0.30	2065	2.17
S2/7	164.95	166.94	7.90	21.40	24.90	45.80	0.51	5398	23.20	27.00	49.80	0.66	5861	1.58
S2/8	166.94	168.95	5.70	19.20	25.10	50.00	0.45	5974	20.40	26.60	53.00	0.48	6335	1.48
Average	---		5.80	37.11	20.84	36.24	0.69	4230	39.41	22.11	38.50	0.75	4492	1.78
DOB9/S3/10	177.27	179.79	3.40	19.20	28.20	49.20	0.42	6087	19.90	29.20	50.90	0.43	6301	1.48
S3/11	179.79	182.31	4.70	28.80	27.90	38.60	0.79	4957	30.20	29.30	40.50	0.83	5201	1.53
Average	---		4.05	24.00	28.05	43.90	0.61	5522	25.05	29.25	45.70	0.63	5751	1.51
DOB9/S4/12	208.53	209.63	3.80	35.10	21.10	40.00	0.59	4659	36.50	21.90	41.60	0.61	4843	1.72
S4/13	209.63	210.73	8.30	16.00	27.00	48.70	0.61	6049	17.50	29.40	53.10	0.67	6597	1.49
S4/14	210.73	211.83	6.20	34.90	17.90	41.00	0.44	4513	37.20	19.10	43.70	0.47	4811	1.75
S4/15	211.83	212.93	9.40	12.40	30.50	47.70	0.96	6128	13.70	33.70	52.60	1.06	6764	1.47
S4/16	212.93	214.03	3.10	58.00	13.10	25.80	0.26	2598	59.90	13.50	26.60	0.27	2681	2.09
S4/17	214.03	215.13	9.30	19.20	23.00	48.50	3.14	5597	21.20	25.40	53.40	3.46	6171	1.56
S4/18	215.13	216.23	8.00	10.90	31.00	50.10	0.64	6468	11.80	33.70	54.50	0.70	7030	1.38
S4/19	216.23	217.33	3.40	67.90	14.70	14.00	0.36	1342	70.30	15.20	14.50	0.37	1389	2.22
S4/20	217.33	218.42	6.10	19.70	23.90	50.30	0.54	5855	21.00	25.50	53.50	0.58	6235	1.48
Average	---		6.40	30.46	22.47	40.68	0.84	4801	32.12	24.16	43.72	0.91	5169	1.68
DOB9/S5/21	238.89	240.07	4.70	19.90	26.00	49.40	0.73	6023	20.90	27.30	51.80	0.77	6320	1.45
S5/22	240.07	241.24	5.20	31.40	22.50	40.90	0.63	4842	33.10	23.70	43.20	0.66	5108	1.55
S5/23	241.87	242.42	3.90	36.90	22.20	37.00	0.53	4634	38.40	23.10	38.50	0.55	4822	1.6
S5/24	242.42	243.67	3.90	40.40	20.40	35.30	2.02	4272	42.00	21.20	36.80	2.10	4445	1.65
Average	---		4.43	32.15	22.78	40.65	0.98	4943	33.60	23.83	42.58	1.02	5174	1.56
DOB9/S6/25	381.62	363.96	3.10	27.10	25.30	44.50	0.54	5507	28.00	26.10	45.90	0.56	5673	1.54
S6/26	383.96	386.30	3.10	27.40	25.00	44.50	0.39	5374	28.30	25.80	45.90	0.40	5546	1.55
S6/27	386.30	388.64	3.70	18.30	29.40	48.60	0.43	6087	19.00	30.50	50.50	0.45	6321	1.44

Sample No	From	To	Moist (%)	Ash (%)	VL (%)	FC (%)	TS (%)	CV (KCal)	Ash (%)	VL (%)	FC (%)	TS (%)	CV (kcal)	Relative Density
S6/28	388.64	390.98	4.50	12.70	30.10	52.70	0.54	6601	13.30	31.50	55.20	0.57	6912	1.39
S6/29	390.98	393.32	5.30	9.60	31.00	54.10	0.45	6765	10.10	32.70	57.20	0.47	7144	1.37
S6/30	393.32	395.66	4.40	12.80	30.20	52.60	0.44	6686	13.40	31.60	55.00	0.46	6994	1.4
S6/31	395.66	398.00	3.40	15.90	29.10	51.60	0.50	6366	16.50	30.10	53.40	0.52	6590	1.48
S6/32	398.00	400.34	4.10	12.70	31.70	51.50	0.42	6708	13.20	33.10	53.70	0.44	6995	1.44
S6/33	400.34	402.68	5.20	10.60	29.80	54.40	0.47	6827	11.20	31.40	57.40	0.50	7202	1.44
S6/34	402.68	405.02	5.20	10.60	29.80	54.40	0.47	6827	11.20	31.40	57.40	0.50	7202	1.44
S6/35	405.02	407.36	3.90	12.60	29.90	53.60	0.57	6755	13.10	31.10	55.80	0.59	7029	1.47
S6/36	407.36	409.70	3.30	15.50	31.30	49.90	0.55	6610	16.00	32.40	51.60	0.57	6836	1.41
S6/37	409.70	412.04	4.40	20.10	26.60	48.90	0.33	5959	21.00	27.80	51.20	0.34	6233	1.47
S6/38	412.04	414.38	4.70	19.30	28.00	48.00	0.40	6009	20.30	29.40	50.30	0.42	6305	1.45
S6/39	414.38	416.72	3.40	16.90	28.90	50.80	0.47	6153	17.50	29.90	52.60	0.49	6370	1.42
S6/40	416.72	419.06	3.90	8.60	27.90	59.60	0.54	6164	8.90	29.00	62.10	0.56	6414	1.43
S6/41	419.06	421.43	4.20	16.60	29.50	49.70	0.57	6227	17.30	30.80	51.90	0.60	6500	1.45
Average	---		4.11	15.72	29.03	51.14	0.48	6331	16.37	30.27	53.36	0.50	6604	1.45

Table 7.2 (continued)

Abbreviations: DOB9 = Deep Observation Borehole No 9; S2 = Seam No 2; S3 = Seam No 3; S5 = Seam No 5; S6 = Seam No 6; VL = Volatile Matter; FC = Fixed Carbon, TS = Total Sulphur; CV = Calorific Value; moist = mois

Table 7-3. Ultimate and maceral analyses of Barapukuria coal (Wardell Armstrong, 1991). Abbreviations: S2 = Seam No 2; S3 = Seam No 3; S5 = Seam No 5; S6 = Seam No 6; U = Upper; L = Lower; A, B, C, D, E, F, G indicate sub-zones of Seam VI; moist = moisture; Ave. = average

Composites	**S2/U**	**S2/L**	**S3/U**	**S4/U**	**S4/L**	**S5**	**S6/A**	**S6/B**	**S6/C**	**S6/D**	**S6/E**	**S6/F**	**S6/G**	**S6/L**	**Ave.**
Equilibrium Moist (%)	4.2	4.8	5	5.3	5.9	4.2	3.9	4.8	4.6	5.8	4.6	4.6	4.6	4.8	4.79
DRY BASIS															
Ash content (%)	18.50	20.40	19.40	16.80	16.60	20.50	24.40	11.40	15.60	11.60	14.20	21.20	18.10	22.60	17.95
Pyrite sulphur (%)	0.29	0.17	0.41	0.34	0.19	0.37	0.33	0.41	0.12	0.14	0.09	0.07	0.38	0.38	0.26
Sulphate sulphur (%)	0.01	0.01	0.01	Nil	0.01	Nil	0.01	0.01	0.01	0.01	0.01	0.07	Nil	Nil	0.02
Organic sulphur (%)	0.18	0.38	0.03	0.36	0.39	0.31	0.14	0.04	0.41	0.42	0.36	0.27	0.13	0.07	0.25
Chlorine (%)	<0.01	0.11	0.06	<0.01	<0.01	<0.01	<0.01	<0.01	<0.01	<0.01	<0.01	<0.01	<0.01	0.13	0.02
Ash analyses (Oxides)															
SiO_2 (%)	50.52	65.35	49.63	63.79	57.57	70.33	59.59	48.32	50.45	47.99	49.67	50.90	49.64	55.37	54.94
Al_2O_3 (%)	36.28	27.84	34.87	27.93	33.91	24.16	30.65	37.22	40.09	39.49	40.08	34.78	33.78	36.27	34.10
Fe_2O_3 (%)	7.74	2.55	9.32	3.09	1.73	1.94	5.37	5.63	2.09	1.89	2.81	8.95	9.54	0.95	4.54
TiO_2 (%)	2.59	2.29	2.89	2.28	3.11	2.65	2..57	2.98	3.34	3.27	3.24	3.04	2.75	3.48	2.71
Mn_3O_4 (%)	0.28	0.10	0.31	0.07	0.06	0.07	0.17	0.16	0.11	0.06	0.10	0.29	0.32	0.05	0.15
CaO (%)	0.87	0.44	0.88	0.71	0.41	0.38	0.65	1.10	1.24	1.23	1.01	0.80	0.87	0.50	0.79
K_2O (%)	0.72	0.44	0.71	0.48	0.32	0.52	0.59	0.77	0.70	0.99	0.91	0.83	0.67	0.78	0.67
Na_2O (%)	0.082	0.071	0.094	0.158	0.076	0.097	0.087	0.105	0.028	0.101	0.097	0.113	0.034	0.109	0.09
MgO (%)	0.706	0.198	0.599	0.248	0.092	0.116	0.371	0.415	0.149	0.200	0.243	0.523	0.457	0.160	0.32
P_2O_5 (%)	0.467	0.274	0.485	0.158	0.159	0.095	0.298	0.768	0.908	0.931	0.773	0.35	0.471	0.348	0.46
SO_3 (%)	0.10	0.02	0.06	0.31	<0.01	0.02	0.04	0.14	0.06	0.04	0.03	0.16	0.10	0.02	0.08
Maceral analyses															
Vitrinite (%)	32.8	17.6	24.4	44.8	34.0	26.4	29.6	38.8	41.6	47.60	34.0	26.4	35.2	31.6	33.2
Liptinite (%)	7.2	5.2	5.6	4.8	5.2	6.8	7.3	6.0	4.0	3.70	8.9	6.9	8.1	6.4	6.1
Inertinite (%)	60.0	77.2	70.0	50.4	60.8	66.8	63.1	55.2	54.4	48.70	57.1	66.7	56.7	62.0	60.5
Mineral matter (%)	10.9	12.0	10.8	9.8	9.7	12.1	14.5	6.7	9.3	6.90	8.5	12.5	10.6	13.4	10.5
Reflectance *Ro* max (%)	0.70	0.73	0.73	0.68	0.69	0.71	0.72	0.72	0.71	0.72	0.75	0.78	0.72	0.72	0.72
DRY ASH FREE BASIS, Ultimate analyses															
Carbon (%)	82.87	83.82	82.94	83.09	83.32	83.65	82.69	84.37	83.71	81.83	84.58	83.12	82.5	82.49	83.21
Hydrogen (%)	4.92	4.69	4.86	4.95	4.77	4.79	4.95	5.05	5.12	5.23	5.12	5.13	5.22	4.97	4.98
Nitrogen (%)	1.72	1.66	1.69	1.79	1.77	1.86	1.76	1.63	1.61	1.62	1.62	1.6	1.59	1.64	1.68
Oxygen (%)	9.9	9.13	9.95	9.33	9.43	8.84	9.97	8.43	8.92	10.68	8.14	9.63	10.07	10.32	9.48
Total sulphur (%)	0.59	0.7	0.56	0.84	0.71	0.86	0.63	0.52	0.64	0.64	0.54	0.52	0.62	0.58	0.64

Average ash content (dry basis) volatile matter, and fixed carbon for Seam VI are 16.37%, 30.27%, and 53.36%, respectively, although these vary within different zones of the seam. Ultimate analyses (dry ash free basis) (Table 7-3) indicate that typical contents of total carbon, hydrogen, nitrogen, oxygen, and sulphur are 83.21%, 4.98%, 1.68%, 9.48%, and 0.64% respectively (Wardell Armstrong, 1991). In Seam VI, the petrographic constituents vary from zone to zone, with inertinite content between 48 - 66%,vitrinite from 26.4% - 47.6%, and an average liptinite content of 6%.

7.2.2. Coal Rank

The Barapukuria coal is high volatile B bituminous rank. From proximate analysis of Seam VI, volatile matter varies between 25.8 and 33.1% (db) and from 34 to 40% (dmmf). Calorific value varies between 5546 and 7202 (kcal/kg). An indicator of rank more usually applied to higher rank coal is the vitrinite reflectance (R_o). In Barapukuria, the mean value of R_o is 0.72%, although this varies from minimum of 0.55 for the shallower coals in the north to about maximum of 0.84% in the deepest part of the deposit (Wardell Armstrong, 1991).

7.3. Characteristics of Cleat

Two cleat sets are identified in Seam VI. The primary cleat (also known as the butt cleat) generally strikes N60^{o}W with an average spacing of 20-25 m^{-1}. A secondary cleat set (face cleat) strikes N30^{o}E with a spacing of 8-10 m m^{-1}. The cleat is well developed in the bright vitrainous coal horizons, and to a lesser extent in the inertinite-dominant layers. Most cleats are perpendicular to the bedding and are usually mineralised with ankeritic calcite. The intersection of both cleat sets has resulted in high permeability of the coal seam (Islam and Islam, 2005).

7.4. Hydrodynamics

The hydrodynamic properties of the coal and associated strata are of fundamental importance to the CBM potential of the deposit, and are controlled by the four principal

formations as defined in section 2.5. The Upper Dupi Tila aquifer is a prolific groundwater reservoir extending over larger areas of Bangladesh (Khan, 1991). This formation is the source of water for irrigation and domestic supply. The Gondwana Sandstone is a poor aquifer, but is in hydraulic connection with the Upper Dupi Tila aquifer in the northern part of the deposit where the Lower Dupi Tila aquiclude is absent. Despite a finite fractured or "weathered" permeability, the Pre-Cambrian Basement is considered to form a basal aquiclude to the overlying Gondwana and Dupi Tila aquifers (Wardell Armstrong, 1991).

There is a proven potential for groundwater flow from the Upper Dupi Tila into the Gondwana sandstones. In the north of the coal basin where the Lower Dupi Tila aquiclude is absent, the Gondwana sandstones are recharged at the Tertiary/Gondwana unconformity. All Gondwana sandstones are typically jointed, although the joints are frequently mineralised or infilled which reduces the secondary permeability of the aquifer. There appears to be a moderate dynamic balance between the Upper Dupi Tila aquifer and the underlying Gondwana, with an almost flat hydraulic gradient (0.0004-0.0006). Average transmissivity, specific yield, storage coefficient, and velocities were 1200m^2/day, 25% to 30%, 0.0004, and 0.02m/day respectively (Wardell Armstrong, 1991).

7.4.1. Porosity and Permeability of Overburden and Seam VI

The porosity of the overburden and the interbedded Gondwana strata varies from 23.90% for very fine-grained sandstone to 33.3% for clays. The Upper Dupi Tila aquifer has a mean porosity of 33%. In the Lower Dupi Tila, with predominantly clayey sands, the porosity is about 41%. In Gondwana sandstones, the average porosity is about 20% (Wardell Armstrong, 1991). Wardell Armstrong Mining Consultants did not measure the coal porosity. They only assumed that in the more permeable coal seams, the porosity is 10%. For CBM production, whenever the porosity in coal is discussed, it is in reference to the cleat porosity and not to the matrix. Cleat porosity of a coal seam can be determined from the coal fabric, such as the cleat spacing (a) and aperture width (b) (Bustin et al., 2008). In the present study, cleat porosity of Barapukuria coal is thereby determined by the following equation (Harpalani and Chen, 1995).

$$\phi = \frac{2b}{a} \qquad (1)$$

If the cleat intensity is about 8/m (cleat spacing, a =125 mm) as mentioned in section 4, and aperture width ranges between 1 – 2 mm, then calculated porosity ranges from 1.6% to 3.2%. In-situ injection packer-tests were carried out by Wardell Armstrong Mining Consultants to determine the permeability values. The permeability of the various lithologies ranges from 3.67 to 75 mD, and 4.81 to 558 mD for medium, and coarse grained sandstone, respectively. The upper coal seams have a permeability between 9.8 mD and 137.8 mD because these seams are comparatively soft and to a varying extent are in hydraulic continuity with the Upper Dupi Tila aquifer. Seam VI has a permeability range from 13 mD to 119 mD (Wardell Armstrong, 1991).

7.5. Geothermal Gradient Strata Temperature

Continuous absolute and differential temperature logs were run in the majority of exploration boreholes drilled by WA and CMC. The holes were generally left 12 to 24 hours prior to logging in order to allow drilling mud to acquire the in-situ strata temperature. The geothermal gradient is determined at 3.2^{o}C/100 m in the Dupi Tila Formation and 3.6^{o}C/100 m in the Gondwana Formation. Temperatures in Seam VI were determined at between 29.5^{o}C in the extreme NW to more than about 40^{o}C in the deepest part of the basin (Wardell Armstrong, 1991). Subsequent to underground development of roadways at the mine, further data have become available regarding the reservoir temperature variation. Measured temperatures vary within the range 31^{o} to 35^{o}C (Islam and Islam, 2005).

7.6. CBM Potential of the Barapukuria Basin

The evaluation of the coal bed methane content at Barapukuria Basin is based on exploration data and the application of Wardell Armstrong (1991), and the use of Nolde and Spears (1998) equation. This is compared with the gas content formulae of Mullen (1988), and Kim (1977), that are primarily based on coal rank and composition. In addition, studies of the cleat and fracture systems in the coal and recent underground temperature data are included.

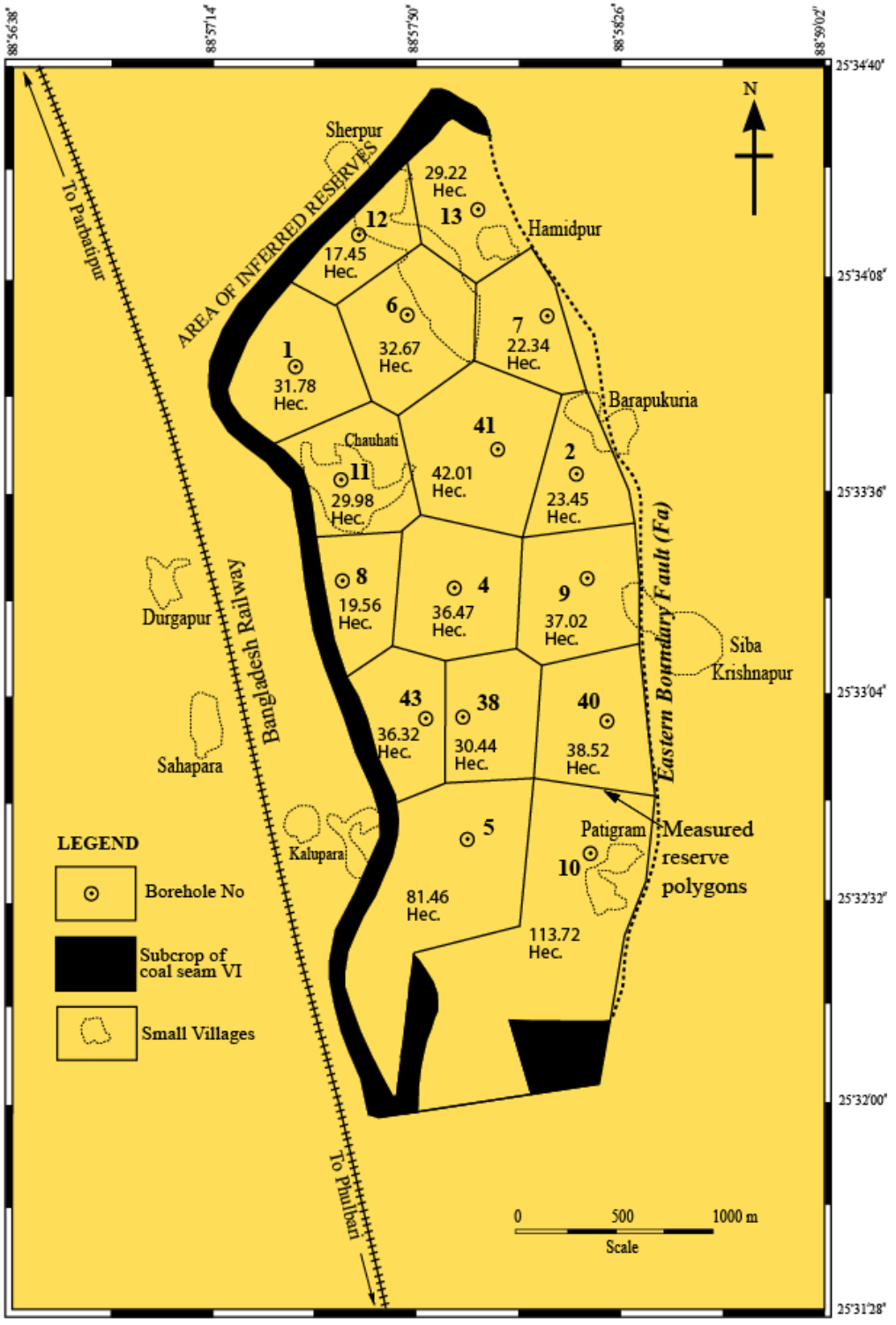

Fig. 7-1. Seam VI in-situ geological reserve area. Main reserve block contains reserve zones 1, 2, 4, 5, 6, 7, 8, 9, 10, 11, 12, 13, 38, 40, 41, and 43, which are named after the included boreholes (modified after Wardell Armstrong, 1991).

7.6.1. Database and Methodology

The critical parameters for the estimation of CBM generation are:

(a) Thickness and extent of coal seams and total resources, and/or desorption and adsorption data
(b) In the absence of desorp and adsorp data, the gas content can be estimated using a coals rank.

The thickness and aerial extent of seams II, III, IV, V, and VI, as determined from boreholes data and seismic surveying have been used for the quantification of the total coal resource (Fig. 7-1). The area of the deposit is subdivided into zones (Polygon Method) as defined by the location of the exploration boreholes. This is considered more accurate and reliable than using arithmetically averaged borehole data due to variation in borehole distribution across the deposit. An average 14,593 tonnes/Ha/m has been assessed at Barapukuria.

In the quantification of the CBM potential, equations 2 and 3 below are applied, (Nolde and Spears, 1998). Estimated gas content (Table 6) is compared with that derived from equations 4 (Mullen, 1988) and 5 (Kim, 1977) to reconcile any discrepancy. The results of all equations show a significant agreement in the CBM potential at Barapukuria. It is emphasised that the resource should be considered as an estimated "gas in-place", and not as a reserve or recoverable gas. The resource estimate is quoted in million cubic meters (Mm^3). The equations referred to above are as follows:

$$Gas\ content\ (m^3/t) = [152 + \{0.2 \times depth\ (m/0.3048)\}] \div 35.3 \qquad (2)$$

Using linear regression to represent the change in gas content with depth, Nolde and Spears (1998) proposed that a minimum depth of 152m (500ft) is generally required for coal to contain gas-in-place. However, this depth is not valid to the all coal reservoirs. For example, in the Powder River Basin, Wyoming, methane was encountered at shallow depth (<100m) coals (Stricker and Flores, 2002).

Formula 3 was also developed to evaluate the in-place CBM resource. Conversion to cubic feet, used a factor of $35.3/m^3$.

$$Gas\ resource = (Gas\ content) \times (density) \times (Av.\ coal\ thickness) \times (Area\ in\ Ha) \times c \qquad (3)$$

Where c = tons of coal per hectare metre of coal = 14,593 tonne (av.)

Average gas content (m^3/ ton) = (- 542ρ_B+ 1053) ÷35.3) (4)

Where, ρ_B = Density of bituminous coal (Barapukuria 1.4 to 1.45)

$$V = \left[(1 - V_M - V_A) \times 0.75 \times \{k_0 \times 0.96h^{n_0} - 0.14\left(\frac{1.8h}{100}\right) + 11\} \right] \div 35.3 \quad (5)$$

This equation (Kim, 1977) involved consideration of coal rank, where:

$$k_0 = 0.8 \times \left(\frac{V_{FC}}{V_M}\right) + 5.6 \quad (6)$$

$$n_0 = 0.39 - 0.1 \times \left(\frac{V_{FC}}{V_M}\right) \quad (7)$$

V= Gas content (m^3/ton)
V_M = Moisture
V_{FC} = Fixed Carbon
h = Depth in metres

7.6.2. Gas Content and Reservoir Saturation

The gas content of the coal seams is estimated using the formulae derived by Nolde and Spears (1998). The application of formulae Nos. 4 and 5 resulted in estimated CBM contents of 8.65 m^3/tonne and 8.33m^3/tonne respectively. The resultant estimated total gas resource at Barapukuria is 5135.32 Mm^3.

The gas content of a coal reservoir can be estimated in two ways:

- Direct measurement of the volume of gas released from a coal sample sealed into a desorption canister (e. g., Stricker and Flores, 2002)
- Indirect estimation based on empirical correlations, or laboratory derived sorption isotherm gas storage capacity data. The latter describe the quantitative relationship between adsorbed methane at varying pressures and a constant temperature, and provide a measure of the maximum methane sorption or storage capacity of the coal sample (Diamond and Schatzel, 1998). Desorption and adsorption data are not available for the Barapukuria coals and further research into this should be considered.

At Barapukuria, estimated gas content data is compared with rank and depth from studies carried out in the USA and Australia. In the Powder River Basin, Wyoming, the desorbed gas contents in subbituminous B coal rises to a maximum of 2.67 m^3/tonne at 396 m depth (Stricker and Flores, 2002). In the Surat Basin, Queensland, Australia, the adsorbed gas contents in the high volatile bituminous coal varies within the range 1 to 14 m^3/t at 400 m depth (Scott et al., 2007). The estimated CBM content of subbituminous B coals at Barapukuria varies within the range 6.76 to 12.68 m^3/tonne (Table 7-4) between the depths of 131 m and 450 m.

The gas saturation of a reservoir is a critical economic factor in the evaluation of a CBM project. Gas saturation refers to the degree to which the gas content of a coal seam approaches the adsorbed gas capacity for the particular reservoir pressure, temperature, and gas composition. Coals that contain less gas than their measured adsorption capacity are referred to as "undersaturated". Conversely, coals that contain more gas than the adsorption capacity are referred to as "oversaturated". This is merely a statement that the measured gas content of a coal is greater than its measured capacity (Bustin and Bustin, 2008).

Gas resource estimates of the Barapukuria basin are based on a full (100%) saturation and represent the best case scenario. Internationally, there is significant variation in the degree of saturation of high-volatile bituminous coals. The degree of saturation of bituminous coals of the Sydney Basin, Australia, rises to a maximum of 85% (Bustin and Clarkson, 1998). The Gates Formation coals, Alberta Inner Foothills, Canada, has maximum holding capacity of about 18.7 m^3/tonne while total gas content from desorption is 16.8 m^3/tonne. This indicates an apparent saturation of 89% (Gentzis and Bolen., 2008). In the Turpan-Hami Basin, China, the degree of gas saturation for subbituminous B coals is 70-91% (Shu et al., 2007). In the Powder River basin, where the gas content determined from desorption is always less than the maximum gas storage capacity, the coals are undersaturated. The undersaturation of gas ranges from 23% for subbituminous A coals to 66% for the subbituminous C coals (Stricker and Flores, 2002). The variation in saturation of the coal at Barapukuria is estimated at between 40% and 90%.

Table 7-4. Estimated gas content (m^3/ton) and gas resource (m^3) of the Barapukuria coal basin (calculated by using eqn. 2 and 3; Nolde and Spears, 1998). For thickness and overburden depth of coal seams see in Tables 3a, and 3b, and in Figs. 5a, 5b, and 5c, respectively. For coal density see in Table 4. Zones and areas (in hectares) are shown in Fig. 7-1.

Coal Seams	**Zones**	**Overburden depth (m)**	**Estimated Gas content (m^3/ton)**	**Density (ρ)**	**Thickness (m)**	**Area (hectares)**	**Estimated Gas resource (Mm^3)** *(based on 100% saturation)*	**Estimated Coal resource (Mt)**
Seam II	Zone-9	155.00	7.18	1.78	13.95	37.02	96.32	7.54
	Zone-40	252.00	9.00	1.78	15.24	38.52	137.24	8.57
Seam III	Zone-4	145.80	7.02	1.51	1.30	36.47	7.33	0.69
	Zone-9	177.47	7.61	1.51	2.33	37.02	14.46	1.26
	Zone-40	276.45	9.45	1.51	6.60	38.52	52.94	3.71
Seam IV	Zone-2	132.90	6.78	1.68	9.60	23.45	37.42	3.29
	Zone-4	170.50	7.48	1.68	7.80	36.47	52.17	4.15
	Zone-9	208.23	8.18	1.68	10.19	37.02	75.65	5.50
	Zone-10	185.34	7.76	1.68	3.80	113.72	82.21	6.31
	Zone-38	162.15	7.32	1.68	8.84	30.44	48.29	3.93
	Zone-40	306.17	10.00	1.68	3.12	38.52	29.46	1.75
	Zone-41	131.96	6.76	1.68	8.69	42.01	60.50	5.33
Seam V	Zone-2	160.03	7.28	1.56	2.31	23.45	8.98	0.79
	Zone-4	206.70	8.15	1.56	1.40	36.47	9.47	0.75
	Zone-5	175.20	7.56	1.56	1.30	81.46	18.23	1.55
	Zone-9	238.89	8.75	1.56	2.26	37.02	16.67	1.22
	Zone-10	208.20	8.18	1.56	2.18	113.72	46.17	3.62
	Zone-38	197.81	7.99	1.56	10.37	30.44	57.42	4.61
	Zone-40	331.01	10.46	1.56	5.49	38.52	50.36	3.09
	Zone-41	162.45	7.33	1.56	6.40	42.01	44.86	3.92
	Zone-43	161.54	7.31	1.56	10.21	36.32	61.71	5.41
Seam VI	Zone-1	131.80	6.76	1.45	29.40	31.78	133.65	13.63
	Zone-2	291.40	9.72	1.45	37.00	23.45	178.45	12.66
	Zone-4	331.15	10.46	1.45	42.50	36.47	343.06	22.62
	Zone-5	249.10	8.94	1.45	21.90	81.46	337.47	26.03
	Zone-6	163.35	7.34	1.45	30.37	32.67	154.10	14.48
	Zone-7	199.55	8.02	1.45	38.05	22.34	144.25	12.40
	Zone-8	195.80	7.95	1.45	21.63	19.56	71.17	6.17
	Zone-9	381.82	11.40	1.45	39.75	37.02	354.97	21.47
	Zone-10	312.70	10.12	1.45	28.70	113.72	698.89	47.63
	Zone-11	180.64	7.67	1.45	33.13	29.98	161.20	14.49
	Zone-12	118.65	6.51	1.45	30.84	17.45	74.13	7.85
	Zone-13	162.00	7.32	1.45	36.00	29.22	162.93	15.35
	Zone-38	331.62	10.47	1.45	39.62	30.44	267.19	17.60
	Zone-40	450.19	12.68	1.45	40.84	38.52	422.09	22.96
	Zone-41	285.27	9.61	1.45	36.29	42.01	310.01	22.25
	Zone-43	286.82	9.64	1.45	42.37	36.32	313.90	22.46
			Mean = 8.20				Total = 5135.32	Total = 377.03

Note: Estimated coal resource = Thickness (m) of seam × Area (in hectares) of regarding zone × c (tons of coal per hectare meter of coal = 14,593 ton average). Basic unit of c value was taken from Nolde and Spears (1998), where they used 1,800 ton of coal per acre foot.

7.7. Summary

The assessment of the CBM potential at Barapukuria involves the consideration of six parameters:

- Thickness and depth of the coal seams
- Coal rank, composition and maceral content
- Characteristic of coal cleats/fractures
- Hydrodynamic properties
- Porosity and permeability of the overburden and coal
- Geothermal gradient and reservoir temperature

Drobniak et al. (2004) concluded that a 1.6 m thick coal seam with overburden up to about 425 m has the potential for CBM exploitation. At Barapukuria, there is a significant resource of coal at depths in excess of 150 m, and this should not be discounted with regard to its CBM potential. Coal seams occurring within the range 60 m and 150 m depth could be of economic interest. Barapukuria is usual in that it contains thick coal seams of limited extent, and appears particularly suitable for CBM exploitation.

Coal rank has a significant effect on its CBM potential. Most CBM projects produce gas from bituminous coals (http://www.fox-davies.com/researchonly.htm:CBM sector overview, 2007). Generally methane manufacture increases with rank from 4.5 m^3/tonne in high volatile B bituminous coal to 15 m^3/tonne in low volatile bituminous coal (Creedy, 1988). Coal rank generally increases with depth of overburden from 0.80% to 1.0% Ro (max), which is equivalent to a high volatile A bituminous coal. At this rank, methane generation from coal is approximately 8 m^3/ton. For coal with between 0.6% and 0.7% Ro, or high volatile B to high volatile C bituminous coal, a methane generation factor of 5m^3 per ton is assumed. The high volatile B bituminous rank coals of Barapukuria, whose Ro (max) ranges between 0.55% and 0.84%, and gas content ranges from 6.51 - 12.68 m^3/tonne, suggest a potential for economic CBM exploitation warranting further research.

Cleats, i.e. natural fractures, are the principal conduits for the release of methane from coal seams (Close, 1993). Typically primary and secondary cleat systems are developed, but in complex structural environments, a tertiary system may also become apparent. Not surprisingly, Diamond et al. (1988) observed that a higher fracture density results in a higher permeability of coal. Coal consists of cleats and matrix. The matrix stores the gas by adsorption and flow of gas in the matrix is by diffusion. As gas is desorbed from the coal, the pressure exerted by the gas in pores decreases. This causes the volume of the coal matrix to reduce in size. A reduction in the matrix size simultaneously acts to widen the cleats thereby increasing permeability. The high intensity of cleat fractures in coal seams at Barapukuria coal is indicative of a relatively high content reservoir of CBM.

The overlying coarse-grained sandstone of Seam VI is effectively permeable, and the water contained within the overlying Upper Dupi Tila aquifer recharges the roof sandstone via faults, joints and fractures. There appears to be a strong hydraulic continuity between the Dupi Tila and the underlying Gondwana sediments (Islam and Islam, 2005). The cleats systems are well developed and are conducive to the vertical passage of water, Hydrofracturing could lead to an increase in the potential for CBM release.

At Barapukuria, high volatile B bituminous coals with a measured porosity of 1.6% to 3.2% predominate, with pores varying between mesopore and micropore sizes (0.95 - 1.35 mm) (Wardell Armstrong, 1991). It is expected, therefore that the CBM storage potential of Barapukuria coal would be comparable to coals with similar pore characteristics elsewhere. The measured range of permeability (9.80 – 137.8 mD) in Barapukuria coals suggest an encouraging prospect for CBM generation. The measured geothermal gradient at Barapukuria of 32^{o}C/km (Dupi Tila) and 36^{o}C/km (Gondwana), and strata temperatures between 29.5^{o}C and 40.5^{o}C suggest a strong potential for CBM production.

Based on the above, exploitation of CBM at Barapukuria could provide an important alternative energy source for Bangladesh. Barapukuria Coal mine is surrounded by many villages, where agriculture is the principal occupation. CBM development could be welcomed by the local population, in favour of open pit or underground mining, both of which will have adverse effects on the agricultural environment.

References

ASTM, 1979. ASTM D1412-07 Standard Test Method for Equilibrium Moisture of Coal at 96 to 97 Percent Relative Humidity and 30°C.

Bustin, M.M.A., and Bustin, R.M., 2008. Coal reservoir saturation: Impact of temperature and pressure. AAPG Bulletin 92, 77-86.

Bustin, R.M., Cui, X., and Chikatamarla, L., 2008. Impacts of volumetric strain on CO_2 sequestration in coals and enhanced CH_4 recovery. AAPG Bulletin 92, 15-29.

Bustin, R.M., and Clarkson, C.R., 1998. Geological controls on coalbed methane reservoir capacity and gas content. International Journal of Coal Geology 38, 3-26.

Close, J.C., 1993. Natural fractures in coal. Am. Assoc. Petrol. Geol. Stud. Geol. 38, 119– 132.

Creedy, D.P., 1988. Geological controls on the formation and distribution of gas in British coal measure strata. International Journal of Coal Geology 10, 1–31.

Desikacher, S.V., 1974. A review of the tectonic and geological history of eastern India in terms of plate tectonic theory. J. Geol. Soc. India 15, 134-149.

Diamond, W.P., and Schatzel, S.J., 1998. Measuring the gas content of coal: A review. International Journal of Coal Geology 35, 311–331.

Diamond, W.P., Elder, C.H., and Jeran, P.W., 1988. Influence of geology on methane emission from coal, U.S. Bureau of Mines Bulletin 687, 26-40.

Drobniak, A., Mastalerz, M., Rupp, J., and Eaton, N., 2004. Evaluation of coalbed gas potential of the Seelyville Coal Member, Indiana, USA. International Journal of Coal Geology 57, 265– 282.

Gentzis, T., and Bolen, D., 2008. The use of numerical simulation in predicting coalbed methane producibility from the Gates coals, Alberta Inner Foothills, Canada: Comparison with Mannville coal CBM production in the Alberta Syncline. International Journal of Coal Geology (article in press).

Harpalani, C., and Chen, G., 1995. Influence of gas production induced volumetric strain on permeability of coal. Geotechnical and Geological Engineering 15, 303-325.

Imam, M.B., Rahman, M., Akhter, S.H., 2002. Coalbed Methane prospects of Jamalganj Coalfield, Bangladesh. The Arabian Journal for Science and Engineering 27, 17-27.

Islam, M.R., and Islam, M.S., 2005. Water Inrush Hazard in Barapukuria Coal Mine, Dinajpur District, Bangladesh. Bangladesh Journal of Geology 24, 1-17.

Kim, A.G., 1977, Estimating methane content of bituminous coalbeds from adsorption data. Report of Investigations, U.S. Bureau of Mines RI 8245, p.22.

Khan, F.H., 1991. Geology of Bangladesh, Willey Eastern Limited, 4835/24 Ansari Road, Daryaganj, New Delhi 110002, India, pp. 33-40.

Mullen, M.J., 1988, Log evaluation in wells drilled for coal-bed methane. in J.E. Fassett, ed., Geology and coal-bed methane resources of the northern San Juan basin, Colorado and New Mexico: Denver, Rocky Mountain Association of Geologists Guidebook, p. 113-124.

National Energy Policy (NEP), 2004. Government of the People's Republic of Bangladesh, Ministry of Power, Energy and Mineral Resources, Dhaka, Bangladesh.

Nolde, J.E., and Spears, D., 1998. A preliminary assessment of in place coalbed methane resources in the Virginia portion of the central Appalachian Basin. International Journal of Coal Geology 38, 115-136.

Petrobangla, 1994. Inauguration Ceremony of the Barapukuria Coal Mine Development Project. A brochure published by Petrobangla, Ministry of Energy and Mineral Resources, Government of the People's Republic of Bangladesh, p.3.

Scott, S., Anderson, B., Crosdale, P., Dingwall, J., and Leblang, G., 2007. Coal petrology and coal seam gas contents of the Walloon Subgroup- Surat Basin, Queensland, Australia. International Journal of Coal Geology 70, 209-222.

Shu, T., Yan, W., and Dai, Z., 2007. A comprehensive appraisal on the characteristics of Coal-Bed Methane reservoir in Tupan-Hami Basin, China. Journal of China University of Mining & Technology 17, 521-725.

Stricker, G.D. and Flores, R.M., 2002. Coalbed Methane Content in the Powder River Basin, Wyoming: Saturation by Coal Rank and Depth. The 19th Annual International Pittsburgh Coal Conference. University of Pittsburgh, Pittsburgh, Pa. pp.1-15.

Wardell Armstrong, 1991, Techno-Economic Feasibility Study of Barapukuria Coal Project (unpubl.), Dinajpur, Bangladesh.